Functionalization of cells, extracellular matrix components and proteins for therapeutic application

Dissertation zur Erlangung des naturwissenschaftlichen Doktorgrades der

Julius-Maximilians-Universität Würzburg

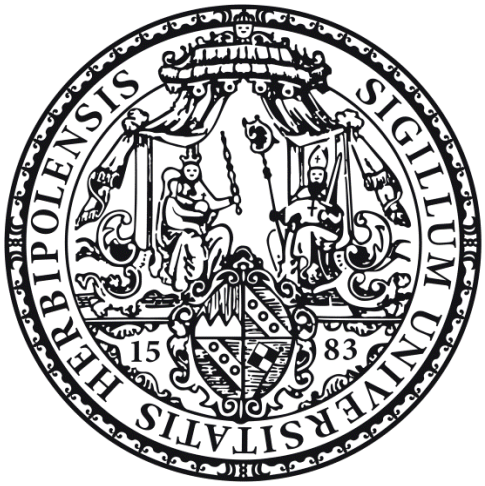

vorgelegt von

Marcus Gutmann

aus Erlangen

Würzburg 2018

Eingereicht bei der Fakultät für Chemie und Pharmazie am

Gutachter der schriftlichen Arbeit

1. Gutachter:

2. Gutachter:

Prüfer des öffentlichen Promotionskolloquiums

1. Prüfer:

2. Prüfer:

3. Prüfer:

Datum des öffentlichen Promotionskolloquiums

Doktorurkunde ausgehändigt am

Die vorliegende Arbeit wurde in der Zeit von Juni 2013 bis Juli 2018 am Institut für Pharmazie und Lebensmittelchemie der Bayerischen Julius-Maximilians-Universität Würzburg unter der Anleitung von Herrn Prof. Dr. Dr. Lorenz Meinel und Frau PD Dr. Tessa Lühmann angefertigt.

Table of contents

Summary

Glycosylation is a biochemical process leading to the formation of glycoconjugates by linking glycans (carbohydrates) to proteins, lipids and various small molecules. The glycans are formed by one or more monosaccharides that are covalently attached, thus offering a broad variety depending on their composition, site of glycan linkage, length and ramification. This special nature provides an exceptional and fine tunable possibility in fields of information transfer, recognition, stability and pharmacokinetic. Due to their intra- and extracellular omnipresence, glycans fulfill an essential role in the regulation of different endogenous processes (e.g. hormone action, immune surveillance, inflammatory response) and act as a key element for maintenance of homeostasis. The strategy of metabolic glycoengineering enables the integration of structural similar but chemically modified monosaccharide building blocks into the natural given glycosylation pathways, thereby anchoring them in the carbohydrate architecture of de novo synthesized glycoconjugates. The available unnatural sugar molecules which are similar to endogenous sugar molecules show minimal perturbation in cell function and - based on their multitude functional groups - offer the potential of side directed coupling with a target substance/structure as well as the development of new biological properties. The chemical-enzymatic strategy of glycoengineering provides a valuable complement to genetic approaches.

This thesis primarily focuses on potential fields of application for glycoengineering and its further use in clinic and research. The last section of this work outlines a genetic approach, using special *Escherichia coli* systems, to integrate chemically tunable amino acids into the biosynthetic pathway of proteins, enabling specific and site-directed coupling with target substances. With the genetic information of the methanogen archaea, *Methanosarcina barkeri*, the *E. coli*. system is able to insert a further amino acid, the pyrrolysine, at the ribosomal site during translation of the protein. The natural stop-codon UAG (amber codon) is used for this newly obtained proteinogenic amino acid.

Chapter I describes two systems for the integration of chemically tunable monosaccharides and presents methods for characterizing these systems. Moreover, it gives a general overview of the structure as well as intended use of glycans and illustrates different glycosylation pathways. Furthermore, the strategy of metabolic glycoengineering is demonstrated. In this context, the structure of basic building blocks and the epimerization of monosaccharides during their metabolic fate are discussed.

Chapter II translates the concept of metabolic glycoengineering to the extracellular network produced by fibroblasts. The incorporation of chemically modified sugar components in the matrix provides an innovative, elegant and biocompatible method for site-directed coupling of target substances. Resident cells, which are involved in the de novo synthesis of matrices, as well as isolated

matrices were characterized and compared to unmodified resident cells and matrices. The natural capacity of the matrix can be extended by metabolic glycoengineering and enables the selective immobilization of a variety of therapeutic substances by combining enzymatic and bioorthogonal reaction strategies. This approach expands the natural ability of extracellular matrix (ECM), like the storage of specific growth factors and the recruitment of surface receptors along with synergistic effects of bound substances. By the selection of the cell type, the production of a wide range of different matrices is possible.

Chapter III focuses on the target-oriented modification of cell surface membranes of living fibroblast and human embryonic kidney cells. Chemically modified monosaccharides are inserted by means of metabolic glycoengineering and are then presented on the cell surface. These monosaccharides can later be covalently coupled, by "strain promoted azide-alkyne cycloaddition" (SPAAC) and/or "copper(I)-catalyzed azide-alkyne cycloaddition" (CuAAC), to the target substance. Due to the toxicity of the copper catalysator in the CuAAC, cytotoxicity analyses were conducted to determine the *in vivo* tolerable range for the use of CuAAC on living cell systems. Finally, the efficacy of both bioorthogonal reactions was compared.

Chapter IV outlines two versatile carrier – spacer – payload delivery systems based on an enzymatic cleavable linker, triggered by disease associated protease. In the selection of carrier systems (i) polyethylene glycol (PEG), a well-studied, Food and Drug Administration approved substance and very common tool to increase the pharmacokinetic properties of therapeutic agents, was chosen as a carrier for non-targeting systems and (ii) Revacept, a human glycoprotein VI antibody, was chosen as a carrier for targeting systems. The protease sensitive cleavable linker was genetically inserted into the N-terminal region of fibroblast growth factor 2 (FGF-2) without jeopardizing protein activity. By exchanging the protease sensitive sequence or the therapeutic payload, both systems represent a promising and adaptable approach for establishing therapeutic systems with bioresponsive release, tailored to pre-existing conditions.

In summary, by site-specific functionalization of various delivery platforms, this thesis establishes an essential cornerstone for promising strategies advancing clinical application. The outlined platforms ensure high flexibility due to exchanging single or multiple elements of the system, individually tailoring them to the respective disease or target site.

Zusammenfassung

Glykosylierung beschreibt einen auf biochemischen Reaktionen basierenden Prozess, welcher durch die Verknüpfung von Glykanen (Kohlenhydraten) mit Proteinen, Lipiden oder einer Vielzahl kleiner organischer Moleküle zur Bildung von Glykokonjugaten führt. Die Entstehung der Kohlenhydratketten erfolgt hierbei durch die kovalente Verknüpfung eines oder mehrerer verschiedener Einfachzucker, welche auf Grund unterschiedlicher Zusammensetzung der Bausteine, Verknüpfungsregion, Länge und Verzweigung eine hohe Diversität aufweisen. Diese Besonderheit ermöglicht eine außergewöhnliche Feinabstimmung im Bereich der Informationsübertragung, Erkennung, Stabilität und Pharmakokinetik. Aufgrund ihrer intra- und extrazellulären Omnipräsenz spielen Glykane zudem eine essentielle Rolle in der Regulierung verschiedenster körpereigener Prozesse (z.B. hormonelle Wirkung, Immunmodulation, Entzündungsreaktionen) und sind folglich ein zentraler Bestandteil bei der Aufrechterhaltung der zellulären Homöostase. Durch die Strategie des „Glycoengineering“ ist man in der Lage, strukturähnliche, aber chemisch modifizierte Zuckerbausteine in die natürlichen Glykosilierungswege einzubinden und diese somit in der Architektur der Kohlenstoffketten von neu-synthetisierten Glykokonjugaten zu verankern. Die hierfür zur Verfügung stehenden, unnatürlichen Zuckermoleküle führen auf Grund ihrer Ähnlichkeit zu körpereigenen Zuckern zu kaum relevanten Störungen der zellulären Funktion, bieten aber durch zahlreiche funktionelle Gruppen die Möglichkeit der gezielten Verknüpfung mit einer Zielsubstanz/-struktur und der Bildung neuer biologischer Eigenschaften. „Glycoengineering“ als chemisch-enzymatische Strategie bietet dabei eine wertvolle Ergänzung zu gentechnischen Ansätzen.

Entsprechend beschäftigt sich diese Dissertation primär mit der Beschreibung potentieller Anwendungsgebiete des „Glycoengineering“ und dessen möglichen Einsatz in Klinik und Forschung. Der letzte Abschnitt dieser Arbeit beschreibt einen gentechnischen Ansatz, bei dem mit Hilfe von speziellen *Escherichia coli* Systemen chemisch modifizierbare Aminosäuren in den Biosyntheseweg von Proteinen eingebunden werden, wodurch anschließend eine spezifische und gerichtete Verknüpfung mit Zielsubstanzen ermöglicht wird. Hierbei benutzt das *E. coli*-System die genetische Information des methanbildenden Archaeas, *Methanosarcina barkeri*, mit der es in der Lage ist, eine weitere Aminosäure, das Pyrrolysin, bei der Translation eines Proteins am Ribosom einzufügen. Als Codon für diese neu gewonnene proteinogene Aminosäure fungiert das natürliche Stopp-Codon („amber codon“) UAG.

Kapitel I beschreibt zwei Systeme für den Einbau von chemisch modifizierten Zuckern und zeigt Methoden für die Charakterisierung dieser Systeme auf. Es gibt zudem eine allgemeine Übersicht über den Aufbau und die Verwendung von Glykanen und veranschaulicht verschiedene Glykosilierungswege. Des Weiteren wird auch die Strategie des „metabolic glycoengineering“

erläutert. Hierbei wird der Aufbau der dabei verwendeten Grundbausteine dargestellt und auf die Epimerisierung der Zucker während deren Metabolismus eingegangen.

Kapitel II überträgt das Konzept des „metabolic glycoengineering“ auf das extrazelluläre Netzwerk von Fibroblasten. Hierbei bietet der Einbau eines chemisch modifizierten Zuckerbausteins in die Matrix eine neue, elegante und biokompatible Möglichkeit der gezielten Verknüpfung von Zielsubstanzen. Die an der Neusynthese der Matrix beteiligten Bindegewebszellen sowie die isolierte Matrix wurden dabei im Vergleich zu nicht modifizierten Bindegewebszellen und Matrices charakterisiert. Durch den Aspekt des “metabolic glycoengineering” wird die natürliche Fähigkeit der Matrix erweitert und ermöglicht durch die Kombination verschiedener enzymatischer und bioorthogonal-chemischer Strategien die selektive Immobilisation einer Vielzahl von therapeutischen Substanzen. Dieser Ansatz erweitert das natürliche Spektrum der Extrazellulärmatrix (ECM), wie Bindung von spezifischen Wachstumsfaktoren, Rekrutierung von Oberflächenrezeptoren und damit einhergehend synergistische Effekte der gebundenen Stoffe. Durch die Auswahl des Zelltyps wird zudem ein breites Spektrum an verschiedenen Matrices ermöglicht.

Kapitel III befasst sich mit der Möglichkeit, die Zellmembran von lebenden Fibroblasten sowie menschliche embryonale Nierenzellen gezielt zu verändern. Durch „metabolic glycoengineering“ werden auch hier chemisch modifizierte Zuckerbausteine eingefügt, die dabei auf der Zelloberfläche präsentiert werden. Anschließend können diese Zucker mittels „ringspannungs-geförderter Azid-Alkin Cycloaddition“ (“strain promoted azide-alkyne cycloaddition“, SPAAC) und „Kupfer(I)-katalysierter Azid-Alkin Cycloaddition“ (“copper(I)-catalyzed azide-alkyne cycloaddition“, CuAAC) umgesetzt werden, was eine kovalente Verknüpfung mit einer Zielsubstanz ermöglicht. Aufgrund der Toxizität des Kupferkatalysators in der CuAAC wurde anhand von zytotoxischen Untersuchungen nach einem *in vivo* vertretbaren Bereich für diese Reaktion gesucht, um die CuAAC auch für lebende Systeme verwendbar zu machen. Zuletzt wurde die Effizienz dieser bioorthogonalen Reaktionen miteinander verglichen.

Kapitel IV beschreibt zwei vielseitig einsetzbare „carrier – spacer – payload“ Therapiesysteme (Träger-Verbindungsstück-Therapeutikum-Systeme), basierend auf einem Verbindungsstück (Linker), dessen Spaltung enzymatisch durch krankheitsspezifisch prävalente Proteasen ausgelöst wird. Bei der Auswahl der Trägersysteme wurde für das nicht-zielgerichtete System Polyethylenglycol (PEG) als Träger eingesetzt, eine gut untersuchte, „Food and Drug Administration“ zugelassene Substanz, welche als sehr gängiges Mittel zur Verbesserung der pharmakologischen Eigenschaften verwendet wird. Für das zielgerichtete System diente Revacept als Träger, ein humaner Glykoprotein VI-Antikörper. Der Protease-sensitive Linker wurde genetisch in der N-terminalen Region des Fibroblasten-Wachstumsfaktor 2 verankert, ohne dabei die

Bioaktivität zu gefährden. Durch den Austausch der Protease-sensitiven Erkennungssequenz oder des Therapeutikums stellen beide Systeme einen vielversprechenden und anpassungsfähigen Ansatz für therapeutische Systeme dar, welche auf ein bereits bestehendes Erkrankungsbild genau zugeschnitten werden können.

Zusammengefasst setzt diese Arbeit durch eine spezifische Funktionalisierung von verschiedenen Therapiesysteme einen wichtigen Meilenstein für vielversprechende Strategien zur Verbesserung der klinischen Anwendbarkeit. Durch den Austausch einer oder mehrerer Komponenten des Systems gewährleisten die hier beschriebenen Therapiesysteme eine hohe Anpassungsfähigkeit, wodurch sie individuell auf die jeweilige Krankheit oder den jeweiligen Zielort angepasst werden können.

Chapter 1: Metabolic glycoengineering of cell derived matrices and cell surfaces - a combination of key principles and step-to-step procedures

Marcus Gutmann[1], Julian Bechold[2], Jürgen Seibel[2], Lorenz Meinel[1] and Tessa Lühmann[1]*

[1]Institute of Pharmacy and Food Chemistry, University of Würzburg, DE-97074 Würzburg, Germany,

[2]Institute of Organic Chemistry, University of Würzburg, DE-97074 Würzburg, Germany

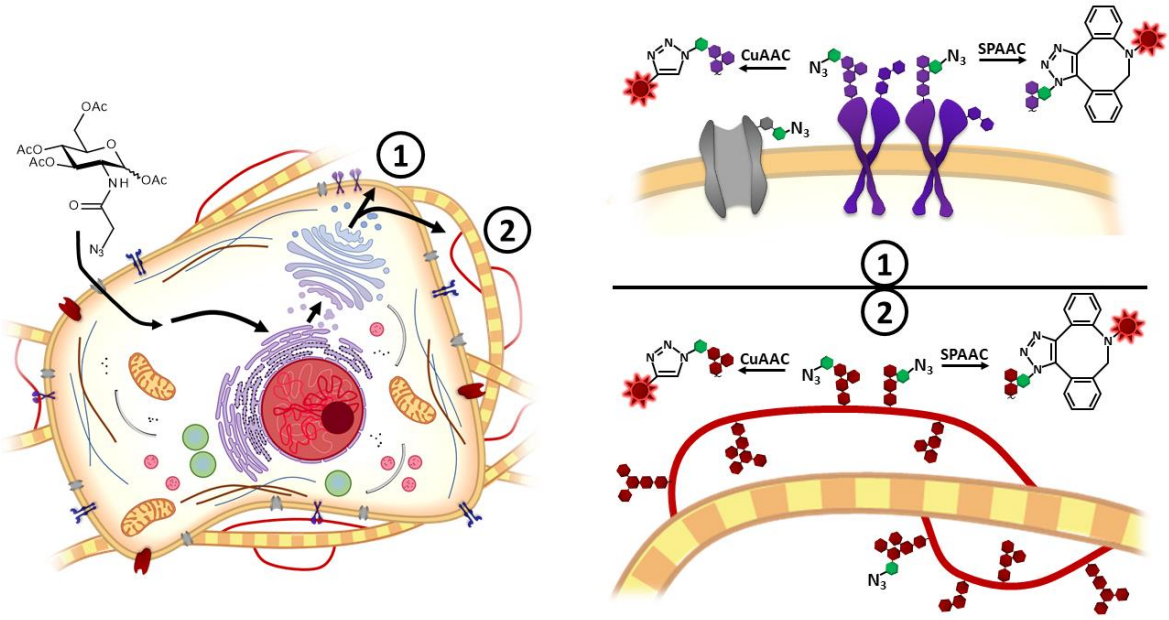

This chapter is currently submitted in ACS Biomaterial Science & Engineering, with permission for figures/tables of John Wiley and Sons, License number 4398120465226 and 4393060950967 and with permission of the American Chemical Society.

Abstract

Metabolic glycoengineering allows insertion of non-natural monosaccharides into glycan structures during biosynthesis thereby enabling extracellular matrices (ECM), cell surfaces or tissues for decoration with functional cues with ultimate spatial control while deploying aqueous and toxicologically benign coupling chemistries. In this work, we discuss relevant methods in the design of metabolic glycoengineered systems, ranging from synthetic procedures to decoration of cell surfaces and ECM components by bioorthogonal chemistries for widespread biomedical applications. As representative example, we chose a tetra-acetylated azide-bearing monosaccharide as model compound to be metabolically incorporated into glycans of the glycocalyx and ECM components generated by NIH 3T3 cells. Detailed guidance in fabrication and functionalization of azide-bearing glycan structures via bioorthogonal click chemistries in glycoengineered extracellular matrices is provided. In addition, a biocompatible design space of the copper (I)-catalyzed azide-alkyne cycloaddition due to the toxicity of the copper catalyst is detailed enabling effective and safe modification of living cell systems. Thereby, this set of methods provides the blueprint enabling the design and characterization of metabolically glycoengineered systems for novel applications in drug delivery and tissue engineering

Introduction

Glycosylation - or linking carbohydrates to proteins, lipids and various small molecules resulting in glycoconjugates – is essential in controlling numerous biological processes. Glycans strongly vary in their composition, site of attachment, length and ramification.[1-2] The complex co- and post-translational process of glycan synthesis fuels the perplexing variety of natural glycosylation patterns. Whereas proteins and nucleic acids result from defined biological templates, carbohydrates are constructed stochastically by a number of enzymes including glycosyltransferases, glycosidases, kinases, phosphorylases, sulfotransferases and sulfatases.[3] Mammalian glycans contain up to ten different monosaccharides – fucose (Fuc), galactose (Gal), glucose (Glc), mannose (Man), sialic acid (SA), *N*-acetylgalactosamine (GalNAc), *N*-acetylglucosamine (GlcNAc), glucuronic acid (GlcA), iduronic acid (IdoA) and xylose (Xyl), whith bacteria and plants deploying substantially higher numbers of monosaccharides.[4-5] It is for this pleiotropy that essential biological processes are directed through sugar side chains, including protein folding and stability, pharmacokinetics or receptor binding.[6-8]

Metabolic glycoengineering builds off these insights, representing a versatile method to insert non-natural monosaccharides – with high similarity to natural precursors – into glycan structures during biosynthesis. Deploying these methods, functional groups are integrated into the sugar side chains

available for further chemical modification,[2, 9-11 12] including hydroxyl,[13] ketone,[14] thiol[15] and azide,[16] alkene,[17] cyclopropane [18] and cyclooctyne.[19] The majority of applied functionalized monosaccharides are thereby derived from Fuc, glucosamine, mannosamine, galactosamine or neuraminic acid.[20-22] The sugars' hydroxyl groups are typically acetylated to allow effective transport across cell membranes, followed by intracellular de-acetylation through esterases, thereby featuring the free sugar for glycosylation. Other protecting groups like propionyl or O-butanoyl have been studied in an effort to maximize the transport across the cellular membranes.[23] Glycosylation most frequently occurs as N-glycosylation, O-glycosylation and glypiation and, less frequently, as C-mannosylation and phosphoglycosylation, the latter of which being limited to parasites and slime molds.[24-25]

N-glycosylation is the transfer of a pre-assembled oligosaccharide from a lipid linked oligosaccharide donor to the amide nitrogen of an asparagine residue within a polysaccharide acceptor sequence of a protein referred to as sequon (Figure 1A). A sequon generally comprises Asn-X-(Ser/Thr) or Asn-X-Cys tripeptide ("X" is any amino acid except proline) consensus sequence.[26-27] O-glycosylation is the transfer of a single monosaccharide to serine (S) and threonine (T) residues and rarely to hydroxyproline and hydroxylysine side chains (Figure 1B).[1, 28] Following the attachment of the first monosaccharide to the hydroxyl-group, subsequent monosaccharides are added consecutively, leading to branched or linear arrangements of the growing oligosaccharide chain. N- and O-glycosylation pathways are further detailed in [28-30].

Occasionally, glycoproteins require anchoring to cell membranes. The necessary post-translational modification - Glypiation - enables a specific recruitment of proteins to the extracellular side on glycosphingolipid/cholesterol rich membrane domains.[31-32] In this process a preassembled glycosylphosphatidylinositol (GPI) anchor is covalently attached to the C terminus of a protein in the presence of a hydrophobic sequence.[33] C-terminal mannosylation of the protein involves covalent attachment of α-mannose to the indole C2 carbon atom of a tryptophan via C-C link.[34] In fact, C-terminal consensus sequences - Trp-x-x-Trp – feature protein C-mannosylation with the first tryptophan residue being mannosylated through specific mannosyltransferases.[35-37]

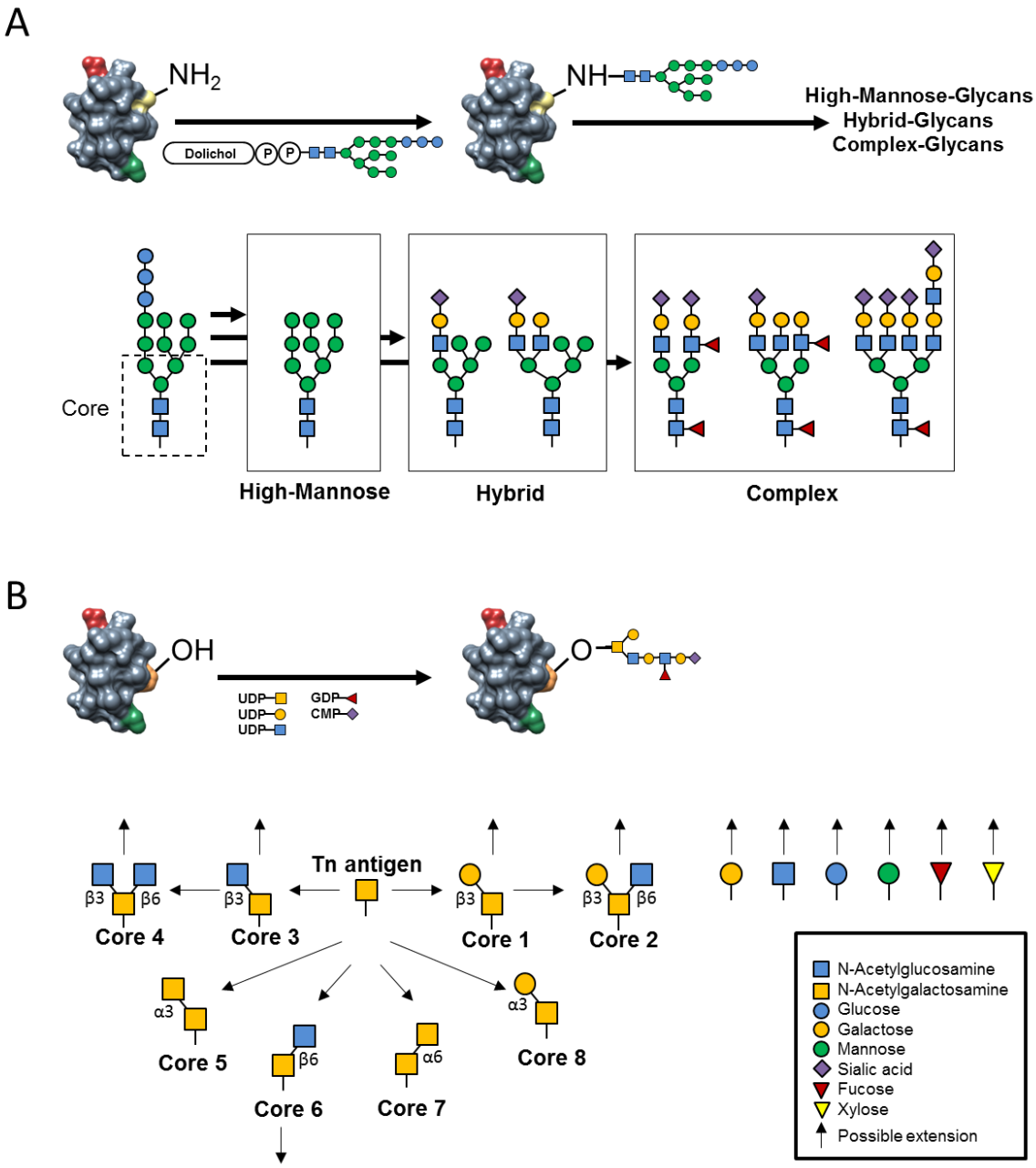

Figure 1: (A) Simplified model of the N-glycosylation. The pre-assembled oligosaccharide chain is transferred by the carrier lipid dolichol-phosphate to the amide of asparagine. By processing the pre-assembled, different types of mature glycoprotein types are generated – High-Mannose; Hybrid and Complex. Each type contains the common $Man_3GlcNAc_2$ core connected to asparagine. **(**B**)** Simplified model of O-glycosylation. The most common mucine-type-O-glycosylation core pathway is initiated by the transfer of the first GalNAc residue forms the Tn-antigen, which is extended to the eight core structures. Other O-glycosylation pathways can be found by the use of different first monosaccharide building blocks.

Typically, monosaccharides for metabolic glycoengineering are analogs of GlcNAc, GalNAc, ManNAc and sialic acid. ManNAc analogs are metabolically converted via ManNAc-6-P, sialic acid-9-P, sialic acid to CMP-sialic acid, representing the terminal monosaccharide in N-glycans.[17, 22, 38-42]

GalNAc analogs – transformed via GalNAc-1-P to UDP-GalNAc – and GlcNAc analogs – transformed via GlcNAc-6-P, GlcNAc-1-P to UDP-GlcNAc – are normally found in O-glycans, with particularly GalNAc analogs in mucin-type-O-glycans.[38-39, 43-45] However, the structure of N- and O-linked glycans is highly cell specific[46] and cellular epimerases are capable of converting some functionalized monosaccharides into their epimeric forms with the result of metabolic cross talk between the different pathways (Figure 2).[20, 43-44, 47-49]

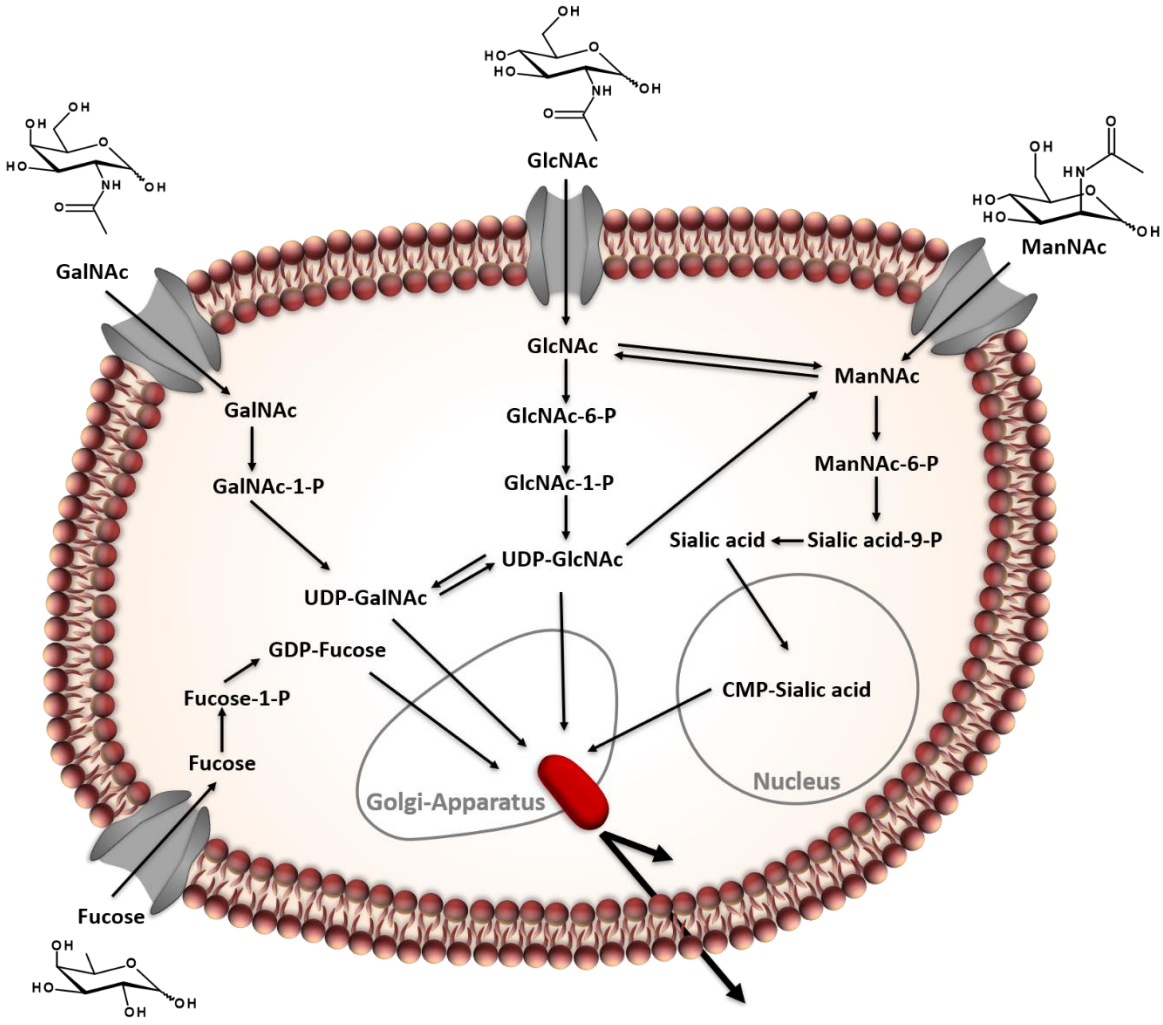

Figure 2: Metabolic fate of different precursor monosaccharides for metabolic glycoengineering and their possible routes for cross talk. Non-natural analogs of GalNAz, GlcNAz and/or ManNAz might not be involved in all cross-talk pathways.

Besides their natural predestination, external influences such as Glc concentration in growth media result into changes in the incorporation pattern of engineered monosaccharides by enhanced synthesis of N-glycans.[44] However, the artificial monosaccharides are subjected to activation procedures with possible enzymatic conversions to other monosaccharide species during endocytosis, trafficking and glycan formation.[50]

In this work, we detail methods for decorating glycan structures within the glycocalyx and cell-derived matrices (CDMs) utilizing metabolic glycoengineering together with guidance in bioorthogonal coupling strategies. CDMs have been previously isolated from fibroblast cell cultures following decellularization procedures.[51-55] As model system we used an azide bearing monosaccharide (Ac_4GlcNAz) to be incorporated either into the glycocalyx or into the ECM network generated by NIH 3T3 fibroblasts as previously reported.[56-57] Ac_4GlcNAz was selected as precursor molecule of glycan biosynthesis and its conversion into different metabolites to ensure incorporation into extracellular matrix components (Figure 2**)**. Ac_4GlcNAz has been shown to be homogenously incorporated into plasma membrane proteins by super-resolution imaging despite lower labeled glycan densities compared to GalNAz and Man NAz analogs, respectively.[42]

These azide-functionalized systems were further functionalized with fluorescent or biotin reporter molecules using bioorthogonal click chemistries (copper(I)-catalyzed azide-alkyne cycloaddition (CuAAC); strain-promoted alkyne-azide cycloaddition (SPAAC)). These methods described here represent only one example of many types of cell surfaces and cell derived matrices of eukaryotic or prokaryotic origin, which are available for further functionalization. Our intention is that the herein provided protocols can be applied to other cell types, CDMs and chemistries, while focusing on cell viability and biocompatibility. Besides Ac_4GlcNAz other functional monosaccharides have been successfully developed in metabolic glycoengineering and could be alternatively used to the here applied Ac_4GlcNAz. Our work is, therefore, organized into three main topics, detailing (i) the synthesis of an azide-bearing monosaccharide (Ac_4GlcNAz), (ii) decoration and functionalization of CDMs and (iii) living cell-surfaces by metabolic glycoengineering (Figure 3).

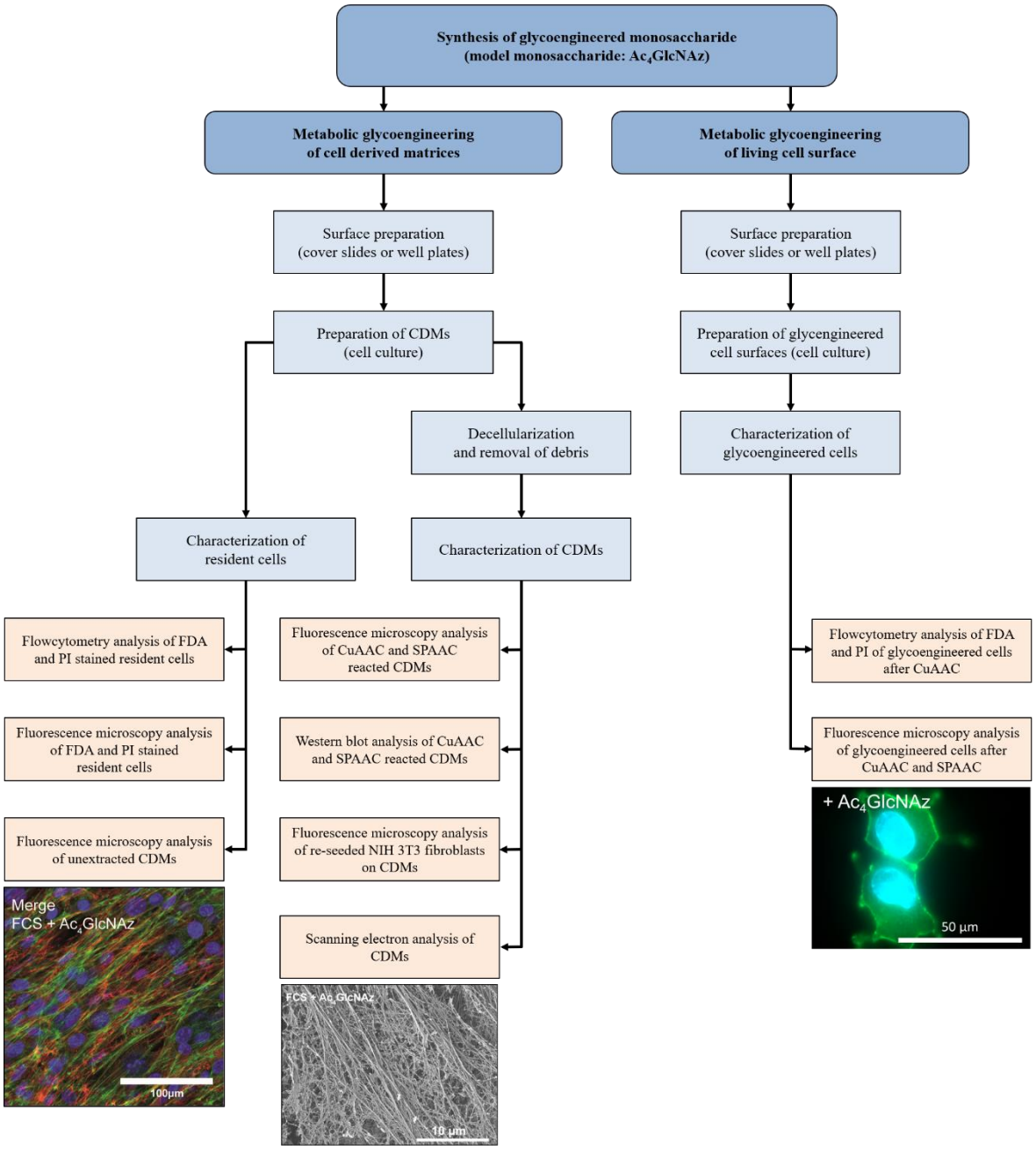

Figure 3: Flow chart for metabolic glycoengineering of CDMs and of living cell surfaces. Besides $Ac_4GlcNAz$ other functional monosaccharides (e.g. $Ac_4GalNAz$ and $Ac_4ManNAz$) are available for incooperation in CDMs and cell surfaces, respectively.

Material

Reagent and Supplies

- (+)-Sodium L-ascorbate (Sigma Aldrich A4034)
- (3-Aminopropyl)triethoxysilane 99 % (APTES) (Sigma Aldrich 440140)
- 12 mm glass cover slides (VWR 631-1577)
- 2-Mercaptoethanol (Sigma Aldrich M6250)
- 4′,6-Diamidino-2-phenylindole dihydrochloride (DAPI) (Sigma Aldrich 32670)
- 8-well Nunc™ Lab-Tek™ II Chamber Slide™ System (VWR 734-2061)
- Acetic acid (Sigma Aldrich A6283)
- Acetic anhydride (Sigma Aldrich 242845)
- Acetone (Sigma Aldrich 270725)
- Acetylene-Fluor 488 (Jena Bioscience CLK-TA106-1)
- Acetylene-PEG_4-Biotin (Jena Bioscience CLK-TA105-25)
- Alexa Fluor™ 488 Phalloidin (Thermo Fisher Scientific A12379)
- Ammonia solution (25 %) (Sigma Aldrich 1054280250)
- Ammonia Solution (VWR 21191.364)
- Anti-Mouse IgG (whole molecule)–Peroxidase antibody produced in goat (Sigma Aldrich A4416)
- BioTrace™ NT Nitrocellulose Transfer Membrane (Pall 66485)
- Bovine Calf Serum (Sigma Aldrich 12133C)
- Bromophenol Blue sodium salt (Sigma Aldrich B8026)
- Chloroacetic anhydride (Sigma Aldrich 215163)
- Copper (II) sulfate (Sigma Aldrich 451657)
- DBCO-Sulfo-Cy5 (Jena Bioscience CLK-A130-1)
- D-(+)-glucosamine hydrochloride (Sigma Aldrich G1514)
- DL-Dithiothreitol (DTT) (Sigma Aldrich 43819)
- Dulbecco’s Modified Eagle’s Medium - high glucose (Sigma Aldrich D5796)
- Ethyl acetate (Sigma Aldrich 270989)
- Ethylenediaminetetraacetic acid (Sigma Aldrich E9884)
- Fetal Bovine Serum, qualified, heat inactivated, E.U.-approved, South America Origin (Thermo Fisher Scientific 10500056)
- Fibronectin Monoclonal Antibody (FBN11) (Thermo Fisher Scientific MA5-11981)
- Filtropur S 0.2 (Sarstedt 83.1826.001)

- Flow cytometry tubes (Sarstedt 55.1579)
- Fluorescein diacetate (Sigma Aldrich F7378)
- Gelatin from bovine skin (Sigma Aldrich G9391)
- Glutaraldehyde solution 50 wt. % in H_2O (Sigma Aldrich 340855)
- Glycerin ≥ 98 %, GPR RECTAPUR® (VWR 24387292)
- Glycine (Sigma Aldrich G7126)
- Goat anti-Mouse IgG (H+L) Cross-Adsorbed Secondary Antibody, Alexa Fluor 488 (Thermo Fisher Scientific A11001)
- Goat anti-Rabbit IgG (H+L) Cross-Adsorbed Secondary Antibody, Alexa Fluor 633 (Thermo Fisher Scientific A21070)
- Greiner CELLSTAR® 96 well plates (Sigma Aldrich M3687)
- Greiner CELLSTAR® multiwell culture plates 24 well (Sigma Aldrich M8812)
- Greiner culture flasks, tissue culture treated surface area 75 cm^2 (Sigma Aldrich C7231)
- H_2O_2 (30 % V/V) (Sigma Aldrich H3410)
- H_2SO_4 (95-97 % V/V) (Sigma Aldrich 30743-M)
- Hoechst 33342 Solution (20 mM) (Thermo Fisher Scientific 62249)
- Hydrochloric acid 37 % (Bernd Kraft 05430.4200)
- Isopropyl alcohol (Sigma Aldrich I9516)
- Methanol (Sigma Aldrich 34885-M)
- N,N-Dimethylformamide ≥ 99.8 % (VWR 84571.320)
- NORM-JECT® 1 mL syringe (VWR 613-2001)
- NORM-JECT® 10 mL syringe (VWR 613-2007)
- NORM-JECT® 20 mL syringe (VWR 613-2009)
- NORM-JECT® 50 mL syringe (VWR 613-2036)
- Paraformaldehyde (Sigma Aldrich P6148)
- Penicillin-Streptomycin (Sigma Aldrich P4333)
- Pierce™ BCA Protein Assay Kit (Thermo Fisher Scientific 23225)
- Ponceau S (Sigma Aldrich P3504)
- Potassium permanganate (Sigma Aldrich 223468)
- Propidium iodide (Sigma Aldrich P4170)
- Pyridine (Sigma Aldrich 270970)
- Roti®-Block, ready-to-use, 10x (Carl Roth A151.4)
- Sodium azide (Sigma Aldrich S2002)
- Sodium dodecyl sulfate (Sigma Aldrich 3771)

- Sodium methoxide (Sigma Aldrich 164992)
- Spectra™ Multicolor High Range Protein Ladder (Thermo Fisher Scientific 26625)
- Streptavidin-HRP Conjugate (Sigma Aldrich RPN1231)
- Sulfo-Cy5-Alkyne (Jena Bioscience CLK-TA116-1)
- SuperSignal™ West Pico PLUS Chemiluminescent Substrate (Thermo Fisher Scientific 34580)
- Triethylamine (Sigma Aldrich T0886)
- Tris(3-hydroxypropyltriazolylmethyl)amine (THPTA) (Sigma Aldrich 762342)
- Triton™ X-100 (Sigma Aldrich T9284)
- Trizma® base (TRIS base) (Sigma Aldrich T6066)
- Trypsin-EDTA solution (Sigma Aldrich T3924)
- TWEEN® 20 (Sigma Aldrich P2287)
- Urea Tech. Grade A (BASF 100001985)

The provided supplier serves as orientation and may be replaced by another source.

Buffers and Solutions

- Potassium permanganate solution (1.5 g $KMnO_4$, 10g K_2CO_3 in 198.75 mL ddH_2O + 1.25 mL 10 % NaOH)
- Phosphate buffered saline (PBS) (137mM NaCl, 2.68 mM KCl, 4.29 mM Na_2HPO_4, 1.47 mM KH_2PO_4 in ddH_2O, pH 7.4)
- Triton-x-ammonia buffer (0.5 % Triton™ X-100, 20 mM NH_4OH in PBS pH 7.4)
- Extraction buffer (15 % (w/w) SDS, 10 % Glycerol (w/w) and 60 mM Tris-HCl in ddH_20, pH 6.8)
- Extraction buffer 2 (8 M urea, 4 % (w/w) SDS, 12.5 mM EDTA and 60 mM Tris-HCl in ddH_2O, pH 6.8)
- 6x sample buffer (30 % glycerol, 0.6 M DTT, 0.356 M SDS, 0.35 M Tris base, 0.18 mM Bromophenol blue in ddH_20, pH 6.8)
- SDS running buffer (25 mM Tris base, 192 mM Glycine, 3.47 mM SDS in ddH_20)
- Western blot buffer (20 % Methanol, 25 mM Tris base, 192 mM Glycine in ddH_20, pH 8.3)
- Tris buffered saline + TWEEN® 20 (TBST) (0.1 % TWEEN® 20, 15.4 mM Tris, 137 mM NaCl in ddH_2O, pH 7.4)
- Mercapto-Ethanol stripping buffer (0.8 % 2-Mercaptoethanol, 69 mM SDS, 62.5 mM Tris in ddH_2O, pH 6.8)
- Ponceau red solution (0.1 % Ponceau S, 1 % Acetic acid in ddH_2O)

Equipment

- Axio Observer.Z1 microscope equipped with an A-Plan 10x/0.25 Ph1 objective (Zeiss), 38 HE Green Fluorescent Protein (λ_{ex}= 450-490 nm λ_{em}= 500-550 nm), 49 DAPI (λ_{ex}= 365 nm λ_{em}= 425-470 nm), 43 DsRed Reflector (λ_{ex}= 538-562 nm λ_{em}= 570-640 nm) and a mercury vapor short-arc lamp
- Facs Calibur system equipped with a 488 nm Laser, emission channel FL1 (530 nm / ± 15 nm) and FL 2 (585 nm / ± 21 nm) with BD CellquestTM Pro and Flowing software
- High-resolution AOBS SP2 confocal laser scanning microscope (Leica microsystem, Wetzla, Ger-many) with a 63x N.A. 1.4-0.60 Oil I BL HCX PL APO I objective
- Critical Point Dryer (Bal-Tec CPD 030)
- Sputter (Bal-Tec SCD 050)
- JSM-7500F filed emission scanning electron microscope (Jeol, Tokyo, Japan)
- General: magnetic stir plate, rotary evaporator, hemocytometer, chromatography columns (Lenz), research pipettes (Eppendorf® Research® plus pipette 0.1-2.5 µL, 1-10 µL, 10-100µL, 100-1000µL), centrifuge (Eppendorf centrifuge 5840 R, Eppendorf Minispin), freezer (−20 °C and −80 °C), thermoblock (Eppendorf thermomixer comfort), electrophoresis power supply (Bio-Rad Model 3000 Xi), shaker (VWR Minishaker), roller mixer (Stuart roller mixer SRT1), incubator (Thermo Fisher Scientific HeraCell 150i), Class II biological safety cabinet (Thermo Fisher Scientific Safe 2020), gel documentation system (Alpha Innotec Fluorchem Fc 2).

Procedure – Synthesis

In this section, we describe the synthesis of monosaccharide 1,3,4,6-tetra-*O*-acetyl-2-(2-azidoacetamido)-2-deoxy-D-glucopyranoside (Ac_4GlcNAz), which is used as model monosaccharide in following procedures. Besides Ac_4GlcNAz, a variety of different chemical tunable monosaccharides such as Ac_4GalNAz and Ac_4ManNAz is commercially available or their synthesis is described in detail elsewhere.[58]

1. Place 500 mg (2.32 mmol) D-glucosamine hydrochloride in a 50 mL round bottom flask equipped with a magnetic stir bar and put it on a magnetic stir plate. Put it under nitrogen atmosphere by equipping a septum on the flask and capping it with a nitrogen filled balloon. Add 10 mL dry methanol using a syringe and needle via the septum to form a slurry.
2. Add 4.64 mL (0.5 M in methanol, 2.32 mmol) sodium methanolate the same way and stir the mixture for 1 h at room temperature.

3. Put the flask into an ice bath to cool it to 0 °C. Add slowly 337 µL (2.44 mmol) triethylamine and 1.98 g (11.6 mmol) chloroacetic anhydride subsequently and stir the mixture for additional 6 h at room temperature.
4. Remove the solvent *in vacuo* (e.g. with a rotary evaporator) and dissolve the obtained yellowish oil in 5 mL dry DMF.
5. Equip the round bottom flask with a condenser and add 1.51 g (23.2 mmol) sodium azide. Heat the suspension to 80 °C and stir for 2 h under reflux cooling.
6. Remove insoluble impurities by column filtration. For this, apply the mixture on a silica pad and elute remaining substance using a mixture of water/isopropyl alcohol/ethyl acetate [V/V/V] 1:3:6 containing 1 % aqueous ammonia solution (10 % w/w ammonia in water).
7. Concentrate the filtrate *in vacuo* (with a rotary evaporator) to obtain a brownish oil. Dissolve the residue in 30 mL pyridine and cool the solution in an ice bath to 0 °C
8. Add 15 mL freshly distilled acetic anhydride and stir the solution for 12 h, while allowing it to reach room temperature.

   Caution! – Possible harsh reaction. Add acetic anhydride slowly.
9. Transfer the solution to a 250 mL separatory funnel and use 10 mL methylene chloride to rinse the round bottom flask.
10. Add 15 mL 1 M HCl and wash the organic phase by shaking the funnel vigorously. For all following steps, the organic phase is the lower layer and contains the compound of interest. Discard the lower (aqueous) layer and repeat the washing step with 15 mL 1 M HCl, then 10 mL saturated $NaHCO_3$-solution, 10 mL water and finally 10 mL brine.

    Caution! – Possible harsh reaction of residue acetic anhydride with water. Add aqueous solutions slowly.
11. Release the organic layer into an Erlenmeyer flask and dry it by adding sodium sulphate (add until the cloudy solution becomes clear). Filter the mixture through a pleated filter into another round bottom flask and remove the organic solvent *in vacuo*.
12. Purify the brownish residue by column chromatography using a gradient of cyclohexane/ethyl acetate [V/V] 3:1-1:1 as eluent.
13. Detect fractions containing $Ac_4GlcNAz$ by thin layer chromatography with visualization by $KMnO_4$ staining solution.
14. Collect all fractions containing the compound and remove residual solvent *in vacuo* to obtain 302 mg (702 µmol, 31 % yield) of product as a colorless foam in an anomeric ratio α/β 2:1.
15. Store $Ac_4GlcNAz$ at -20 °C.

R_f-Value: 0.1 (cyclohexane/ethyl acetate 2:1).

^{1}H-NMR (400 MHz, $CDCl_3$): δ = [α-anomer] 6.41 (br. d, 1H, J = 8.9 Hz, NH), 6.21 (d, 1H, J = 3.7 Hz, H1), 5.30 (dd, 1H, J = 9.7, 10.8 Hz, H3) 5.21 (dd, 1H, J = 9.7, 9.8 Hz, H4), 4.45 (ddd, 1H, J = 3.7, 8.9, 10.8 Hz, H2), 4.27 (dd, 1H, J = 4.1, 12.5 Hz, $H6_a$), 4.08 (dd, 1H, J = 2.4, 12.5 Hz, H6b), 4.02 (ddd, 1H, J = 2.4, 4.1, 9.8 Hz, H5), 3.93 (s, 2H, CH_{2ab}-N_3), 2.21, 2.06, 2.05, 2.09 (4x s, 3H, CH3); [β-anomer] 6.38 (br. d, 1H, J = 9.4 Hz, NH), 5.79 (d, 1H, J = 8.7 Hz, H1) 5.23 (dd, 1H, J = 9.6, 10.5 Hz, H3), 5.14 (dd, 1H, J = 9.6, 9.7 Hz, H4), 4.28 (dd, 1H, J = 4.7, 12.6 Hz, H6a), 4.21 (ddd, 1H, J = 8.7, 9.4, 10.5 Hz, H2), 4.13 (dd, 1H, J = 2.5, 12.6 Hz, $H6_b$), 3.91 (s, 2H, CH_{2ab}-N_3), 3.83 (ddd, 1H, J = 2.5, 4.7, 9.7 Hz, H5), 2.11, 2.09, 2.04, 2.04 (4x s, 3H, CH3) ppm.

^{13}C-NMR (100 MHz, CDCl3): δ = [α-anomer] 171.67, 170.79, 169.26, 168.78 (4x COO), 166.97 (CON), 90.44 (C1), 70.51 (C3), 69.99 (C5), 67.58 (C4), 61.65 (C6), 52.62 (CH_2N_3), 51.42 (C2), 21.03, 20.82, 20.72, 20.70 (4x CH_3); [β-Anomer] 170.99, 170.76, 169.43, 169.39 (4x COO), 167.14 (CON), 92.40 (C1), 73.13 (C5), 72.31 (C3), 67.82 (C4), 61.75 (C6), 53.48 (C2), 52.76 (CH_2N_3), 21.00, 20.85, 20.72, 20.70 (4x CH_3) ppm.

HRMS (ESI-pos): m/z calc. $C_{16}H_{22}NaN_4O_{10}$ $[M+Na]^+$: 453.12281; found: 453.12242, Δppm: 0.86.

Procedure – Cell derived extracellular matrices

In this part of the work, we describe the introduction of functionalized monosaccharides into ECM derived components using metabolic glycoengineering. As model, Ac_4GlcNAz is used and incorporated into NIH 3T3 fibroblast derived matrices. Through the incorporation of chemically tunable monosaccharides for covalent modification, the natural capacity of ECM – (I) storage of growth factors with natural bearing ECM binding sites or through enzymatic reactions (e.g. transglutaminase) and (II) synergy effect (matricrin effects[59]) of growth factors bound to ECM-molecules together with the recruitment of integrin receptors with the result of an increased and prolonged signaling[60] – is expanded.

NIH 3T3 fibroblasts were seeded and maintained at a confluent state on pretreated surfaces for nine days. The metabolic engineered monosaccharide and sodium ascorbate, which acts as cofactor for the synthesis of new collagen fibrils and stabilizes the secreted matrices,[61] was exchanged every 24-48 h during the period of nine days. After culture, the synthesized CDMs were decellularized and remaining debris were removed using a combination of hypoosmotic and alkaline treatment to isolate the 3D network. The resident cells during the time of matrix assembly were monitored and received matrices were characterized.

Step 1: Surface preparation

Step 2: Cell culture and preparation of CDMs

Step 3: Decellularization and removal of cellular debris

Step 4: Characterization of resident cells

- Flowcytometry analysis of FDA and PI stained resident cells
- Fluorescence microscopy analysis of FDA and PI stained resident cells
- Fluorescence microscopy analysis of unextracted CDMs

Step 5: Modification and characterization of CDMs

- Fluorescence microscopy analysis of CuAAC and SPAAC reacted CDMs
- Western blot analysis of CuAAC and SPAAC reacted CDMs
- Fluorescence microscopy analysis of re-seeded NIH 3T3 fibroblasts on CDMs
- Scanning electron analysis of CDMs

1. Surface preparation

Coating of the surfaces and cover slides for matrix deposition is highly recommended to avoid disruption of the generated matrix during cell culture and isolation steps. Glass surfaces require a special treatment, whereas a simple gelatin coating is sufficient for tissue culture polystyrene (TCPS) dishes. However, treatment of the surface may impact the deposition of matrix components resulting in variations of thickness and composition.[62]

Note – Piranha solution cleaning should not be performed for glass surfaces surrounded by non-glass framework. For surface preparation including plastics, turn to point 4.

1. Prepare a fresh piranha solution by mixing 7 parts H_2SO_4 (97 % V/V) with 3 parts H_2O_2 (30 % V/V) on ice using a small glass beaker. Add the H_2SO_4 (97 % V/V) drop-wise using a glass pipette to the ice-cold H_2O_2 (30 % V/V) and ensure proper mixing.
   Caution! – Volatile and corrosive, always wear personal protective equipment and work under the fume hood.
2. Place glass cover slides in a glass petri dish or use a PTFE carrier, and cover with piranha solution for 45-60 min at room temperature.
   Caution! – Volatile and corrosive, always wear personal protective equipment and work under fume hood.
3. Aspirate the piranha solution using a glass pipette and wash glass cover slides 3 times, 5 min each time, with extensive amount of double distilled water. Transfer glass cover slides to a well plate using needle and tweezer and make sure, that treated surface points upwards.

Note – Dispose piranha solution by cooling down for several hours (overnight). Neutralize the cooled solution with 1N NaOH on ice. If the neutralized solution does not contain any regulated metals (arsenic, barium, cadmium, chromium, copper, lead, mercury, nickel, selenium, silver, zinc), the neutralized solution can be poured down the drain.

4. Apply a freshly prepared 2 % APTES solution in water for 15 min at room temperature.
   Note – APTES is hydrolyzed in water.
5. Aspirate APTES solution and wash glass cover slides 3 times, 5 min each time, with double distilled water.
6. Apply a 0.125 % glutaraldehyde solution in water for 30 min at room temperature.
7. Aspirate glutaraldehyde solution and wash glass cover slides 3 times, 5 min each time, with double distilled water.
8. Transfer glass cover slides to a new well plate using needle and tweezer and sterilize by UV irradiation under laminar air flow (LAF) for 1 h.
9. Apply sterile filtered 2 % gelatin solution in PBS and incubate under the LAF for 60 min.
10. Aspirate 2 % gelatin solution and wash glass cover slides 3 times, 5 min each time, with sterile PBS.
    Note – Do not let the glass cover slides run dry.
    Note – The use of non-tissue plastic can avoid cell growth beneath cover slides.

2. Cell culture and preparation of CDMs

To generate glycoengineered CDMs derived from NIH 3T3 fibroblasts, the cell morphology of fibroblasts is important and a flat (not elongated) phenotype is recommended. Cells have to be cultured in Dulbecco's modified Eagle medium with high glucose (4.5 g/L) containing heat inactivated BCS (10 %), penicillin G (100 U mL^{-1}) and streptomycin (100 µg mL^{-1}). Medium supplemented with low glucose (1 g/L) is not suitable as we have experienced enhanced cell apoptosis.

Note – Do not allow the cells to become confluent.

Note – 20 passages prior to matrix generation is recommended to reduce contact inhibition.

Note – Carry out cell culture under aseptic conditions. Incubate at 37° C and 5 % CO_2. All solutions and equipment have to be sterile.

Note – FCS and BCS can be filtered through a 0.22 µm sterile filter to avoid background particles during microscopy analysis.

1. Prepare wanted amount of well plates using DMEM with high glucose (4.5 g/L) containing heat inactivated FCS (20 %), penicillin G (100 U mL^{-1}) and streptomycin (100 µg mL^{-1}) with or – for controls – without the addition of azide-monosaccharide (100 µM).
    a. 24-well – 300 µL per well
    b. 96-well – 125 µL per well
    c. 8-well Nunc™ Lab-Tek™ II Chamber Slide™ System – 150 µL per well
2. Aspirate growth medium from cell culture dish, wash with PBS and apply trypsin-EDTA (0.005 % trypsin [m/V] and 0.025 % EDTA [m/V]) at approximately 80 % confluency for 1 min. Carefully tap cell culture dish and check detachment of the cells under light microscope.
3. Resuspend fibroblasts in DMEM with high glucose (4.5 g/L) containing heat inactivated FCS (20 %), penicillin G (100 U mL^{-1}) and streptomycin (100 µg mL^{-1}) and centrifuge (5 min at 218xg).
4. Aspirate the growth medium and resuspend fibroblasts in DMEM with high glucose (4.5 g/L) containing heat inactivated FCS (20 %), penicillin G (100 U mL^{-1}) and streptomycin (100 µg mL^{-1}).
5. Count the cells with a hemocytometer according to manufacturer instructions and resuspend the desired number of cells in DMEM with high glucose (4.5 g/L) containing heat inactivated FCS (20 %), penicillin G (100 U mL^{-1}) and streptomycin (100 µg mL^{-1}) and incubate for 24 h.
    a. 24 Well – $66.8x10^4$ cells mL^{-1}, 300 µL growth medium per well.
    b. 96 Well – $28x10^4$ cells mL^{-1}, 125 µl growth medium per well.
    c. 8-well Nunc™ Lab-Tek™ II Chamber Slide™ System – $33.4x10^4$ cells mL^{-1}, 150 µL growth medium per well.

    Note – A slightly higher amount of cells may be needed when using glass cover slides due to potential cell growth under the slides.

    Note – 100 µM azido-monosaccharide becomes diluted to 50 µM during seeding.

    Note – Decreased azido-monosaccharide concentration results in insufficient incorporation. (Figure 4)

    Note – Initial 20 % FCS concentration during cell seeding is necessary to increase cell survival.
6. Confirm confluency under the light microscope, aspirate the medium and replace it by DMEM with high glucose (4.5 g/L) containing heat inactivated FCS (10 %), penicillin G (100 U mL^{-1}), streptomycin (100 µg mL^{-1}), sodium L-ascorbate (50 µg mL^{-1}) and with or – for controls – without the addition of azide-monosaccharide (50 µM). The medium has to be changed every 48 h up to day 6 and later every 24 h to obtain best possible cell culture parameters. (Table 1)

    Note – The usage of 10 % BCS will reduce the time until matrix generation to 6 days but will lead to a failure in incorporation of glycoengineered monosaccharide.

Note – Gently aspirate the growth medium without touching the ground and replace the medium by gently pipetting on the wall to avoid disruption and washing of the matrix.

Note – Ascorbic acid has to be replaced at least every 48 h based on rapid degradation.

Table 1: Time plan for growth medium exchange.

Time	Action	Growth medium
Day 0	Seeding	DMEM high glucose + FCS (20 %) + P/S + monosaccharide (50 µM)
Day 1	Maintenance	DMEM high glucose + FCS (10 %) + P/S + monosaccharide (50 µM) + Sodium L-ascorbate (50 µg mL^{-1})
Day 2	Maintenance	DMEM high glucose + FCS (10 %) + P/S + monosaccharide (50 µM) + Sodium L-ascorbate (50 µg mL^{-1})
Day 4	Maintenance	DMEM high glucose + FCS (10 %) + P/S + monosaccharide (50 µM) + Sodium L-ascorbate (50 µg mL^{-1})
Day 6	Maintenance	DMEM high glucose + FCS (10 %) + P/S + monosaccharide (50 µM) + Sodium L-ascorbate (50 µg mL^{-1})
Day 7	Maintenance	DMEM high glucose + FCS (10 %) + P/S + monosaccharide (50 µM) + Sodium L-ascorbate (50 µg mL^{-1})
Day 8	Maintenance	DMEM high glucose + FCS (10 %) + P/S + monosaccharide (50 µM) + Sodium L-ascorbate (50 µg mL^{-1})
Day 9	Decellularization	

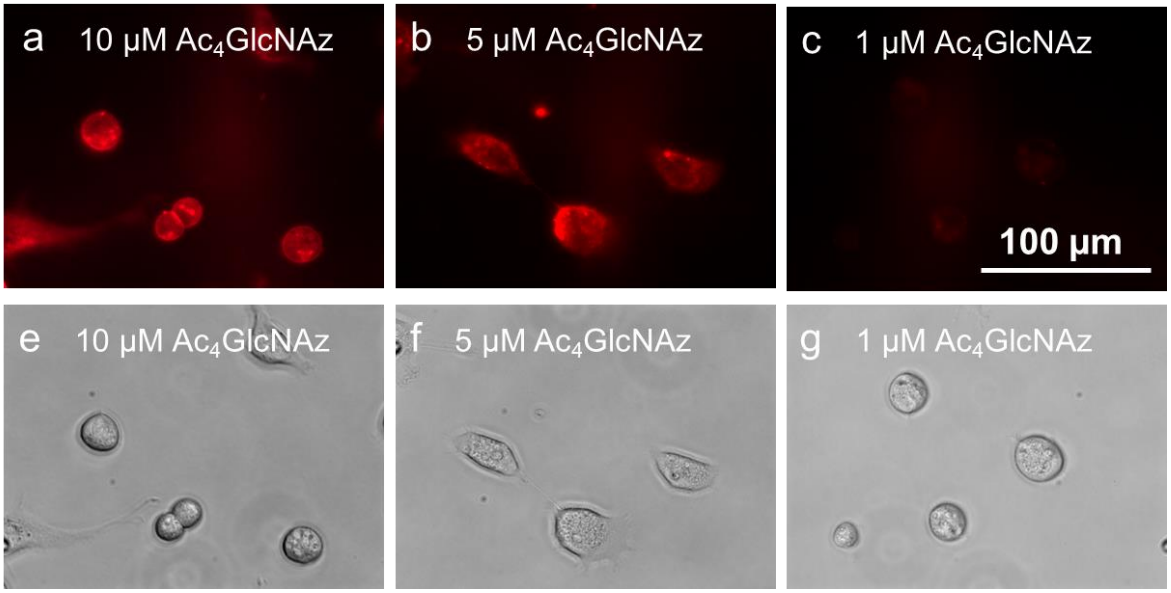

Figure 4: Fluorescent image (a-c) and transmitted light images (e-g) of NIH 3T3 fibroblasts, treated with different concentration of the glycoengineered monosaccharide Ac4GlcNAz. Incorporated azide-monosaccharide is show in red after Sulfo-Cy5-Alkyne-labeling using CuAAC.

3. Decellularization and removal of cellular debris

All matrices should be handled with extreme care during the decellularization process and further treatment due to strong destabilization of the generated matrices after cell extraction.

Note – Glass cover slides should be gently lifted with a needle to reach cells growing beneath.

1. Aspirate growth medium from cell culture dish and rinse the matrix two times with PBS.
2. Incubate the matrix with double distilled water for 15 min and again for 30 min.
   Note – Cells should be detaching during incubation.
3. Aspirate double distilled water and rinse the matrix three times with PBS.
4. Incubate the matrix with triton-x-ammonia buffer (0.5 % Triton™ X-100 and 20 mM NH_4OH in PBS, pH 7.4) for 10 min at 37 °C, 5 % CO_2.
   Note – Incubation times can be easily increase up to 30 min.
   Note – triton-x-ammonia buffer has a shelf life of 3 month.
5. Aspirate triton-x-ammonia buffer and rinse the matrix 5 times with PBS.
   Note – Matrices should be exchanged to PBS with penicillin G (100 U mL^{-1}) and streptomycin (100 µg mL^{-1}) to store at 4 °C. Sodium azide should be avoided for preservation if performing azide-alkyne reactions.
   Note – Additional treatment with DNase I (200 U mL^{-1}) for 30 min at 37 °C and/or 0.5 % deoxycholate for 10 min can be performed for better DNA/ RNA removal.

4. Characterization of resident cells

Characterization of resident cells is performed prior to decellularization and during the period of matrix deposition.

Note – Carry out cell culture under aseptic conditions. Incubate at 37° C and 5 % CO_2. All solutions and equipment have to be sterile.

4.1 Flow cytometry analysis of FDA and PI stained resident cells

1. Aspirate growth medium from cell culture dish and rinse the matrix twice with PBS.
2. Apply trypsin-EDTA (0.005 % trypsin [m/V] and 0.025 % EDTA [m/V]) to the cell culture dish and incubate for 5 min.
3. Add DMEM with high glucose (4.5 g/L) containing heat inactivated FCS (10 %), penicillin G (100 U mL^{-1}) and streptomycin (100 µg mL^{-1}) to the trypsin-EDTA solution. Resuspend and centrifuge (5 min at 218xg) the cells.
   Note – Remove remaining ECM with a tip.
4. Resuspend the cells in PBS and count the cells with a hemocytometer according to manufacturer instructions.
5. Divide cells in equal parts and incubate either with 0.01 µg/10^4 cells fluorescein diacetate (FDA) or with 0.003 µg/10^4 cells propidium iodide (PI) for 3 min at room temperature.
   Note – To avoid cell harm, stained cells should be stored on ice after 3 min of incubation.
   Note – Cells should be stained either with FDA or PI to avoid fluorescence cross-talk.
   Note – FDA is light sensitive. All samples and stock solutions should be kept in the dark.
6. For analysis, use a flow cytometer equipped with a 488 nm Laser and Forward scatter (FSC) diode, side scatter (SSC) diode, Fluorescence channel 1 (FL1) diode [530 nm filter] and Fluorescence channel 2 (FL2) diode [585 nm filter]. Count 5000-10000 cells and assess the geometric mean of FL1 and FL2. Here, a FacsCalibur system and BD CellquestTM Pro and Flowing software (version 2.5.1; Turku Bioimaging) was used (Figure 5 B).
   Note – Use standard cultured cells as positive control and 70 % isopropanol treated cells as negative control.

4.2 Fluorescence microscopy analysis of FDA and PI stained resident cells

1. Aspirate growth medium from cell culture dish and rinse the matrix three times with PBS.
2. Apply a FDA (15 µg mL^{-1}) – PI (2 µg mL^{-1}) solution and incubate for 5 min at room temperature.
   Note – FDA is light sensitive. All samples and stock solutions should be kept in the dark.
   Note – To avoid cell harm, stained cells should be stored on ice after 3 min of incubation.

3. Gently aspirate the FDA-PI solution a wash three times with PBS.
4. For analysis, use an epifluorescence or confocal microscope. Here, an Axio Observer.Z1 microscope equipped with an A-Plan 10x/0.25 Ph1 objective (Zeiss) was used (Figure 5 A).

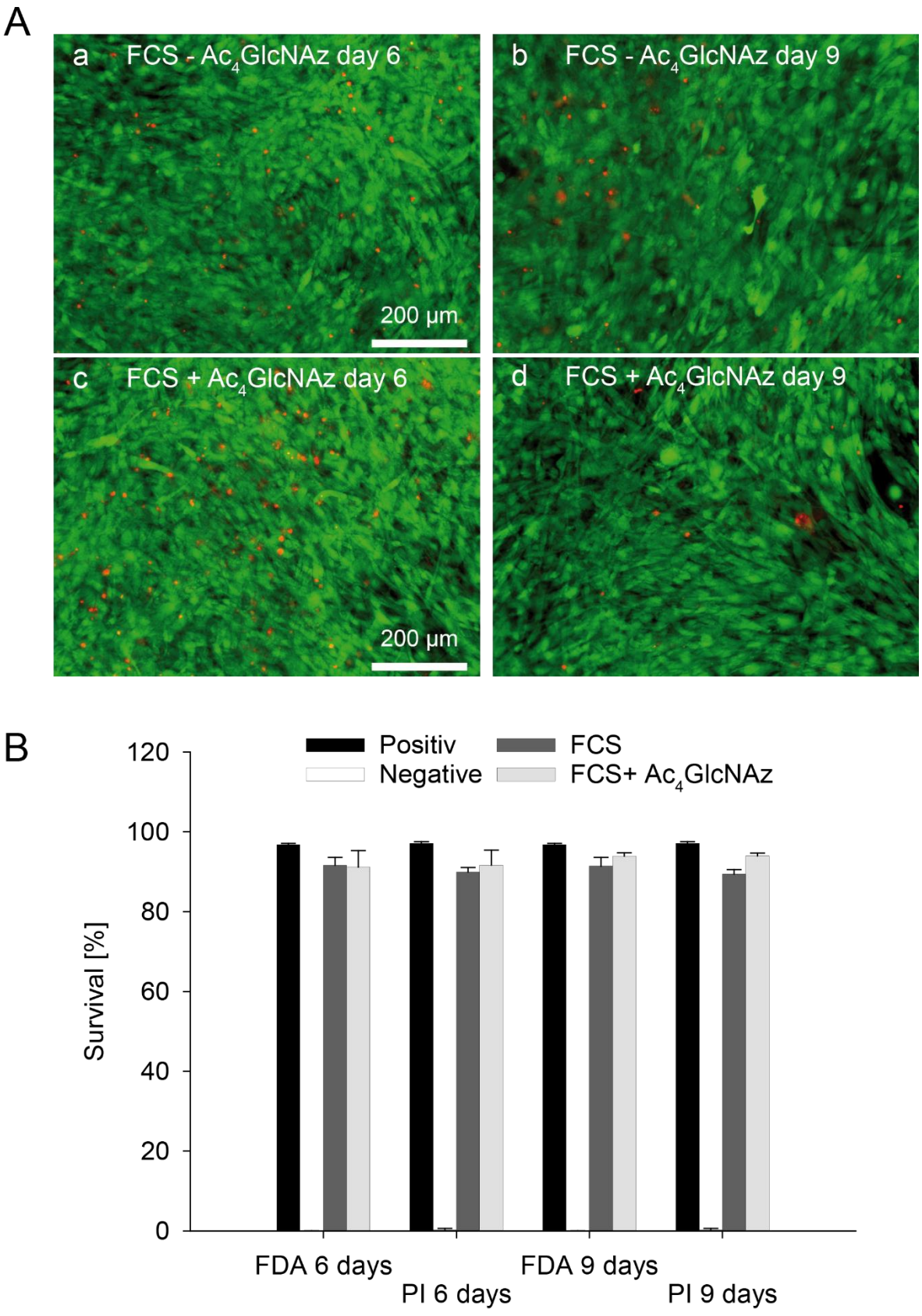

Figure 5: (A) Fluorescent images of fluorescein diacetate (green) and propidium iodide (red) stained resident cells from Ac_4GlcNAz treated (c, d) and untreated (a, b) CDMs after 6 (a, c) and 9 (b, d) days. (B) Flow

cytometry of FDA/PI stained resident cells from Ac_4GlcNAz treated and untreated CDMs after 6 and 9 days. Standard cultured fibroblasts were used as positive control and 70 % 2-propanol treated cells as negative control. Results are displayed as mean with standard deviation. Reprinted (adapted) with permission from[57].Copyright 2018 American Chemical Society.

4.3 Fluorescent microscopy analysis of unextracted CDMs

1. Aspirate growth medium from cell culture dish and rinse the matrix three times with PBS.
2. Fix cells with 2 % paraformaldehyde (PFA) in PBS for 15 min at room temperature.
   Note – Methanol fixation is sufficient for antibody staining but may lead to low staining efficacy using actin staining by phalloidin.
3. Aspirate PFA solution and rinse the matrix three times with PBS.
4. Permeabilize cells with 0.2 % triton-x in PBS for 15 min at room temperature.
5. Aspirate triton-x solution and rinse the matrix three times with PBS.
6. Apply 1x Roti®-Block for 60 min at room temperature.
   Note – 0.22 µm filtered 5 % BSA in PBS can be used as an alternative to 1x Roti®-Block.
7. Aspirate 1x Roti®-Block and rinse the matrix three times with PBS.
8. Incubate samples overnight at 4 °C with primary antibody, here rabbit anti-Fibronectin antibody 1:500 in PBS.
9. Aspirate the primary antibody and rinse the matrix twice with PBS.
10. Incubate samples with second antibody for 90 min at room temperature, here goat anti-rabbit IgG H&L Alexa Fluor® 633 antibody 1:200 in PBS.
11. Aspirate second antibody and rinse the matrix twice with PBS.
12. Incubate with Alexa Fluor™ 488 Phalloidin (165 nM in PBS) for 20 min at room temperature.
    Note – Anti-alpha smooth muscle actin antibody can be used as an alternative to phalloidin.
13. Aspirate phalloidin and rinse the matrix twice with PBS.
14. Incubate with DAPI 1:1000 in PBS for 10 min at room temperature.
15. Aspirate DAPI and rinse the matrix three times with PBS.
16. For analysis, use an epifluorescence or confocal microscope. Here, an AOBS SP2 confocal laser scanning microscope (Leica microsystem, Wetzla, Germany) with a 63x N.A. 1.4-0.60 Oil I BL HCX PL APO I objective was used. (Figure S1)

5. Modification and characterization of CDMs

Modification and characterization of CDMs is performed after decellularization and removal of debris.

5.1 Fluorescence microscopy analysis of CuAAC and SPAAC reacted CDMs

1.1 Calculate total volume and prepare CuAAC mixture of 250 µM THPTA, 50 µM $CuSO_4$, 2.5 mM sodium L-ascorbate and 20 µM alkyne-dye in PBS. (Figure 6)

a. Apply THPTA to a tube to obtain a final concentration of 250 µM using a 10 mM stock solution of THPTA in ddH_2O.

b. Add $CuSO_4$ to obtain a final concentration of 50 µM using a 100 mM stock solution of $CuSO_4$ in ddH_2O.

Note – Color of the solution should turn yellow. A brownish precipitate indicates the generation of copper (0) and the wrong order of the used substances.

Note – THPTA and $CuSO_4$ should be used at least in a 5:1 molar ratio.

c. Add sodium L-ascorbate to obtain a final concentration of 2.5 mM using a 100 mM stock solution of L-ascorbate in ddH_2O.

Note – Sodium L-ascorbate solution has to be prepared freshly.

d. Add PBS to obtain the former calculated concentrations.

e. Add alkyne-dye to obtain the final concentration of 20 µM, here Sulfo-Cy5-Alkyne was used.

Note – The order of the substances is mandatory to avoid copper (0) generation.

Note – The use of Tris-buffer instead of PBS will lead to a low yield based on its complexing character.

1.2 Prepare SPAAC mixture by adding DBCO-dye to PBS to obtain a final concentration of 20 µM, here DBCO-Sulfo-Cy5 was used. (Figure 6)

2. Aspirate PBS, apply SPAAC mixture and incubate for 1 h or apply CuAAC mixture and incubate for 5 min at room temperature, respectively.

Note – Previously stored matrices should be rinsed with PBS twice to clear off remaining antibacterial and antifungal protecting agents.

Note – Reaction time, temperature and THPTA + copper sulfate concentration can be increased but may lead to unspecific side reactions.

3. Aspirate SPAAC or CuAAC mixture and apply growth medium or EDTA-solution to stop the reaction.
4. Aspirate growth medium and rinse the matrix three times with PBS.
5. Apply 1x Roti®-Block for 60 min at room temperature.
6. Aspirate 1x Roti®-Block and rinse the matrix three times with PBS.
7. Incubate samples with primary antibody overnight at 4 °C, here mouse anti-Fibronectin antibody 1:500 in PBS.
8. Aspirate the primary antibody and rinse the matrix twice with PBS.

9. Incubate samples with second antibody for 90 min at room temperature, here goat anti-mouse IgG H&L Alexa Fluor® 488 antibody 1:200 in PBS.
10. Aspirate second antibody and rinse the matrix twice with PBS.
11. For analysis, use an epifluorescence or confocal microscope. Here, an AOBS SP2 confocal laser scanning microscope (Leica microsystem, Wetzla, Germany) with a 63x N.A. 1.4-0.60 Oil I BL HCX PL APO I objective was used. (Figure 7 A)

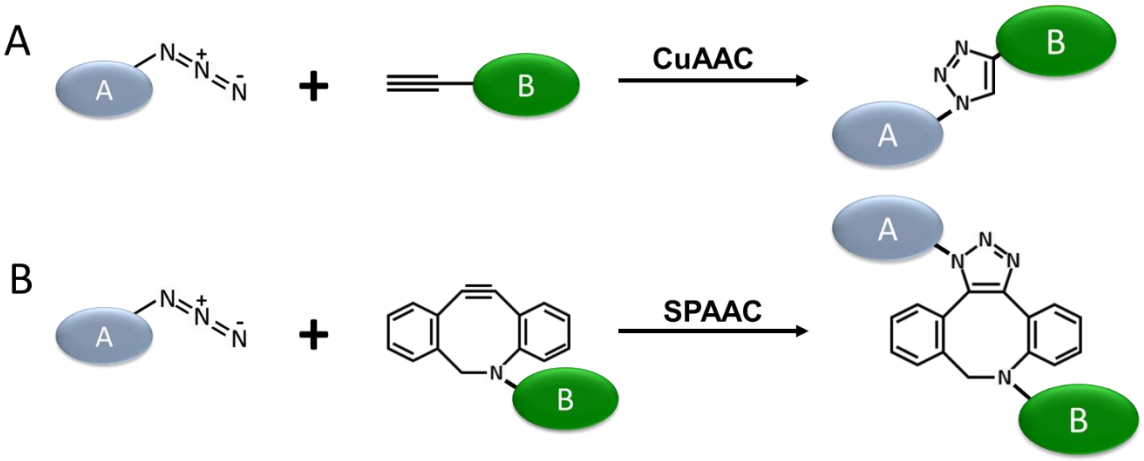

Figure 6: (A) Schematic overview of the copper(I)-catalyzed azide-alkyne cycloaddition (CuAAC). (B) Schematic overview of the strain-promoted alkyne-azide cycloaddition (SPAAC).

5.2 Western blot analysis of CuAAC and SPAAC reacted CDMs

1. Analogous to 5.1 steps 1-4, 20 µM acetylene-PEG_4-biotin is used here.
2. Apply extraction buffer 1 (5 % (w/w) SDS, 10 % glycerol (w/w) and 60 mM Tris-HCl in ddH_20, pH 6.8) and collect the CDM suspension using a cell scraper.
3. Incubate the suspension at 95 °C for 5 min and centrifuge (10 min, $16x10^3xg$)
4. Separate the supernatant (soluble fraction) from the pellet (insoluble and urea soluble fraction).
5. Incubate the pellet with extraction buffer 2 (8 M urea, 4 % (w/w) SDS, 12.5 mM EDTA and 60 mM Tris-HCl in ddH_20, pH 6.8) with half of the volume used in step 2. Incubate for 30 min at room temperature and centrifuge (10 min, $16x10^3xg$).
6. Separate the supernatant (urea soluble fraction) from the pellet (insoluble fraction).
   Note – Supernatants can be combined or stored separately.
7. Determine the total protein concentration by BCA assay.
8. Add a sixth of 6x sample buffer to 10 µg total protein sample and incubate at 95 °C for 5 min.
9. Load samples and 5 µL of a pre-stained broad range marker on a 5 % SDS-PAGE gel.
10. Use 1x SDS running buffer to separate the proteins by electrophoresis at 120 V until the bromophenol blue reaches the bottom of the gel.

11. Transfer the proteins from the gel to a nitrocellulose membrane using 1x WB buffer at 80 V for 1.5 h and 4 °C.
12. Rinse the nitrocellulose membrane twice with deionized water.
13. Incubate the nitrocellulose membrane with Ponceau red solution for 5 min on an orbital shaker with 150 RPM.
14. Rinse the nitrocellulose membrane twice with deionized water.
    Note – The use of ddH_2O will rapidly decrease Ponceau red staining.
15. Analyze Ponceau red staining using a gel documentation system.
16. Wash the nitrocellulose membrane twice with ddH_2O for 10 min on an orbital shaker with 150 RPM.
17. Wash the nitrocellulose membrane three times with TBST for 10 min on an orbital shaker with 150 RPM.
18. Incubate the nitrocellulose membrane 1x Roti®-Block for 60 min on an orbital shaker with 150 RPM.
    Note – 0.22 µm filtered 5 % BSA in TBST can be used as an alternative to 1x Roti®-Block.
19. Wash the nitrocellulose membrane three times with TBST for 10 min on an orbital shaker with 150 RPM.
20. Incubate nitrocellulose membrane in a 50 mL falcon with primary antibody overnight at 4 °C on a roller mixer, here mouse anti-Fibronectin antibody 1:2000 in TBST.
21. Wash the nitrocellulose membrane three times with TBST for 10 min on an orbital shaker with 150 RPM.
22. Incubate nitrocellulose membrane in a 50 mL falcon with a peroxidase conjugated secondary antibody for 90 min at room temperature on a roller mixer, here goat anti-mouse HRP conjugated antibody 1:2000 in TBST.
23. Wash the nitrocellulose membrane three times with TBST for 10 min on an orbital shaker with 150 RPM.
24. Rinse the nitrocellulose membrane twice with deionized water.
25. Incubate the nitrocellulose membrane with SuperSignal™ West Pico PLUS Chemiluminescent Substrate kit and analyze using a gel documentation system.
26. Wash the nitrocellulose membrane three times with TBST for 10 min on an orbital shaker with 150 RPM.
27. Rinse the nitrocellulose membrane twice with deionized water.
28. Strip the nitrocellulose membrane with Mercapto-Ethanol stripping buffer for 45 min at 50 °C.
29. Rinse the nitrocellulose membrane for 60 min under running water.
    Note – Fix membrane with small magnets on a plastic board.

30. Wash the nitrocellulose membrane three times with TBST for 10 min on an orbital shaker with 150 RPM.
31. Incubate the nitrocellulose membrane with Streptavidin-HRP Conjugate overnight at 4 °C, here 1:2000 in TBST.

    Note – An incubation of 60 min at room temperature can be used alternatively.
32. Wash the nitrocellulose membrane three times with TBST for 10 min on an orbital shaker with 150 RPM.
33. Rinse the nitrocellulose membrane twice with deionized water.
34. Incubate the nitrocellulose membrane with SuperSignal™ West Pico PLUS Chemiluminescent Substrate kit and analyze using a gel documentation system (Figure 7 B).

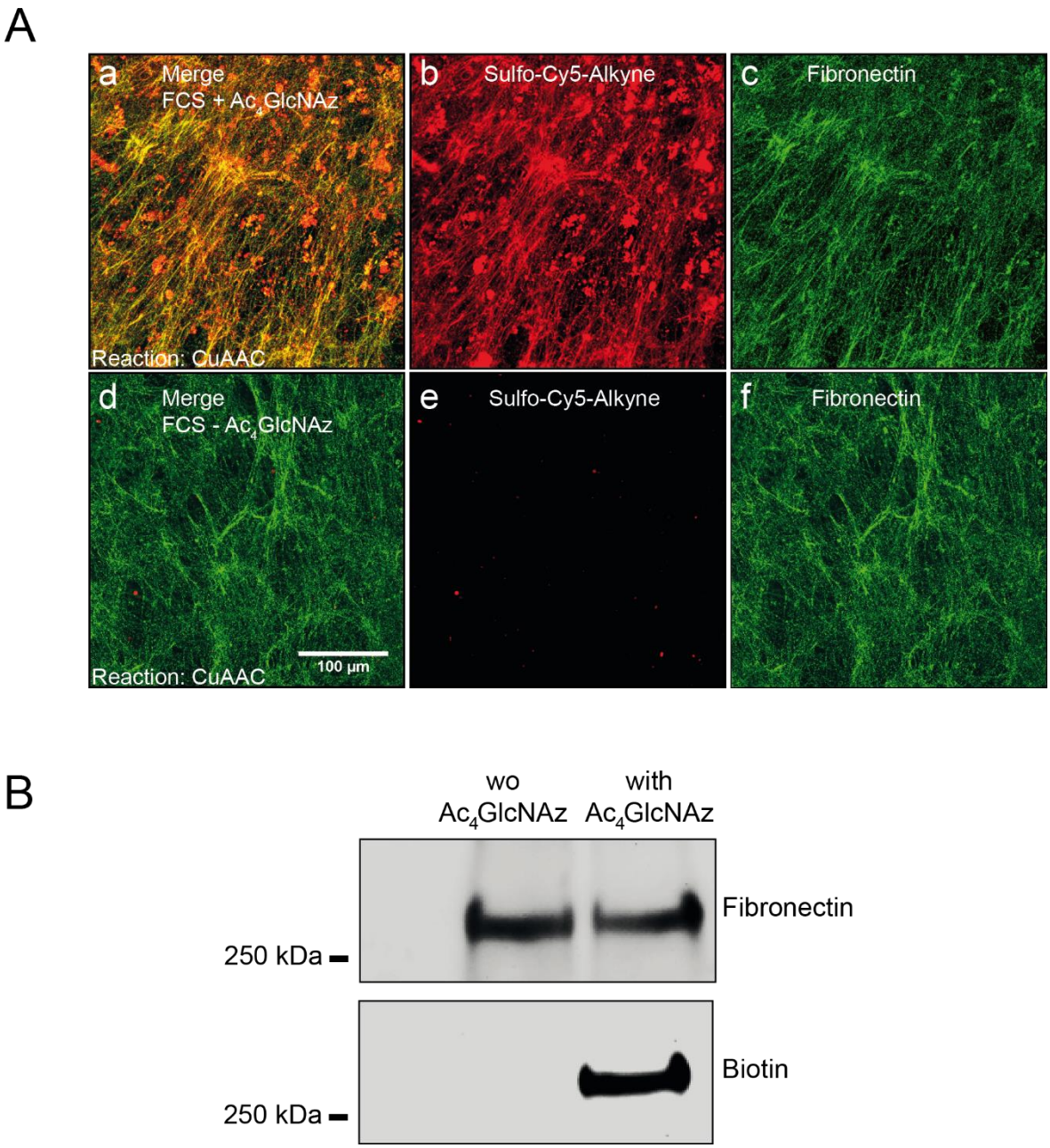

Figure 7: (A) Confocal images of CuAAC reacted CDMs. CDMs were generated with (a, b, c) or without (d, e, f) the addition of Ac_4GlcNAz and reacted with Sulfo-Cy5-Alkyne using CuAAC. Incorporated azide-monosaccharide is shown in red after Cy5-labeling (b, e). Fibronectin is shown in green (d, f). Merge is shown in yellow (a, d). (B) Western blot of CuAAC reacted CDM extracts. CDMs were generated with or without addition of Ac_4GlcNAz and were reacted with acetlyen-PEG4-biotin. The matrix extracts were analysed for fibronectin, stripped and analysed for biotin using streptavidin HRP. Reprinted (adapted) with permission from[57]. Copyright 2018 American Chemical Society.

5.3 Fluorescence microscopy analysis of re-seeded NIH 3T3 fibroblasts on CDMs

Note – Carry out cell culture under aseptic conditions. Incubate at 37° C and 5 % CO_2. All solutions and equipment have to be sterile.

Note – Decellularization and removal of debris have to be carried out under aseptic conditions using sterile solutions (0.22 µm filtered) and equipment.

Note – Fibronectin coated wells can be used for control. Use mouse fibronectin-solution (5 µg mL^{-1} in PBS) for 1 h at 37 °C and washed once with PBS.

1. Use a semi-confluent culture dish containing NIH 3T3 fibroblasts.
2. Aspirate the growth medium and rinse the cells with PBS.
3. Apply PBS with Hoechst 33342 Solution [20 mM] (1 µL mL^{-1}) for 15 min at 37 °C, 5 % CO_2.
4. Aspirate the solution and rinse the cells with PBS.
5. Apply trypsin-EDTA (0.005 % trypsin [m/V] and 0.025 % EDTA [m/V]) for 1 min. Carefully tap cell culture dish and check detachment of the cells under light microscope.
6. Resuspend fibroblasts in DMEM with high glucose (4.5 g/L) containing heat inactivated BCS (10 %), penicillin G (100 U mL^{-1}) and streptomycin (100 µg mL^{-1}).
7. Count the cells with a hemocytometer according to manufacturer instructions and centrifuge (5 min at 218xg).
8. Aspirate the growth medium and resuspend fibroblasts in DMEM with high glucose (4.5 g/L) containing heat inactivated BCS (10 %), penicillin G (100 U mL^{-1}) and streptomycin (100 µg mL^{-1}) to the desired number.
    a. 24 Well – 6700 cells mL^{-1}, 600 µL growth medium per well.
    b. 96 Well – 2720 cells mL^{-1}, 250 µl growth medium per well.
    c. 8-well NuncTM Lab-TekTm II Chamber SlideTM System – 6400 cells mL^{-1}, 250 µL growth medium per well.
9. Aspirate PBS from matrix and fibronectin coated wells, apply calculated cells and incubate overnight.
10. Aspirate growth medium and rinse the matrix with attached cells using PBS.
11. Apply FDA-solution (15 µg mL^{-1}) for 5 min at room temperature.
    Note – FDA is light sensitive. All samples and stock solutions should be kept in the dark.
12. Aspirate FDA solution and rinse matrix with attached cells using PBS.
13. For analysis, use an epifluorescence or confocal microscope. Here, an Axio Observer.Z1 microscope equipped with an A-Plan 10x/0.25 Ph1 objective (Zeiss) was used.

14. Process images using ImageJ (http://imagej.nih.gov/ij/). The Fluorescein image shows the whole cell.
15. Outline every cell and add the results to the ROI manager of ImageJ to calculate the circularity.
16. The morphology of the cells can be measured by means of the $circularity = 4\pi \frac{area}{perimeter^2}$ which indicates a perfect circle with a value of 1.0 and elongation by reaching the value 0 (Figure S2 A,B).

5.4 Scanning electron analysis of CDMs

Note – CDMs have to be prepared on a glass cover slide to attach them on a standard SEM specimen mount.

1. Aspirate PBS, apply 2.5 % glutaraldehyde solution in PBS and incubate for 30 min at room temperature.

   Note – Previously stored matrix should be rinsed with PBS twice to clear off remaining antibacterial and antifungal protecting agents.
2. Aspirate glutaraldehyde solution and rinse the matrix three times with PBS.
3. Aspirate PBS and rinse the matrix twice with ddH_2O.

   Note – Matrix can be stored at 4 °C.
4. Remove glass cover slides from well plate using a tweezer and needle and transfer to a Teflon waver to perform an acetone series to dry the glass cover slides. Stepwise transfer the Teflon waver to different glass beakers with acetone.
   a. 30 % acetone for 10 min.
   b. 50 % acetone for 10 min.
   c. 70 % acetone for 10 min.
   d. 90 % acetone for 10 min.
   e. 100 % acetone for 10 min.
   f. 100 % acetone for 10 min.
   g. Water free acetone for 10 min.
5. Apply to a water free acetone beaker, seal with parafilm and incubate overnight at 4 °C.
6. Apply samples to a critical point drying system and fill the chamber with water free acetone until all samples are covered.
   a. Allow the system to cool to < 5 °C and start stirrer.
   b. Apply CO_2 until the chamber is filled and mix for 5 min.
   c. Remove CO_2 until surface of the samples is reached and repeat step b and c approximately 8 times.
   d. Stop cooling and increase temperature to 40 °C to remove CO_2 gas.

7. Apply carbon planchet to standard SEM specimen mount.
8. Transfer samples form Teflon waver to the carbon planchet on a standard SEM specimen mount using a needle and tweezer.
9. Apply colloidal silver paste at one edge of the sample.
10. Sputter the sample with 10-15 nm Au/Pd and analyze using a scanning electron microscope. Here, JSM-7500F filed emission scanning electron microscope (Jeol, Tokyo, Japan) was used (Figure S2 C).

Timing

Note – Times are calculated according to a triplicate/quadruplicate of one condition.

Step 1: Surface preparation = 4.5 h

- Piranha solution treatment = 60 min
- APTES treatment = 30 min
- Glutaraldehyde treatment = 45 min
- UV sterilization = 60 min
- Gelatin coating = 75 min

Step 2: Cell culture and preparation of CDMs = 9 days

Step 3: Decellularization and removal of cellular debris = 1.5 h

- ddH_2O treatment = 60 min
- triton-x-ammonia treatment = 30 min

Step 4: Characterization of resident cells

Step 4.1: Flowcytometry analysis of FDA and PI stained resident cells = 1 h

- Sample preparation = 30 min
- Flowcytometry analysis = 30 min

Step 4.2: Fluorescence microscopy analysis of FDA and PI stained resident cells = 1 h

- Sample preparation = 20 min
- Microscopy analysis = 40 min

Step 4.3: Fluorescence microscopy analysis of unextracted CDMs = 2-3 days

- Day 1 – Fixation + Permeabilization + Blocking + Primary Antibody = 140 min

- Day 2 –Secondary Antibody + Phalloidin staining + DAPI staining = 150 min
- Microscopy analysis = 120 min

Step 5: Modification and characterization of CDMs

Step 5.1: Fluorescence microscopy analysis of CuAAC and SPAAC reacted CDMs = 2-3 days

- Day 1 – CuAAC/SPAAC + Blocking + Primary Antibody = 95 – 140 min
- Day 2 – Secondary Antibody = 100 min
- Microscopy analysis = 120 min

Step 5.2: Western blot analysis of CuAAC and SPAAC reacted CDMs = 3-4 days

- Day 1 – CuAAC + Extraction + Determination of protein concentration = 140 min
- Day 2 – SDS-PAGE electrophoresis + Western blot + Ponceau red + Primary antibody = 310 min
- Day 3 – Secondary Antibody + Stripping + Streptavidin-HRP + Western blotting = 415 min

Step 5.3: Fluorescence microscopy analysis of re-seeded NIH 3T3 fibroblasts on CDMs = 1-2 days

- Day 1 – Fibronectin coating + DAPI staining + Seeding = 100 min
- Day 2 – FDA staining + microcopy analysis = 130 min

Step 5.4: Scanning electron analysis of CDMs = 1-3 days

- Day 1 – Fixation + Acetone series = 115 min
- Day 2 – Critic point drying + Sputtering = 200 min
- Day 3 – Microscopy analysis = 120 min

Procedure – Cells

In this part of the work, we describe the method for the incorporation of functionalized monosaccharides as demonstrated by Ac_4GlcNAz into the glycocalyx of NIH 3T3 fibroblasts using metabolic glycoengineering. The incorporated monosaccharides enable a biocompatible, rapid and specific way for cell surface modification using bioorthogonal chemistries.

NIH 3T3 fibroblasts were seeded in the presence of the monosaccharide and incubated for 48 h. During this time, the chemical tunable monosaccharide is incorporated into glycoproteins and transported to the glycocalyx.

Step 1: Surface preparation

Step 2: Cell culture

Step 3: Modification and characterization of glycoengineered cells

- Flowcytometry analysis of FDA and PI of glycoengineered cells after CuAAC
- Fluorescence microscopy analysis of glycoengineered cells after CuAAC and SPAAC

1. Surface preparation

The preparation of surfaces is necessary when working with glass to avoid failure in attachment of cells and thereby occurring cell death. Glass surfaces require a special treatment, whereas tissue culture plastic is normally sufficient and does not require any preparation.

Note – Surface preparation is carried out under aseptic conditions and solutions are sterilized or at least sterile filtered.

1. Prepare one pipetting reservoir with 70 % 2-propanol and two reservoirs with ddH_2O.
2. Immerse glass cover slides in the pipetting reservoir with 70 % 2-propanol for 1 min.
3. Transfer glass cover slides from the pipetting reservoir with 70 % 2-propanol to the first reservoir containing ddH_2O using a small tweezer and immerse for 1 min.
4. Transfer glass cover slides from first pipetting reservoir with ddH_2O to the second pipetting reservoir containing ddH_2O using a small tweezer and immerse for 1 min.
5. Transfer glass cover slides from second pipetting reservoir with ddH_2O on top of a petri dish.
   Note - Place the glass cover slides with slight protruding edges to ease the later transfer.
6. Sterilize and dry glass cover slides by UV irradiation under laminar air flow (LAF) for 1 h.
7. Transfer glass cover slides to well plate, apply sterile filtered 2 % gelatin solution in PBS and incubate under the LAF for 60 min.
8. Aspirate 2 % gelatin solution and wash glass cover slides 3 times, 5 min each time, with sterile PBS.
   Note – Do not let the glass cover slides run dry.
   Note – The use of non-tissue plastic can avoid cell growth beneath cover slides.

2. Cell culture

NIH 3T3 fibroblasts are at least subcultured five times to avoid any dysfunctions from thawing. Dulbecco's modified Eagle medium with high glucose (4.5 g/L) containing heat inactivated FCS (10 %), penicillin G (100 U mL^{-1}) and streptomycin (100 µg mL^{-1}) is used as standard growth medium.

Note – Carry out cell culture under aseptic conditions. Incubate at 37° C and 5 % CO_2. All solutions and equipment have to be sterile.

Note – FCS can be filtered through a 0.22 µm sterile filter to avoid background particles during microscopy analysis.

1. Prepare wanted amount of well plates using DMEM with high glucose (4.5 g/L) containing heat inactivated FCS (10 %), penicillin G (100 U mL^{-1}) and streptomycin (100 µg mL^{-1}) with or – for controls – without the addition of azide-monosaccharide (100 µM).
   24 Well – 500 µL per well
   8-well NuncTM Lab-TekTm II Chamber SlideTM System – 150 µL per well
2. Aspirate growth medium from cell culture dish, wash with PBS and apply trypsin-EDTA (0.005 % trypsin [m/V] and 0.025 % EDTA [m/V]) at approximately 80 % confluency for 1 min. Carefully tap cell culture dish and check detachment of the cells under light microscope.
3. Resuspend fibroblasts in DMEM with high glucose (4.5 g/L) containing heat inactivated FCS (10 %), penicillin G (100 U mL^{-1}) and streptomycin (100 µg mL^{-1}) and centrifuge (5 min at 218xg).
4. Aspirate the growth medium and resuspend fibroblasts in DMEM with high glucose (4.5 g/L) containing heat inactivated FCS (10 %), penicillin G (100 U mL^{-1}) and streptomycin (100 µg mL^{-1}).
5. Count the cells with a hemocytometer according to manufacturer instructions and resuspend the desired number of cells in DMEM with high glucose (4.5 g/L) containing heat inactivated FCS (10 %), penicillin G (100 U mL^{-1}) and streptomycin (100 µg mL^{-1}) and incubate for 48 h.
   24 Well – $5x10^4$ cells mL^{-1}, 500 µL growth medium per well.
   8-well NuncTM Lab-TekTm II Chamber SlideTM System – $1.7x10^4$ cells mL^{-1}, 150 µL growth medium per well.
   Note – A slightly higher amount of cells may be needed when using glass cover slides due to cell growth under the slides.
   Note – 100 µM azido-monosaccharide becomes diluted to 50 µM during seeding.

3. Modification and characterization of glycoengineered cells

Both alkyne-azide cycloadditions can be performed under aseptic conditions depending on further use. Solutions should be prewarmed or at least be conditioned to room temperature.

3.1 Flowcytometry analysis of FDA and PI of glycoengineered cells after CuAAC

Note – For testing the CuAAC conditions, the alkyne-dye can be exchanged by PBS (skip step 1.1 e).

Note – Concentration and incubation times can be changed to find the perfect conditions. Molar ratios have to be maintained.

1. Calculate total volume and prepare CuAAC mixture of 250 µM THPTA, 50 µM $CuSO_4$, 2.5 mM sodium L-ascorbate and 20 µM alkyne-dye in PBS
    a. Apply THPTA to a tube to obtain a final concentration of 250 µM using a 10 mM stock solution of THPTA in ddH_2O.
    b. Add $CuSO_4$ to obtain a final concentration of 50 µM using a 100 mM stock solution of $CuSO_4$ in ddH_2O.

       Note – Color of the solution should turn yellow. A brownish precipitate indicates the generation of copper (0) and the wrong order of used substances.

       Note – THPTA and $CuSO_4$ should be used at least in a 5:1 molar ratio.

       Note – Increased $CuSO_4$ concentration can lead to cell damage and should be kept below 125 µM.
    c. Add sodium L-ascorbate to obtain a final concentration of 2.5 mM using a 100 mM stock solution of L-ascorbate in ddH_2O.

       Note – Sodium L-ascorbate solution has to be freshly prepared.
    d. Add PBS to obtain the former calculated concentrations.
    e. Add alkyne-dye to obtain the final concentration of 20 µM, here Sulfo-Cy5-Alkyne was used.

       Note – For testing the CuAAC conditions, the alkyne-dye can be exchanged by PBS.

       Note – The order of the substances is mandatory to avoid copper (0) generation.

       Note – The use of Tris-buffer instead of PBS will lead to a low yield based on the complexing character.
2. Rinse the cells twice with prewarmed PBS.
3. Aspirate PBS, apply CuAAC mixture and incubate for 5 min at room temperature.
4. Aspirate growth medium from cell culture dish and rinse the matrix twice with PBS.
5. Apply trypsin-EDTA (0.005 % trypsin [m/V] and 0.025 % EDTA [m/V]) for 5 min.
6. Add DMEM with high glucose (4.5 g/L) containing heat inactivated FCS (10 %), penicillin G (100 U mL^{-1}) and streptomycin (100 µg mL^{-1}), resuspend and centrifuge (5 min at 218xg).
7. Resuspend in PBS and count the cells with a hemocytometer according to manufacturer instructions.

8. Divide cells in equal parts and incubate either with 0.01 µg/10^4 cells fluorescein diacetate (FDA) or with 0.003 µg/10^4 cells propidium iodide (PI) for 3 min at room temperature.
   Note – To avoid cell harm, stained cells should be stored on ice after 3 min of incubation.
   Note – Cells should be stained either with FDA or PI to avoid fluorescence cross-talk.
   Note – FDA is light sensitive. All samples and stock solutions should be kept in the dark.
9. For analysis, use a flow cytometer equipped with a 488 nm Laser and Forward scatter (FSC) diode, side scatter (SSC) diode, Fluorescence channel 1 (FL1) diode [530 nm filter] and Fluorescence channel 2 (FL2) diode [585 nm filter]. Count 5000-10000 cells and assess the geometric mean of FL1 and FL2. Here, a FacsCalibur system and BD CellquestTM Pro and Flowing software (version 2.5.1; Turku Bioimaging) was used. (Figure S3)
   Note – Use standard cultured cells as positive control and 70 % isopropanol treated cells as negative control.

3.2 Fluorescence microscopy analysis of glycoengineered cells after CuAAC and SPAAC

Characterization of modified glycoengineered cells has to be performed immediately after alkyne-azide cycloaddition for live cell applications (e.g. imaging). Otherwise, cells can be fixed using methanol or paraformaldehyde. Concentrations and reaction times are mandatory unless otherwise noticed to avoid cell damage and cell death.

1.1. Calculate total volume and prepare CuAAC mixture of 250 µM THPTA, 50 µM $CuSO_4$, 2.5 mM sodium L-ascorbate and 20 µM alkyne-dye in PBS.
   a. Apply THPTA to a tube to obtain a final concentration of 250 µM using a 10 mM stock solution of THPTA in ddH_2O.
   b. Add $CuSO_4$ to obtain a final concentration of 50 µM using a 100 mM stock solution of $CuSO_4$ in ddH_2O.
      Note – Color of the solution should turn yellow. A brownish precipitate indicates the generation of copper (0) and the wrong order of used substances.
      Note – THPTA and $CuSO_4$ should be used at least in a 5:1 molar ratio.
      Note – Increased $CuSO_4$ concentration can lead to cell damage and should be kept below 125 µM.
   c. Add sodium L-ascorbate to obtain a final concentration of 2.5 mM using a 100 mM stock solution of L-ascorbate in ddH_2O.
      Note – Sodium L-ascorbate solution has to be freshly prepared.
   d. Add PBS to obtain the former calculated concentrations.

e. Add alkyne-dye to obtain the final concentration of 20 µM, here Sulfo-Cy5-Alkyne or Acetylene-Fluor 488 were used.

Note – The order of the substances is mandatory to avoid copper (0) generation.

Note – The use of Tris-buffer instead of PBS will lead to a low yield based on the complexing character.

1.2 Prepare SPAAC mixture by adding DBCO-dye to PBS to obtain a final concentration of 20 µM, here DBCO-Sulfo-Cy5 was used.

2. Rinse the cells twice with prewarmed PBS.
3. Aspirate PBS, apply SPAAC mixture and incubate for 1 h or apply CuAAC mixture and incubate for 5 min at room temperature, respectively.
4. Aspirate SPAAC or CuAAC mixture and apply growth medium to stop the reaction.
5. Aspirate growth medium and wash the cells three times with PBS.

   Note – Cells can be fixed using ice-cold methanol for 10 min at room temperature or 2 % paraformaldehyde solution in PBS for 15 min at room temperature.
6. For analysis, use an epifluorescence or confocal microscope. Here, an AOBS SP2 confocal laser scanning microscope (Leica microsystem, Wetzla, Germany) with a 63x N.A. 1.4-0.60 Oil I BL HCX PL APO I objective and an Axio Observer.Z1 microscope equipped with an 63x Plan-Apochromat 100x/1.40 Oil DIC M77 objective (Zeiss) were used. (Figure S4)

Timing

Step 1: Surface preparation = 2 h

- Cleaning of cover slides = 15 min
- UV sterilization = 60 min
- Gelatin coating = 75 min

Step 2: Cell culture = 48 h

Step 3: Modification and characterization of glycoengineered cells

Step 3.1: Flowcytometry analysis of FDA and PI of glycoengineered cells after CuAAC = 1 h

- Sample preparation = 30 min
- Flowcytometry analysis = 30 min

Step 3.2: Fluorescence microscopy analysis of glycoengineered cells after CuAAC and SPAAC = 1-2 h

- Sample preparation = 25-80 min

- Microscopy analysis = 40 min

Troubleshooting

Table 2: Troubleshooting for different critical steps.

Problem	Cause	Solution
Step 2 Cell culture and preparation of ECM		
Cell death after cell seeding.	a) Incomplete surface modification. a) Residues of surface modification substances. b) Possible cytotoxicity of engineered monosaccharide.	a) Increase washing steps during and after surface preparation. b) Decrease the amount of engineered monosaccharide.
Cell death after stimulation with sodium ascorbate (day 1).	a) Low confluence of seeded cells.	a) Cell should be 100 % confluent prior to sodium ascorbate stimulation. a) Increase number of cells.
Step 5 Modification and characterization of CDMs		
Low yields after SPAAC	a) Insufficient incorporation of engineered monosaccharide	a) Increase the amount of engineered monosaccharide (50 µM) b)
Low yields after CuAAC	a) Insufficient incorporation of engineered monosaccharide b) Slow reaction, His_6-Tag or other complexing structures and buffers. c) Slow reaction or covered azide/alkyne moiety.	a) Increase the amount of engineered monosaccharide (50 µM is typical) b) Increase the amount of $CuSO_4$ and THPTA (keep 1:5 ratio). c) Increase reaction time and temperature. c) Perform the reaction using co-solvents (DMSO, NMP, DMF).
General remarks		
Low incooperation of the used monosaccharide Ac_4GlcNAz into CDMs and/or cellular surfaces.	a) Incorporation efficiency dependent on the used cell type and type of functionalized monosaccharide.	a) Exchange to Gal or Man analogues (e.g. Ac_4GalNAz, Ac_4ManNAz).

Anticipated Results

Metabolic glycoengineering presents a versatile strategy for controlled and specific modification of naturally integrated chemically tunable monosaccharides into glycans of the glycocalyx and ECM

components, thus offering a comprehensive range of possibilities (vide infra). The herein presented protocols provide a complete set of tools for metabolic glycoengineering of CDMs and living cell surfaces. NIH 3T3 fibroblasts were selected for all protocols due to their (i) robustness [63] and (ii) ability to generate ECM *in vitro*.[55, 62]

Through the incorporation of chemically tunable monosaccharides for covalent modification, the natural capacity of the ECM – (i) storage of growth factors with natural bearing ECM binding sites or through enzymatic reactions (e.g. transglutaminase) and (ii) synergy effects (matricrin effects[59]) of growth factors bound to ECM-molecules together with the recruitment of integrin receptors with the result of an increased and prolonged signaling [60] – is expanded by chemical modification. According to this, glycoengineered ECM scaffolds represent a powerful development tool for designing drug delivery platforms by providing superior functional diversity and flexibility, thus enabling a selective adaptation of these CDMs to specific conditions.[64] Glycoengineered CDMs are currently featured as cover material for synthetic surfaces, thereby rendering these former incompatible materials in terms of biocompatibility available for the health care sector.[65] By using glycoengineering approaches on CDMs, specific stimuli for cell proliferation and differentiation by covalent immobilization of e.g. growth factors, or cytokines can be provided to support regenerative outcome.[66-68] Bioresponsive release of immobilized therapeutics from CDMs can be further trigged by upregulated proteases – acting as surrogate of a disease – by incooperation of matrix metalloproteinase sensitive linkers as we have reported before.[69-71] By demonstrating the incorporation and specific reactivity of the azide-bearing monosaccharide in the glycan structure of the extracellular matrix structure (Figure 7) in line with uncompromised cell viability of the generated glycoengineered CDM material, our protocols set the starting point for deploying CDMs, specially tailored to multiple needs in generative medicine. In fact, many more perspectives are possible in respect to the chosen cell-type and bioorthogonal chemistries as outlined here. Even a combination of bioorthogonal chemistries for immobilizing different molecules at the same time by combining different synthetic monosaccharides and coupling strategies are conceivable. Substitution of the added monosaccharide from GlcNAz to ManNAz or GalNAz represents an easy strategy to tune modified glycan densities. Densities of modified glycans were doubled for ManNAz and were found highest for GalNAz compared to GlcNAz in neuroblastoma (SK-N-MC) and osteosarcoma (U2OS) cell-lines.[42] GlcNAz has been suggested to intracellularly label O-glycosylated glycoproteins.[38] This aspect might favor glycoengineering of extracellular matrix components (e.g. fibronectin), which are secreted into the extracellular space. It will be thus of interest to compare modified glycan densities of extracellular matrix components in respect to ManNAz or GalNAz incorporation in the future.

Besides the modification of ECM components *in vitro*, glycans in the glycocalyx of living cell organisms can be addressed via metabolic glycoengineering and bioorthogonal coupling methods

without jeopardizing cellular performances. Metabolic glycoengineering of living cell surfaces has been successfully performed in diagnostics and therapy for cancer treatment. By directly applying the azide-bearing monosaccharide into the tumor tissue, new target azide-moieties were created to be locally accessible for DBCO-modified bioactive substances.[72] Furthermore, endogenous T cells were modified by means of metabolic glycoengineering combined with SPAAC for targeted immunotherapy. By tethering tumor-targeting moieties onto glycoengineered T cell surfaces, immune responses in tumor tissues were boosted effectively.[73] Further metabolic glycoengineering approaches include monitoring of biological processes in the fields of tissue development and cell tracking by *in vitro* generated glycoengineered and labeled cells prior before *in vivo* application.[74-76] Our optimized protocols pave the way for an efficient and rapid customization of cell surfaces using azide-bearing monosaccharides coupled with bioorthogonal click reactions, here demonstrated by specific and transient fluorescence detection of the cell membrane (Figure S 4 A, B). It has to be emphasized that incooperation of the respective functionalized monosaccharide is highly cell-type depandant and needs to be adjusted for each case.[77] Our protocols include a design space (reaction time – copper concentration) for CuAAC reaction in consideration to cell viability (Figure S3) as well as further studies that cover the minimum monosaccharide concentration that should be used (Figure 4) and the expected resident time of metabolic engineered glycans on the cell surface prior to fading off due to sequestration processes (Figure S4 C). The results outlined here suggest applications aiming at short term biological processes and labeling procedures as outlined above.

Summary

The ECM provides an essential biochemical and biophysical scaffold, secreted by resident cells enabling higher organization into tissues and organs.[78] Composed of fibrous proteins as core structure and glycoproteins and proteoglycans as the gel-like interstitial space, the ECM features a highly structured interconnected network,[79] regulating important cell functions including morphogenesis, cell differentiation and homeostasis.[60, 80] Fulfilling the key characteristics of drug delivery systems, namely (i) available sites for physio-adsorption of the therapeutic, (ii) improved stability of the embedded therapeutic[60] and (iii) local release of the therapeutic,[81] the ECM represents an excellent candidate material for application in drug delivery.[65] Various attempts with different strategies for immobilization and release of therapeutic substances for drug delivery were performed by changing the biochemical/physical properties of the ECM[82] (e.g. charge, hydrophobicity, viscosity) or linking the therapeutic agent covalently – by chemical means (e.g. *N*-hydroxysuccinimide chemistry) – to ECM components. Given the fact that different components of the ECM like fibronectin, fibrinogen, tenascin and vitronectin hold the natural ability to bind different growth factors,[83-84] diverse ECM-like biomaterials have recently emerged.[85] Incorporation of chemically tunable monosaccharides into

ECM components or into the glycocalyx offers an elegant approach for covalent immobilization of substances for therapeutic or diagnostic application. The outlined CuAAC protocol allows an efficient and rapid modification of living cells and CDMs.[56-57] However, the decorated glycocalyx is limited in time determined by the membrane turnover of the specific cell type. Recently, several fields for metabolic glycoengineering emerged with applications in *in vivo* cell tracking, imaging of tissue development as well as tumor therapy and diagnostics.[10] The outlined techniques can easily be applied and adapted for other cell-lines and generated CDMs. The given practical guide for metabolic glycoengineering of CDMs and cellular surfaces provides a starting point for the experiment to effectively use and study (i) cellular inertness of the synthetic sugar, (ii) generation of glycoengineered CDMs and cellular surfaces, and (iii) biocompatible and effective decoration of (living) glycoengineered systems deploying bioorthogonal chemistries.

Supporting Information

Supporting Figures

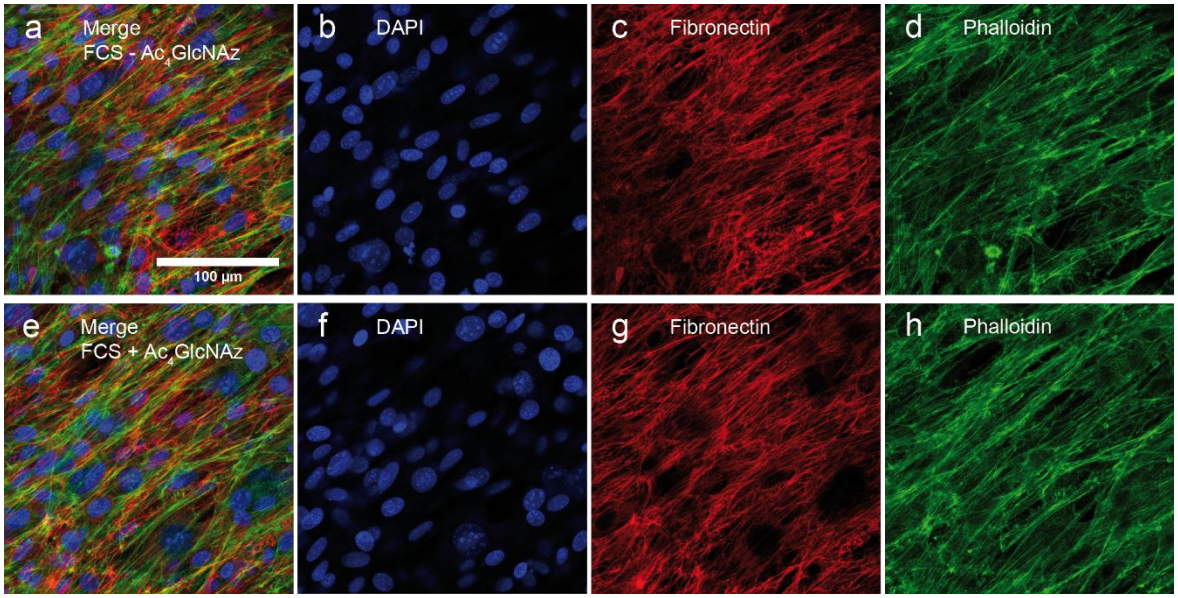

Figure S 1: Confocal images of resident cells and surrounding extracellular matrix network. Matrices were generated with or without the addition of $Ac_4GlcNAz$ and fixed with paraformaldehyde. Fibronectin was stained with a red fluorescent Alexa Fluor® 633 antibody conjugate (c, g). Actin was stained with a green fluorescent Alexa Fluor® 488 phalloidin conjugate (d, h). Nuclei were stained with DAPI (b, f). Merge is shown in yellow (a, e). Reprinted (adapted) with permission from[57].Copyright 2018 American Chemical Society.

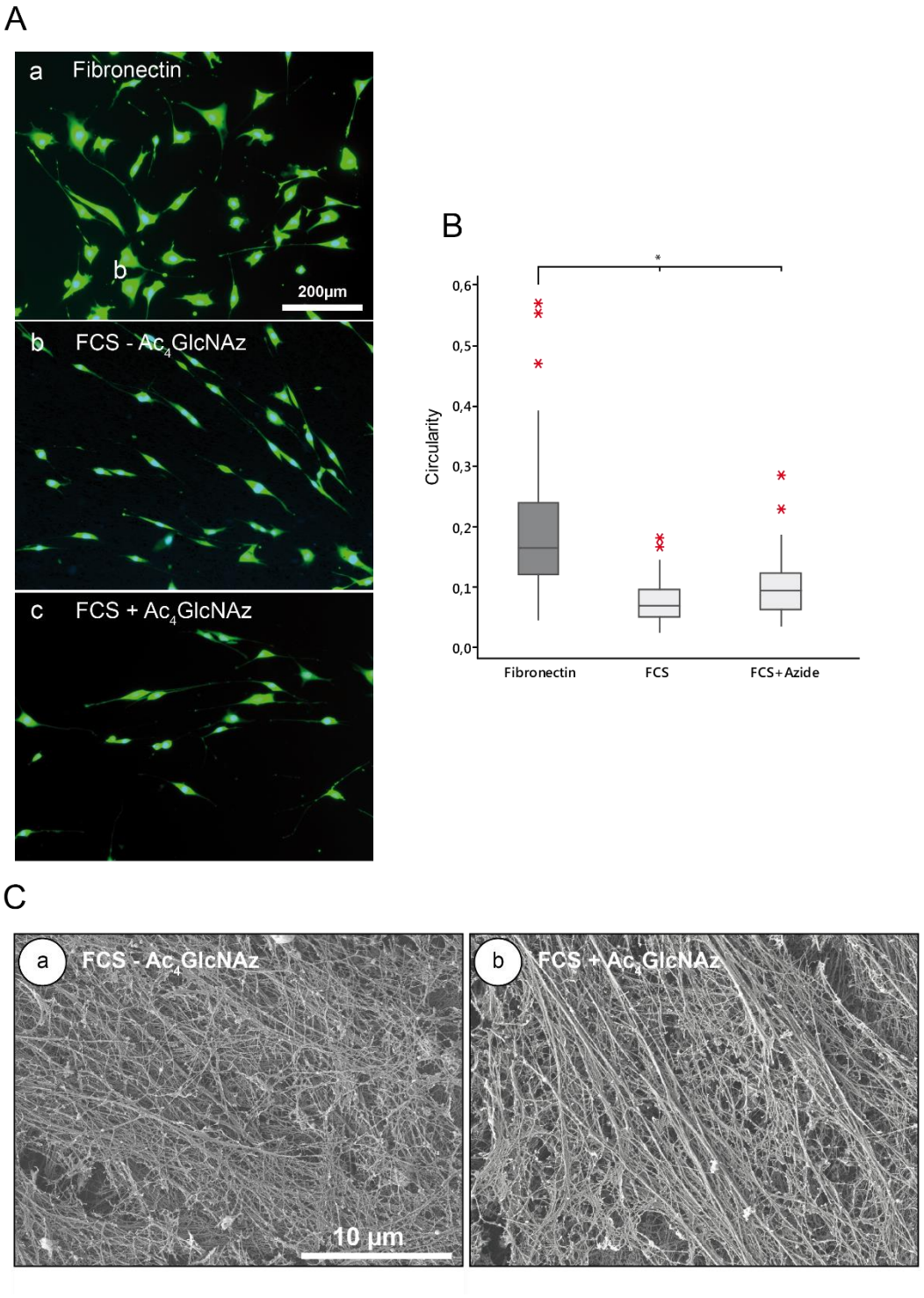

Figure S 2: (A) Fluorescent images of reseeded NIH 3T3 fibroblast on CDMs. CDMs were generated with (c) or without (b) the addition of $Ac_4GlcNAz$. Cultured fibroblasts were stained with Hoechst, seeded and stained with fluorescein diacetate. Fibronectin coated wells were used for control (a). (B) Circularity was determined, and results were displayed as mean with standard deviation. Outliners are shown with red stars. (C) CDMs were generated with (a) or without (b) the addition of $Ac_4GlcNAz$ and characterized using scanning electron microscopy with a 4000x magnification. Reprinted (adapted) with permission from[57].Copyright 2018 American Chemical Society.

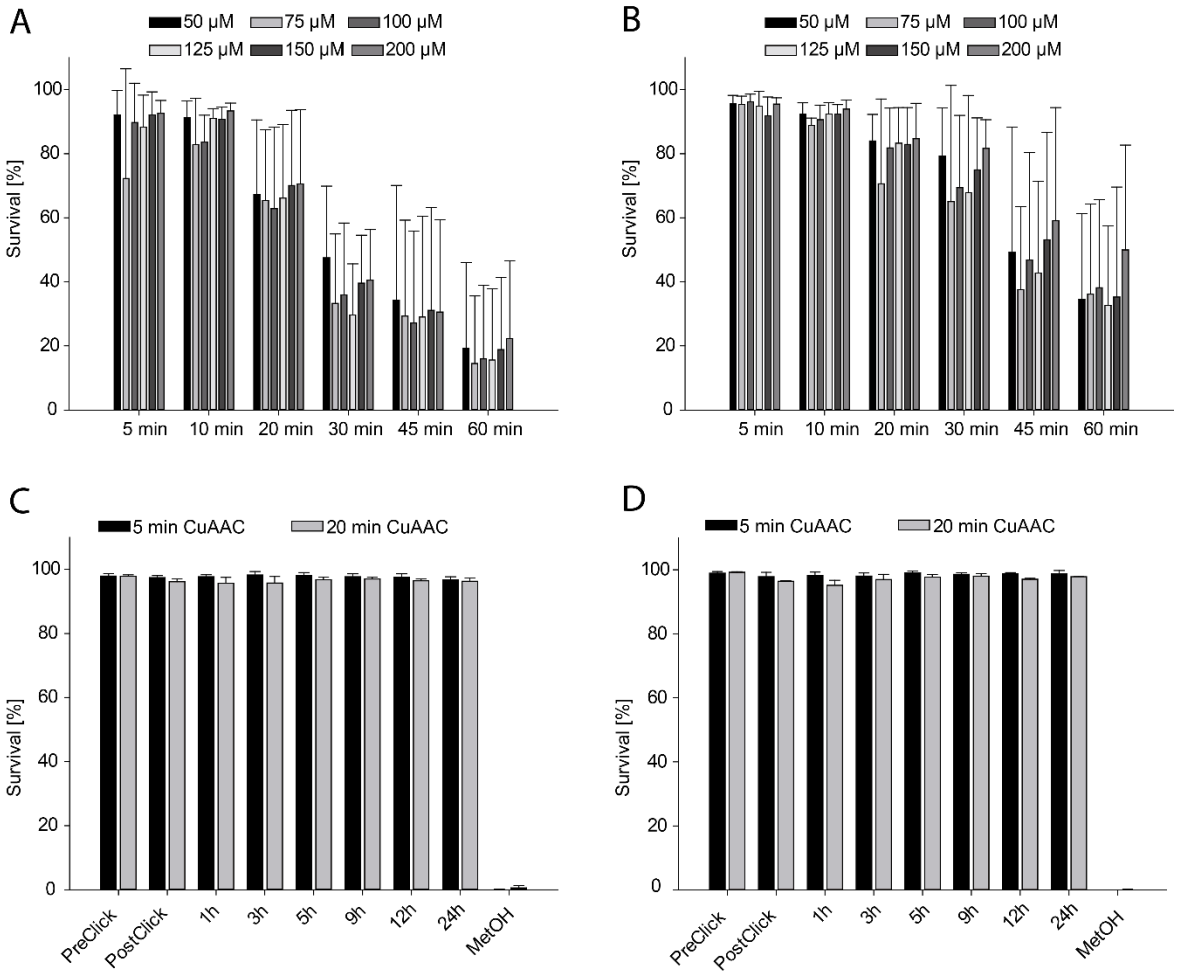

Figure S 3: Cell viability of NIH 3T3 fibroblasts after $CuSO_4$, THPTA and sodium L-ascorbate treatment as a function of copper concentration and exposure time as analyzed by FDA (A) and PI (B) staining and subsequent FACS analysis (n=4). Cell viability of NIH 3T3 fibroblasts stained with PI (C) and FDA (D) after click reaction for 5 minutes or 20 minutes. Pre-clicked cells were untreated cells and post clicked cells were analyzed directly after the click reaction ($p < 0.05$, $n = 3$). Reprinted with permission from[56].Copyright 2016 John Wiley and Sons.

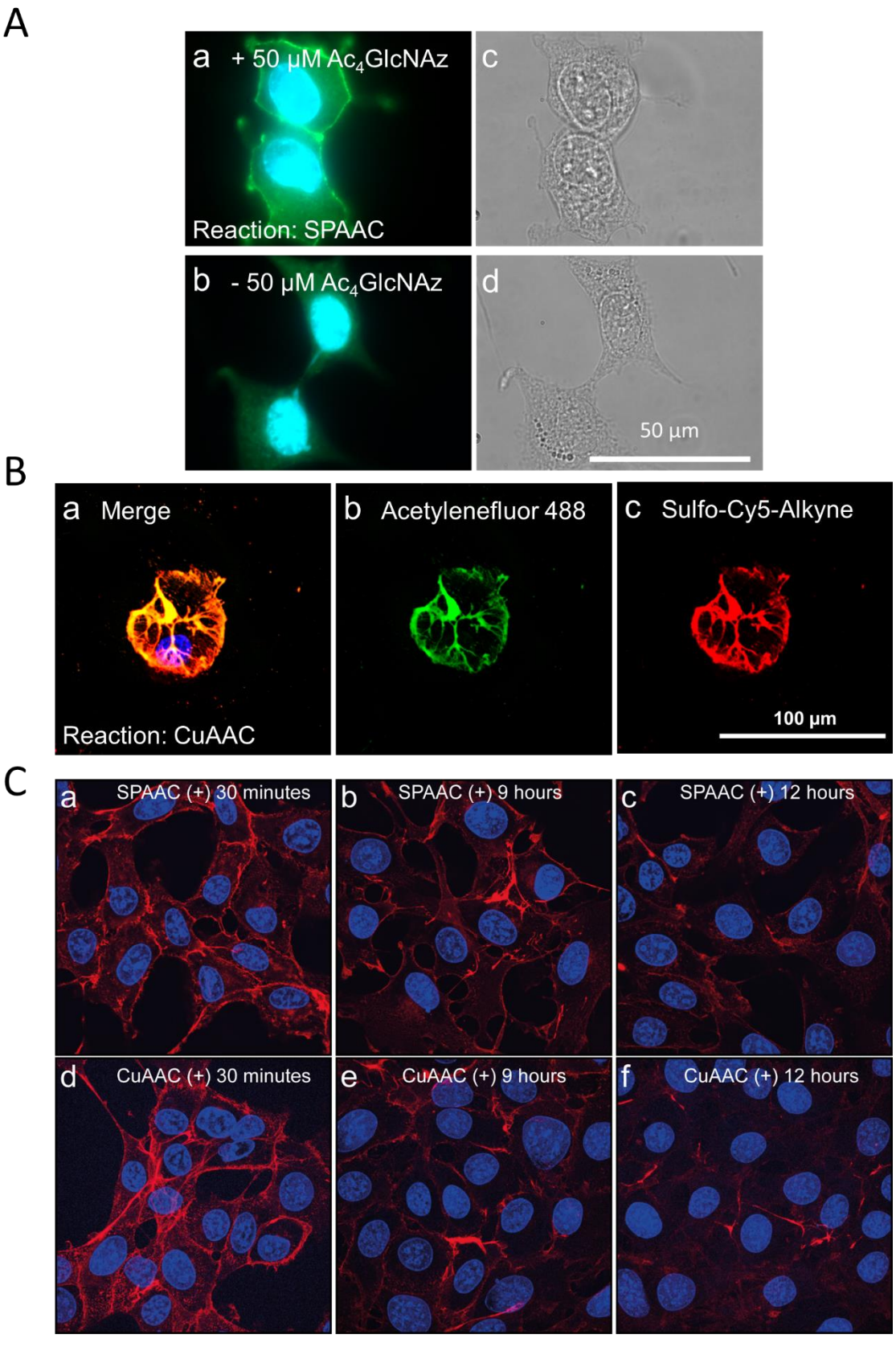
A
a + 50 µM Ac4GlcNAz
Reaction: SPAAC
c
b - 50 µM Ac4GlcNAz
d
50 µm
B
a Merge
Reaction: CuAAC
b Acetylenefluor 488
c Sulfo-Cy5-Alkyne
100 µm
C
a SPAAC (+) 30 minutes
b SPAAC (+) 9 hours
c SPAAC (+) 12 hours
d CuAAC (+) 30 minutes
e CuAAC (+) 9 hours
f CuAAC (+) 12 hours

Figure S 4: (A) Fluorescent image (a) and transmitted light image (b) of Ac_4GlcNAz treated NIH 3T3 fibroblasts. Incorporated azide-monosaccharide is shown in green after DBCO-PEG4-5/6-Carboxyrhodamine 110 labeling using SPAAC. Nuclei were stained with DAPI (blue). (B) Confocal image of CuAAC reacted glycoengineered NIH 3T3 fibroblast. NIH 3T3 cells were grown in presence of Ac4GlcNAz for 48 hours, reacted and again grown in presence of Ac_4GlcNAz for 12 hours. Incorporated azide-monosaccharide was labelled green with acetlyenfluor 488 (b) after 48 hours and red with Sulfo-Cy5-Alkyne (c) after 36 hours using CuAAC. Merge is shown in yellow (a). Nucleus was stained with DAPI (blue). (C) Fluorescent images of Ac_4GlcNAz treated and CuAAC (d-f) or SPAAC (a-c) reacted NIH 3T3 fibroblasts after 30 minutes (a, d), 9 hours (b, e) and 12 hours (c, f). Incorporated azide-monosaccharide is shown in red after Sulfo-Cy5-Alkyne labeling using CuAAC (d-f) or DBCO-Sulfo-Cy5 labeling using SPAAC (a-c). Nuclei were stained with DAPI. Reprinted with permission from[56].Copyright 2016 John Wiley and Sons.

Acknowledgments

This work was supported by the German Research Foundation (DFG) within the collaborative research centre SFB TRR225 (subprojects A03 and B05).

References

1. Moremen, K. W.; Tiemeyer, M.; Nairn, A. V., Vertebrate protein glycosylation: diversity, synthesis and function. *Nature reviews. Molecular cell biology* **2012,** *13* (7), 448-62. DOI: 10.1038/nrm3383.
2. Wratil, P. R.; Horstkorte, R.; Reutter, W., Metabolic Glycoengineering with N-Acyl Side Chain Modified Mannosamines. *Angew Chem Int Ed Engl* **2016,** *55* (33), 9482-512. DOI: 10.1002/anie.201601123.
3. Laughlin, S. T.; Agard, N. J.; Baskin, J. M.; Carrico, I. S.; Chang, P. V.; Ganguli, A. S.; Hangauer, M. J.; Lo, A.; Prescher, J. A.; Bertozzi, C. R., Metabolic labeling of glycans with azido sugars for visualization and glycoproteomics. *Methods in enzymology* **2006,** *415*, 230-50. DOI: 10.1016/S0076-6879(06)15015-6.
4. Herget, S.; Toukach, P. V.; Ranzinger, R.; Hull, W. E.; Knirel, Y. A.; von der Lieth, C. W., Statistical analysis of the Bacterial Carbohydrate Structure Data Base (BCSDB): characteristics and diversity of bacterial carbohydrates in comparison with mammalian glycans. *BMC Struct Biol* **2008,** *8*, 35. DOI: 10.1186/1472-6807-8-35.
5. Marino, K.; Bones, J.; Kattla, J. J.; Rudd, P. M., A systematic approach to protein glycosylation analysis: a path through the maze. *Nat Chem Biol* **2010,** *6* (10), 713-23. DOI: 10.1038/nchembio.437.
6. Bertozzi, C. R.; Kiessling, L. L., Chemical glycobiology. *Science* **2001,** *291* (5512), 2357-64. DOI: 10.1126/science.1059820.
7. Varki, A.; Gagneux, P., Biological Functions of Glycans. In *Essentials of Glycobiology*, 3rd ed.; rd; Varki, A.; Cummings, R. D.; Esko, J. D.; Stanley, P.; Hart, G. W.; Aebi, M.; Darvill, A. G.; Kinoshita, T.; Packer, N. H.; Prestegard, J. H.; Schnaar, R. L.; Seeberger, P. H., Eds. Cold Spring Harbor (NY), 2015; pp 77-88. DOI: 10.1101/glycobiology.3e.007.
8. Seibel, J.; Konig, S.; Gohler, A.; Doose, S.; Memmel, E.; Bertleff, N.; Sauer, M., Investigating infection processes with a workflow from organic chemistry to biophysics: the combination of metabolic glycoengineering, super-resolution fluorescence imaging and proteomics. *Expert Rev Proteomics* **2013,** *10* (1), 25-31. DOI: 10.1586/epr.12.72.
9. Du, J.; Meledeo, M. A.; Wang, Z.; Khanna, H. S.; Paruchuri, V. D.; Yarema, K. J., Metabolic glycoengineering: sialic acid and beyond. *Glycobiology* **2009,** *19* (12), 1382-401. DOI: 10.1093/glycob/cwp115.

10. Yoon, H. Y.; Koo, H.; Kim, K.; Kwon, I. C., Molecular imaging based on metabolic glycoengineering and bioorthogonal click chemistry. *Biomaterials* **2017,** *132*, 28-36. DOI: 10.1016/j.biomaterials.2017.04.003.
11. Agard, N. J.; Bertozzi, C. R., Chemical approaches to perturb, profile, and perceive glycans. *Acc Chem Res* **2009,** *42* (6), 788-97. DOI: 10.1021/ar800267j.
12. Kayser, H.; Zeitler, R.; Kannicht, C.; Grunow, D.; Nuck, R.; Reutter, W., Biosynthesis of a nonphysiological sialic acid in different rat organs, using N-propanoyl-D-hexosamines as precursors. *J Biol Chem* **1992,** *267* (24), 16934-8.
13. Collins, B. E.; Fralich, T. J.; itonori, S.; Ichikawa, Y.; Schnaar, R. L., Conversion of cellular sialic acid expression from N-acetyl- to N-glycolylneuraminic acid using a synthetic precursor, N-glycolylmannosamine pentaacetate: inhibition of myelin-associated glycoprotein binding to neural cells. *Glycobiology* **2000,** *10* (1), 11-20. DOI: 10.1093/glycob/10.1.11.
14. Mahal, L. K.; Yamada, K. M.; Bertozzi, C. R., Engineering Chemical Reactivity on Cell Surfaces Through Oligosaccharide Biosynthesis. *Science* **1997,** *276* (5315), 1125-1128. DOI: 10.1126/science.276.5315.1125.
15. Sampathkumar, S. G.; Li, A. V.; Jones, M. B.; Sun, Z.; Yarema, K. J., Metabolic installation of thiols into sialic acid modulates adhesion and stem cell biology. *Nat Chem Biol* **2006,** *2* (3), 149-52. DOI: 10.1038/nchembio770.
16. Saxon, E.; Bertozzi, C. R., Cell surface engineering by a modified Staudinger reaction. *Science* **2000,** *287* (5460), 2007-10. DOI: 10.1126/science.287.5460.2007.
17. Niederwieser, A.; Spate, A. K.; Nguyen, L. D.; Jungst, C.; Reutter, W.; Wittmann, V., Two-color glycan labeling of live cells by a combination of Diels-Alder and click chemistry. *Angew Chem Int Ed Engl* **2013,** *52* (15), 4265-8. DOI: 10.1002/anie.201208991.
18. Patterson, D. M.; Nazarova, L. A.; Xie, B.; Kamber, D. N.; Prescher, J. A., Functionalized cyclopropenes as bioorthogonal chemical reporters. *J Am Chem Soc* **2012,** *134* (45), 18638-43. DOI: 10.1021/ja3060436.
19. Agarwal, P.; Beahm, B. J.; Shieh, P.; Bertozzi, C. R., Systemic Fluorescence Imaging of Zebrafish Glycans with Bioorthogonal Chemistry. *Angew Chem Int Ed Engl* **2015,** *54* (39), 11504-10. DOI: 10.1002/anie.201504249.
20. Nischan, N.; Kohler, J. J., Advances in cell surface glycoengineering reveal biological function. *Glycobiology* **2016,** *26* (8), 789-96. DOI: 10.1093/glycob/cww045.
21. Zhang, X.; Zhang, Y., Applications of azide-based bioorthogonal click chemistry in glycobiology. *Molecules* **2013,** *18* (6), 7145-59. DOI: 10.3390/molecules18067145.
22. Homann, A.; Qamar, R. U.; Serim, S.; Dersch, P.; Seibel, J., Bioorthogonal metabolic glycoengineering of human larynx carcinoma (HEp-2) cells targeting sialic acid. *Beilstein journal of organic chemistry* **2010,** *6*, 24. DOI: 10.3762/bjoc.6.24.
23. Almaraz, R. T.; Aich, U.; Khanna, H. S.; Tan, E.; Bhattacharya, R.; Shah, S.; Yarema, K. J., Metabolic oligosaccharide engineering with N-Acyl functionalized ManNAc analogs: cytotoxicity, metabolic flux, and glycan-display considerations. *Biotechnol Bioeng* **2012,** *109* (4), 992-1006. DOI: 10.1002/bit.24363.
24. Haynes, P. A., Phosphoglycosylation: a new structural class of glycosylation? *Glycobiology* **1998,** *8* (1), 1-5.
25. Spiro, R. G., Protein glycosylation: nature, distribution, enzymatic formation, and disease implications of glycopeptide bonds. *Glycobiology* **2002,** *12* (4), 43R-56R. DOI: 10.1093/glycob/12.4.43R.
26. Shrimal, S.; Cherepanova, N. A.; Gilmore, R., Cotranslational and posttranslocational N-glycosylation of proteins in the endoplasmic reticulum. *Semin Cell Dev Biol* **2015,** *41*, 71-8. DOI: 10.1016/j.semcdb.2014.11.005.
27. Kelleher, D. J.; Gilmore, R., An evolving view of the eukaryotic oligosaccharyltransferase. *Glycobiology* **2006,** *16* (4), 47R-62R. DOI: 10.1093/glycob/cwj066.
28. Van den Steen, P.; Rudd, P. M.; Dwek, R. A.; Opdenakker, G., Concepts and principles of O-linked glycosylation. *Crit Rev Biochem Mol Biol* **1998,** *33* (3), 151-208. DOI: 10.1080/10409239891204198.

29. Stanley, P.; Taniguchi, N.; Aebi, M., N-Glycans. In *Essentials of Glycobiology*, rd; Varki, A.; Cummings, R. D.; Esko, J. D.; Stanley, P.; Hart, G. W.; Aebi, M.; Darvill, A. G.; Kinoshita, T.; Packer, N. H.; Prestegard, J. H.; Schnaar, R. L.; Seeberger, P. H., Eds. Cold Spring Harbor (NY), 2015; pp 99-111. DOI: 10.1101/glycobiology.3e.009.
30. Kudelka, M. R.; Ju, T.; Heimburg-Molinaro, J.; Cummings, R. D., Simple sugars to complex disease--mucin-type O-glycans in cancer. *Adv Cancer Res* **2015,** *126*, 53-135. DOI: 10.1016/bs.acr.2014.11.002.
31. Friedrichson, T.; Kurzchalia, T. V., Microdomains of GPI-anchored proteins in living cells revealed by crosslinking. *Nature* **1998,** *394* (6695), 802-5. DOI: 10.1038/29570.
32. Walker-Nasir, E.; Ahmad, I.; Saleem, M.; Hoessli, D., Glycosyltransferase and Glypiation Inhibitors. *Current Organic Chemistry* **2007,** *11* (7), 591-607. DOI: 10.2174/138527207780598837.
33. Low, M. G., Biochemistry of the glycosyl-phosphatidylinositol membrane protein anchors. *Biochemical Journal* **1987,** *244* (1), 1-13.
34. Furmanek, A.; Hofsteenge, J., Protein C-mannosylation: facts and questions. *Acta biochimica Polonica* **2000,** *47* (3), 781-9.
35. Ihara, Y.; Inai, Y.; Ikezaki, M.; Matsui, I.-S. L.; Manabe, S.; Ito, Y., C-Mannosylation: Modification on Tryptophan in Cellular Proteins. In *Glycoscience: Biology and Medicine*, Taniguchi, N.; Endo, T.; Hart, G. W.; Seeberger, P. H.; Wong, C.-H., Eds. Springer Japan: Tokyo, 2015; pp 1091-1099. DOI: 10.1007/978-4-431-54841-6_67.
36. Hartmann, S.; Hofsteenge, J., Properdin, the positive regulator of complement, is highly C-mannosylated. *J Biol Chem* **2000,** *275* (37), 28569-74. DOI: 10.1074/jbc.M001732200.
37. Doucey, M. A.; Hess, D.; Cacan, R.; Hofsteenge, J., Protein C-mannosylation is enzyme-catalysed and uses dolichyl-phosphate-mannose as a precursor. *Molecular Biology of the Cell* **1998,** *9* (2), 291-300.
38. Laughlin, S. T.; Bertozzi, C. R., Metabolic labeling of glycans with azido sugars and subsequent glycan-profiling and visualization via Staudinger ligation. *Nat Protoc* **2007,** *2* (11), 2930-44. DOI: 10.1038/nprot.2007.422.
39. Mongis, A.; Piller, F.; Piller, V., Coupling of Immunostimulants to Live Cells through Metabolic Glycoengineering and Bioorthogonal Click Chemistry. *Bioconjug Chem* **2017,** *28* (4), 1151-1165. DOI: 10.1021/acs.bioconjchem.7b00042.
40. Memmel, E.; Homann, A.; Oelschlaeger, T. A.; Seibel, J., Metabolic glycoengineering of Staphylococcus aureus reduces its adherence to human T24 bladder carcinoma cells. *Chemical communications* **2013,** *49* (66), 7301-3. DOI: 10.1039/c3cc43424a.
41. Mertsch, A.; Letschert, S.; Memmel, E.; Sauer, M.; Seibel, J., Synthesis and application of water-soluble, photoswitchable cyanine dyes for bioorthogonal labeling of cell-surface carbohydrates. *Z Naturforsch C* **2016,** *71* (9-10), 347-354. DOI: 10.1515/znc-2016-0123.
42. Letschert, S.; Gohler, A.; Franke, C.; Bertleff-Zieschang, N.; Memmel, E.; Doose, S.; Seibel, J.; Sauer, M., Super-resolution imaging of plasma membrane glycans. *Angewandte Chemie* **2014,** *53* (41), 10921-4. DOI: 10.1002/anie.201406045.
43. Boyce, M.; Carrico, I. S.; Ganguli, A. S.; Yu, S. H.; Hangauer, M. J.; Hubbard, S. C.; Kohler, J. J.; Bertozzi, C. R., Metabolic cross-talk allows labeling of O-linked beta-N-acetylglucosamine-modified proteins via the N-acetylgalactosamine salvage pathway. *Proc Natl Acad Sci U S A* **2011,** *108* (8), 3141-6. DOI: 10.1073/pnas.1010045108.
44. Zaro, B. W.; Yang, Y. Y.; Hang, H. C.; Pratt, M. R., Chemical reporters for fluorescent detection and identification of O-GlcNAc-modified proteins reveal glycosylation of the ubiquitin ligase NEDD4-1. *Proceedings of the National Academy of Sciences of the United States of America* **2011,** *108* (20), 8146-51. DOI: 10.1073/pnas.1102458108.
45. Li, S.; Zhu, H.; Wang, J.; Wang, X.; Li, X.; Ma, C.; Wen, L.; Yu, B.; Wang, Y.; Li, J.; Wang, P. G., Comparative analysis of Cu (I)-catalyzed alkyne-azide cycloaddition (CuAAC) and strain-promoted alkyne-azide cycloaddition (SPAAC) in O-GlcNAc proteomics. *Electrophoresis* **2016,** *37* (11), 1431-6. DOI: 10.1002/elps.201500491.

46. Woo, C. M.; Iavarone, A. T.; Spiciarich, D. R.; Palaniappan, K. K.; Bertozzi, C. R., Isotope-targeted glycoproteomics (IsoTaG): a mass-independent platform for intact N- and O-glycopeptide discovery and analysis. *Nat Methods* **2015,** *12* (6), 561-7. DOI: 10.1038/nmeth.3366.
47. Chugh, S. S.; Mace, C.; Clement, L. C.; Del Nogal Avila, M.; Marshall, C. B., Angiopoietin-like 4 based therapeutics for proteinuria and kidney disease. *Front Pharmacol* **2014,** *5*, 23. DOI: 10.3389/fphar.2014.00023.
48. Huizing, M.; Krasnewich, D. M., Hereditary inclusion body myopathy: a decade of progress. *Biochim Biophys Acta* **2009,** *1792* (9), 881-7. DOI: 10.1016/j.bbadis.2009.07.001.
49. Luchansky, S. J.; Yarema, K. J.; Takahashi, S.; Bertozzi, C. R., GlcNAc 2-epimerase can serve a catabolic role in sialic acid metabolism. *J Biol Chem* **2003,** *278* (10), 8035-42. DOI: 10.1074/jbc.M212127200.
50. Luchansky, S. J.; Hang, H. C.; Saxon, E.; Grunwell, J. R.; Yu, C.; Dube, D. H.; Bertozzi, C. R., Constructing Azide-Labeled Cell Surfaces Using Polysaccharide Biosynthetic Pathways. **2003,** *362*, 249-272. DOI: 10.1016/s0076-6879(03)01018-8.
51. Mao, Y.; Schwarzbauer, J. E., Stimulatory effects of a three-dimensional microenvironment on cell-mediated fibronectin fibrillogenesis. *J Cell Sci* **2005,** *118* (Pt 19), 4427-36. DOI: 10.1242/jcs.02566.
52. Kubow, K. E.; Vukmirovic, R.; Zhe, L.; Klotzsch, E.; Smith, M. L.; Gourdon, D.; Luna, S.; Vogel, V., Mechanical forces regulate the interactions of fibronectin and collagen I in extracellular matrix. *Nature communications* **2015,** *6*, 8026. DOI: 10.1038/ncomms9026.
53. Hakkinen, K. M.; Harunaga, J. S.; Doyle, A. D.; Yamada, K. M., Direct comparisons of the morphology, migration, cell adhesions, and actin cytoskeleton of fibroblasts in four different three-dimensional extracellular matrices. *Tissue Eng Part A* **2011,** *17* (5-6), 713-24. DOI: 10.1089/ten.TEA.2010.0273.
54. Cukierman, E., Cell migration analyses within fibroblast-derived 3-D matrices. *Methods Mol Biol* **2005,** *294*, 79-93.
55. Castello-Cros, R.; Cukierman, E., Stromagenesis during tumorigenesis: characterization of tumor-associated fibroblasts and stroma-derived 3D matrices. *Methods in molecular biology* **2009,** *522*, 275-305. DOI: 10.1007/978-1-59745-413-1_19.
56. Gutmann, M.; Memmel, E.; Braun, A. C.; Seibel, J.; Meinel, L.; Luhmann, T., Biocompatible Azide-Alkyne "Click" Reactions for Surface Decoration of Glyco-Engineered Cells. *Chembiochem : a European journal of chemical biology* **2016,** *17* (9), 866-75. DOI: 10.1002/cbic.201500582.
57. Gutmann, M.; Braun, A.; Seibel, J.; Lühmann, T., Bioorthogonal Modification of Cell Derived Matrices by Metabolic Glycoengineering. *ACS Biomaterials Science & Engineering* **2018,** *4* (4), 1300-1306. DOI: 10.1021/acsbiomaterials.8b00264.
58. Zhao, X.; Cai, L.; Adogla, E. A.; Guan, H.; Lin, Y.; Wang, Q., Labeling of Enveloped Virus via Metabolic Incorporation of Azido Sugars. *Bioconjug Chem* **2015,** *26* (9), 1868-72. DOI: 10.1021/acs.bioconjchem.5b00310.
59. Tada, S.; Kitajima, T.; Ito, Y., Design and synthesis of binding growth factors. *Int J Mol Sci* **2012,** *13* (5), 6053-72. DOI: 10.3390/ijms13056053.
60. Briquez, P. S.; Hubbell, J. A.; Martino, M. M., Extracellular Matrix-Inspired Growth Factor Delivery Systems for Skin Wound Healing. *Adv Wound Care (New Rochelle)* **2015,** *4* (8), 479-489. DOI: 10.1089/wound.2014.0603.
61. Canty, E. G.; Kadler, K. E., Procollagen trafficking, processing and fibrillogenesis. *J Cell Sci* **2005,** *118* (Pt 7), 1341-53. DOI: 10.1242/jcs.01731.
62. Yamada, K. M., Extracellular Matrix. *Current Protocols in Cell Biology* **2009,** *45* (1), 10.0.1-10.0.3. DOI: 10.1002/0471143030.cb1000s45.
63. Xia, M.; Huang, R.; Witt, K. L.; Southall, N.; Fostel, J.; Cho, M. H.; Jadhav, A.; Smith, C. S.; Inglese, J.; Portier, C. J.; Tice, R. R.; Austin, C. P., Compound cytotoxicity profiling using quantitative high-throughput screening. *Environ Health Perspect* **2008,** *116* (3), 284-91. DOI: 10.1289/ehp.10727.

64. Park, S. N.; Kim, J. K.; Suh, H., Evaluation of antibiotic-loaded collagen-hyaluronic acid matrix as a skin substitute. *Biomaterials* **2004,** *25* (17), 3689-98. DOI: 10.1016/j.biomaterials.2003.10.072.
65. Hinderer, S.; Layland, S. L.; Schenke-Layland, K., ECM and ECM-like materials - Biomaterials for applications in regenerative medicine and cancer therapy. *Adv Drug Deliv Rev* **2016,** *97*, 260-9. DOI: 10.1016/j.addr.2015.11.019.
66. Lühmann, T.; Jones, G.; Gutmann, M.; Rybak, J.-C.; Nickel, J.; Rubini, M.; Meinel, L., Bio-orthogonal Immobilization of Fibroblast Growth Factor 2 for Spatial Controlled Cell Proliferation. *ACS Biomaterials Science & Engineering* **2015,** *1* (9), 740-746. DOI: 10.1021/acsbiomaterials.5b00236.
67. Luhmann, T.; Spieler, V.; Werner, V.; Ludwig, M. G.; Fiebig, J.; Mueller, T. D.; Meinel, L., Interleukin-4-Clicked Surfaces Drive M2 Macrophage Polarization. *Chembiochem* **2016,** *17* (22), 2123-2128. DOI: 10.1002/cbic.201600480.
68. Tabisz, B.; Schmitz, W.; Schmitz, M.; Luehmann, T.; Heusler, E.; Rybak, J. C.; Meinel, L.; Fiebig, J. E.; Mueller, T. D.; Nickel, J., Site-Directed Immobilization of BMP-2: Two Approaches for the Production of Innovative Osteoinductive Scaffolds. *Biomacromolecules* **2017,** *18* (3), 695-708. DOI: 10.1021/acs.biomac.6b01407.
69. Ritzer, J.; Luhmann, T.; Rode, C.; Pein-Hackelbusch, M.; Immohr, I.; Schedler, U.; Thiele, T.; Stubinger, S.; Rechenberg, B. V.; Waser-Althaus, J.; Schlottig, F.; Merli, M.; Dawe, H.; Karpisek, M.; Wyrwa, R.; Schnabelrauch, M.; Meinel, L., Diagnosing peri-implant disease using the tongue as a 24/7 detector. *Nat Commun* **2017,** *8* (1), 264. DOI: 10.1038/s41467-017-00340-x.
70. Braun, A. C.; Gutmann, M.; Mueller, T. D.; Luhmann, T.; Meinel, L., Bioresponsive release of insulin-like growth factor-I from its PEGylated conjugate. *J Control Release* **2018,** *279*, 17-28. DOI: 10.1016/j.jconrel.2018.04.009.
71. Braun, A. C.; Gutmann, M.; Ebert, R.; Jakob, F.; Gieseler, H.; Luhmann, T.; Meinel, L., Matrix Metalloproteinase Responsive Delivery of Myostatin Inhibitors. *Pharm Res* **2017,** *34* (1), 58-72. DOI: 10.1007/s11095-016-2038-6.
72. Yoo, J. W.; Irvine, D. J.; Discher, D. E.; Mitragotri, S., Bio-inspired, bioengineered and biomimetic drug delivery carriers. *Nat Rev Drug Discov* **2011,** *10* (7), 521-35. DOI: 10.1038/nrd3499.
73. Wang, W.; Zhao, Z.; Zhang, Z.; Zhang, C.; Xiao, S.; Ye, X.; Zhang, L.; Xia, Q.; Zhou, D., Redirecting Killer T Cells through Incorporation of Azido Sugars for Tethering Ligands. *Chembiochem* **2017,** *18* (21), 2082-2086. DOI: 10.1002/cbic.201700340.
74. Gu, E.; Chen, W. Y.; Gu, J.; Burridge, P.; Wu, J. C., Molecular imaging of stem cells: tracking survival, biodistribution, tumorigenicity, and immunogenicity. *Theranostics* **2012,** *2* (4), 335-45. DOI: 10.7150/thno.3666.
75. Kang, S. W.; Lee, S.; Na, J. H.; Yoon, H. I.; Lee, D. E.; Koo, H.; Cho, Y. W.; Kim, S. H.; Jeong, S. Y.; Kwon, I. C.; Choi, K.; Kim, K., Cell labeling and tracking method without distorted signals by phagocytosis of macrophages. *Theranostics* **2014,** *4* (4), 420-31. DOI: 10.7150/thno.7265.
76. Laughlin, S. T.; Baskin, J. M.; Amacher, S. L.; Bertozzi, C. R., In vivo imaging of membrane-associated glycans in developing zebrafish. *Science* **2008,** *320* (5876), 664-7. DOI: 10.1126/science.1155106.
77. Luchansky, S. J.; Hang, H. C.; Saxon, E.; Grunwell, J. R.; Yu, C.; Dube, D. H.; Bertozzi, C. R., Constructing Azide-Labeled Cell Surfaces Using Polysaccharide Biosynthetic Pathways. *Methods in Enzymologys* **2003,** *362*, 249-272. DOI: 10.1016/s0076-6879(03)01018-8.
78. Frantz, C.; Stewart, K. M.; Weaver, V. M., The extracellular matrix at a glance. *J Cell Sci* **2010,** *123* (Pt 24), 4195-200. DOI: 10.1242/jcs.023820.
79. Fitzpatrick, L. E.; McDevitt, T. C., Cell-derived matrices for tissue engineering and regenerative medicine applications. *Biomater Sci* **2015,** *3* (1), 12-24. DOI: 10.1039/C4BM00246F.
80. Zhu, J.; Clark, R. A. F., Fibronectin at select sites binds multiple growth factors and enhances their activity: expansion of the collaborative ECM-GF paradigm. *J Invest Dermatol* **2014,** *134* (4), 895-901. DOI: 10.1038/jid.2013.484.

81. Minardi, S.; Taraballi, F.; Pandolfi, L.; Tasciotti, E., Patterning Biomaterials for the Spatiotemporal Delivery of Bioactive Molecules. *Front Bioeng Biotechnol* **2016,** *4*, 45. DOI: 10.3389/fbioe.2016.00045.
82. Lee, K.; Silva, E. A.; Mooney, D. J., Growth factor delivery-based tissue engineering: general approaches and a review of recent developments. *J R Soc Interface* **2011,** *8* (55), 153-70. DOI: 10.1098/rsif.2010.0223.
83. Martino, M. M.; Briquez, P. S.; Guc, E.; Tortelli, F.; Kilarski, W. W.; Metzger, S.; Rice, J. J.; Kuhn, G. A.; Muller, R.; Swartz, M. A.; Hubbell, J. A., Growth factors engineered for super-affinity to the extracellular matrix enhance tissue healing. *Science* **2014,** *343* (6173), 885-8. DOI: 10.1126/science.1247663.
84. Mitchell, A. C.; Briquez, P. S.; Hubbell, J. A.; Cochran, J. R., Engineering growth factors for regenerative medicine applications. *Acta biomaterialia* **2016,** *30*, 1-12. DOI: 10.1016/j.actbio.2015.11.007.
85. Parmaksiz, M.; Dogan, A.; Odabas, S.; Elcin, A. E.; Elcin, Y. M., Clinical applications of decellularized extracellular matrices for tissue engineering and regenerative medicine. *Biomed Mater* **2016,** *11* (2), 022003. DOI: 10.1088/1748-6041/11/2/022003.

Chapter 2: Bioorthogonal Modification of Cell Derived Matrices by Metabolic Glycoengineering

Marcus Gutmann[1], Alexandra C. Braun[1], Jürgen Seibel[2], and Tessa Lühmann[1]*

[1]Institute of Pharmacy and Food Chemistry, University of Würzburg, DE-97074 Würzburg, Germany,

[2]Institute of Organic Chemistry, University of Würzburg, DE-97074 Würzburg, Germany

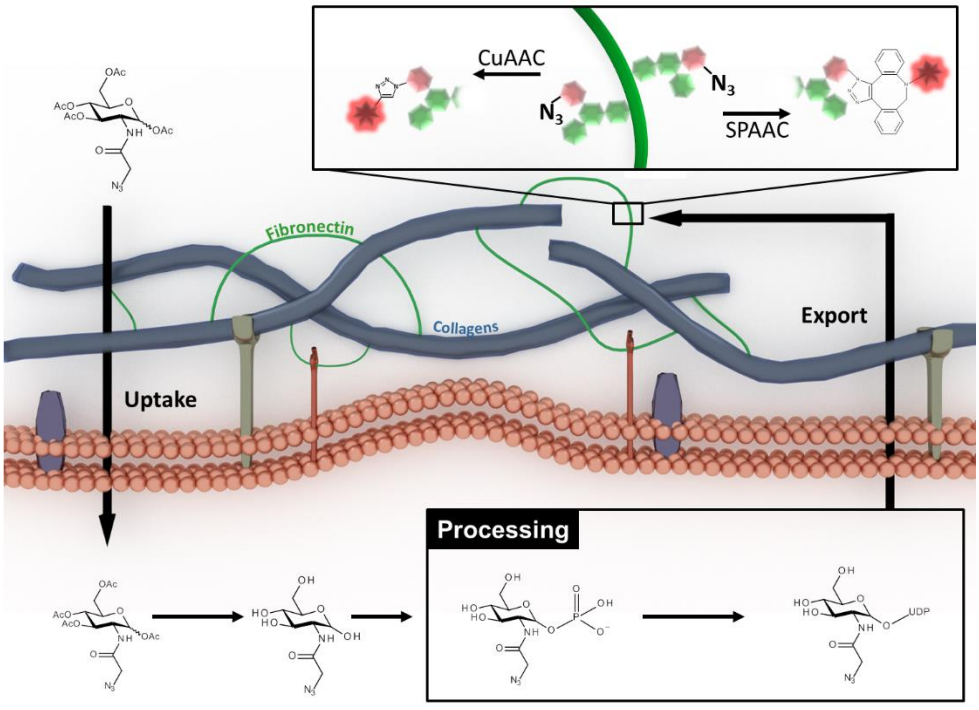

This chapter was originally published in ACS Biomaterial Science & Engineering, vol. 4 (4), pp. 1300-6, 2018; DOI: 10.1021/acsbiomaterials.8b00264, with permission of American Chemical Society.

Abstract

Cell-derived matrices (CDMs) emerged as an attractive biomaterial in regenerative medicine. Here we present a strategy for site-specific decoration of CDMs with bioactive molecules deploying metabolic glycoengineering. NIH 3T3 fibroblasts were cultured in the presence of a tetra acetylated azide bearing monosaccharide to metabolically incorporate the synthetic sugar into the glycan structure of extracellular matrix proteins. Glycoengineered CDMs were isolated and analyzed for fibronectin as one of the most abundant ECM species by western blotting and fluorescence labeling of the azide-monosaccharides deploying bioorthogonal chemistries. Glycoengineered CDMs were biocompatible for incorporated and reseeded NIH 3T3 fibroblasts, respectively. Successful modification of glycoengineered CDMs was demonstrated by a therapeutic peptide inhibitor against myostatin. This study details a site-specific, effective, and biocompatible strategy for the decoration of glycan structures within CDMs for future tissue engineering application.

Introduction

Decoration of biodegradable matrices with small molecules, therapeutic peptides and proteins is essential to drive cellular performances towards tissue repair in regenerative medicine and tissue engineering applications. Biodegradable materials have been intensively investigated in drug delivery as they provide sites for cellular adhesion and growth factor interaction[1], enabling spatio-temporal delivery[2-3] and contributing to improved stability[2] of the embedded molecules[4]. These scaffolds are either generated synthetically, including poly-L-lactide [5-6], polyurethanes[7-9] and poly(ε-caprolactone)[10], or are based on natural compounds, such as chitosan[11-12], alginate[13-15], silk[16-18], and extracellular matrix (ECM) components.[19] The ECM is a complex and highly organized 3D network, assembled by secreted macromolecules from various cell types[20], comprising an intertwining mesh of fibrous proteins (e.g. collagens, elastin) as core structure, and glycoproteins (e.g. tenascin, laminin, fibronectin) and proteoglycans (e.g. perlecan) to provide the gel-like intermediate space.[2]

The ECM plays a crucial role in tissue development, homeostasis and repair through regulating cell behavior, migration, differentiation, proliferation, survival and cell differentiation.[21] To this end, ECM components and cell derived matrices (CDMs) have emerged as bioengineered 3D microenvironments based on their unique properties providing mechanical stability, stimulating cell adhesion and migration via exposed cell-binding sites, modulating cell processes and acting as reservoir for growth factors. [4, 21-24] Commercially available ECM derived scaffold materials are, therefore, already profiled in clinical trials.[25-26] However, ECM derived scaffolds – besides their endogenous regenerative potential – lack specific molecular triggers. Covalent immobilization of active compounds onto ECM derived materials is one emerging strategy to boost their regenerative

outcome. In light of future translation, such decorated ECMs provide maximal control over attachment sites at the active compound, particularly important for replacement therapy due to immunogenic considerations, i.e. enzymes, endogenous growth factors or cytokines, etc. Several growth factors possess specific binding sites with fibronectin, fibrinogen, tenascin, vitronectin and heparan sulfates, enabling non-covalent interaction onto ECM-materials without further modification.[27-28] Moreover, recombinantly expressed proteins were enzymatically immobilized to the ECM proteins fibronectin and fibrinogen using a transglutaminase recognition peptide sequence.[29-32]

We report – to the best of our knowledge for the first time - a novel strategy with control of attachment sites by inserting azide moieties into glycan structures of the extracellular network via metabolic glycoengineering by taking advantage of the natural cell machinery of the de novo synthesized and assembled glycoproteins. Using this approach, the glycoengineered CDM is featured for bioorthogonal conjugation chemistries including copper (I)-catalyzed azide-alkyne cycloaddition (CuAAC) or strain-promoted alkyne-azide cycloaddition (SPAAC). Chemically tunable monosaccharides, including 2-azidoacetylamino-2-deoxy-(1,3,4,6)-tetra-O-acetyl-D gluco pyranoside (Ac_4GlcNAz) were previously used to decorate the glycocalyx – the outer cellular surface – with azide functionalized groups.[33-36] These tailored monosaccharides enter the cell by passive diffusion[35, 37] or by active transport mechanisms. [38] Inside the cell they function as substrates for enzymatic post translational modification processes. Incorporated via the glycosylation machinery through the Golgi apparatus or the endoplasmic reticulum, the monosaccharides are inserted in glycoproteins and glycolipids, which in turn are shuttled through the cell membrane by secretory pathways and become part of the membrane bound, extracellular glycocalyx and of the interstitial space.[36]

Here, we aimed at expanding the metabolic glycoengineering approach towards modulation of secreted glycoproteins of the ECM to be accessible for bioorthogonal conjugation chemistries, allowing glycan modification.

First, we established a protocol to fabricate glycoengineered CDMs from NIH 3T3 fibroblasts with introduced azide functionalized monosaccharides into the glycoprotein architecture suitable for covalent modification using bioorthogonal click chemistries (Figure 1). Purity and identity of Ac_4GlcNAz was assessed by ^{1}H-NMR and high-resolution mass spectrometry (HRMS) (Figure S1). For this purpose, two different approaches for generating CDMs from NIH 3T3 fibroblasts were compared by continuously stimulating collagen fibrillogenesis[39] with 50 µg/mL sodium ascorbate and by using growth medium supplemented either with FCS (fetal calf serum) or BCS (bovine calf serum), respectively, following existing protocols.[40-41] Introduction of azide moieties into secreted ECM components was achieved by supplementing the monosaccharide Ac_4GlcNAz (50 µM) into the

growth medium (Figure 1). On the basis of this procedure, CDMs were formed by NIH 3T3 fibroblasts in the presence or absence of $Ac_4GlcNAz$ within 9 days and subsequent harvest by extracting the embedded cells.

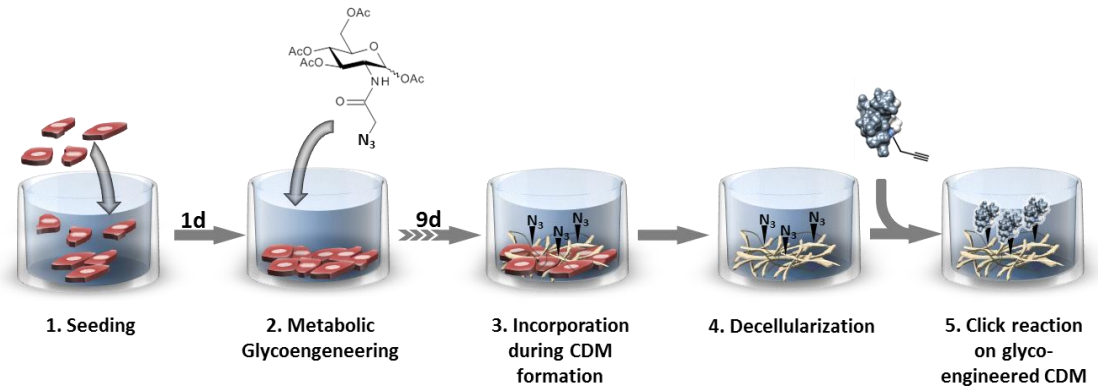

Figure 1: Scheme for fabrication of glycoengineered cell-derived matrices (CDM). Fibroblasts were (1) seeded and (2) grown in monolayers in the presence of sodium ascorbate and azide-monosaccharides for 9 days. (3) After deposition of a network of secreted matrix molecules bearing azide functionalized sugars, CDMs were isolated by decellularization. (4) Deposited matrix molecules containing azide moieties are accessible for (5) modification via CuAAC or SPAAC.

Next, we studied the integrity and functionality of the azide functionalized glycoengineered CDMs compared to non-functionalized controls (without addition of $Ac_4GlcNAz$) by following standard CuAAC and SPAAC procedures.[36] CDMs were exposed to DBCO-Sulfo-Cy5 a copper free variant of the alkyne-azide cycloaddition for 1 h and fluorescence of fibrillary components was assessed by confocal laser scanning microscopy (CLSM) (Figure 2). Fibronectin – as major fibrillar glycoprotein within the ECM[42] – was visualized by coimmunostaining. A strong and defined fluorescence of high-order fibrillar structures was observed after the SPAAC reaction for $Ac_4GlcNAz$ treated CDMs derived from NIH 3T3 cells incubated in FCS. These structures colocalized with immuno-stained fibronectin fibrils (Figure S2 and white arrows in Figure 2 a-c). In contrast, CDMs, which were generated without supplementation of the azide-monosaccharide (Figure 2 d-f, k-m) or CDMs using BCS containing growth medium showed no detectable fluorescence (Figure 2 g-m). We then switched to the copper variant of the alkyne-azide cycloaddition and modified azide functionalities within the CDM with a CuAAC click reaction mixture (Sulfo-Cy5-Alkyne, $CuSO_4$, THPTA, sodium L-ascorbate) for 5 min prior CLSM analysis (Figure S3). Glycoengineered CDMs generated in FCS supplemented growth medium and in the presence of $Ac_4GlcNAz$ were fluorescently labeled with strong intensity as indicated by defined fibrillar structures, which colocalized with the fibronectin counterstain (Figure S4 and white arrows in Figure S3 a-c). These findings indicate that our metabolic glycoengineering approach followed by modification by bioorthogonal chemistries did not interfere with fibronectin fibrillogenesis and might be a suitable approach to study dynamics of fibronectin fiber formation and matrix turnover in cellular systems in a physiological context. In line with the

results obtained for the SPAAC chemistry (vide supra), we did not succeed to modify fibrillar structures of glycoengineered CDM fabricated in the presence of Ac_4GlcNAz and BCS containing growth medium (Figure S3 g-j).

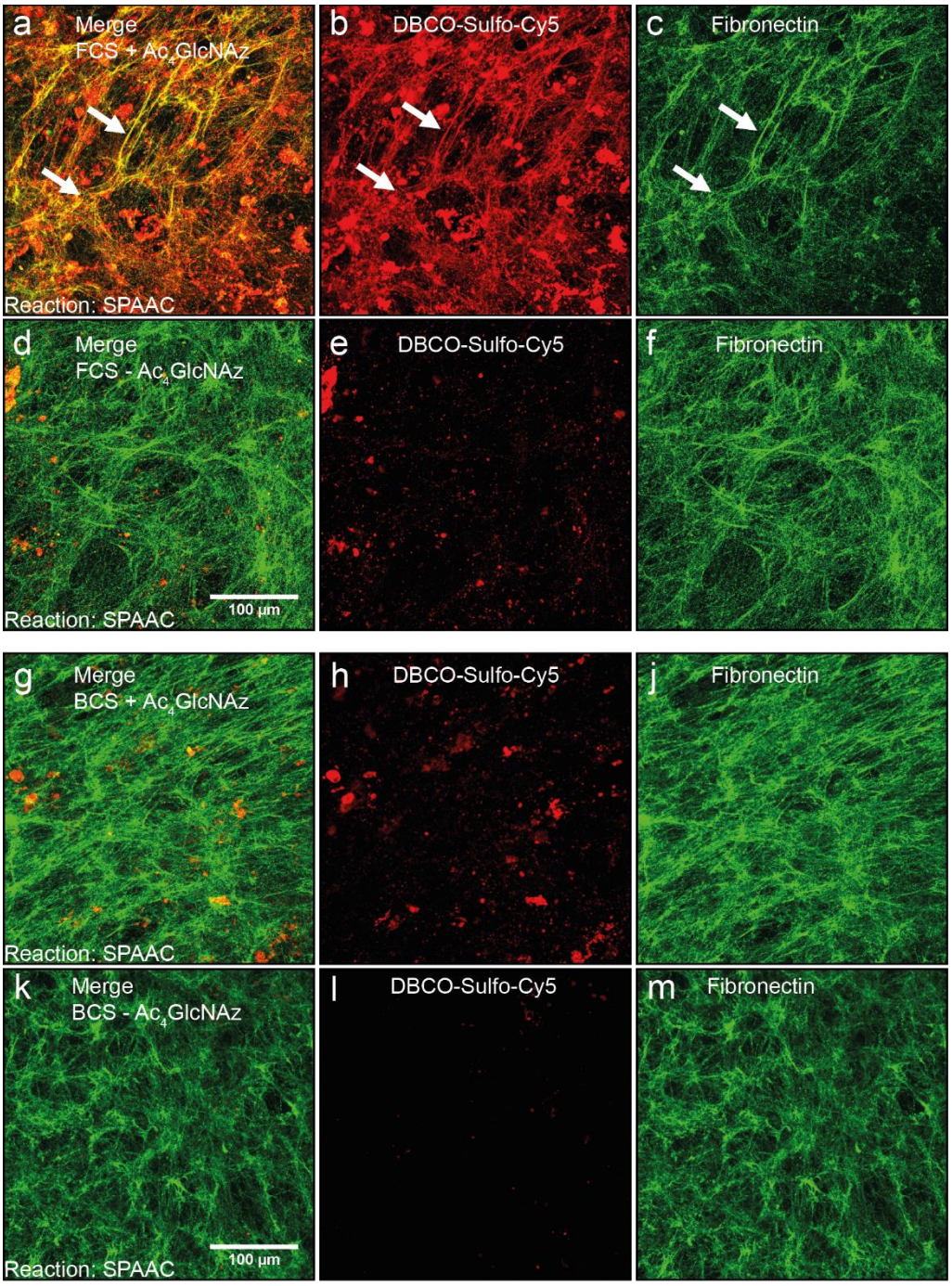

Figure 2: Confocal images CDMs derived from (a−f) FCS and (g−m) BCS with or without the addition of Ac4GlcNAz. The CDMs were reacted with DBCO-Sulfo-Cy5 using SPAAC. (b, e, h, l) Incorporated azide-monosaccharide is shown in red after Cy5-labeling using SPAAC; (c, f, j, m) Fibronectin is shown in green; (a, d, g, k) merge is shown in yellow.

Fibronectin is expressed and secreted into the plasma with average concentrations of 300-400 µg/mL by hepatocytes in the liver (plasma fibronectin), whereas different fibronectin isoforms are synthesized and secreted into the intercellular space in tissues (cellular fibronectin).[42] The assembly of fibronectin into multimeric fibronectin fibrils is a cell-mediated process with plasma and cellular fibronectin having diverse structures and rates of assembly into three-dimensional matrices from each other.[42-44] For this reason, we analyzed the applied growth medium supplemented with either FCS or BCS for generation of glyco-engineered CDMs for the presence of plasma fibronectin. Western blot analysis revealed a strong level of plasma fibronectin in BCS as demonstrated by positive lanes at 250 kDa in contrast to the analyzed FCS serum, lacking detectable amounts of plasma fibronectin (Figure S5).

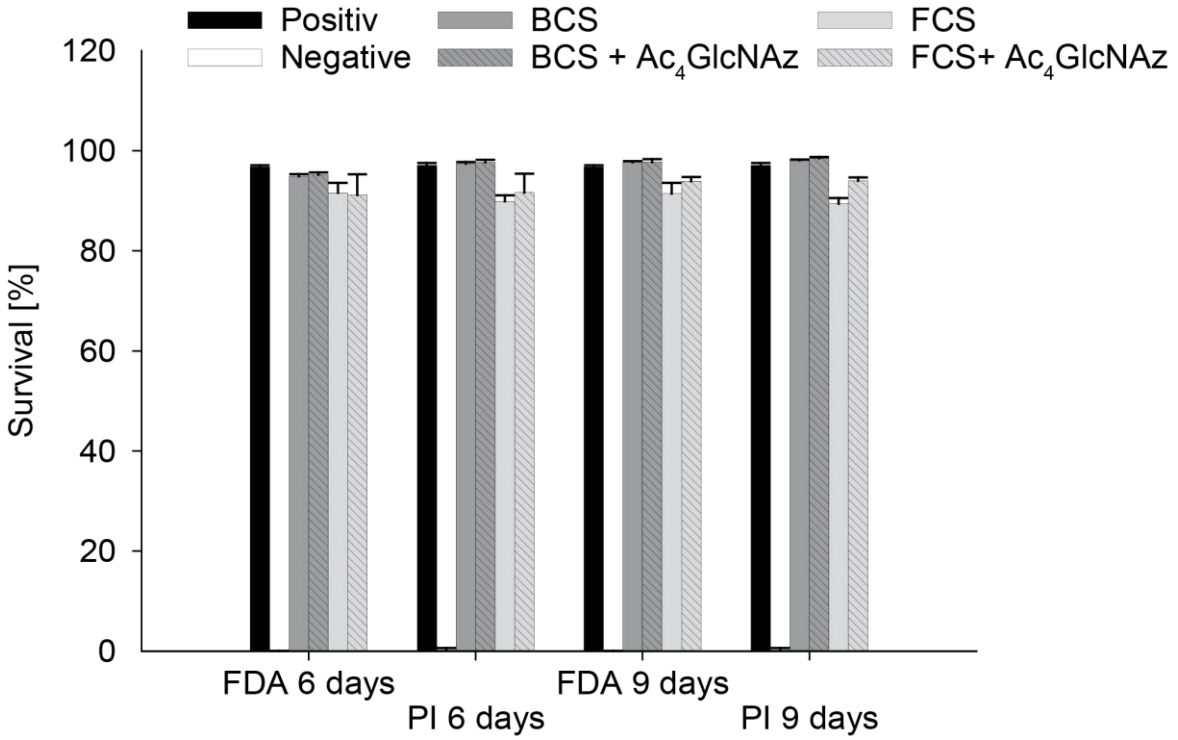

Figure 3: Cytotoxicity analysis of Ac4GlcNAz treated and untreated FCS and BCS derived CDMs after 6 and 9 days. NIH 3T3 fibroblasts cultured on tissue culture polystyrene were used as positive control and 70% 2-propranol treatment as negative control. NIH 3T3 fibroblasts were extracted from matrices and stained either with fluorescein diacetate or propidium iodide before analysis by flow cytometry. Results are displayed as mean with standard deviation.

We than analyzed the biocompatibility of extracted and unextracted glycoengineered CDMs according to existing protocols.[40-41] To analyze the viability of the resident NIH-3T3 fibroblasts during ECM assembly, we monitored cytotoxicity after 6 and 9 days, respectively. NIH-3T3 Fibroblasts were stained with fluorescein diacetate (FDA) for enzymatic activity and in parallel with propidium iodide (PI) for analysis of cell-membrane integrity. For quantification, the cells were

subsequently analyzed by flow cytometry (Figure 3) and were qualitatively visualized by florescence microscopy (Figure S6). Cell viability as assessed by FDA and PI staining revealed more than 90 % of living cells for all conditions analyzed, indicating that incorporation of azide-bearing monosaccharides into de novo synthesized glycan structures is a biocompatible cellular process. NIH-3T3 fibroblasts within their ECM were than visualized by actin staining and labeling of fibronectin as ECM component by CLSM (Figure S7). Intact ECMs displayed a defined fibronectin network, in which NIH-3T3 fibroblasts were observed to be well-aligned with strong actin stress fibers.

The morphology of extracted CDMs derived from FCS and BCS supplemented growth media was assessed by scanning electron microscopy (SEM) imaging (Figure S8). The CDMs exhibit a mesh like appearance with defined fibrillar components. Together SEM and CLSM imaging revealed a similar morphology of the ECM after treatment with the azide modified monosaccharide. To evaluate the biocompatibility of different glycoengineered CDMs as potential biomaterial substrate, the generated matrices were extracted, washed and re-plated with NIH-3T3 fibroblasts.[40-41] After overnight incubation, the cells were stained with FDA and cell shape was analyzed (Figure S9). As control, tissue culture surfaces coated with murine fibronectin were used. The morphology of the cells was quantified by circularity analysis (defined as a perfect circle with a value of 1.0 and cell elongation with a value of 0) (Figure S9 B). Round shaped fibroblasts were predominantly present on fibronectin coated 2D surfaces, whereas elongated shaped fibroblasts were observed on all tested glycoengineered CDMs and unmodified controls.

To gain further insights into the glycan-modification of glycoengineered CDMs, fibronectin as the most abundant species of glycoproteins within the ECM was chosen. Glycoengineered CDMs were prepared and were functionalized with acetylene-PEG4-Biotin via CuAAC chemistry in comparison to controls lacking the azide bearing sugar. CDM components were isolated in a two-step manner by separately extracting the soluble protein fraction and urea-solubilizing insoluble components, respectively.[45] Both fractions of each CDM extraction were combined and analyzed for biotin modification using western blot analysis for verification of bands corresponding to fibronectin and HRP-labeled streptavidin for visualization of the conjugated biotin probe (Figure 4A). Ponceau red staining was performed as loading control (Figure S10). CDMs generated in the presence of the azide monosaccharide revealed an intensive band corresponding to biotin with identical molecular size of fibronectin and in contrast to the unmodified controls (CDMs without Ac_4GlcNAz treatment). Interestingly, biotin-modification of fibronectin was observed within fractions of glycoengineered CDMs generated in both tested media but with a lower intensity in BCS supplemented medium relative to fibronectin as qualitatively assessed. The source of the

applied serum (bovine or fetal origin) is therefore critical for generation of glycan modified ECM components by metabolic glycoengineering.

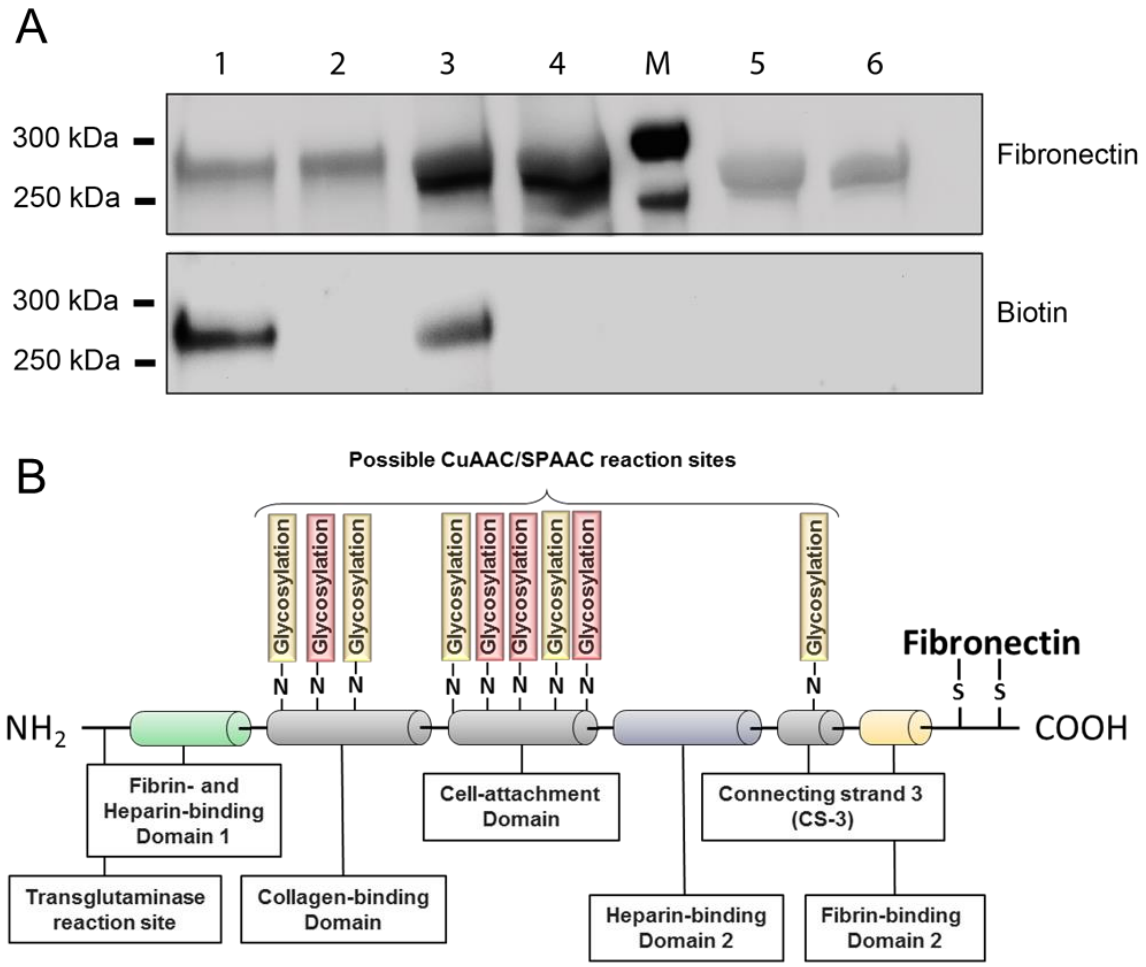

Figure 4: (A) Western blot analysis of CuAAC modified CDMs derived from FCS with (a) or without (b) the addition of Ac_4GlcNAz and BCS with (c) or without (d) the addition of Ac_4GlcNAz. 10 µg (e) and 5 µg (f) mouse fibronectin was used as control. (m) shows the 250 kDa and 300 kDa bands of the marker. CDMs were incubated with alkyne-biotin and matrix extracts were analyzed for fibronectin, stripped and analyzed for biotin using streptavidin-HRP. (B) Structure of mouse fibronectin with potential N-glycosylation sites; (red) published glycosylation[46-49] (yellow) predicted glycosylation sites (UniProtKB P11276). Potential O-glycosylation sites of murine fibronectin are not illustrated.

We conclude that specific labeling of cellular fibronectin was achieved by incorporation of azide-functionalities into its oligosaccharides– as demonstrated by covalent biotin modification – using metabolic glycoengineering. Cellular fibronectin possesses different glycosylation sites (Figure 4B), in which processed monosaccharides of the precursor Ac_4GlcNAz are incorporated during post-translational modification. As glycoproteins are the target for the incorporation of functionalized sugars during metabolic glycoengineering, fibronectin as ubiquitous and major structural glycoprotein within the ECM was analyzed. In fact, other structural glycoproteins are simultaneously secreted and incorporated into the ECM, presenting potential targets for azide-monosaccharide

modification during glycosylation, being subject of ongoing studies in our laboratory. $Ac_4GlcNAz$ is metabolized in the cytosol to GlcNAz via deacetylation and is further enzymatically converted to other stereoisomers (GalNAz; ManNAz), resulting in a variety of different azide-functionalized sugars. [50-51] Because of this reason, multiple modification sites within the ECM are possible beyond the analysis of fibronectin (as done here) and might be the focus of future studies in the context of matrix biology.

Together, these findings might explain the successful modification using CuAAC and SPAAC chemistries of glycoengineered CDMs from NIH-3T3 cells cultured in FCS being absent from external ECM compounds, primarily plasma fibronectin. Under this condition, cellular fibronectin is de novo expressed, metabolically glycoengineered in the presence of $Ac_4GlcNAz$ and secreted by NIH-3T3 fibroblasts and assembled into fibronectin fibrils. We hypothesize that in the presence of ECM compounds (as shown here for the BCS containing medium), NIH 3T3 cells incorporate a substantial amount of plasma fibronectin into their surrounding ECM, which lacks the incorporated azide monosaccharide and is thus not available for functional modification by bioorthogonal click chemistries.[52-53]

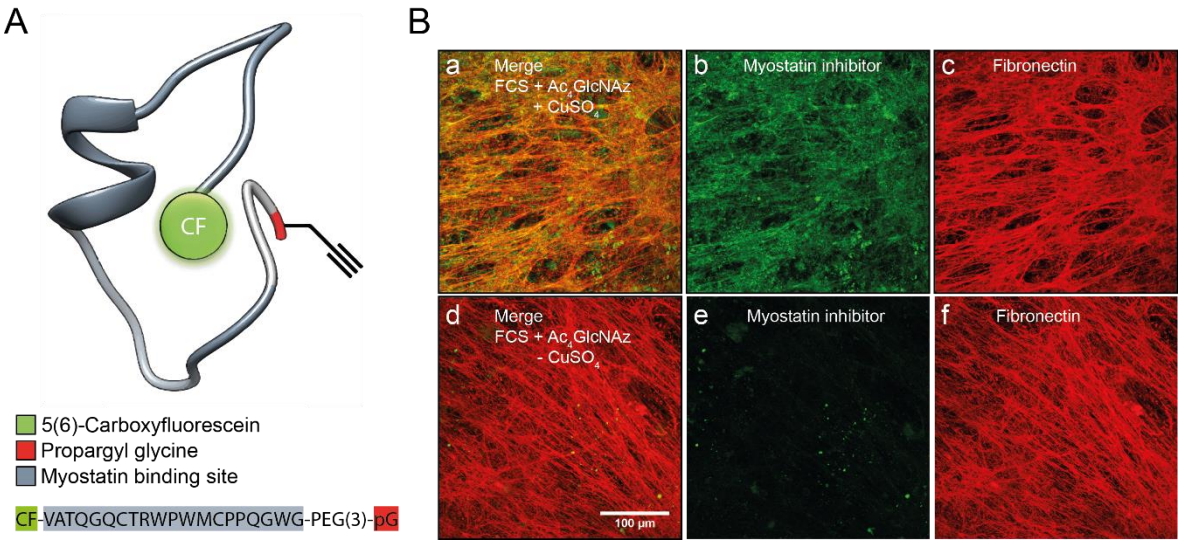

Figure 5: Immobilization of a therapeutic myostatin inhibitor (MI) on glycoengineered CDMs. (A) Predicted structure of the MI according to PEPFOLD 3.0. The MI moiety is highlighted in dark gray and the N-terminus with CF in green and C-terminus in red, respectively. (B) Confocal images of the covalent immobilization of the MI after CuAAC on CDMs derived from FCS with or without the addition of Ac4GlcNAz. (c, f) Fibronectin (red); (b, e) MI (green); (a, d) merge (yellow).

As next, we chose a therapeutic peptide as proof of concept for functional modification of glycoengineered CDMs. The myostatin inhibitor (MI) peptide antagonizes myostatin, an important player in the formation of muscle atrophy and during wound healing. Although most of the studies focus on myostatin in muscle atrophy where it acts as strong inhibitor of muscle differentiation via interacting with cell membrane associated heterodimeric receptors, the activin receptors IIB (ActRIIB) and activin receptor-like kinase receptor (ALK4/5), recent studies unveil a potential in

facilitating wound healing by reducing scars and decreasing inflammation response. [54-56] Many current therapies for myostatin targeting the ActRIIB receptor via scavenger antibodies or antagonizing myostatin and preventing the activation of the heterodimeric receptor.[57-58] To this end, the MI was synthesized via solid phase peptide synthesis as previously described.[59] At the C-terminus, the unnatural amino acid propargyl glycine was introduced to render the peptide suitable for modification via click chemistry. The N-terminus was modified with carboxyfluorescein to enable visualization by fluorescence imaging (Figure 5A). Purity and identity of the MI-carboxyfluorescein peptide was assessed by RP-HPLC and HRMS (Figure S11). The MI was effectively conjugated to fibrillar structures within the glycoengineered CDMs in the presence of copper-(I) (Figure5 B a-c), whereas the reaction without the catalyst showed only weak background fluorescence (Figure 5 B d-f), demonstrating that the glycoengineered CDM material was effectively decorated by the therapeutic peptide.

In contrast to natural compounds, CDMs display a versatile material by selection of the type of cells to generate the ECM.[20] In fact, many more perspectives are possible: glycoengineered CDMs offer (i) decoration of multiple therapeutic substances by combining different specific immobilization strategies[60] such as enzymatic modification with bioorthogonal chemistries (ii) the ability of ECM components to store growth factors with naturally occurring ECM binding sites, and (iii) induction of synergistic effects[61] of growth factors bound to ECM-molecules together with the recruitment of integrin receptors, resulting in an increased and prolonged signaling.[2] The metabolic glycoengineering approach of CDMs presented herein, can be easily expanded with protease sensitive linkers, being recognized by disease specific enzymes and connected either into the CDM or directly into the structure of the therapeutic to link its release to the activity of upregulates enzymes.[59, 62] Finally, it will be of interest to cover synthetic scaffold surfaces with glycoengineered CDMs to modulate their biocompatibility and render them accessible for functionalization and future biomedical applications.

In summary, we have established an efficient, rapid and versatile method for site-specific modification of glycan structures within the CDMs deploying metabolic glycoengineering. Future work will have to detail the outcome of decorated glyco-engineered CDMs, including assessments of immunogenicity, stability, and clinical performances.

Supporting Information

Materials

Dulbecco's modified Eagle's medium (DMEM), copper-(II) sulfate, sodium L-ascorbate, tris(3-hydroxypropyltriazolylmethyl) amine (THPTA), 3-aminopropyldimethylmethoxysilane (APTES),

Glutaraldehyde and bovine calf serum (BCS – Lot 15B526) were purchased from Sigma–Aldrich (Schnelldorf, Germany). Fetal bovine serum (FBS – Lot 41A1692K) was from Gibco (Darmstadt, Germany). Penicillin G and streptomycin were purchased from Biochrom AG (Berlin, Germany). Pierce BCA Protein Assay Kit, NuncTM Lab-TekTM II Chamber SlideTM System, Alexa Fluor™ 488 Phalloidin, Hoechst 33342, Mouse Anti-Fibronectin antibody, rabbit Anti-Fibronectin, Goat Anti-Mouse IgG H&L Alexa Fluor® 633 antibody and Goat Anti-Mouse IgG H&L Alexa Fluor® 488 antibody were from ThermoFisher Scientific (Dreieich, Germany). DBCO-Sulfo-Cy5, Sulfo-Cy5-Alkyne and acetlyen-PEG_4-Biotin were from Jena Bioscience (Jena, Germany). 24-well plates and 100 mm culture dishes were from Greiner Bio One (Frickenhausen, Germany). Roti®-Block was purchased from Carl Roth (Karlsruhe, Germany). Mouse fibronectin was purchased from Innovative Research (Novi, MI, USA). SuperSignal West Dura Substrate, Bradford Protein Assay Kit were from Pierce (Rockford, USA). All other chemicals were at least of pharmaceutical grade and were purchased from Sigma–Aldrich.

Methods

Chemical synthesis of 2-azidoacetylamino-2-deoxy-(1,3,4,6)-tetra-O-acetyl-D-glucopyranoside

Synthesis of the azide analogue Ac_4GlcNAz was performed according to existing protocols.[50, 63-64] D-glucosamine hydrochloride (500 mg, 2.32 mmol) was dissolved in dry methanol (10 mL), sodium methanolate (0.5 M in methanol, 4.64 mL, 2.32 mmol) was added and the solution stirred for 1 h at room temperature. Triethylamine (337 µL, 2.44 mmol) and chloroacetic anhydride (1.98 g, 11.6 mmol) were added and the mixture stirred for further 6 h at room temperature. The solvent was removed in vacuum and the residue dissolved in DMF (5 mL). Sodium azide (1.51 g, 23.2 mmol) was added and the suspension stirred for 2 h at 80 °C. Insoluble residues were removed by filtration through a silica pad (elution with water/isopropyl alcohol/ethyl acetate v/v/v 1:3:6 + 1 % aqueous ammonia). The solvent was removed in vacuum and the brown oily residue was redissolved in pyridine (30 mL). At 0 °C acetic anhydride (15 mL) was added and the mixture was stirred for 12 h at room temperature. Methylene chloride was added, and the solution was washed twice with 1 M HCl, sat. $NaHCO_3$, water and brine. The organic layer was dried with sodium sulphate and the solvent was removed in vacuum. Ac_4GlcNAz was obtained as a colorless foam (302 mg, 702 µmol, 31 %) after column chromatography (gradient cyclohexane/ethyl acetate v/v 3:1-1:1) in an anomeric ratio of α/β = 2:1, Rf value: 0.07 (cyclohexane/ethyl acetate 2:1).1H-NMR (400 MHz, $CDCl_3$): δ = [α-anomer] 6.41 (br. d, 1H, J = 8.9 Hz, NH), 6.21 (d, 1H, J = 3.7 Hz, H1), 5.30 (dd, 1H, J = 9.7, 10.8 Hz, H3) 5.21 (dd, 1H, J = 9.7, 9.8 Hz, H4), 4.45 (ddd, 1H, J = 3.7, 8.9, 10.8 Hz, H2), 4.27 (dd, 1H, J = 4.1, 12.5 Hz, H6a), 4.08 (dd, 1H, J = 2.4, 12.5 Hz, H6b), 4.02 (ddd, 1H, J = 2.4, 4.1, 9.8 Hz, H5),

3.93 (s, 2H, CH2ab-N3), 2.21, 2.06, 2.05, 2.09 (4x s, 3H, CH3); [β-anomer] 6.38 (br. d, 1H, J = 9.4 Hz, NH), 5.79 (d, 1H, J = 8.7 Hz, H1) 5.23 (dd, 1H, J = 9.6, 10.5 Hz, H3), 5.14 (dd, 1H, J = 9.6, 9.7 Hz, H4), 4.28 (dd, 1H, J = 4.7, 12.6 Hz, H6a), 4.21 (ddd, 1H, J = 8.7, 9.4, 10.5 Hz, H2), 4.13 (dd, 1H, J = 2.5, 12.6 Hz, H6b), 3.91 (s, 2H, CH2ab-N3), 3.83 (ddd, 1H, J = 2.5, 4.7, 9.7 Hz, 2 H5), 2.11, 2.09, 2.04, 2.04 (4x s, 3H, CH3) ppm.13C-NMR (100 MHz, CDCl3): δ = [α-anomer] 171.67, 170.79, 169.26, 168.78 (4x COO), 166.97 (CON), 90.44 (C1), 70.51 (C3), 69.99 (C5), 67.58 (C4), 61.65 (C6), 52.62 (CH2N3),51.42 (C2), 21.03, 20.82, 20.72, 20.70 (4x CH3); [β- anomer] 170.99, 170.76, 169.43, 169.39 (4x COO), 167.14 (CON), 92.40 (C1), 73.13 (C5), 72.31 (C3), 67.82 (C4), 61.75 (C6), 53.48 (C2), 52.76 (CH2N3), 21.00, 20.85, 20.72, 20.70 (4x CH3) ppm. HRMS (ESI-pos): m/z calc. for $C_{16}H_{22}NaN_4O_{10}$ [M+Na^+]: 453.12281; found: 453.12242, Δppm: 0.86.

Surface modification

Glass cover slides (35 mm, Menzel Gläser, Braunschweig, Germany) and 8-Well NuncTM LabTekTM II Chamber SlideTM System were covalently functionalized with gelatin. Briefly, glass cover slides were treated with piranha solution (7 mL H_2SO_4 (97 % v/v) and 3 mL H_2O_2 (30 % v/v) for 45 minutes and washed subsequently three times with ultrapure water for 5 minutes. The first step was not performed for the NuncTM Lab-TekTM II Chamber SlideTM Systems. Surfaces were treated with a 2 % aqueous solution of 3-aminopropyldimethylmethoxysilane (APTES) for 15 minutes and washed three times with ultrapure water. Both surfaces were then incubated with a 0.125 % aqueous solution of glutaraldehyde for 30 minutes, washed with ultrapure water and subsequently sterilized by UV irradiation for 60 minutes. Finally, the surfaces were incubated with a 2 % gelatin solution in PBS for 60 minutes and washed three times with PBS prior to use. [65]

Cell culture

NIH 3T3 fibroblasts (CRL-1658; ATCC, Manassas, VA) were maintained in 100 mm culture dishes in growth medium (DMEM containing heat-inactivated BCS (10 %), penicillin G (100 U mL^{-1}) and streptomycin (100 µg $µL^{-1}$)) at 37 °C under CO_2 (5 %). Prior to use, the cells were seeded (16.7x10^4 cells mL^{-1}, 300 µL growth medium per well) in 8-well NuncTM Lab-TekTM II Chamber SlideTM System or in 24-well plates (33.4x104 cells mL^{-1}, 600 µL growth medium per well) using two different growth media schemata. For **schema A** the cells were seeded using DMEM containing heat-inactivated FCS (20 %), penicillin G (100 U mL^{-1}) and streptomycin (100 µg $µL^{-1}$) and grown for 24 h at 37 °C under CO2 (5 %) with or without addition of Ac_4GlcNAz (50 µM). After 24 h the medium was changed to DMEM containing heat-inactivated FCS (10 %), penicillin G (100 U mL-1), streptomycin (100 µg $µL^{-1}$) and sodium L-ascorbate (50 µg mL^{-1}) with or without addition of Ac_4GlcNAz (50 µM). The medium was changed every 48 h up to day 6 and later every 24. For

schema B the cells were seeded using DMEM containing heat-inactivated BCS (10 %), penicillin G (100 U mL^{-1}) and streptomycin (100 µg $µL^{-1}$) and grown for 24 h at 37 °C under CO2 (5 %) with or without the addition of Ac4GlcNAz (50 µM). After 24 h the medium was changed using DMEM containing heat-inactivated BCS (10 %), penicillin G (100 U mL-1), streptomycin (100 µg $µL^{-1}$) and sodium L-ascorbate (50 µg mL^{-1}) with or without addition of Ac_4GlcNAz (50 µM). The medium was changed every 48 h up to day 6 and later every 24.

Isolation of cell derived matrices

Extracellular matrix components were isolated following existing protocols[40-41]. The medium was carefully aspirated and the cells were washed two times with PBS and subsequently incubated with ultrapure water for 15 minutes and a second time for 30 minutes followed by three additional washing steps with PBS. After water incubation, the cells were extracted using a triton-x-ammoniac buffer (0.5 % (v/v) triton-X and 20 mM NH_4OH in PBS pH 7.4) for 10 minutes at 37 °C. After that, the extraction buffer was removed by washing with PBS for five times.

Fluorescence imaging after click reaction on functionalized cell derived matrices

NIH 3T3 cells were cultured in 8-well NuncTM Lab-TekTM II Chambers for 9 days (Schema A and B) and the ECM was isolated as described. For the copper catalyzed click reaction, a mixture of $CuSO_4$ (50 µM), THPTA (250 µM), and sodium-L-ascorbate (2.5 mM) in PBS, which had been incubated for 10 minutes, was combined with Sulfo-Cy5-Alkyne (20 µM), and the solution was given on the ECM for 5 minutes at RT. For the strain-promoted azide-alkyne cycloaddition, DBCO-Sulfo-Cy5 (20 µM in PBS) was given to the ECM for 60 minutes at RT[36]. After the reaction, the cells were washed one time with growth medium followed by three washing steps using PBS. The ECM was blocked using 1x Roti®-Block for 60 minutes at RT and washed once with PBS. The ECM was visualized by detecting fibronectin using a combination of Mouse AntiFibronectin antibody (1:500 in PBS, overnight at 4 °C) and Goat Anti-Mouse IgG H&L Alexa Fluor® 488 antibody (1:200 in PBS, 90 minutes at RT). ECM was analyzed on a high-resolution AOBS SP2 confocal laser scanning microscope (Leica microsystem, Wetzla, Germany) with a 63x N.A. 1.4-0.60 Oil I BL HCX PL APO I objective. To avoid cross talk the emission signals were collected independently. Image processing was performed in ImageJ (http://imagej.nih.gov/ij/).

Western blot analysis of FCS and BCS sera

A series dilution of each serum (2, 1 and 0.5 µL of FCS and BCS, respectively) was analyzed using standard SDS-Page and Western blotting procedures. For detection of fibronectin, a mouse anti-fibronectin antibody (1:2000 in Tris buffered saline (TBS), containing 0.1 % (w/w) Tween20

(TBST)) was used. After incubation of the blot with a peroxidase conjugated second antibody, detection was performed by an enhanced chemiluminescence substrate and signals were subsequently monitored by a FluorChem FC 2 imaging system (Protein Simple, Santa Clara, USA).

Flow cytometry of FDA and PI stained un-extracted cell derived matrices

NIH 3T3 cells were cultured in 24-well plates for 9 days (Schema A and B) as described before. The medium was gently aspirated and the cells were washed with PBS and detached using an aqueous 0.005 % trypsin [m/V] and 0.025% EDTA [m/V] solution. Trypsin/EDTA activity was stopped by the addition of growth medium and resuspended in PBS. Prior, remaining ECM was removed manually with a tip. Cells were counted and equally divided in two parts and stained either with 0.01 µg/10^4 cells fluorescein diacetate (FDA) (λ_{ex}= 492 nm λ_{em}= 517 nm) or 0.003 µg/10^4 cells propidium iodide (PI) (λ_{ex}= 540 nm λ_{em}= 608 nm) dissolved in PBS for 3 minutes at room temperature. The cells were subsequently analyzed by flow cytometry on a FACS Calibur system. For detection a 488 nm Laser was chosen with the emission channel FL1 (530 nm / ± 15 nm) for FDA and FL 2 (585 nm / ± 21 nm) for PI, respectively. A total number of 5000 events were counted with BD CellQuestTM Pro and the geometric mean fluorescence intensity was determined for each condition using Flowing Software (version 2.5.1; Turku Bioimaging).

Fluorescence imaging of FDA and PI stained un-extracted cell derived matrices

NIH-3T3 cells were cultured in 24-well plates for 9 days as (Schema A and B) described before. The medium was gently aspirated and the cells were washed three times with PBS. A solution of FDA (15 µg/mL) and PI (2 µg/mL) in PBS was added to the cells. After incubation for 5 minutes at room temperature cells were washed three times with PBS. Matrices were analyzed using an Axio Observer.Z1 microscope equipped with an A-Plan 10x/0.25 Ph1 objective (Zeiss). The images were recorded with a phase-contrast channel, 38 HE Green Fluorescent Protein (λ_{ex}= 450-490 nm λ_{em}= 500-550 nm) and a 43 DsRed Reflector (λ_{ex}= 538-562 nm λ_{em}= 570-640 nm) with a mercury vapor short-arc lamp.

Fluorescence imaging of un-extracted cell derived matrices

NIH 3T3 cells were cultured in in 8-well NuncTM Lab-TekTM II Chambers for 9 days (Schema A and B) as described before. The medium was gently aspirated and cells were washed three times with PBS before fixation with 2 % PFA solution in PBS for 15 minutes at room temperature. Cells were washed twice with PBS following by permeabilization using a 0.2 % triton-x solution in PBS for 15 minutes at room temperature. After fixation the Cells were washed again twice with PBS and blocked using 1x Roti®-Block for 60 minutes at RT and washed twice with PBS. Cells and derived matrices

were visualized by detecting fibronectin using a combination of Mouse Anti-Fibronectin antibody (1:500 in PBS, overnight at 4 °C) and goat anti-rabbit IgG H&L Alexa Fluor® 633 antibody (1:200 in PBS, 90 minutes at RT), filamentous actin using phalloidin-488 (165 nM in PBS, 20 minutes at RT) and DAPI (1:1000 in PBS, 10 minutes at RT). ECM was analyzed on a high-resolution AOBS SP2 confocal laser scanning microscope (Leica microsystem, Wetzla, Germany) with a 63x N.A. 1.4-0.60 Oil I BL HCX PL APO I objective. To avoid cross talk the emission signals were collected independently. Image processing was performed in ImageJ (http://imagej.nih.gov/ij/).

Scanning electron microscopy of cell derived matrices

Cells were cultured in 24-well plates on surface modified glass cover slides (vide supra) for 9 days (Schema A and B). CDMs were isolated as described before, fixed with 2.5 % glutaraldehyde for 30 minutes at RT and were subsequently dried using a series of acetone dilutions (30 %-50 %-70 %-90 %-100 %, each step was performed for 10 minutes at RT). Samples were sputter and images were recorded using a JSM-7500F filed emission scanning electron microscope (Jeol, Tokyo, Japan).

Fluorescence imaging of re-seeded extracted cell derived matrices

NIH 3T3 cells were cultured in in 8-well NuncTM LabTekTM II Chambers for 9 days (Schema A and B) and ECM was isolated as described before. Fibronectin coated 8-well NuncTM LabTekTM II Chambers were used as control. For this purpose, the chambers were coated with a mouse fibronectin-solution (5 µg/mL in PBS) for 1 hour at 37 °C and washed once with PBS.[40] NIH 3T3 cells were stained with Hoechst 33342 (1 µL/mL) for 15 minutes at 37 °C, washed three times with PBS and seeded (2000 cells per well in 300 µl growth medium) on the CDMs and fibronectin coated chambers. After 16 hours the cells were washed with PBS and stained with FDA (15 µg FDA per mL PBS) for 5 minutes and washed three times with PBS. CDMs and Fibronectin coated chambers were analyzed using an Axio Observer.Z1 microscope equipped with an A-Plan 10x/0.25 Ph1 objective (Zeiss).. The images were recorded with a phase-contrast channel, 38 HE Green Fluorescent Protein (λ_{ex}= 450-490 nm λ_{em}= 500-550 nm) and a 49 DAPI (λ_{ex}= 365 nm λ_{em}= 425-470 nm) with a mercury vapor short-arc lamp. Image processing was performed in ImageJ (http://imagej.nih.gov/ij/).

Western blot analysis of functionalized cell derived matrices

Cells were treated in 24-well plates for 9 days (Schema A and B) and the ECM was isolated as described before. After isolation of the extracellular matrix components, the glycoengineered CDM was reacted with acetylene-PEG_4-Biotin using copper catalyzed click reaction as described[36]. A mixture of $CuSO_4$ (50 µM), THPTA (250 µM), and sodium-L-ascorbate (2.5 mM) in PBS, which

had been incubated for 10 minutes, was combined with acetylen-PEG_4-biotin (20 µM), and the solution was given on the CDM for 5 minutes at RT. The CDM was flushed with growth medium followed by three PBS washing steps. The ECM-proteins were extracted according to a two-step protocol[45]. The soluble fraction was obtained by scratching the ECM using an SDS containing buffer (5 % (w/w) SDS, 10 % glycerol (w/w) and 60 mM Tris-HCl, pH 6.8) and by collecting the suspension. The mixture was heated up to 95 °C for 5 minutes and was centrifuged at $1.6x10^4$ g for 10 minutes to separate soluble from insoluble components. The supernatant was collected. Insoluble ECM components were extracted by incubating the pellet with SDSurea-buffer (8 M urea, 4 % (w/w) SDS, 12.5 mM EDTA and 60 mM Tris-HCl pH 6.8) for 30 minutes at RT. The mixture was centrifuged at $1.6x10^4$ g, 10 minutes and the supernatant was pooled with the soluble fraction. Protein concentration of each fraction was assessed using a standard BCA assay. 20 µg of each sample were used for analysis following standard SDS-Page and Western blotting procedures. Prior to antibody staining, Ponceau red staining was performed. For detection of fibronectin, a mouse anti-fibronectin antibody (1:2000 in Tris buffered saline (TBS), containing 0.1% (w/w) Tween-20 (TBST)) was used. After incubation of the blot with a peroxidase conjugated second antibody, signals were detected using an enhanced chemiluminescence substrate and were subsequently monitored by a FluorChem FC 2 imaging system (Protein Simple, Santa Clara, USA). After detection of fibronectin signals, the blot was stripped (50 mM Tris-HCl, 2 % (w/w) SDS and 0.8 % 2-mercaptoethanol pH 6.8) for 45 minutes at 50 °C and was washed subsequently under rinsing water for 1 hour. Biotin signals were detected using streptavidin-HRP (1:2000 in TBST) as described above.

Fluorescence imaging after myostatin immobilization on glycoengineered cell derived matrices

NIH-3T3 cells were cultured in 8-well NuncTM Lab-TekTM II Chambers for 9 days (Schema A) with the addition of Ac_4GlcNAz and the ECM was isolated as described before. After isolation, CDMs were reacted with carboxyfluorescein-alkyne-myostatin inhibitor using CuAAC procedures. Two different mixtures were used for the CuAAC. A mixture of $CuSO_4$ (100 µM), THPTA (500 µM), and sodium-L-ascorbate (2.5 mM) in PBS and a mixture where the $CuSO_4$ was replaced by PBS, were combined with carboxyfluorescein-alkyne-myostatin inhibitor (100 µM), and the click reaction mixtures were added to the glycoengineered CDM for 1 hour at RT, respectively. After the reaction, the CDM was washed four times with PBS and blocked using 1x Roti®-Block for 60 minutes at RT. ECM was washed with PBS prior incubation with a rabbit AntiFibronectin antibody (1:500 in PBS, overnight at 4 °C) and goat anti-rabbit IgG H&L Alexa Fluor® 633 antibody (1:200 in PBS, 90 minutes at RT). CDMs were analyzed on a high resolution AOBS SP2 confocal laser scanning microscope (Leica microsystem, Wetzla, Germany) with a 63x N.A. 1.4-0.60 Oil I BL HCX

PL APO I objective. To avoid cross-talk the emission signals were collected independently. Image processing was performed in ImageJ (http://imagej.nih.gov/ij/).

Solid phase peptide synthesis of a myostatin inhibitor peptide

Synthesis of the myostatin inhibitor was performed according to existing protocols[59]. In brief, the myostatin inhibitor was synthesized manually using Fmoc strategy as described before[66]. The sequence for the MI was VATQGQCTRWPWMCPPQGW-Peg(3)-propargyl glycine with 5(6)-Carboxyfluorescein coupled to the N-terminal region. The purified peptide was analyzed by RP-HPLC and HRMS (ESI-pos) m/z calc. for $C_{137}H_{178}N_{36}O_{32}S_3$ [M+3H$^+$] 982.08262; found 982.08308.

Statistics

All data were displayed as mean ± standard deviation (SD) unless specified otherwise. All statistical analyses were performed using Minitab 16 (Minitab, Coventry, UK). Statistical significance was calculated using one-way ANOVA followed by pairwise comparison using Tukey's post-test. Results were considered statistically significant at $*p \leq 0.01$.

Supporting Information

Supporting Figures

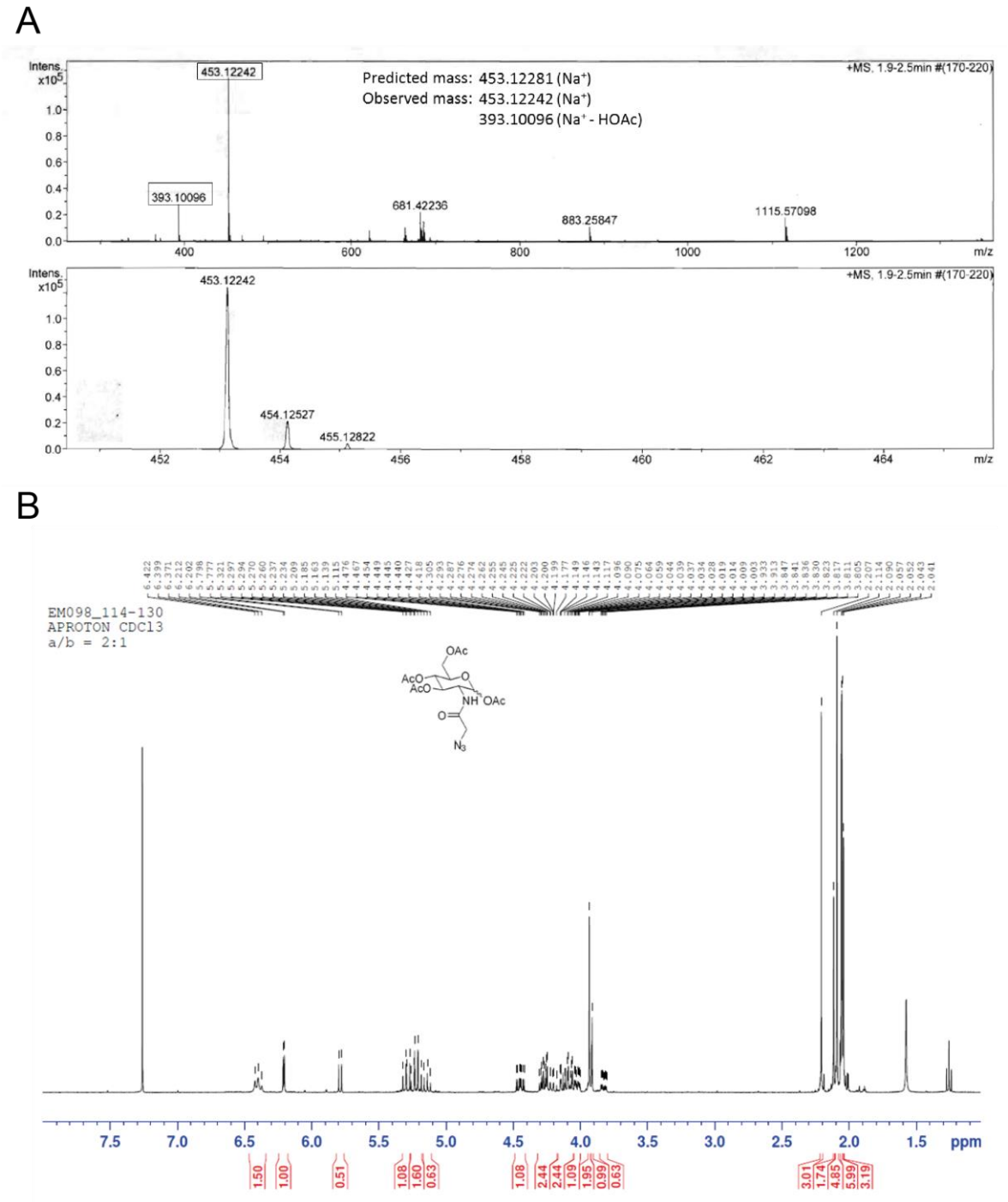

Figure S 1: (A) HRMS Esi-pos spectra and (B) 1H-NMR spectra of synthesized Ac4GlcNAz to asses identification and purity. Obs. average mass [M+Na+] = 453.12242 Da, calc. average mass [M+Na+] = 453.12281 Da.

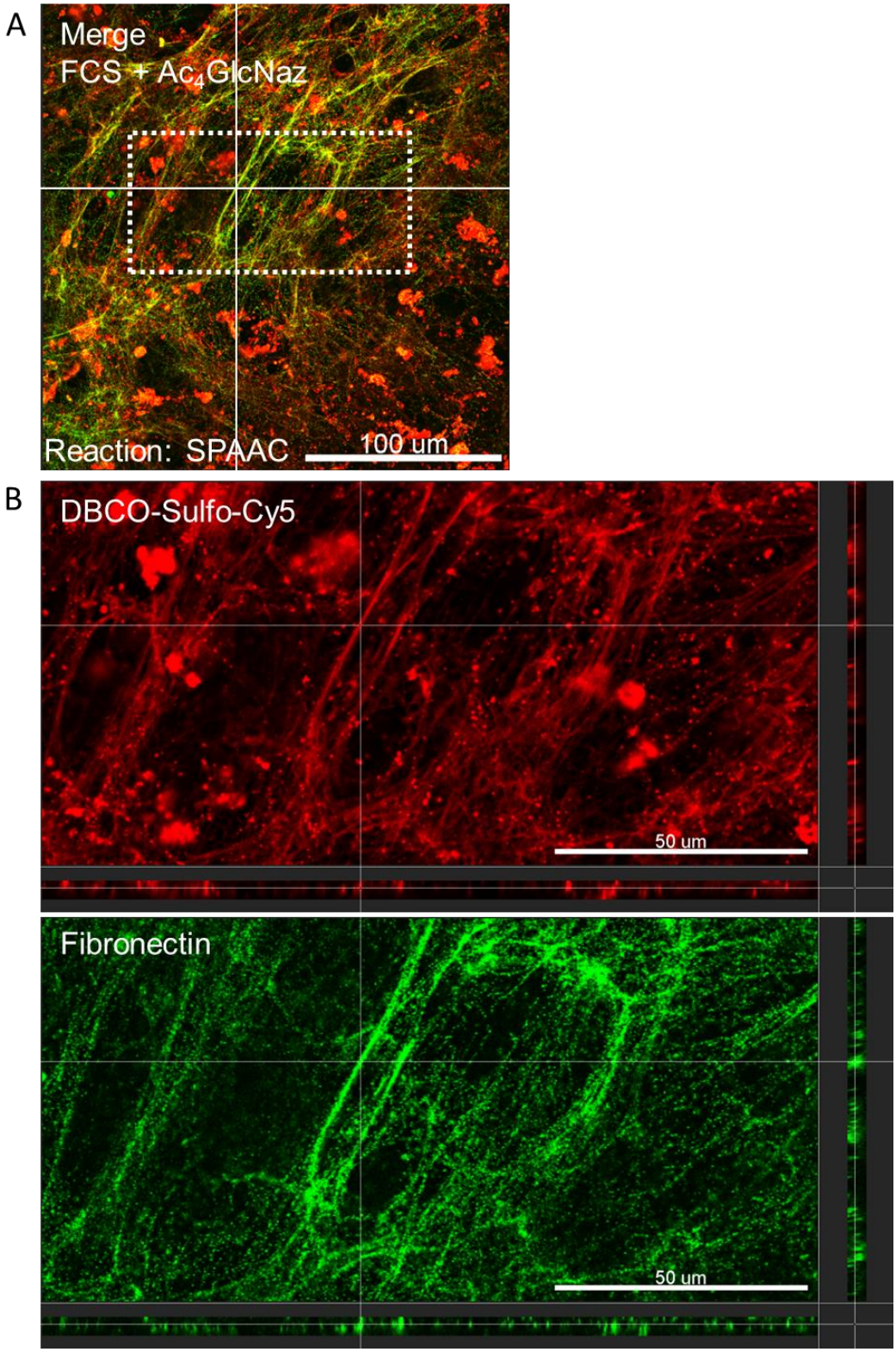

Figure S 2: (A) Merged confocal images of CDM derived from FCS with the addition of Ac4GlcNAz. Incorporation of the azide-monosaccharide is shown in red after SPAAC reaction using DBCO-Sulfo-Cy5; Fibronectin is shown in green. Dashed white square displays the region of interest for the orthogonal view (B).

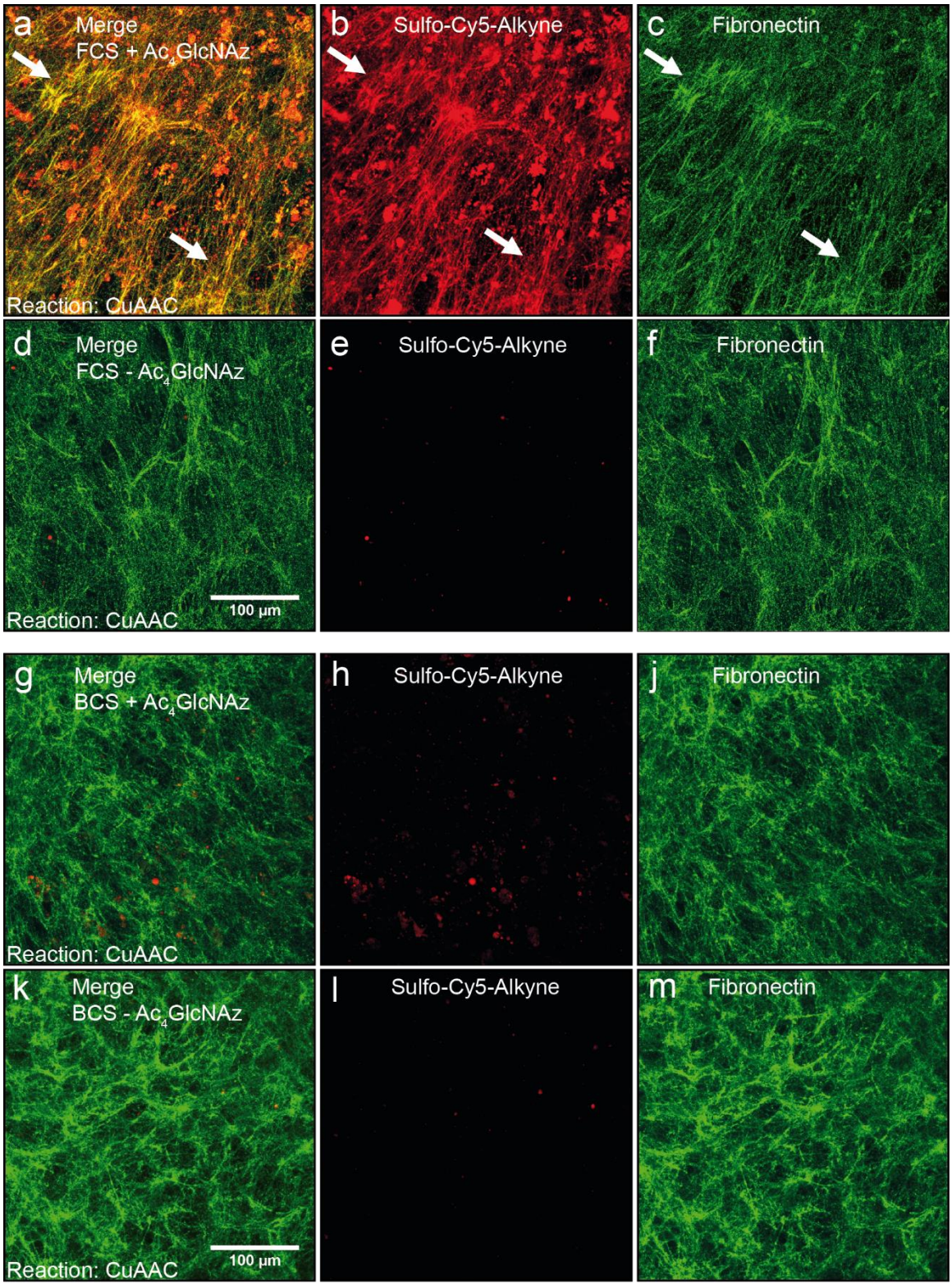

Figure S 3: Confocal images of CDMs derived from FCS (a-f) and BCS (g-m) with or without the addition of Ac4GlcNAz. The CDMs were reacted with Sulfo-Cy5-Alkyne using CuAAC. Incorporation of the azide-monosaccharide is shown in red after Cy5-labeling using CuAAC (b,e,h,l); Fibronectin is shown in green (c,f,j,m); Merge is shown in yellow (a,d,g,k).

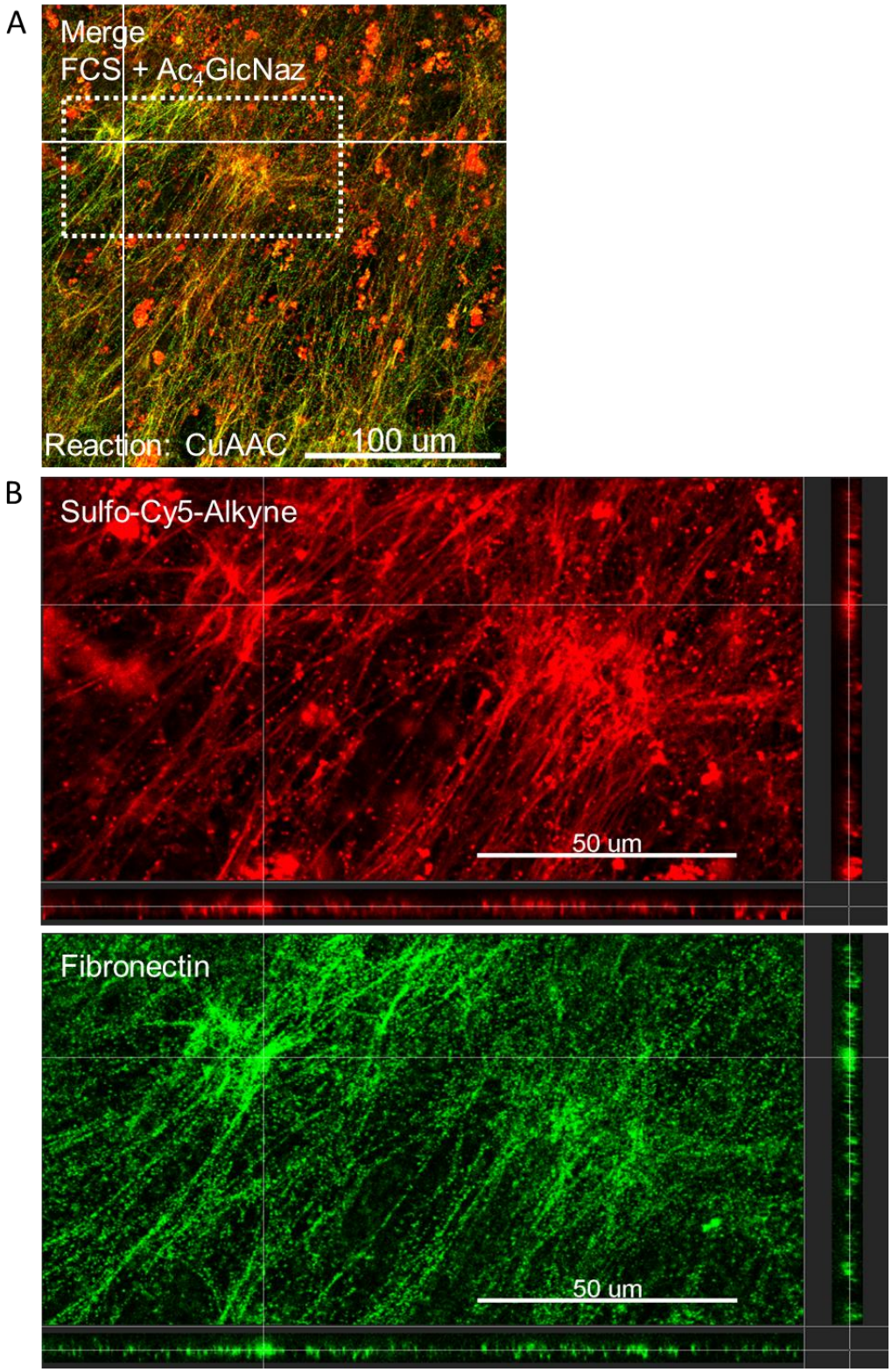

Figure S 4: (A) Merged confocal images of CDM derived from FCS with the addition of Ac4GlcNAz. Incorporation of the azide-monosaccharide is shown in red after CuAAC reaction S16 using Sulfo-Cy5-Alkyne; Fibronectin is shown in green. Dashed white square displays the region of interest for the orthogonal view (B).

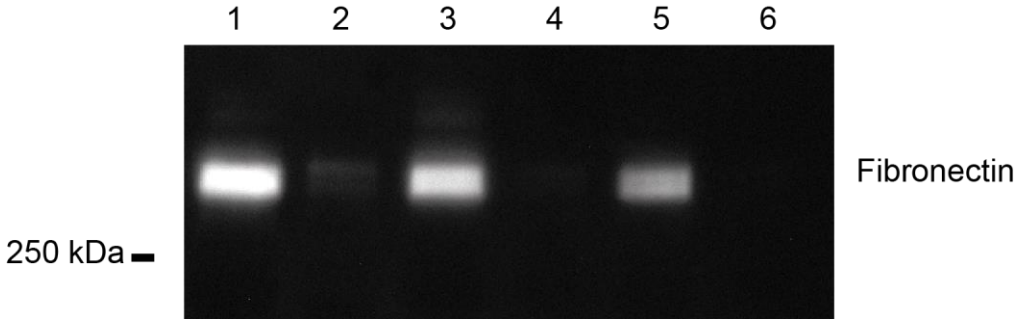

Figure S 5: Western blot analysis of 2µl, 1µL and 0.5µL BCS (Lane 1, 3, 5) and FCS (Lane 2, 4, 6) undiluted sera.

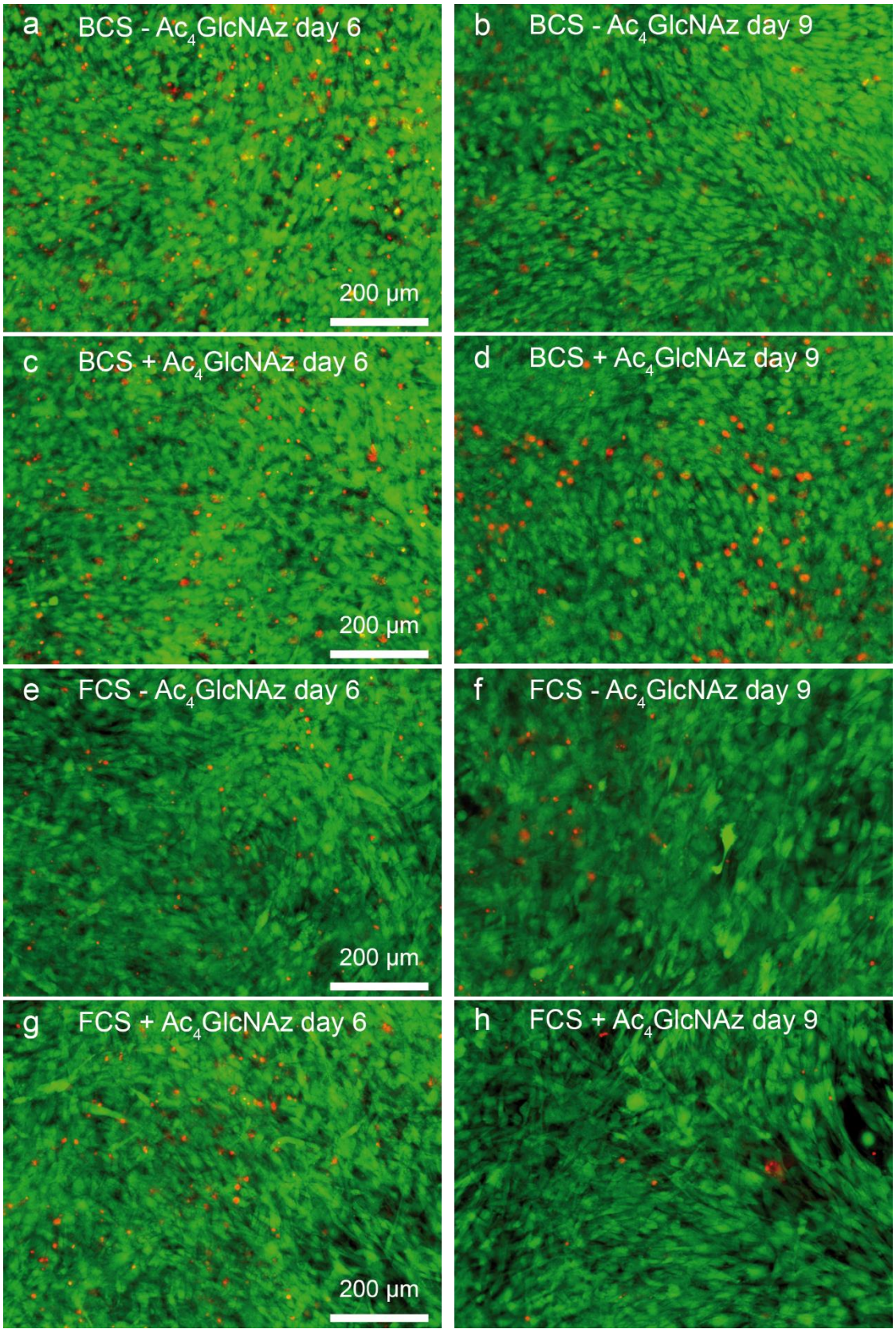

Figure S 6: Fluorescent images of Ac4GlcNAz treated and untreated BCS (a-d) and FCS (e-h) derived CDMs after 6 and 9 days stained with fluorescein diacetate (green) and propidium iodide (red).

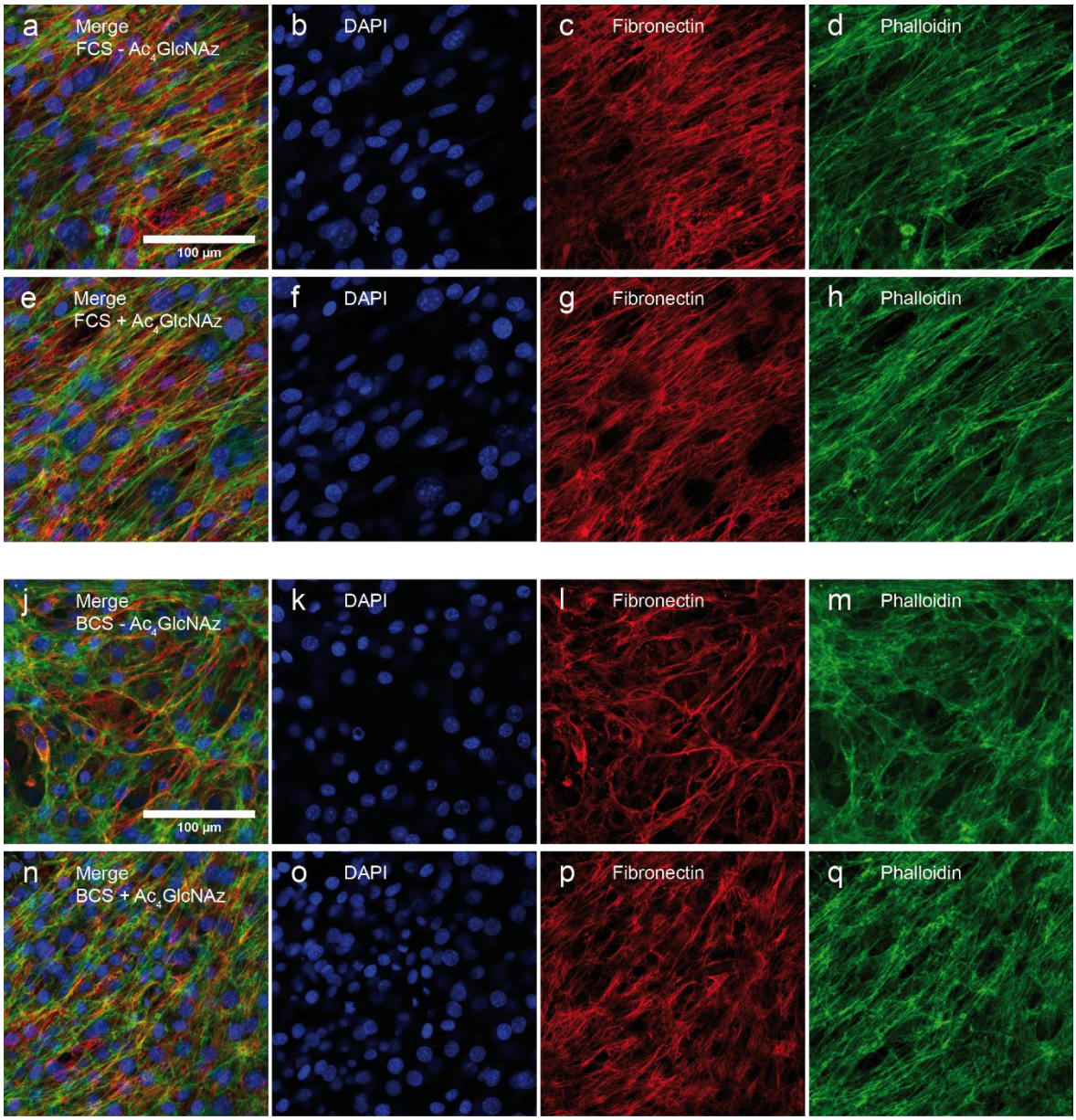

Figure S 7: Confocal images of unextracted CDMs derived from FCS (a-h) and BCS (j-q) with or without the addition of Ac4GlcNAz after 9 days. The CDMs were fixed with paraformaldehyde and stained for fibronectin with a red fluorescent Alexa Fluor® 633 antibody conjugate (c, g, l, p). F-actin was visualized with a green fluorescent AlexaFluor® 488 phalloidin conjugate (d, h, m, q). Nuclei were stained with Dapi (b, f, k, o). (a, e, j, n) shows the merge.

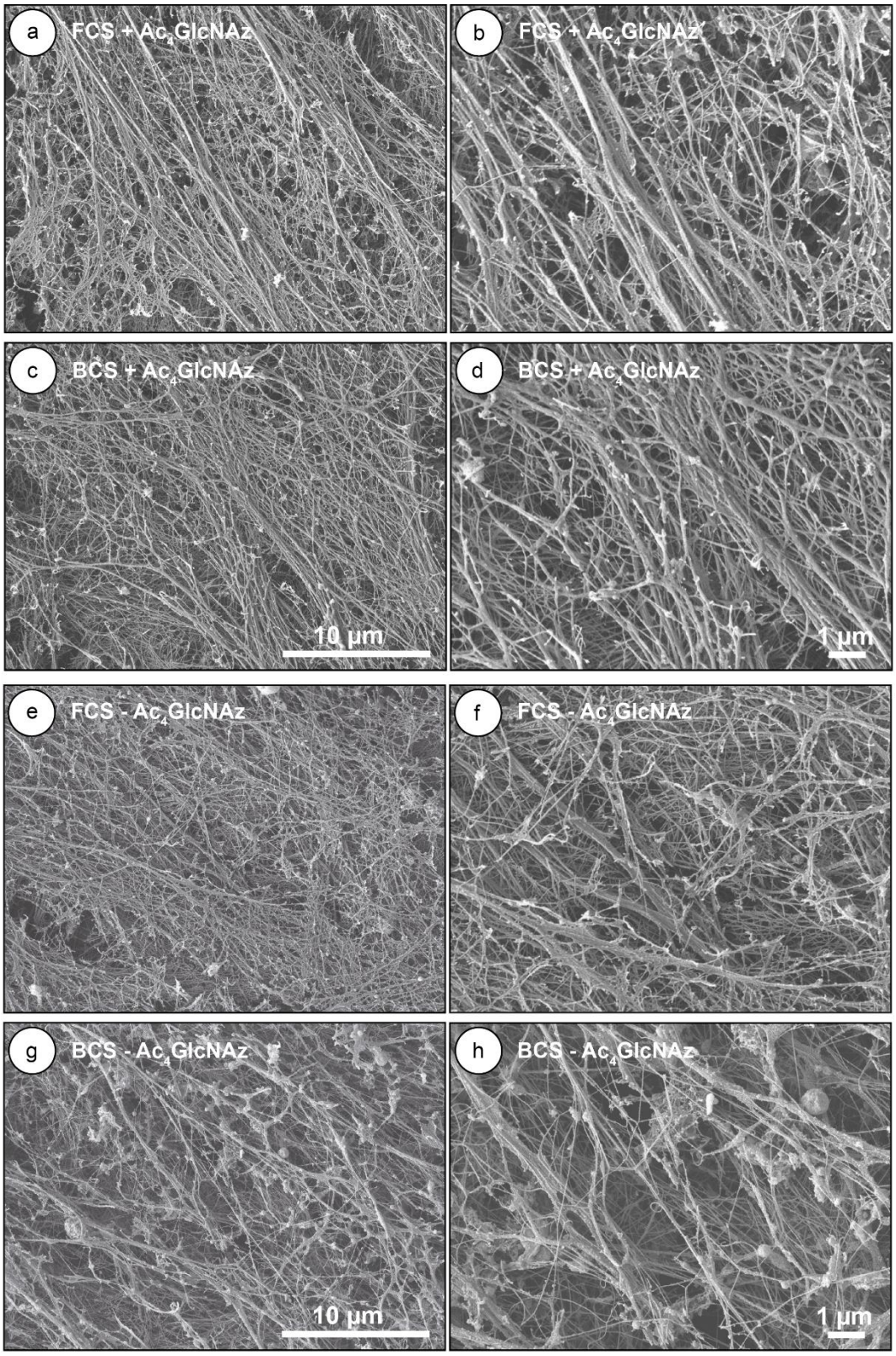

Figure S 8: Scanning electron images of CDMs derived from FCS with (a,b) or without (c,d) the addition of Ac4GlcNAz and BCS with (e,f) or without (g,h) the addition of Ac4GlcNAz. (a,c,e,g) shows 4000x magnification. (b,d,f,h) shows 10,000x magnification.

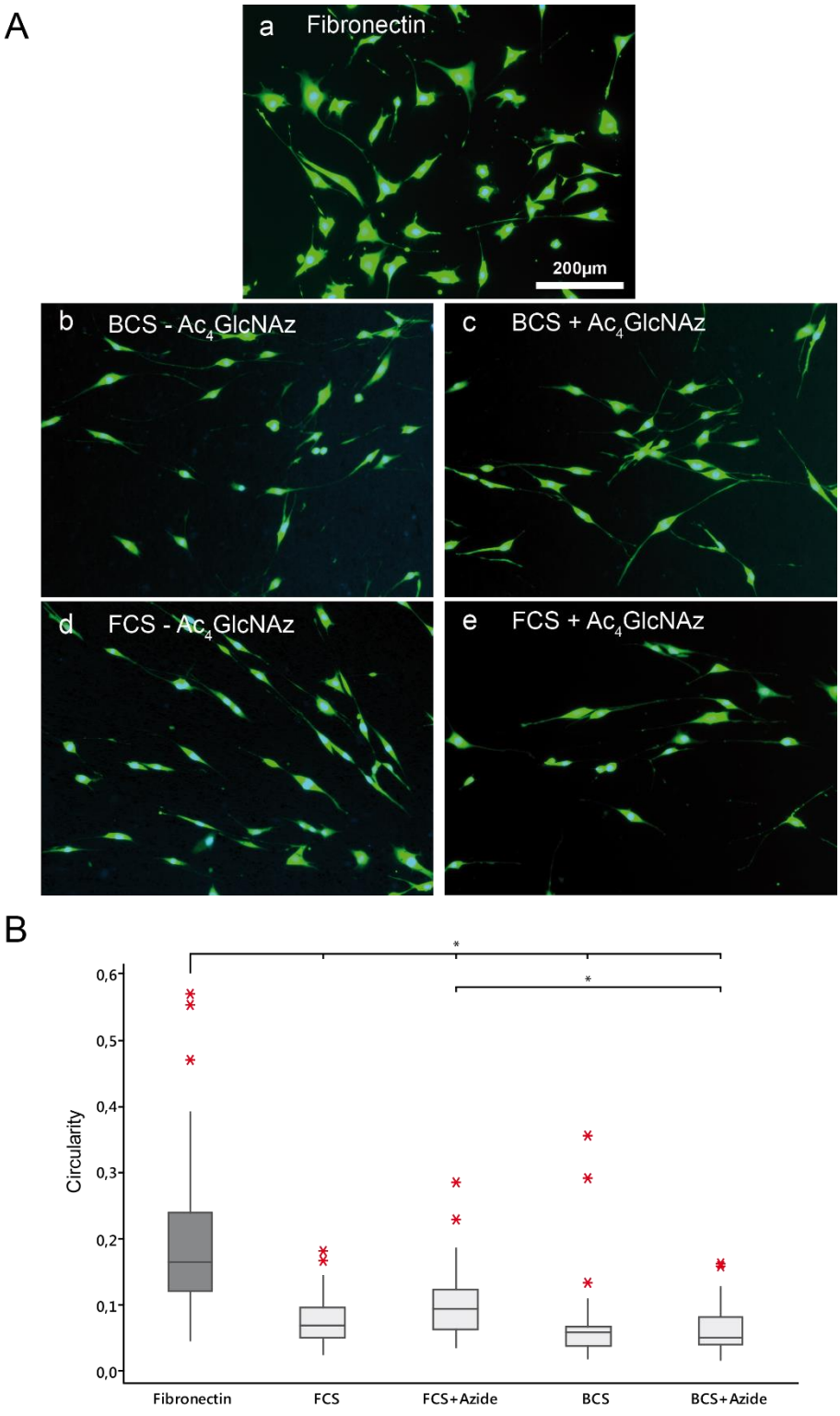

Figure S 9: (A) Fluorescent images of replated NIH 3T3 fibroblasts on mouse fibronectin coated surfaces (a) as well as Ac4GlcNAz treated and untreated BCS (b, c) and FCS (d, e) extracted CDMs. Cells were preincubated with Hoechst 33342 (blue) prior to seeding and were stained S21 after incubation on the surfaces with fluorescein diacetate. (B) Determination of the circularity of replated cells on mouse fibronectin coated wells and CDMs, respectively. Results were displayed as mean with standard deviation ($p \leq 0.01$, $n > 30$).

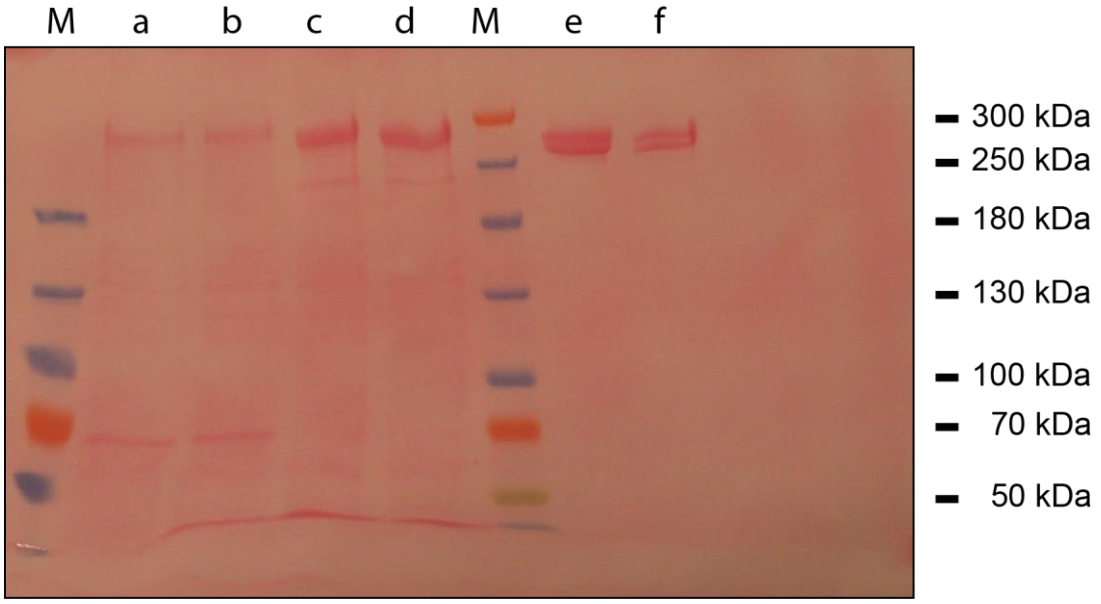

Figure S 10: Ponceau red staining of CDMs derived from FCS with (a) or without (b) the addition of Ac4GlcNAz and BCS with (c) or without (d) the addition of Ac4GlcNAz after CuAAC reaction with acetylen-PEG4-biotin. 10 µg (e) and 5 µg (f) mouse fibronectin was used as control. (M) shows the markers.

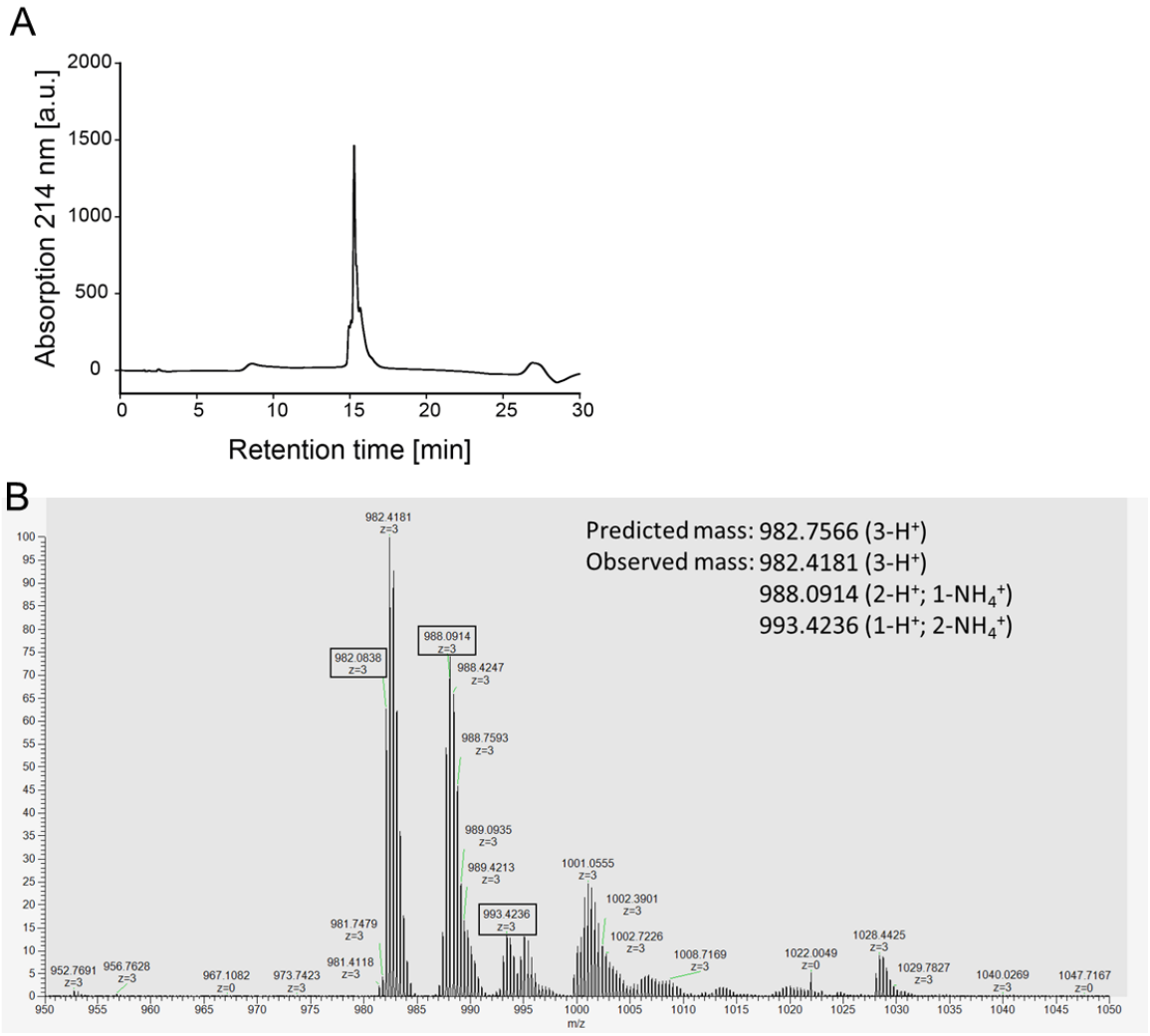

Figure S 11: RP-HPLC analytics and HRMS ESI-pos spectra of synthesized myostatin inhibitor (MI) for identification and purity. (A) RP-HPLC chromatogram and (B) HMRS spectra of the carboxyfluorescein-modified variant. Obs. average mass [M+3H+] = 982.08308 Da, calc. average mass [M+3H+] = 982.08262 Da.

Acknowledgments

The financial support of the Sino-German center for the promotion of sciences (Grant GZ1094), the German Research Foundation (Grant ME 3820/3-1), and the TRR SFB 225 (397978692) Biofabrikation are gratefully acknowledged.

References

1. Neffe, A. T.; Wischke, C.; Racheva, M.; Lendlein, A., Progress in biopolymer-based biomaterials and their application in controlled drug delivery. *Expert Rev Med Devices* **2013,** *10* (6), 813-33. DOI: 10.1586/17434440.2013.839209.

2. Briquez, P. S.; Hubbell, J. A.; Martino, M. M., Extracellular Matrix-Inspired Growth Factor Delivery Systems for Skin Wound Healing. *Adv Wound Care (New Rochelle)* **2015,** *4* (8), 479-489. DOI: 10.1089/wound.2014.0603.
3. Minardi, S.; Taraballi, F.; Pandolfi, L.; Tasciotti, E., Patterning Biomaterials for the Spatiotemporal Delivery of Bioactive Molecules. *Front Bioeng Biotechnol* **2016,** *4*, 45. DOI: 10.3389/fbioe.2016.00045.
4. Hinderer, S.; Layland, S. L.; Schenke-Layland, K., ECM and ECM-like materials - Biomaterials for applications in regenerative medicine and cancer therapy. *Adv Drug Deliv Rev* **2016,** *97*, 260-9. DOI: 10.1016/j.addr.2015.11.019.
5. Jiang, B.; Akar, B.; Waller, T. M.; Larson, J. C.; Appel, A. A.; Brey, E. M., Design of a composite biomaterial system for tissue engineering applications. *Acta Biomater* **2014,** *10* (3), 1177-86. DOI: 10.1016/j.actbio.2013.11.029.
6. Zhu, Y.; Pyda, M.; Cebe, P., Electrospun fibers of poly(l

-lactic acid) containing lovastatin with potential applications in drug delivery. *Journal of Applied Polymer Science* **2017,** *134* (36), 45287. DOI: 10.1002/app.45287.
7. Chiono, V.; Mozetic, P.; Boffito, M.; Sartori, S.; Gioffredi, E.; Silvestri, A.; Rainer, A.; Giannitelli, S. M.; Trombetta, M.; Nurzynska, D.; Di Meglio, F.; Castaldo, C.; Miraglia, R.; Montagnani, S.; Ciardelli, G., Polyurethane-based scaffolds for myocardial tissue engineering. *Interface Focus* **2014,** *4* (1), 20130045. DOI: 10.1098/rsfs.2013.0045.
8. Martin, J. R.; Gupta, M. K.; Page, J. M.; Yu, F.; Davidson, J. M.; Guelcher, S. A.; Duvall, C. L., A porous tissue engineering scaffold selectively degraded by cell-generated reactive oxygen species. *Biomaterials* **2014,** *35* (12), 3766-76. DOI: 10.1016/j.biomaterials.2014.01.026.
9. Gogolewski, S.; Gorna, K.; Turner, A. S., Regeneration of bicortical defects in the iliac crest of estrogen-deficient sheep, using new biodegradable polyurethane bone graft substitutes. *J Biomed Mater Res A* **2006,** *77* (4), 802-10. DOI: 10.1002/jbm.a.30669.
10. Dash, T. K.; Konkimalla, V. B., Poly-small je, Ukrainian-caprolactone based formulations for drug delivery and tissue engineering: A review. *J Control Release* **2012,** *158* (1), 15-33. DOI: 10.1016/j.jconrel.2011.09.064.
11. Williams, P. A.; Campbell, K. T.; Gharaviram, H.; Madrigal, J. L.; Silva, E. A., Alginate-Chitosan Hydrogels Provide a Sustained Gradient of Sphingosine-1-Phosphate for Therapeutic Angiogenesis. *Ann Biomed Eng* **2017,** *45* (4), 1003-1014. DOI: 10.1007/s10439-016-1768-2.
12. Wu, Z. M.; Zhang, X. G.; Zheng, C.; Li, C. X.; Zhang, S. M.; Dong, R. N.; Yu, D. M., Disulfide-crosslinked chitosan hydrogel for cell viability and controlled protein release. *Eur J Pharm Sci* **2009,** *37* (3-4), 198-206. DOI: 10.1016/j.ejps.2009.01.010.
13. Gombotz, W., Protein release from alginate matrices. *Advanced Drug Delivery Reviews* **1998,** *31* (3), 267-285. DOI: 10.1016/s0169-409x(97)00124-5.
14. Rong, J. J.; Liang, M.; Xuan, F. Q.; Sun, J. Y.; Zhao, L. J.; Zhen, H. Z.; Tian, X. X.; Liu, D.; Zhang, Q. Y.; Peng, C. F.; Yao, T. M.; Li, F.; Wang, X. Z.; Han, Y. L.; Yu, W. T., Alginate-calcium microsphere loaded with thrombin: a new composite biomaterial for hemostatic embolization. *Int J Biol Macromol* **2015,** *75*, 479-88. DOI: 10.1016/j.ijbiomac.2014.12.043.
15. Mejia Oneto, J. M.; Gupta, M.; Leach, J. K.; Lee, M.; Sutcliffe, J. L., Implantable biomaterial based on click chemistry for targeting small molecules. *Acta Biomater* **2014,** *10* (12), 5099-105. DOI: 10.1016/j.actbio.2014.08.019.
16. Uebersax, L.; Mattotti, M.; Papaloizos, M.; Merkle, H. P.; Gander, B.; Meinel, L., Silk fibroin matrices for the controlled release of nerve growth factor (NGF). *Biomaterials* **2007,** *28* (30), 4449-60. DOI: 10.1016/j.biomaterials.2007.06.034.
17. Wenk, E.; Merkle, H. P.; Meinel, L., Silk fibroin as a vehicle for drug delivery applications. *J Control Release* **2011,** *150* (2), 128-41. DOI: 10.1016/j.jconrel.2010.11.007.
18. Numata, K.; Kaplan, D. L., Silk-based delivery systems of bioactive molecules. *Adv Drug Deliv Rev* **2010,** *62* (15), 1497-508. DOI: 10.1016/j.addr.2010.03.009.

19. Germershaus, O.; Lühmann, T.; Rybak, J. C.; Ritzer, J.; Meinel, L., Application of natural and semi-synthetic polymers for the delivery of sensitive drugs. *International Materials Reviews* **2014,** *60* (2), 101-131. DOI: 10.1179/1743280414y.0000000045.
20. Fitzpatrick, L. E.; McDevitt, T. C., Cell-derived matrices for tissue engineering and regenerative medicine applications. *Biomater Sci* **2015,** *3* (1), 12-24. DOI: 10.1039/C4BM00246F.
21. Zhu, J.; Clark, R. A., Fibronectin at select sites binds multiple growth factors and enhances their activity: expansion of the collaborative ECM-GF paradigm. *J Invest Dermatol* **2014,** *134* (4), 895-901. DOI: 10.1038/jid.2013.484.
22. von der Mark, K.; Park, J.; Bauer, S.; Schmuki, P., Nanoscale engineering of biomimetic surfaces: cues from the extracellular matrix. *Cell Tissue Res* **2010,** *339* (1), 131-53. DOI: 10.1007/s00441-009-0896-5.
23. Martino, M. M.; Hubbell, J. A., The 12th-14th type III repeats of fibronectin function as a highly promiscuous growth factor-binding domain. *FASEB J* **2010,** *24* (12), 4711-21. DOI: 10.1096/fj.09-151282.
24. Taipale, J.; Keski-Oja, J., Growth factors in the extracellular matrix. *FASEB J* **1997,** *11* (1), 51-9.
25. Badylak, S. F.; Freytes, D. O.; Gilbert, T. W., Extracellular matrix as a biological scaffold material: Structure and function. *Acta Biomater* **2009,** *5* (1), 1-13. DOI: 10.1016/j.actbio.2008.09.013.
26. Parmaksiz, M.; Dogan, A.; Odabas, S.; Elcin, A. E.; Elcin, Y. M., Clinical applications of decellularized extracellular matrices for tissue engineering and regenerative medicine. *Biomed Mater* **2016,** *11* (2), 022003. DOI: 10.1088/1748-6041/11/2/022003.
27. Martino, M. M.; Briquez, P. S.; Guc, E.; Tortelli, F.; Kilarski, W. W.; Metzger, S.; Rice, J. J.; Kuhn, G. A.; Muller, R.; Swartz, M. A.; Hubbell, J. A., Growth factors engineered for super-affinity to the extracellular matrix enhance tissue healing. *Science* **2014,** *343* (6173), 885-8. DOI: 10.1126/science.1247663.
28. Mitchell, A. C.; Briquez, P. S.; Hubbell, J. A.; Cochran, J. R., Engineering growth factors for regenerative medicine applications. *Acta biomaterialia* **2016,** *30*, 1-12. DOI: 10.1016/j.actbio.2015.11.007.
29. Fruh, S. M.; Spycher, P. R.; Mitsi, M.; Burkhardt, M. A.; Vogel, V.; Schoen, I., Functional modification of fibronectin by N-terminal FXIIIa-mediated transamidation. *Chembiochem* **2014,** *15* (10), 1481-6. DOI: 10.1002/cbic.201402099.
30. Jones, M. E.; Messersmith, P. B., Facile coupling of synthetic peptides and peptide-polymer conjugates to cartilage via transglutaminase enzyme. *Biomaterials* **2007,** *28* (35), 5215-24. DOI: 10.1016/j.biomaterials.2007.08.026.
31. Zisch, A. H.; Schenk, U.; Schense, J. C.; Sakiyama-Elbert, S. E.; Hubbell, J. A., Covalently conjugated VEGF--fibrin matrices for endothelialization. *J Control Release* **2001,** *72* (1-3), 101-13.
32. Luhmann, T.; Hanseler, P.; Grant, B.; Hall, H., The induction of cell alignment by covalently immobilized gradients of the 6th Ig-like domain of cell adhesion molecule L1 in 3D-fibrin matrices. *Biomaterials* **2009,** *30* (27), 4503-12. DOI: 10.1016/j.biomaterials.2009.05.041.
33. Hong, V.; Steinmetz, N. F.; Manchester, M.; Finn, M. G., Labeling live cells by copper-catalyzed alkyne--azide click chemistry. *Bioconjugate chemistry* **2010,** *21* (10), 1912-6. DOI: 10.1021/bc100272z.
34. Baskin, J. M.; Prescher, J. A.; Laughlin, S. T.; Agard, N. J.; Chang, P. V.; Miller, I. A.; Lo, A.; Codelli, J. A.; Bertozzi, C. R., Copper-free click chemistry for dynamic in vivo imaging. *Proceedings of the National Academy of Sciences of the United States of America* **2007,** *104* (43), 16793-7. DOI: 10.1073/pnas.0707090104.
35. Laughlin, S. T.; Bertozzi, C. R., Metabolic labeling of glycans with azido sugars and subsequent glycan-profiling and visualization via Staudinger ligation. *Nat Protoc* **2007,** *2* (11), 2930-44. DOI: 10.1038/nprot.2007.422.
36. Gutmann, M.; Memmel, E.; Braun, A. C.; Seibel, J.; Meinel, L.; Luhmann, T., Biocompatible Azide-Alkyne "Click" Reactions for Surface Decoration of Glyco-Engineered Cells.

Chembiochem : a European journal of chemical biology **2016,** *17* (9), 866-75. DOI: 10.1002/cbic.201500582.
37. Sarkar, A. K.; Fritz, T. A.; Taylor, W. H.; Esko, J. D., Disaccharide uptake and priming in animal cells: inhibition of sialyl Lewis X by acetylated Gal beta 1-->4GlcNAc beta-O-naphthalenemethanol. *Proceedings of the National Academy of Sciences* **1995,** *92* (8), 3323-3327. DOI: 10.1073/pnas.92.8.3323.
38. Homann, A.; Qamar, R. U.; Serim, S.; Dersch, P.; Seibel, J., Bioorthogonal metabolic glycoengineering of human larynx carcinoma (HEp-2) cells targeting sialic acid. *Beilstein journal of organic chemistry* **2010,** *6*, 24. DOI: 10.3762/bjoc.6.24.
39. Canty, E. G.; Kadler, K. E., Procollagen trafficking, processing and fibrillogenesis. *J Cell Sci* **2005,** *118* (Pt 7), 1341-53. DOI: 10.1242/jcs.01731.
40. Yamada, K. M., Extracellular Matrix. **2009**. DOI: 10.1002/0471143030.cb1000s45.
41. Castello-Cros, R.; Cukierman, E., Stromagenesis during tumorigenesis: characterization of tumor-associated fibroblasts and stroma-derived 3D matrices. *Methods in molecular biology* **2009,** *522*, 275-305. DOI: 10.1007/978-1-59745-413-1_19.
42. To, W. S.; Midwood, K. S., Plasma and cellular fibronectin: distinct and independent functions during tissue repair. *Fibrogenesis Tissue Repair* **2011,** *4*, 21. DOI: 10.1186/1755-1536-4-21.
43. Frantz, C.; Stewart, K. M.; Weaver, V. M., The extracellular matrix at a glance. *J Cell Sci* **2010,** *123* (Pt 24), 4195-200. DOI: 10.1242/jcs.023820.
44. Schwarzbauer, J. E.; DeSimone, D. W., Fibronectins, their fibrillogenesis, and in vivo functions. *Cold Spring Harb Perspect Biol* **2011,** *3* (7). DOI: 10.1101/cshperspect.a005041.
45. Harvey, A.; Yen, T. Y.; Aizman, I.; Tate, C.; Case, C., Proteomic analysis of the extracellular matrix produced by mesenchymal stromal cells: implications for cell therapy mechanism. *PLoS One* **2013,** *8* (11), e79283. DOI: 10.1371/journal.pone.0079283.
46. Bernhard, O. K.; Kapp, E. A.; Simpson, R. J., Enhanced analysis of the mouse plasma proteome using cysteine-containing tryptic glycopeptides. *J Proteome Res* **2007,** *6* (3), 987-95. DOI: 10.1021/pr0604559.
47. Ghesquiere, B.; Van Damme, J.; Martens, L.; Vandekerckhove, J.; Gevaert, K., Proteome-wide characterization of N-glycosylation events by diagonal chromatography. *J Proteome Res* **2006,** *5* (9), 2438-47. DOI: 10.1021/pr060186m.
48. Gundry, R. L.; Raginski, K.; Tarasova, Y.; Tchernyshyov, I.; Bausch-Fluck, D.; Elliott, S. T.; Boheler, K. R.; Van Eyk, J. E.; Wollscheid, B., The mouse C2C12 myoblast cell surface N-linked glycoproteome: identification, glycosite occupancy, and membrane orientation. *Mol Cell Proteomics* **2009,** *8* (11), 2555-69. DOI: 10.1074/mcp.M900195-MCP200.
49. Wollscheid, B.; Bausch-Fluck, D.; Henderson, C.; O'Brien, R.; Bibel, M.; Schiess, R.; Aebersold, R.; Watts, J. D., Mass-spectrometric identification and relative quantification of N-linked cell surface glycoproteins. *Nat Biotechnol* **2009,** *27* (4), 378-86. DOI: 10.1038/nbt.1532.
50. Luchansky, S. J.; Hang, H. C.; Saxon, E.; Grunwell, J. R.; Yu, C.; Dube, D. H.; Bertozzi, C. R., Constructing Azide-Labeled Cell Surfaces Using Polysaccharide Biosynthetic Pathways. **2003,** *362*, 249-272. DOI: 10.1016/s0076-6879(03)01018-8.
51. Zaro, B. W.; Yang, Y. Y.; Hang, H. C.; Pratt, M. R., Chemical reporters for fluorescent detection and identification of O-GlcNAc-modified proteins reveal glycosylation of the ubiquitin ligase NEDD4-1. *Proceedings of the National Academy of Sciences of the United States of America* **2011,** *108* (20), 8146-51. DOI: 10.1073/pnas.1102458108.
52. Kubow, K. E.; Vukmirovic, R.; Zhe, L.; Klotzsch, E.; Smith, M. L.; Gourdon, D.; Luna, S.; Vogel, V., Mechanical forces regulate the interactions of fibronectin and collagen I in extracellular matrix. *Nature communications* **2015,** *6*, 8026. DOI: 10.1038/ncomms9026.
53. Zhang, Y.; Lin, Z.; Foolen, J.; Schoen, I.; Santoro, A.; Zenobi-Wong, M.; Vogel, V., Disentangling the multifactorial contributions of fibronectin, collagen and cyclic strain on MMP expression and extracellular matrix remodeling by fibroblasts. *Matrix Biol* **2014,** *40*, 62-72. DOI: 10.1016/j.matbio.2014.09.001.

54. Tsuchida, K.; Nakatani, M.; Uezumi, A.; Murakami, T.; Cui, X., Signal transduction pathway through activin receptors as a therapeutic target of musculoskeletal diseases and cancer. *Endocr J* **2008,** *55* (1), 11-21.
55. Cohen, S.; Nathan, J. A.; Goldberg, A. L., Muscle wasting in disease: molecular mechanisms and promising therapies. *Nat Rev Drug Discov* **2015,** *14* (1), 58-74. DOI: 10.1038/nrd4467.
56. Wallner, C., Targeting Myostatin Signaling in Skin Healing. *Journal of Dermatology Research and Therapy* **2016,** *2* (1). DOI: 10.23937/2469-5750/1510014.
57. Lach-Trifilieff, E.; Minetti, G. C.; Sheppard, K.; Ibebunjo, C.; Feige, J. N.; Hartmann, S.; Brachat, S.; Rivet, H.; Koelbing, C.; Morvan, F.; Hatakeyama, S.; Glass, D. J., An antibody blocking activin type II receptors induces strong skeletal muscle hypertrophy and protects from atrophy. *Mol Cell Biol* **2014,** *34* (4), 606-18. DOI: 10.1128/MCB.01307-13.
58. Gilson, H.; Schakman, O.; Kalista, S.; Lause, P.; Tsuchida, K.; Thissen, J. P., Follistatin induces muscle hypertrophy through satellite cell proliferation and inhibition of both myostatin and activin. *Am J Physiol Endocrinol Metab* **2009,** *297* (1), E157-64. DOI: 10.1152/ajpendo.00193.2009.
59. Braun, A. C.; Gutmann, M.; Ebert, R.; Jakob, F.; Gieseler, H.; Luhmann, T.; Meinel, L., Matrix Metalloproteinase Responsive Delivery of Myostatin Inhibitors. *Pharm Res* **2017,** *34* (1), 58-72. DOI: 10.1007/s11095-016-2038-6.
60. Braun, A. C.; Gutmann, M.; Luhmann, T.; Meinel, L., Bioorthogonal strategies for site-directed decoration of biomaterials with therapeutic proteins. *J Control Release* **2018,** *273*, 68-85. DOI: 10.1016/j.jconrel.2018.01.018.
61. Tada, S.; Kitajima, T.; Ito, Y., Design and synthesis of binding growth factors. *Int J Mol Sci* **2012,** *13* (5), 6053-72. DOI: 10.3390/ijms13056053.
62. Ritzer, J.; Luhmann, T.; Rode, C.; Pein-Hackelbusch, M.; Immohr, I.; Schedler, U.; Thiele, T.; Stubinger, S.; Rechenberg, B. V.; Waser-Althaus, J.; Schlottig, F.; Merli, M.; Dawe, H.; Karpisek, M.; Wyrwa, R.; Schnabelrauch, M.; Meinel, L., Diagnosing peri-implant disease using the tongue as a 24/7 detector. *Nat Commun* **2017,** *8* (1), 264. DOI: 10.1038/s41467-017-00340-x.
63. Bernardin, A.; Cazet, A.; Guyon, L.; Delannoy, P.; Vinet, F.; Bonnaffe, D.; Texier, I., Copper-free click chemistry for highly luminescent quantum dot conjugates: application to in vivo metabolic imaging. *Bioconjugate chemistry* **2010,** *21* (4), 583-8. DOI: 10.1021/bc900564w.
64. Saxon, E., Cell Surface Engineering by a Modified Staudinger Reaction. *Science* **2000,** *287* (5460), 2007-2010. DOI: 10.1126/science.287.5460.2007.
65. Kubow, K. E.; Klotzsch, E.; Smith, M. L.; Gourdon, D.; Little, W. C.; Vogel, V., Crosslinking of cell-derived 3D scaffolds up-regulates the stretching and unfolding of new extracellular matrix assembled by reseeded cells. *Integrative biology : quantitative biosciences from nano to macro* **2009,** *1* (11-12), 635-48. DOI: 10.1039/b914996a.
66. Coin, I.; Beyermann, M.; Bienert, M., Solid-phase peptide synthesis: from standard procedures to the synthesis of difficult sequences. *Nat Protoc* **2007,** *2* (12), 3247-56. DOI: 10.1038/nprot.2007.454.

Chapter 3: Biocompatible Azide–Alkyne "Click" Reactions for Surface Decoration of Glyco-Engineered Cells

Marcus Gutmann[1], Elisabeth Memmel[2], Alexandra C. Braun[1], Jürgen Seibel[2], Lorenz Meinel[1] and Tessa Lühmann[1]*

[1]Institute of Pharmacy and Food Chemistry, University of Würzburg, DE-97074 Würzburg, Germany,
[2]Institute of Organic Chemistry, University of Würzburg, DE-97074 Würzburg, Germany

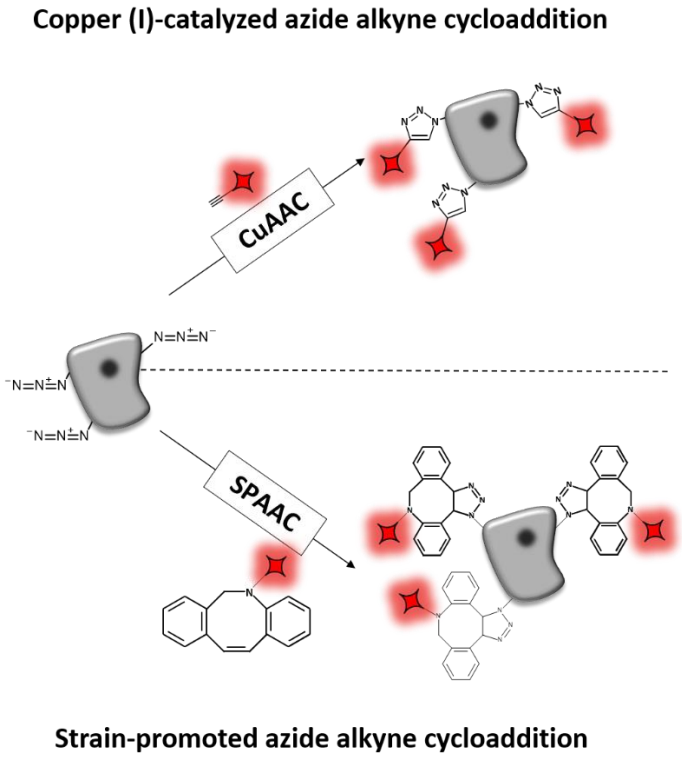

This chapter was originally published in CHEMBIOCHEM, vol. 17 (9), pp. 866-75, 2016; DOI: 10.1002/cbic.201500582. With permission of John Wiley and Sons, License number 4398110929928.

Abstract

Bio-orthogonal copper (I)-catalyzed azide–alkyne cycloaddition (CuAAC) has been widely used to modify azide- or alkyne-bearing monosaccharides on metabolic glycoengineered mammalian cells. Here, we present a systematic study to elucidate the design space for the cytotoxic effects of the copper catalyst on NIH 3T3 fibroblasts and on HEK 293-F cells. Monitoring membrane integrity by flow cytometry and RT-PCR analysis with apoptotic and anti-apoptotic markers elucidated the general feasibility of CuAAC, with exposure time of the CuAAC reaction mixture having the major influence on biocompatibility. A high labeling efficiency of HEK 293-F cells with a fluorescent alkyne dye was rapidly achieved by CuAAC in comparison to copper free strain-promoted azide–alkyne cycloaddition (SPAAC). The study details effective and biocompatible conditions for CuAAC-based modification of glycoengineered cells in comparison to its copper free alternative.

Introduction

The outer cell surface is covered by a cell-specific glycocalyx, which is involved in physiological functions, including cell signaling, storage of growth factors, and regulation of endocytotic processes.[1-3] Chemically tunable monosaccharides such as azide-functionalized N-acetyl-d-glucosamine (Ac_4GlcNAz) are used to decorate cell surfaces with azide functional groups, thus opening the glycocalyx to elegant chemical decoration strategies.[4-6] These functionalized monosaccharides can readily diffuse through the cell membrane, either by passive diffusion (when polar hydroxy groups, e.g., N-acetyl-glucosamine monosaccharide are acetylated)[7] or by active transport mechanisms[4-6] (Figure 1). Within the cytosol the monosaccharides are processed by organelles[8] and incorporated into the structure of glycoproteins and glycolipids, which in turn shuttle through the cell membrane by secretory pathways and become expressed on the cell surface (Figure 1). Ac_4GlcNAz (and its azide group) becomes integrated into N-linked and mucin O-linked glycan structures,[9-11] thus serving as a target for elegant bioconjugation, for example, the bioorthogonal copper (I)-catalyzed azide–alkyne cycloaddition (click reaction).[12-16] Click reactions such as CuAAC[17-19] and copper-free strain-promoted alkyne–azide cycloaddition (SPAAC)[20-21] strictly confine the covalent decoration to the unnatural functional group of the glycocalyx while leaving all natural functional groups of the glycocalyx unaffected. CuAAC and SPAAC are chemically robust, tolerating large pH and temperature ranges, respectively. The advantages of CuAAC over SPAAC include faster reaction kinetics[22] and the use of more stable and better water-soluble educts,[23] thus arguably rendering CuAAC more suitable for fast and specific bioconjugation reactions in cell systems.[15, 24] However, the advantage of CuAAC comes at a price, thus posing formidable limitations to the decoration of cell surfaces, namely the delicate yet inevitable exposure of cells to copper

cations ($Cu^{+/++}$) during CuAAC decoration, as this has a profound cytotoxic effect. The toxicity of Cu is associated with the formation of reactive oxygen species (ROS) thereby leading to DNA strand breaks,[25-26] oxidative processes,[27] and the cleavage[28] and cross-linking of amino acids in proteins.[29] The reported cytotoxicity of copper cations spans from 0.1 to 1000 µM.[30-32] This quite broad range results, at least in part, from the different cell culture conditions of the studies: some used Tris(3-hydroxypropyltriazolyl-methyl)amine (THPTA) or Tris((1-benzyl-1H-1,2,3-triazol-4-yl)methyl)amine (TBTA) as Cu^{I}-stabilizing ligands; some used different reducing molecules, including sodium l- ascorbate or Tris-(2-carboxyethyl)phosphine (TCEP). [16, 28, 33-36]

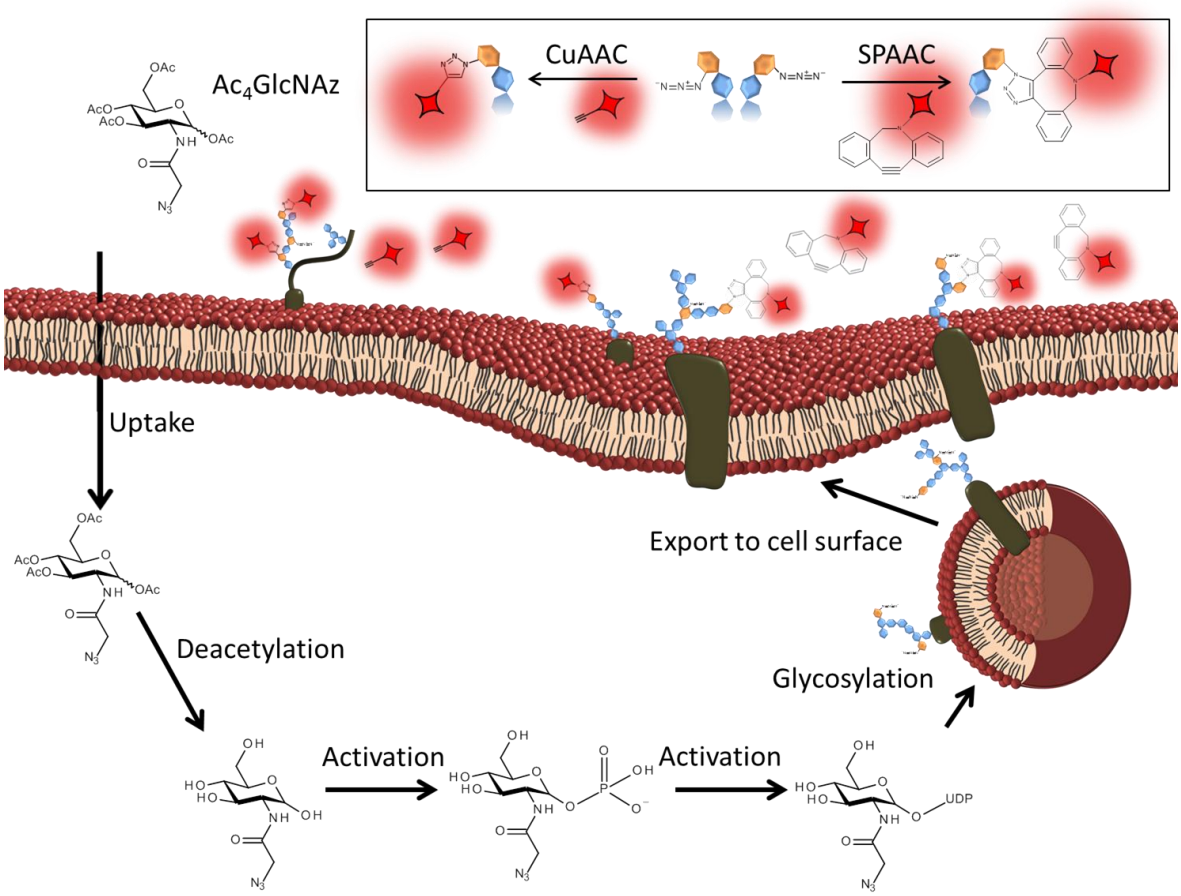

Figure 1: Cell-surface decoration and labeling of modified glycoproteins by CuAAC and SPAAC. Ac_4GlcNAz enters the cytosol by diffusion through the membrane, is processed, activated by cell organelles (Golgi apparatus and endoplasmic reticulum), and connected to glycosylated proteins. The latter are transported to the cell surface and are available for CuAAC or SPAAC.

Metabolic glycoengineering with CuAAC or SPAAC has been successfully performed in various living organisms, and the more general challenges of cytotoxicity were discussed.[37-44] Therefore, we aimed at detailing the mechanistic challenges of CuAAC with living cells, with the goal of providing a design space for the effective and rapid decoration of living and healthy glycoengineered cells.

Results

Cell viability after click reaction analyzed by fluorescein diacetate and propidium iodide

Cu species are responsible for toxic side-effects due to ROS formation in living cells, but they are required as the catalyst in the CuAAC reaction. Cell membrane integrity and intracellular esterase activity after treatment with various CuAAC reaction mixture concentrations were studied in NIH 3T3 fibroblasts by using double staining with fluorescein diacetate (FDA) and propidium iodide (PI) and subsequent flow cytometry analysis. FDA (Figure 2 A, C) and PI (Figure 2 B, D) fluorescence intensity were used to monitor metabolic and membrane damage as a result of exposure to 50, 75, 100, 125, 150, and 200 µM $CuSO_4$ in the presence of sodium l-ascorbate (reducing agent) and THPTA (CuI-stabilizing ligand). Cell viability, as assessed by FDA fluorescence, was not significantly reduced after 5 and 10 min, and was approximately 90 % on average for all Cu concentrations, comparable to the viability of unexposed cells (Figure 2 C). However, after 20 min of exposure to the click reaction mixtures, cell viability dropped significantly (to ~70 %) for all Cu concentrations. Incubation for longer than 20 min further impaired cell viability (50 % relative to unexposed cells). Cell viability was not significantly affected by Cu concentration at each exposure time. Cell viability (membrane integrity as assessed by PI fluorescence) was analyzed in parallel (Figure 2 D), and was unaffected for short incubations (5, 10, or 20 min) in all applied CuAAC reaction mixtures, but longer incubation (30, 45, or 60 min) resulted in a decrease in cell viability (<50 % living cells). As second cell line (human kidney-derived HEK 293-F) was similarly treated and analyzed for cell membrane integrity and esterase activity (Figure 2 E, F). Cell viability (FDA fluorescence) decreased after 30 min of exposure to the click reaction mixture and reached ~50 % (relative to unexposed cells) after 60 min at all tested Cu concentrations (Figure 2 E). Membrane integrity (PI staining) declined after 30 min, and less than 60 % of cells were living after 60 min (Figure 2 F).

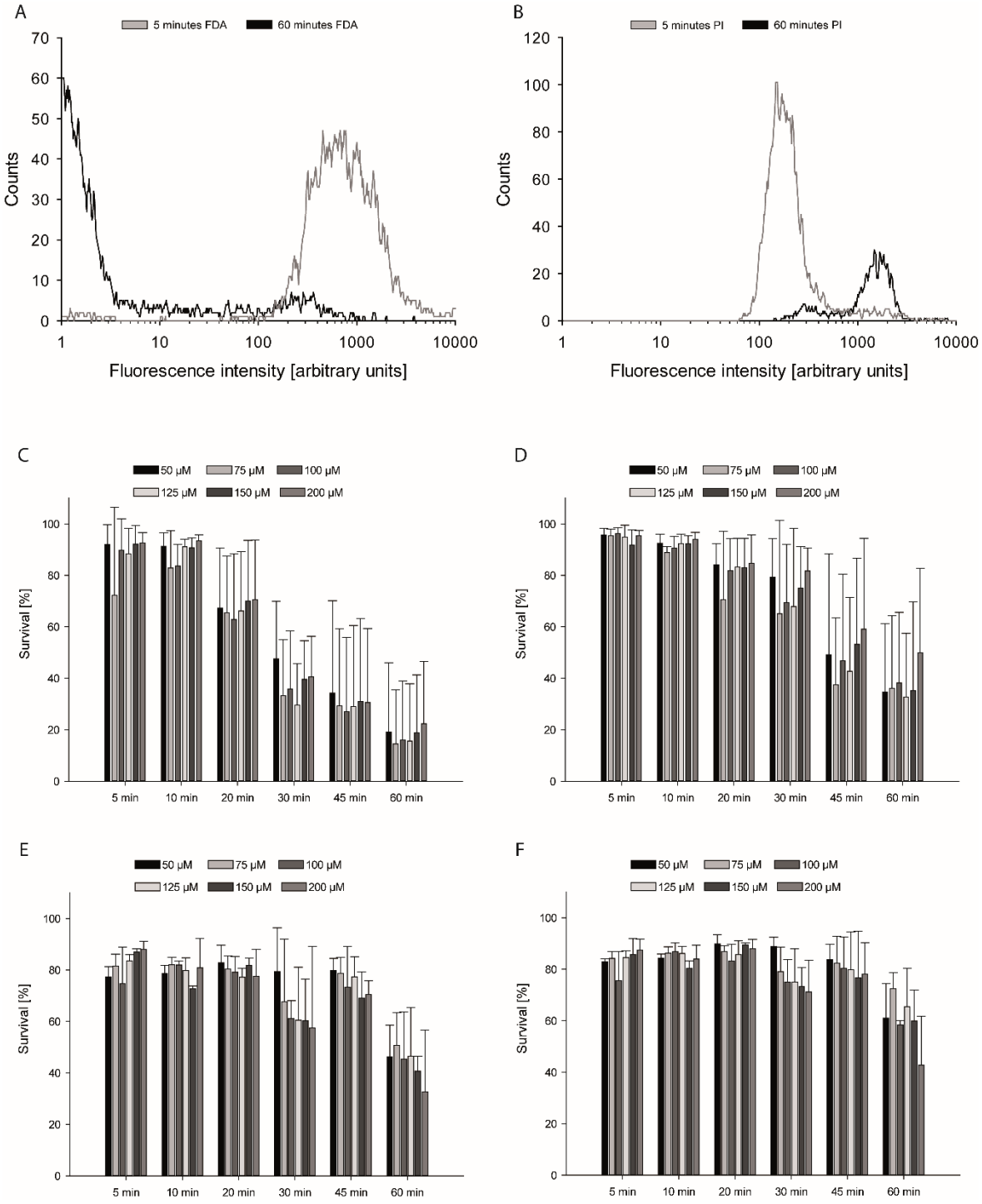

Figure 2: Cell viability of NIH 3T3 fibroblasts and HEK 293-F cells after $CuSO_4$, THPTA, and sodium L-ascorbate treatment as a function of copper concentration and exposure time, as analyzed by A), C), E) FDA or B), D), F) PI staining and subsequent FACS analysis. A) and B) Fluorescence intensities of NIH 3T3 fibroblasts treated with 50 µM $CuSO_4$, 250 µM THPTA, and 2.5 mM sodium L-ascorbate for 5 min and 60 min. C) and D) Fluorescence intensities of NIH 3T3 cells (n=4). E) and F) Fluorescence intensities of HEK 293-F cells (n=3).

Cell recovery after click reaction by fluorescein diacetate and propidium iodide staining

To determine late-stage effects of the CuAAC reaction mixture, NIH 3T3 cell viability (FDA and PI fluorescence) was further analyzed after exposure for 5 and 20 min to 50 µM $CuSO_4$ in the presence of sodium l-ascorbate and THPTA (Figure 3). These CuAAC reaction mixtures did not affect cell viability.

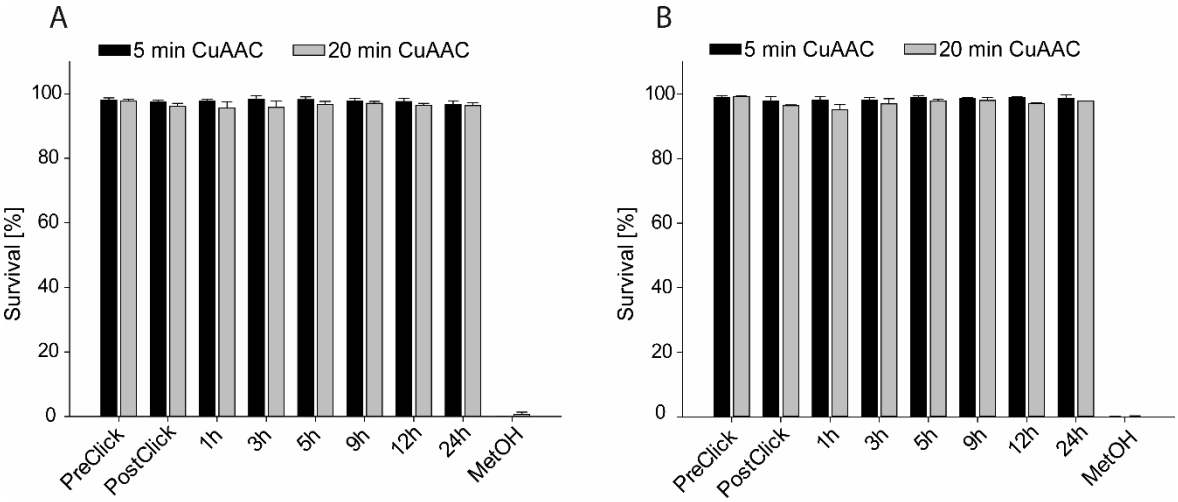

Figure 3: Flow cytometry analysis of NIH 3T3 fibroblasts stained with A) PI or B) FDA after click reaction for 5 min or 20 min. PreClick: untreated cells; PostClick: cells analyzed directly after click reaction (p<0.05, n=3).

Quantitative real-time PCR of apoptosis markers

In order to study the impact of the CuAAC reaction mixture (20 µM sulfo-Cy5-alkyne for coupling to the azide functionalized glycocalyx, 50 µM CuSO4, 250 µM THPTA, and 2.5 mM sodium l-ascorbate) and of SPAAC (20 µM DBCO-Sulfo-Cy5 for coupling to the azide functionalized glycocalyx) on apoptosis, the transcriptome of apoptotic and anti-apoptotic genes covering the essential parts of cell-death downstream signaling[45-47] were analyzed by RT-PCR (Figure 4). Ac4GlcNAz-functionalized NIH 3T3 fibroblasts were incubated with the CuAAC reaction mixture for 5 min (Figure 4 A) and 20 min (Figure 4 B), then mRNA expression of apoptotic genes (caspase 2, APAF1, BAX and Bcl-2) was quantified (normalized to GAPDH expression; Figure 4 A, B). The cells were similarly analyzed after 1 hour of incubation with DBCO-Sulfo-Cy5 (Figure 4 C). Caspase 2 has been linked to total DNA damage,[48-49] whereas BAX (Bcl 2 associated X protein) is a marker for both mitochondrial[50-51] and DNA damage.[52] APAF1 (apoptotic protease activating factor 1)[53-54] was chosen as additional indicator of mitochondrial damage; Bcl-2 (B cell lymphoma 2) was used as a control pre-apoptotic marker.[55-56] None of the tested conditions significantly increased mRNA expression (defined as >1.5-fold) of the apoptotic genes after 5 min of exposure to the CuAAC

reaction mixture, in contrast to the positive control (G418 as inducer of cell death), with the exception of Bcl-2. Bcl-2 is marker for cellular stress, possibly leading to apoptosis. In concert with BAX upregulation, however, apoptosis is manifested.[57-58] Comparable results were found at 20 min and for Ac_4GlcNAz-functionalized NIH 3T3 fibroblasts treated by SPAAC (Figure 4 C).

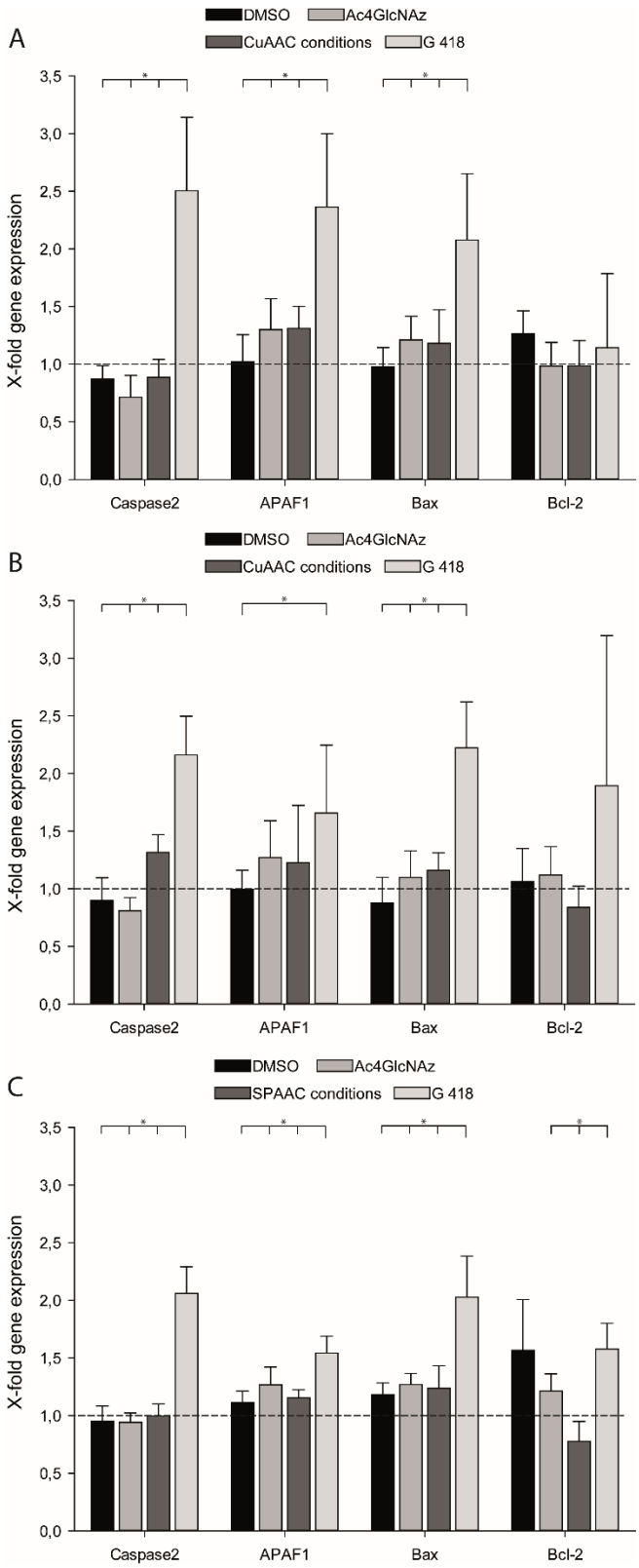

Figure 4: Expression of apoptotic marker genes Caspase 2, APAF1, and Bax and the pre-apoptotic marker gene Bcl-2 in NIH 3T3 fibroblasts after A) 5 and B) 20 min of CuAAC or C) 1 hour of SPAAC. Data are normalized to GAPDH expression and depicted relative to expression in untreated cells by the comparative C_T method (p<0.05, n=3).

Quantification of hydrogen peroxide

ROS, including hydrogen peroxide, are causative for oxidative stress and harbinger to cell damage. [59-62] Hydrogen peroxide was detected during the CuAAC reaction to assess the kinetics of ROS formation in the absence or presence of THPTA (Figure 5). In the absence of THPTA hydrogen peroxide was significantly elevated after 10 min (15±0.45 µMol L^{-1}) and after 30 min (19±0.09 µMol L^{-1}), whereas in presence of THPTA hydrogen peroxide formation was lowest after 2 min (6±0.35 µMol L^{-1}) and continuously increased up to 60 min (12±0.24 µMol L^{-1}; no later time points were assessed).

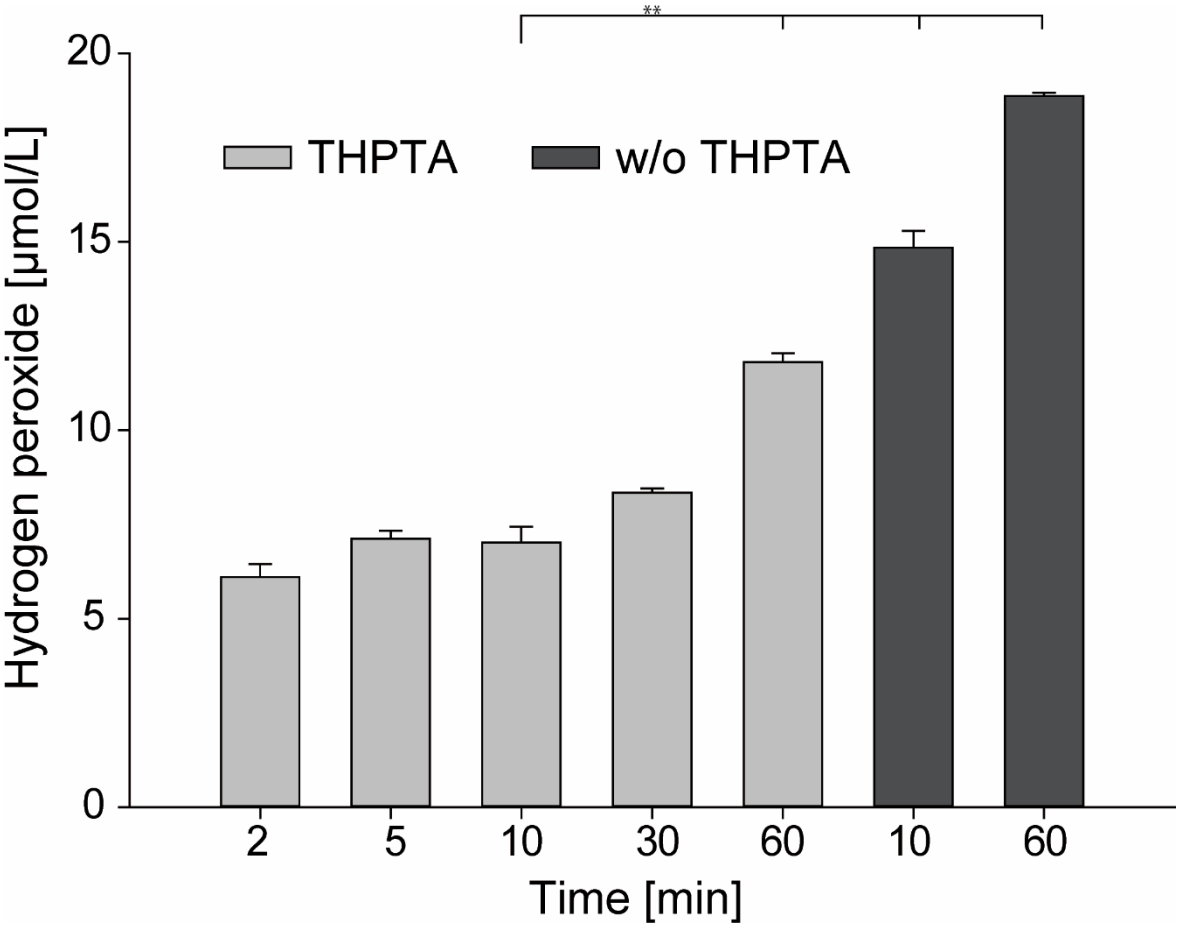

Figure 5: Determination of reactive oxygen species (ROS) during the copper mediated click reaction (p<0.01, n=3).

Cell surface labeling of HEK 293-F cells

HEK 293-F cells were used to quantify and compare labeling on the cell surface by flow cytometry analysis for CuAAC and SPAAC (Figure 6). Ac_4GlcNAz-functionalized cells (and non-functionalized controls) were exposed to the CuAAC reaction mixture (Sulfo-Cy5-alkyne, CuSO4, THPTA, sodium l-ascorbate), and cellular fluorescence was monitored after 5, 10, and 20 min.

SPAAC was assessed in a similar manner with Sulfo-Cy5 (DBCO-sulfo-Cy5) to enable direct comparison between the two types of azide–alkyne click chemistries. The fluorescence intensity increased continuously from 27 771±5805 a.u. after 5 min to 90 838±9136 a.u. after 20 min exposure to the click reaction mixture and was significantly higher than for the negative controls (Figure 6 C). The fluorescence of non-functionalized cells increased significantly from 5454±1253 a.u. after 5 min to 22 755±1705 after 20 min of exposure to the copper(I)-containing click reaction mixture.

Copper-free treatment for 5 min resulted in a lower fluorescence intensity (15 558±4716 a.u.) compared to the CuAAC-treated cells, and it increased threefold to 49 118±2527 a.u after 60 min (Figure 6 D).In contrast to the CuAAC negative control, the intensities of the negative controls exposed to SPAAC remained constant at all time points (Figure 6 D).

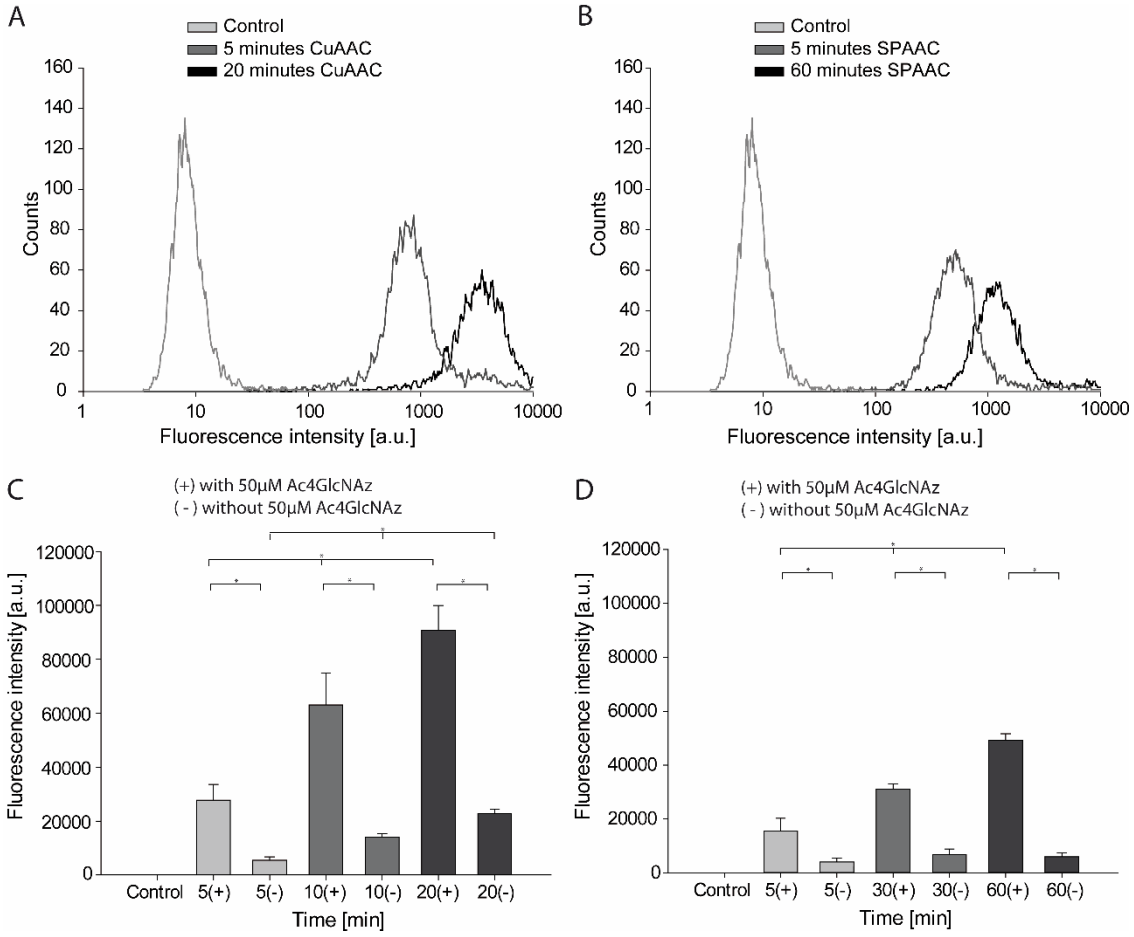

Figure 6: Flow cytometry analysis of HEK 293-F cells. Representative fluorescence intensity histograms of cells with 50 µM $Ac_4GlcNAz$ after conjugation with A) Sulfo-Cy5-alkyne for 5 and 20 min or B) DBCO-Sulfo-Cy5 for 5 and 60 min compared to control cells. Mean fluorescence after C) CuAAC or D) SPAAC, with (+) or without (−) 50 µM $Ac_4GlcNAz$ at different time points. Data were analyzed by a paired Student's t-test for pairwise comparison within groups and one-way ANOVA for comparison between groups (p<0.05, n=4).

Fluorescence imaging after click reaction on the cell surface of adherent NIH 3T3 fibroblasts

Ac_4GlcNAz-treated NIH 3T3 fibroblasts were labeled with Sulfo-Cy5-alkyne under CuAAC click conditions (CuSO4, THPTA, sodium l-ascorbate) for 5 min and by SPAAC with DBCO-Sulfo-Cy5 for 1 h. The cells were analyzed after 30 min, 3 h, and 12 h to quantitatively assess the kinetics of the fluorescence signal loss of the covalently modified glycans on the cellular surface. Strong and specific fluorescence of the cell membrane and weak fluorescence in the entire cytoplasm were observed after 30 min for both types of click chemistry (Figure 7 A). Cell-surface fluorescence intensity decreased strongly for both after 3 h (Figure 7 B) and were only marginally detectable after 12 h (Figure 7 C). Control cells (lacking Ac_4GlcNAz) showed no detectable membrane fluorescence (Figure 7D–F).

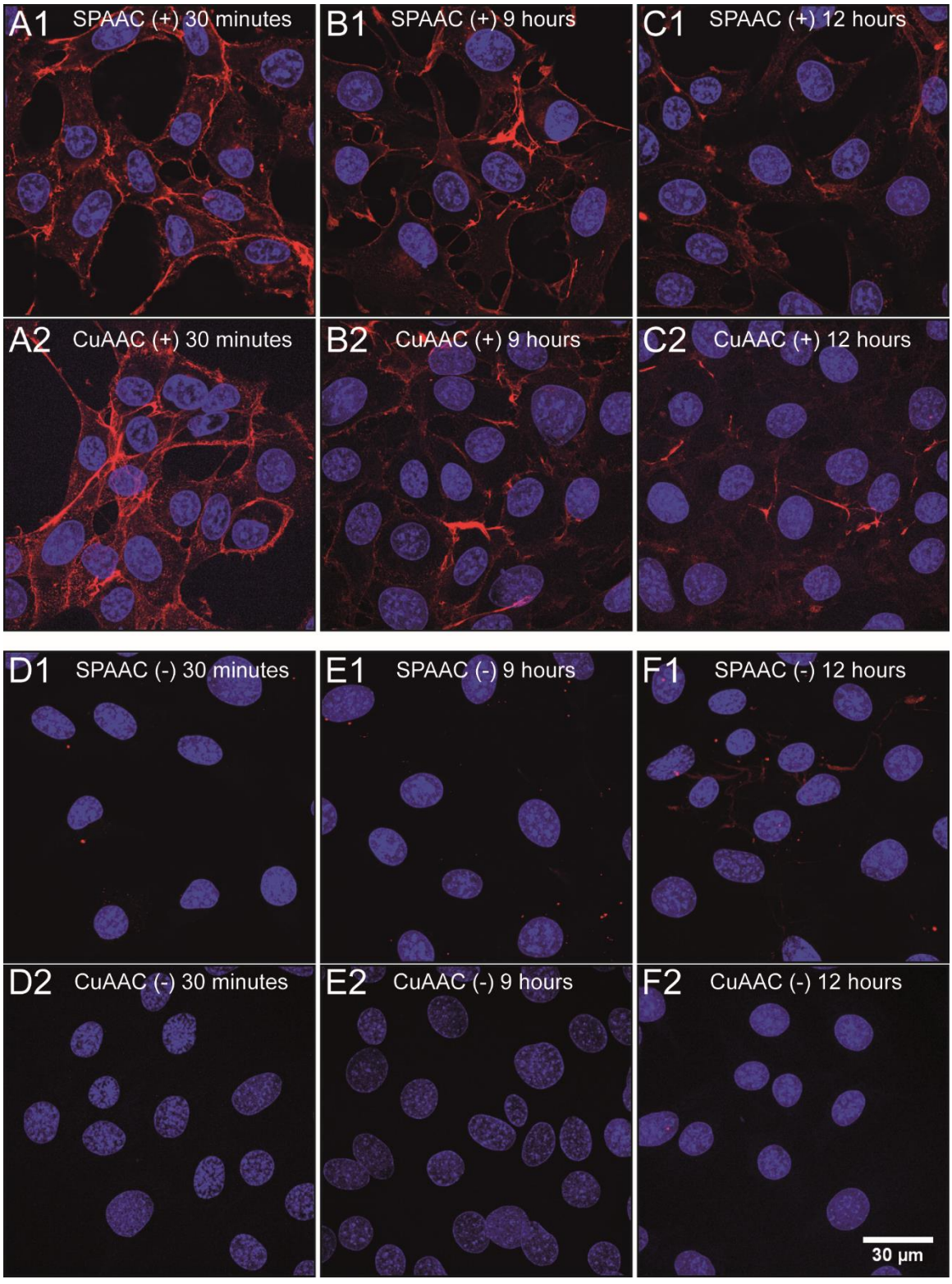

Figure 7: Labeling of NIH 3T3 cell membranes. Cells were treated, as indicated, for 1 hour by SPAAC (with 20 µM DBCO-Sulfo-Cy5) or for 5 min by CuAAC (with 20 µM Sulfo-Cy5-alkyne) in the presence of 50 µM $CuSO_4$, 250 µM THPTA, and 2.5 mM sodium L-ascorbate. Cells were grown with (+) or without (−) 50 µM Ac_4GlcNAz and were imaged at the indicated times after the labeling reactions. Blue is DAPI fluorescence (cell nuclei); red fluorescence is Sulfo-Cy5-labeling. Corresponding phase contrast images are in Figure S1.

Discussion

Cu species are essential cofactors for various enzymes, such as superoxide dismutase, but have toxic oxidative side effects, including DNA strand breaks or cleavage and cross linking of amino acid residues in proteins. [25-28] For these reasons, it is crucial to tightly control the exposure of living cell systems to copper species during CuAAC reactions, in order to obtain efficient decoration and retain high cell viability.

Early studies in the field illustrated the feasibility of CuAAC-based bioconjugation in living cells. Cell viability was determined by ATP production as an indicator of metabolically active HeLa, CHO, and Jurkat cells after treatment with azide monosaccharides and after the CuAAC reaction. The focus was on different ratios between CuSO4 and the ligand THPTA.[63] Optimization of the CuAAC reaction in terms of the types of reducing agent, ligand, and buffer system in respect to ROS generation has been described.[63] Proliferation and Cu^{I} and Cu^{II} ion-uptake assays were performed at different Cu^{II} ligand concentrations (2 mM to 1 μM including the complexing ligands EDTA, TBTA, THPTA, BPS or l-histidine) without the presence of ascorbic acid, in Huh7.5, MDA-MB-468, HEK 293T, and HeLa cells for 24 h to determine the best-performing Cu^{II} ligand combined with the lowest cytotoxic effect. [36] However, the lack of ascorbic acid in this study might be critical. The majority of the studies on cytotoxic effects of CuAAC confined the analysis of cell viability to assessment of cell proliferation. [36, 63] Although cell-proliferation assays, such as the commonly used tetrazolium/formazan salt conversion method, provide general conclusions about biocompatibility, they are based on cell number and, therefore, only indirectly quantify cytotoxic effects.

Our study aimed to define a design space for the CuAAC reaction in respect to cell cytotoxicity in mouse-derived NIH 3T3 fibroblasts and human-kidney-derived HEK 293-F cells. Assessed parameters included metabolic activity and membrane integrity, by FDA/PI staining and subsequent flow cytometry, as well as apoptotic downstream processes as determined by RT-PCR, with a peroxide assay to quantify ROS species. The CuAAC reaction on living cells was performed according to existing protocols. [28, 33, 35, 63]

$CuSO_4$, THPTA, and sodium l-ascorbate were premixed and incubated for 10 min before use in all experiments to reduce generated ROS species and thereby, limit the oxidative effects. Conventional CuAAC reactions (50–200 μM CuSO4, THPTA in a molar ratio of 1:5, and 2.5 mM sodium l-ascorbate as reducing agent) were well tolerated for up to 20 min in the case of NIH 3T3 fibroblasts, without critical loss in cell viability (>90 % cell viability after 5 and 10 min; 70 % cell viability after 20 min; Figure 2 A, C); there were no long-term side-effects in respect to FDA and PI staining (100 % cell viability; Figure 4). A similar finding was observed for HEK 293-F cells. The click

reaction was well tolerated for 20 min, with cell viability equal to that for untreated cells (Figure 2 E). Interestingly, exposure time of the click reaction mixture but not Cu concentration (50–200 μM CuSO4) critically impacted cell viability for both cell lines (Figure 2). Overall, HEK 293-F cells showed higher CuSO4 tolerance compared to NIH 3T3, which were more sensitive to $CuSO_4$ exposure time. The antimicrobial properties of copper are well known[64] leading to bacterial cell death. We speculate that ROS formation by the CuAAC reaction was primarily responsible for the increase in PI-positive cells (indicative of loss of cell membrane integrity) after exposure to the click reaction mixture, and as observed for exposure times exceeding 20 min of incubation (Figure 2 B, D). This hypothesis was corroborated by hydrogen peroxide formation during the CuAAC reaction, which was already double after 2 min and further increased up to 60 min (Figure 5). In contrast to previous reports,[63] a constant development of hydrogen peroxide over time was observed during the CuAAC reaction, and this was significantly reduced in the presence THPTA (Figure 5).These results indicate that ROS formation during CuAAC cannot be avoided (but can be reduced); it nevertheless poses a threat for possible alteration of proteins, carbohydrates, or lipids within or on the cell, or in the extracellular space; previous studies have demonstrated efficient transport of peroxide through lipid membranes.[65] Interestingly, we observed that the fluorescence background intensity of cells that had not been modified with Ac_4GlcNAz increased continuously during the CuAAC reaction (Figure 6). Although cyclooctynes are more hydrophobic and thus enable non-covalent sticking to hydrophobic surfaces (such as membranes) more effectively than non-cyclic alkynes, the background fluorescence intensity of Ac_4GlcNAz-unmodified cells remained constant during SPAAC. This indicates that the alkyne fluorophore reacted nonspecifically with endogenous nucleophiles on the cellular surface when ROS were present, such as during CuAAC (and in contrast to SPAAC). Future studies should detail the impact of the side reactions on the safety of this approach, particularly when these glycoengineered cells are profiled for *in vivo*/clinical use.

In order to obtain a more detailed insight into CuAAC-induced apoptotic processes after Ac_4GlcNAz metabolic glycoengineering and treatment with the best-performing click reaction mixture (best conditions for cell compatibility: 50 μM CuSO4, 250 μM THPTA, and 2.5 mM sodium l-ascorbate, as determined by FDA/PI staining, Figure 2), RT-PCR on apoptotic gene markers and an anti-apoptotic gene marker was conducted. As representative markers for apoptosis, we chose caspase 2 (a marker for DNA damage),[48-49] BAX (a marker for DNA damage and mitochondria-mediated damage),[50-52] and APAF (a marker for mitochondrial breakdown),[53-54] in order to assess the transcription of essential genes involved in apoptotic pathways.[45] Gene expression of Bcl-2 was previously linked to a pre-apoptotic status.[55-56] RT-PCR analysis of all tested gene markers revealed no upregulation of the pre-apoptotic marker or apoptotic marker genes in fibroblasts after exposure to the optimized click reaction mixture (Figure 3 A, B). This further corroborated the finding that the

Cu^{I} species in the click reaction mixture are not harmful in cellular systems when low Cu^{I} concentration (50 µM $CuSO_4$) and short-term exposure (5 min) are applied. Gene markers were not increased after treatment with SPAAC for 1 hour, thus indicating that the copper-free azide–alkyne alternative does not trigger apoptotic signals (Figure 3 C).

In order to confirm our findings regarding CuAAC optimization in living cell systems, we determined the efficacy and duration of the labeling with an alkyne dye over time. As most of the current applications of glycoengineered cell systems focus on cell modification for cellular imaging, Ac_4GlcNAz-treated NIH 3T3 fibroblasts (and untreated cells) were labeled with fluorescent dyes by CuAAC (for 5 min) or SPAAC (for 1 h) to aim for comparable fluorescence labeling efficiencies. Strong and specific Cy5-fluorescence was observed on the cell membrane 30 min and 3 h after both click reactions (Figure 7). As glyco-modification on the cell surface is a transient process (because of, for example, sequestration or general endocytotic processes), Cy5-fluorescence declined within 12 h, thus indicating that metabolic processes and glyco-trafficking within the cytoplasm are not impaired by the conjugated fluorophore or by SPAAC/CuAAC chemistry. This suggests that decoration following glycoengineering is particularly interesting for mechanistic *in vitro* studies aimed at rapid biological processes (ideally proceeding within 3 h; e.g., internalization and sequestration), but less appropriate for studies on interactions requiring prolonged decoration of the glycocalyx (e.g., tissue engineering). Here the optimized CuAAC protocol is beneficial because of the short exposure to the click reaction mixture (5 min) and intensive labeling of the cell surface, compared to SPAAC. In fact, current alternatives to CuAAC (such as SPAAC) have slower reaction kinetics and pose other technical hurdles related to reactant solubility; this is why some laboratories favour CuAAC over SPAAC (or alternatives) for the spatially controlled decoration of the glycocalyx in living systems.[15, 23-24]However, other cell lines and primary cell sources display other kinetics, and the fading decoration as observed for the cell line studied here should be considered when extrapolated to other cell lines. Obviously, the best conditions for cell decoration would use chemistries avoiding Cu; possibly viable alternatives will be developed. One limitation of this study is our assessment of cellular performance in response to medium exposure during CuAAC. In fact, many more perspectives are possibly required to conclude cellular inertness to these media, beyond the assessment of membrane integrity, cell viability, and apoptotic and non-apoptotic gene expression (as used here). This is to say that a possible bias of the CuAAC procedure itself deployed for specific biological functionalities must be carefully separated, through proper controls, from the impact of the decoration. Finally, it is interesting to translate these protocols for decorating cells with fluorescent dyes to more complex macromolecules including DNA, lipids, and proteins. Studies are required to detail the extent to which the conditions reported here are adequate for an expansion to larger decoration molecules in living cell systems.

Conclusion

CuAAC is well tolerated by living cells. However, the cytotoxicity is limiting, and exposure times exceeding 30 min are critical. Interestingly, the amounts of Cu used in this study 'did not induce cytotoxicity. A proper design of the decoration conditions of the cells is essential to yield uncompromised cell membrane integrity, cell metabolism, and avoid apoptotic responses. The optimized CuAAC protocol resulted in efficient labeling and rapid modification of the cell membrane compared to the copper-free alternative SPAAC. Both click-chemistry-based decoration strategies lead to functionalized glycocalyx, thus allowing exciting studies of glycoengineered living-cell systems. The presentation of the decorated glycocalyx is transient for both types of click chemistry (fading within 12 h of conjugation), thus suggesting particular application of this technique for studying quite rapid biological processes in living cells.

Materials and methods

Materials

Dulbecco's modified Eagle's medium (DMEM), copper(II) sulfate, sodium l-ascorbate, tris(3-hydroxypropyltriazolylmethyl)amine (THPTA), 4′,6-diamidino-2-phenylindole (DAPI), fluorescein diacetate (FDA), and propidium iodide (PI) were purchased from Sigma–Aldrich. Penicillin G and streptomycin were purchased from Biochrom AG (Merck Millipore). Fetal bovine serum (FBS) was from Gibco. DBCO-Sulfo-Cy5 and Sulfo-Cy5-alkyne were from Jena Bioscience (Jena, Germany). TaqMan Gene Expression Master Mix, High Capacity cDNA Reverse Transcription Kit, as well as GAPDH-, Bax-, Bcl-, APAF1- and Caspase 2 TaqMan Gene Expression Assays were purchased from Applied Biosystems (ThermoFisher Scientific). Tissue culture polystyrene (TCPS) cell culture flasks (75 cm^2) were from Nunc (ThermoFisher); 24-well plates were from Greiner Bio One (Frickenhausen, Germany); Mowiol 4-88 was from Carl Roth; 125 mL Erlenmeyer flasks from Corning Incorporated (Oneonta, NY). All other chemicals were at least of pharmaceutical grade and were purchased from Sigma–Aldrich.

Methods

Synthesis of 2-azidoacetylamino-2-deoxy-(1,3,4,6)-tetra-O-acetyl-d-glucopyranoside

Synthesis of the azide analogue Ac_4GlcNAz was performed according to existing protocols.[11, 66-69] A detailed description is in the Supporting Information.

Cell culture

NIH 3T3 fibroblasts (CRL-1658; ATCC, Manassas, VA) were maintained in 100 mm culture dishes in growth medium (DMEM containing heat-inactivated FBS (10 %), penicillin G (100 U mL^{-1}) and streptomycin (100 μg $μL^{-1}$)) at 37 °C under CO2 (5 %). Before use, the cells were seeded ($2.5×10^4$ cells mL^{-1}, 1 mL growth medium per well) in 24-well plates and grown for 48 h at 37 °C under CO2 (5 %), with or without addition of Ac_4GlcNAz (50 μM). HEK 293-F cells (Freestyle 293-F #R790-07, Life Technologies) were maintained in 125 mL Erlenmeyer flasks in Freestyle 293 growth medium containing penicillin G (100 U mL^{-1}) and streptomycin (100 μg $μL^{-1}$) at 37 °C under CO2 (8 %), on a Mini shaker (150 rpm; VWR). Before use, the cells were seeded ($5×10^4$ cells mL^{-1}, 1 mL per well) in 24-well plates in growth medium and cultured for 48 h at 37 °C under CO2 (8 %) on a platform shaker (230 rpm) with or without Ac_4GlcNAz (50 μM).

Cell viability after click reaction by fluorescein diacetate and propidium iodide staining

NIH 3T3 and HEK 293-F cells were investigated for the cytotoxic effects of the commonly used CuAAC mixture containing $CuSO_4$, THPTA, and sodium l-ascorbate. NIH 3T3 fibroblasts were incubated for 24 h in growth medium in 24-well plates. The medium was gently aspirated, and the cells were washed twice with PBS (1 mL). CuSO4 and THPTA were mixed (molar ratio, 1:5), and freshly prepared stock solution of sodium l-ascorbate (100 mM) was added. The mixture was incubated for 10 min at RT before adding PBS (137 mM NaCl, 2.7 mM KCl, 4.3 mM Na_2HPO_4, 1.47 mM KH_2PO_4, pH 7.4) to finally contain $CuSO_4$ (50, 75, 100, 125, 150, 200 μM), THPTA (×5 concentration), and sodium l-ascorbate (2.5 mM). The mixture was added to the cells. After incubation (5 to 60 min) at RT, the reaction was stopped by gently aspirating the mixture and by washing with growth medium to remove residual copper species. After washing with PBS, the cells were detached by trypsin (0.005 %) with EDTA (0.025 %). Trypsin/EDTA activity was stopped by the addition of growth medium, and cells were resuspended in PBS. HEK 293-F cells ($5.0×10^4$) were maintained in 125 mL Erlenmeyer flasks in growth medium. After one washing step with PBS including centrifugation and aspiration, the cells were incubated with $CuSO_4$, THPTA, and sodium l-ascorbate as described above. After incubation (5 to 60 min) at RT, the reaction was stopped by adding EDTA (1 μL, 250 mM in PBS). The cells were washed with growth medium and resuspended in PBS. Cells were counted, divided in two equal parts and stained with either FDA (0.01 μg per 10^4 cells) or PI (0.003 μg per 10^4 cells) in PBS for 3 min at RT. Non-fluorescent FDA substrate is a viability marker for enzymatic activity and cell-membrane integrity after active conversion to fluorescein ($λ_{ex}$=492 nm $λ_{em}$=517 nm) by intracellular esterases in living cells. PI ($λ_{ex}$=540 nm $λ_{em}$=608 nm) does not penetrate intact membranes and intercalates stoichiometrically with nucleic

acids in dead cells.[70-72] The cells were subsequently analyzed on a FACSCalibur flow cytometer (BD Biosciences): 488 nm laser; channel FL2 (585 nm/±21 nm) for PI; channel FL1 (530 nm/±15 nm) for FDA. A total of 5000 events were counted with CellQuest Pro (BD Biosciences), and mean fluorescence was determined with Flowing Software (version 2.5.1; Turku Bioimaging, Turku, Finland).

Cell recovery after click reaction by FDA and PI staining

NIH 3T3 fibroblasts were incubated for 24 h in growth medium in 24-well plates. The medium was gently aspirated, and cells were washed twice with PBS (1 mL). $CuSO_4$ and THPTA were mixed as above, and PBS was used to prepare a solution containing $CuSO_4$ (50 μM), THPTA (250 μM), and sodium l-ascorbate (2.5 mM). Cells were incubated with the reaction mixture, and the click reactions were stopped after 5 or 20 min by gently aspirating the reagents and washing with growth medium to remove all traces of copper species. Cells were then incubated (1 to 24 h) in growth medium and maintained at 37 °C under CO2 (5 %). At time points the cells were washed with PBS and detached with trypsin/EDTA and stained with FDA (0.01 μg per 10^4 cells) or PI (0.003 μg per 10^4 cells) for 3 min at RT. Flow cytometry was performed as above.

Real-time PCR for the analysis of apoptotic marker genes

Apoptotic processes caused by the copper-mediated click reaction were evaluated, with geneticin (G418) as a positive control as previously described.[73] NIH 3T3 cells (2.5×10^4 cells mL^{-1}, 1 mL per well) were seeded in 24-well plates in growth medium for 24 h, followed by medium exchange to growth medium containing G418 (400 μg mL^{-1}). After 72 h, RNA was extracted with a PureLink RNA Mini Kit (Life Technologies). A set of conditions was used to monitor the effects of the CuAAC and SPAAC reaction. DMSO (4 μL mL^{-1}) was added to the cells to evaluate the impact of the solvent for Ac_4GlcNAz; it was also used as negative control. Ac_4GlcNAz (50 μM) was added, and cells were maintained for 48 h. For CuAAC and SPAAC, the medium was aspirated, and the cells were gently washed with PBS. For SPAAC, DBCO-Sulfo-Cy5 (20 μM in PBS) was added, and cells were incubated for 1 h at RT. For CuAAC, a mixture of $CuSO_4$ (50 μM), THPTA (250 μM), and sodium l-ascorbate (2.5 mM) in PBS (premixed as above) and Sulfo-Cy5-alkyne (20 μM) were added, and the cells were incubated for 5 or 20 min at RT. The click reaction was stopped by washing the cells with growth medium to remove copper species. Untreated cells were used as a negative control. Total RNA was isolated after 30 min with a Pure Link RNA Mini Kit in the incubator. cDNA was prepared from equal amounts of total RNA by using oligo(dT) primers and the High Capacity cDNA Reverse Transcriptase Kit (Applied Biosystems). cDNA (100 ng) was amplified in an ABI prism7900 HT Real-Time PCR System (Applied Biosystems) in TaqMan

Gene Expression Master Mix and appropriate probes as apoptosis markers (Table S1): 50 °C for 2 min; increased to 95 °C over 10 min; 40 cycles of 95 °C for 15 s, 60 °C for 1 min. cDNA levels were normalized to the expression of the housekeeping gene GAPDH; relative values were calculated by the comparative CT Method.[74]

Quantification of hydrogen peroxide formation

Peroxide content was determined with a Pierce Quantitative Peroxide Assay Kit (Thermo Scientific). Samples were prepared by combining $CuSO_4$ and THPTA (1:5 as above), then adding sodium l-ascorbate, and incubation in the absence of air (in a parafilm-sealed Eppendorf tube) for 2 to 60 min. At time points, the stock solution was diluted with PBS buffer to obtain $CuSO_4$ (50 µM), THPTA (250 µM), and sodium l-ascorbate (2.5 mM). The diluted samples (20 µL) were mixed with the detection reagent (200 µL; ammonium ferrous sulfate (250 µM), xylenol orange (125 µM), sorbitol (100 µM), sulfuric acid (25 mM)) and incubated for 20 min at RT before analysis on a Spectramax 250 automated microplate reader (λ=595 nm; Molecular Devices). Hydrogen peroxide (30 %) was used as the standard. Peroxide levels are expressed as µMol L^{-1}.

Quantification of cell-surface staining of HEK 293-F cells

Cells were incubated in growth medium with or without Ac_4GlcNAz (50 µM) for 48 h in a 24-well plate on a platform shaker (230 rpm). After 48 h, the cells were centrifuged (218 g, 5 min, RT) and washed twice with PBS. For the CuAAC reaction, $CuSO_4$ (50 µM), THPTA (250 µM), and sodium l-ascorbate (2.5 mM) were incubated for 10 min (as above). Sulfo-Cy5-alkyne (20 µM) was added, and the mixture was given to the cells. After 5, 10, and 20 min, the reaction was stopped by adding EDTA (1 µL, 250 mM in PBS). For SPAAC, DBCO-Sulfo-Cy5 (20 µM in PBS containing FCS (1 %)) was given to the cells. After 5, 30, and 60 min the reaction was stopped by centrifugation and by washing the cells with PBS. Samples were analyzed on a FACSAria III flow cytometer (BD Biosciences): 633 nm laser; PE-Cy5 (670 nm/±14 nm). A total of 5000 events were counted with FACSDiva software (BD Biosciences); mean fluorescence was determined with Flowing Software (version 2.5.1; Turku Bioimaging).

Fluorescence imaging after click reaction on the cell surface

Cells were seeded on glass cover slides (35 mm, Menzel Gläser, Braunschweig, Germany) in 24-well plates coated with gelatine (2 %) and were grown for 48 h in growth medium with or without Ac_4GlcNAz (50 µM). After 48 h the medium was gently aspirated, and the cells were washed twice with PBS before performing the copper-catalyzed click reaction with Sulfo-Cy5-alkyne or the strain-promoted click reaction with DBCO-Sulfo-Cy5 on the cell surface. For the copper-catalyzed

click reaction, a mixture of $CuSO_4$ (50 µM), THPTA (250 µM), and sodium l-ascorbate (2.5 mM), which had been incubated for 10 min, was combined with Sulfo-Cy5-alkyne (20 µM), and the solution was incubated with the cells for 5 min at RT. For SPAAC, the cells were treated with DBCO-Sulfo-Cy5 (20 µM in PBS containing FCS (1 %)) for 1 h. After the reaction, the cells were washed with growth medium and incubated for additional 30 min to 12 h in the incubator. Cells were removed from the incubator after 30 min, 3 h, and 12 h and fixed with ice-cold methanol for 10 min at RT. After washing with PBS four times, cell nuclei were stained with DAPI. The cells on the cover slides were mounted on microscope slides with Mowiol 4-88, before analysis on a high resolution AOBS SP2 confocal laser scanning microscope (Leica microsystem, Wetzlar, Germany) with a 63× N.A. 1.4-0.60 Oil l BL HCX PL APO l objective. To avoid cross-talk the emission signals were collected independently. Image processing was performed in ImageJ (http://imagej.nih.gov/ij/).

Statistical analysis

Data were analyzed by a paired Student's t-test for pairwise comparison or one-way ANOVA after comparing the mean values by a Tukey–Kramer post-hoc test. SigmaPlot (Systat Software, San Jose, CA) and Minitab 16 (Minitab, Coventry, UK) were used. Presented data are mean±SD; results were considered statistically significant at $p \leq 0.05$(*) or $p \leq 0.01$(**).

Acknowledgments

This work was supported by DAAD grant, Kooperation in Pharmazeutische Wissenschaften und Lehre, 57058983 and by the European project MANAQA, "Magnetic Nano Actuators for Quantitative Analysis", 296679.

Supporting Information

Methods

Synthesis and analysis of 2-azidoacetylamino-2-deoxy-(1,3,4,6)-tetra-O-acetyl-d-glucopyranoside

D-glucosamine hydrochloride (500 mg, 2.32 mmol) was dissolved in dry methanol (10 mL), sodium methanolate (0.5 M in methanol, 4.64 mL, 2.32 mmol) was added and the solution stirred for 1 h at room temperature. Triethylamine (337 µL, 2.44 mmol) and chloroacetic anhydride (1.98 g, 11.6 mmol) were added and the mixture stirred for further 6 h at room temperature. The solvent was removed in vacuum and the residue dissolved in DMF (5 mL).

Sodium azide (1.51 g, 23.2 mmol) was added and the suspension stirred for 2 h at 80 °C. Insoluble residues were removed by filtration through a silica pad (elution with water/isopropyl alcohol/ethyl acetate v/v/v 1:3:6 + 1 % aqueous ammonia). The solvent was removed in vacuum and the brown oily residue was redissolved in pyridine (30 mL). At 0 °C acetic anhydride (15 mL) was added and the mixture was stirred for 12 h at room temperature. Methylene chloride was added and the solution was washed twice with 1 M HCl, sat. $NaHCO_3$, water and brine. The organic layer was dried with sodium sulphate and the solvent was removed in vacuum. Ac_4GlcNAz was obtained as a colorless foam (302 mg, 702 µmol, 31 %) after column chromatography (gradient cyclohexane/ethyl acetate v/v 3:1-1:1) in an anomeric ratio of α/β = 2:1, Rf value: 0.07 (cyclohexane/ethyl acetate 2:1).1H-NMR (400 MHz, $CDCl_3$): δ = [α-anomer] 6.41 (br. d, 1H, J = 8.9 Hz, NH), 6.21 (d, 1H, J = 3.7 Hz, H1), 5.30 (dd, 1H, J = 9.7, 10.8 Hz, H3) 5.21 (dd, 1H, J = 9.7, 9.8 Hz, H4), 4.45 (ddd, 1H, J = 3.7, 8.9, 10.8 Hz, H2), 4.27 (dd, 1H, J = 4.1, 12.5 Hz, H6a), 4.08 (dd, 1H, J = 2.4, 12.5 Hz, H6b), 4.02 (ddd, 1H, J = 2.4, 4.1, 9.8 Hz, H5), 3.93 (s, 2H, CH2ab-N3), 2.21, 2.06, 2.05, 2.09 (4x s, 3H, CH3); [β-anomer] 6.38 (br. d, 1H, J = 9.4 Hz, NH), 5.79 (d, 1H, J = 8.7 Hz, H1) 5.23 (dd, 1H, J = 9.6, 10.5 Hz, H3), 5.14 (dd, 1H, J = 9.6, 9.7 Hz, H4), 4.28 (dd, 1H, J = 4.7, 12.6 Hz, H6a), 4.21 (ddd, 1H, J = 8.7, 9.4, 10.5 Hz, H2), 4.13 (dd, 1H, J = 2.5, 12.6 Hz, H6b), 3.91 (s, 2H, CH2ab-N3), 3.83 (ddd, 1H, J = 2.5, 4.7, 9.7 Hz, H5), 2.11, 2.09, 2.04, 2.04 (4x s, 3H, CH3) ppm.13C-NMR (100 MHz, CDCl3): δ = [α-anomer] 171.67, 170.79, 169.26, 168.78 (4x COO), 166.97 (CON), 90.44 (C1), 70.51 (C3), 69.99 (C5), 67.58 (C4), 61.65 (C6), 52.62 (CH2N3),51.42 (C2), 21.03, 20.82, 20.72, 20.70 (4x CH3); [β-anomer] 170.99, 170.76, 169.43, 169.39 (4x COO), 167.14 (CON), 92.40 (C1), 73.13 (C5), 72.31 (C3), 67.82 (C4), 61.75 (C6), 53.48 (C2), 52.76 (CH2N3), 21.00, 20.85, 20.72, 20.70 (4x CH3) ppm. HRMS (ESI-pos): m/z calc. for C16H22NaN4O10 [M+Na]+: 453.12281; found: 453.12242, Δppm: 0.86.[11, 68-69]

Supporting Figures

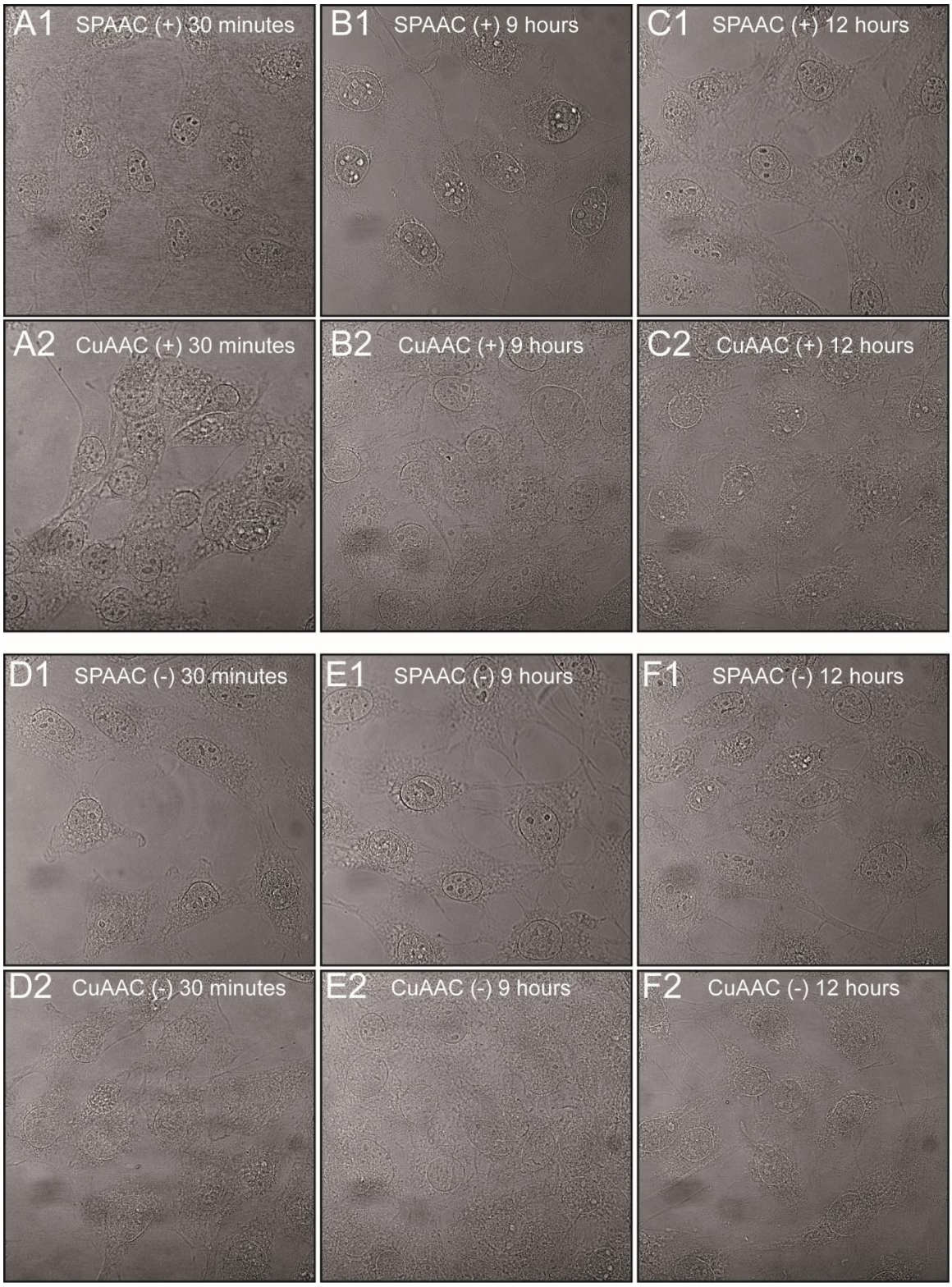

Figure S 1: Individual phase contrast (PC) images of NIH 3T3 fibroblasts labeled via SPAAC (A1-F1) or CuAAC (A2-F2). NIH 3T3 cells were grown with (A-C) or without (D-F) 50 µM Ac4GlcNAz and were imaged after 30 minutes (A,D), 3 hours (B, E) and 12 hours (C, F) after the labeling reaction.

Supporting Tables

Table S 1: TaqMan Gene Expression primer; species = mouse; Fluorescent dye = fluorescein amidite (FAM).

Applied Biosystems Assay ID	Gene
Mm99999915_g	GAPDH (Glycerinaldehyd-3-phosphat-Dehydrogenase)
Mm00432314_m1	Caspase 2
Mm01223702_m1	APAF 1 (Apoptotic protease activating factor 1)
Mm00477631_m1	Bcl 2 (B cell lymphoma 2)
Mm00432051_m1	BAX (Bcl 2 associated X protein)

References

1. Freeze, H. H., Genetic defects in the human glycome. *Nature reviews. Genetics* **2006,** *7* (7), 537-51. DOI: 10.1038/nrg1894.
2. Hart, G. W.; Housley, M. P.; Slawson, C., Cycling of O-linked beta-N-acetylglucosamine on nucleocytoplasmic proteins. *Nature* **2007,** *446* (7139), 1017-22. DOI: 10.1038/nature05815.
3. Moremen, K. W.; Tiemeyer, M.; Nairn, A. V., Vertebrate protein glycosylation: diversity, synthesis and function. *Nature reviews. Molecular cell biology* **2012,** *13* (7), 448-62. DOI: 10.1038/nrm3383.
4. Homann, A.; Qamar, R. U.; Serim, S.; Dersch, P.; Seibel, J., Bioorthogonal metabolic glycoengineering of human larynx carcinoma (HEp-2) cells targeting sialic acid. *Beilstein journal of organic chemistry* **2010,** *6*, 24. DOI: 10.3762/bjoc.6.24.
5. Letschert, S.; Gohler, A.; Franke, C.; Bertleff-Zieschang, N.; Memmel, E.; Doose, S.; Seibel, J.; Sauer, M., Super-resolution imaging of plasma membrane glycans. *Angewandte Chemie* **2014,** *53* (41), 10921-4. DOI: 10.1002/anie.201406045.
6. Memmel, E.; Homann, A.; Oelschlaeger, T. A.; Seibel, J., Metabolic glycoengineering of Staphylococcus aureus reduces its adherence to human T24 bladder carcinoma cells. *Chemical communications* **2013,** *49* (66), 7301-3. DOI: 10.1039/c3cc43424a.
7. Sarkar, A. K.; Fritz, T. A.; Taylor, W. H.; Esko, J. D., Disaccharide uptake and priming in animal cells: inhibition of sialyl Lewis X by acetylated Gal beta 1-->4GlcNAc beta-O-naphthalenemethanol. *Proceedings of the National Academy of Sciences of the United States of America* **1995,** *92* (8), 3323-7.
8. Sarkar, A. K.; Rostand, K. S.; Jain, R. K.; Matta, K. L.; Esko, J. D., Fucosylation of disaccharide precursors of sialyl LewisX inhibit selectin-mediated cell adhesion. *The Journal of biological chemistry* **1997,** *272* (41), 25608-16.
9. Zaro, B. W.; Yang, Y. Y.; Hang, H. C.; Pratt, M. R., Chemical reporters for fluorescent detection and identification of O-GlcNAc-modified proteins reveal glycosylation of the ubiquitin ligase NEDD4-1. *Proceedings of the National Academy of Sciences of the United States of America* **2011,** *108* (20), 8146-51. DOI: 10.1073/pnas.1102458108.
10. Saxon, E.; Luchansky, S. J.; Hang, H. C.; Yu, C.; Lee, S. C.; Bertozzi, C. R., Investigating cellular metabolism of synthetic azidosugars with the Staudinger ligation. *Journal of the American Chemical Society* **2002,** *124* (50), 14893-902.
11. Luchansky, S. J.; Hang, H. C.; Saxon, E.; Grunwell, J. R.; Yu, C.; Dube, D. H.; Bertozzi, C. R., Constructing Azide-Labeled Cell Surfaces Using Polysaccharide Biosynthetic Pathways. *Methods in Enzymologys* **2003,** *362*, 249-272. DOI: 10.1016/s0076-6879(03)01018-8.
12. Hsu, T. L.; Hanson, S. R.; Kishikawa, K.; Wang, S. K.; Sawa, M.; Wong, C. H., Alkynyl sugar analogs for the labeling and visualization of glycoconjugates in cells. *Proceedings of the National Academy of Sciences of the United States of America* **2007,** *104* (8), 2614-9. DOI: 10.1073/pnas.0611307104.

13. Boyce, M.; Bertozzi, C. R., Bringing chemistry to life. *Nature methods* **2011,** *8* (8), 638-42. DOI: 10.1038/nmeth.1657.
14. Laughlin, S. T.; Bertozzi, C. R., Imaging the glycome. *Proceedings of the National Academy of Sciences of the United States of America* **2009,** *106* (1), 12-7. DOI: 10.1073/pnas.0811481106.
15. Prescher, J. A.; Bertozzi, C. R., Chemistry in living systems. *Nature chemical biology* **2005,** *1* (1), 13-21. DOI: 10.1038/nchembio0605-13.
16. Jiang, H.; Zheng, T.; Lopez-Aguilar, A.; Feng, L.; Kopp, F.; Marlow, F. L.; Wu, P., Monitoring dynamic glycosylation in vivo using supersensitive click chemistry. *Bioconjugate chemistry* **2014,** *25* (4), 698-706. DOI: 10.1021/bc400502d.
17. Huisgen, R., Kinetics and Mechanism of 1,3-Dipolr Cycloadditions. *Angewandte Chemie International Edition in English* **1963,** *2* (11), 633-645. DOI: 10.1002/anie.196306331.
18. Tornoe, C. W.; Christensen, C.; Meldal, M., Peptidotriazoles on solid phase: [1,2,3]-triazoles by regiospecific copper(i)-catalyzed 1,3-dipolar cycloadditions of terminal alkynes to azides. *The Journal of organic chemistry* **2002,** *67* (9), 3057-64.
19. Rostovtsev, V. V.; Green, L. G.; Fokin, V. V.; Sharpless, K. B., A Stepwise Huisgen Cycloaddition Process: Copper(I)-Catalyzed Regioselective "Ligation" of Azides and Terminal Alkynes. *Angewandte Chemie International Edition* **2002,** *41* (14), 2596-2599. DOI: 10.1002/1521-3773(20020715)41:14<2596::aid-anie2596>3.0.co;2-4.
20. Agard, N. J.; Prescher, J. A.; Bertozzi, C. R., A strain-promoted [3 + 2] azide-alkyne cycloaddition for covalent modification of biomolecules in living systems. *Journal of the American Chemical Society* **2004,** *126* (46), 15046-7. DOI: 10.1021/ja044996f.
21. Baskin, J. M.; Prescher, J. A.; Laughlin, S. T.; Agard, N. J.; Chang, P. V.; Miller, I. A.; Lo, A.; Codelli, J. A.; Bertozzi, C. R., Copper-free click chemistry for dynamic in vivo imaging. *Proceedings of the National Academy of Sciences of the United States of America* **2007,** *104* (43), 16793-7. DOI: 10.1073/pnas.0707090104.
22. Lang, K.; Chin, J. W., Bioorthogonal reactions for labeling proteins. *ACS chemical biology* **2014,** *9* (1), 16-20. DOI: 10.1021/cb4009292.
23. Elchinger, P.-H.; Faugeras, P.-A.; Boëns, B.; Brouillette, F.; Montplaisir, D.; Zerrouki, R.; Lucas, R., Polysaccharides: The "Click" Chemistry Impact. *Polymers* **2011,** *3* (4), 1607-1651. DOI: 10.3390/polym3041607.
24. Jewett, J. C.; Sletten, E. M.; Bertozzi, C. R., Rapid Cu-free click chemistry with readily synthesized biarylazacyclooctynones. *Journal of the American Chemical Society* **2010,** *132* (11), 3688-90. DOI: 10.1021/ja100014q.
25. Gaetke, L., Copper toxicity, oxidative stress, and antioxidant nutrients. *Toxicology* **2003,** *189* (1-2), 147-163. DOI: 10.1016/s0300-483x(03)00159-8.
26. Brewer, G. J., Risks of copper and iron toxicity during aging in humans. *Chemical research in toxicology* **2010,** *23* (2), 319-26. DOI: 10.1021/tx900338d.
27. Stadtman, E. R.; Oliver, C. N., Metal-catalyzed oxidation of proteins. Physiological consequences. *The Journal of biological chemistry* **1991,** *266* (4), 2005-8.
28. Hong, V.; Presolski, S. I.; Ma, C.; Finn, M. G., Analysis and optimization of copper-catalyzed azide-alkyne cycloaddition for bioconjugation. *Angewandte Chemie* **2009,** *48* (52), 9879-83. DOI: 10.1002/anie.200905087.
29. Liu, Y.; Sun, G.; David, A.; Sayre, L. M., Model studies on the metal-catalyzed protein oxidation: structure of a possible His-Lys cross-link. *Chemical research in toxicology* **2004,** *17* (1), 110-8. DOI: 10.1021/tx034167s.
30. Trivedy, C.; Meghji, S.; Warnakulasuriya, K. A.; Johnson, N. W.; Harris, M., Copper stimulates human oral fibroblasts in vitro: a role in the pathogenesis of oral submucous fibrosis. *Journal of oral pathology & medicine : official publication of the International Association of Oral Pathologists and the American Academy of Oral Pathology* **2001,** *30* (8), 465-70.
31. Cao, B.; Zheng, Y.; Xi, T.; Zhang, C.; Song, W.; Burugapalli, K.; Yang, H.; Ma, Y., Concentration-dependent cytotoxicity of copper ions on mouse fibroblasts in vitro: effects of

copper ion release from TCu380A vs TCu220C intra-uterine devices. *Biomedical microdevices* **2012,** *14* (4), 709-20. DOI: 10.1007/s10544-012-9651-x.
32. Tchounwou, P. B.; Newsome, C.; Williams, J.; Glass, K., Copper-Induced Cytotoxicity and Transcriptional Activation of Stress Genes in Human Liver Carcinoma (HepG(2)) Cells. *Metal ions in biology and medicine : proceedings of the ... International Symposium on Metal Ions in Biology and Medicine held ... = Les ions metalliques en biologie et en medecine : ... Symposium international sur les ions metalliques* **2008,** *10*, 285-290.
33. Uttamapinant, C.; Sanchez, M. I.; Liu, D. S.; Yao, J. Z.; Ting, A. Y., Site-specific protein labeling using PRIME and chelation-assisted click chemistry. *Nat Protoc* **2013,** *8* (8), 1620-34. DOI: 10.1038/nprot.2013.096.
34. Uttamapinant, C.; Tangpeerachaikul, A.; Grecian, S.; Clarke, S.; Singh, U.; Slade, P.; Gee, K. R.; Ting, A. Y., Fast, cell-compatible click chemistry with copper-chelating azides for biomolecular labeling. *Angewandte Chemie* **2012,** *51* (24), 5852-6. DOI: 10.1002/anie.201108181.
35. Presolski, S. I.; Hong, V. P.; Finn, M. G., Copper-Catalyzed Azide-Alkyne Click Chemistry for Bioconjugation. *Current protocols in chemical biology* **2011,** *3* (4), 153-162. DOI: 10.1002/9780470559277.ch110148.
36. Kennedy, D. C.; McKay, C. S.; Legault, M. C.; Danielson, D. C.; Blake, J. A.; Pegoraro, A. F.; Stolow, A.; Mester, Z.; Pezacki, J. P., Cellular consequences of copper complexes used to catalyze bioorthogonal click reactions. *Journal of the American Chemical Society* **2011,** *133* (44), 17993-8001. DOI: 10.1021/ja2083027.
37. Chang, P. V.; Prescher, J. A.; Hangauer, M. J.; Bertozzi, C. R., Imaging cell surface glycans with bioorthogonal chemical reporters. *Journal of the American Chemical Society* **2007,** *129* (27), 8400-1. DOI: 10.1021/ja070238o.
38. Baskin, J. M.; Dehnert, K. W.; Laughlin, S. T.; Amacher, S. L.; Bertozzi, C. R., Visualizing enveloping layer glycans during zebrafish early embryogenesis. *Proceedings of the National Academy of Sciences of the United States of America* **2010,** *107* (23), 10360-5. DOI: 10.1073/pnas.0912081107.
39. Laughlin, S. T.; Bertozzi, C. R., In vivo imaging of Caenorhabditis elegans glycans. *ACS chemical biology* **2009,** *4* (12), 1068-72. DOI: 10.1021/cb900254y.
40. Dehnert, K. W.; Beahm, B. J.; Huynh, T. T.; Baskin, J. M.; Laughlin, S. T.; Wang, W.; Wu, P.; Amacher, S. L.; Bertozzi, C. R., Metabolic labeling of fucosylated glycans in developing zebrafish. *ACS chemical biology* **2011,** *6* (6), 547-52. DOI: 10.1021/cb100284d.
41. Dehnert, K. W.; Baskin, J. M.; Laughlin, S. T.; Beahm, B. J.; Naidu, N. N.; Amacher, S. L.; Bertozzi, C. R., Imaging the sialome during zebrafish development with copper-free click chemistry. *Chembiochem : a European journal of chemical biology* **2012,** *13* (3), 353-7. DOI: 10.1002/cbic.201100649.
42. Chang, P. V.; Prescher, J. A.; Sletten, E. M.; Baskin, J. M.; Miller, I. A.; Agard, N. J.; Lo, A.; Bertozzi, C. R., Copper-free click chemistry in living animals. *Proceedings of the National Academy of Sciences of the United States of America* **2010,** *107* (5), 1821-6. DOI: 10.1073/pnas.0911116107.
43. Breidenbach, M. A.; Palaniappan, K. K.; Pitcher, A. A.; Bertozzi, C. R., Mapping yeast N-glycosites with isotopically recoded glycans. *Molecular & cellular proteomics : MCP* **2012,** *11* (6), M111 015339. DOI: 10.1074/mcp.M111.015339.
44. Beahm, B. J.; Dehnert, K. W.; Derr, N. L.; Kuhn, J.; Eberhart, J. K.; Spillmann, D.; Amacher, S. L.; Bertozzi, C. R., A visualizable chain-terminating inhibitor of glycosaminoglycan biosynthesis in developing zebrafish. *Angewandte Chemie* **2014,** *53* (13), 3347-52. DOI: 10.1002/anie.201310569.
45. Elmore, S., Apoptosis: a review of programmed cell death. *Toxicologic pathology* **2007,** *35* (4), 495-516. DOI: 10.1080/01926230701320337.
46. Fulda, S.; Debatin, K. M., Extrinsic versus intrinsic apoptosis pathways in anticancer chemotherapy. *Oncogene* **2006,** *25* (34), 4798-811. DOI: 10.1038/sj.onc.1209608.

47. Pradelli, L. A.; Beneteau, M.; Ricci, J. E., Mitochondrial control of caspase-dependent and -independent cell death. *Cellular and molecular life sciences : CMLS* **2010,** *67* (10), 1589-97. DOI: 10.1007/s00018-010-0285-y.
48. Zhivotovsky, B.; Orrenius, S., Caspase-2 function in response to DNA damage. *Biochemical and biophysical research communications* **2005,** *331* (3), 859-67. DOI: 10.1016/j.bbrc.2005.03.191.
49. Kumar, S., Caspase 2 in apoptosis, the DNA damage response and tumour suppression: enigma no more? *Nature reviews. Cancer* **2009,** *9* (12), 897-903. DOI: 10.1038/nrc2745.
50. Lalier, L.; Cartron, P. F.; Juin, P.; Nedelkina, S.; Manon, S.; Bechinger, B.; Vallette, F. M., Bax activation and mitochondrial insertion during apoptosis. *Apoptosis : an international journal on programmed cell death* **2007,** *12* (5), 887-96. DOI: 10.1007/s10495-007-0749-1.
51. Westphal, D.; Kluck, R. M.; Dewson, G., Building blocks of the apoptotic pore: how Bax and Bak are activated and oligomerize during apoptosis. *Cell death and differentiation* **2014,** *21* (2), 196-205. DOI: 10.1038/cdd.2013.139.
52. Milosevic, J.; Hoffarth, S.; Huber, C.; Schuler, M., The DNA damage-induced decrease of Bcl-2 is secondary to the activation of apoptotic effector caspases. *Oncogene* **2003,** *22* (44), 6852-6. DOI: 10.1038/sj.onc.1206716.
53. Purring-Koch, C.; McLendon, G., Cytochrome c binding to Apaf-1: the effects of dATP and ionic strength. *Proceedings of the National Academy of Sciences of the United States of America* **2000,** *97* (22), 11928-31. DOI: 10.1073/pnas.220416197.
54. Li, P.; Nijhawan, D.; Budihardjo, I.; Srinivasula, S. M.; Ahmad, M.; Alnemri, E. S.; Wang, X., Cytochrome c and dATP-Dependent Formation of Apaf-1/Caspase-9 Complex Initiates an Apoptotic Protease Cascade. *Cell* **1997,** *91* (4), 479-489. DOI: 10.1016/s0092-8674(00)80434-1.
55. Garcia-Saez, A. J., The secrets of the Bcl-2 family. *Cell death and differentiation* **2012,** *19* (11), 1733-40. DOI: 10.1038/cdd.2012.105.
56. Lindsay, J.; Esposti, M. D.; Gilmore, A. P., Bcl-2 proteins and mitochondria--specificity in membrane targeting for death. *Biochimica et biophysica acta* **2011,** *1813* (4), 532-9. DOI: 10.1016/j.bbamcr.2010.10.017.
57. Deng, G.; Su, J. H.; Ivins, K. J.; Van Houten, B.; Cotman, C. W., Bcl-2 facilitates recovery from DNA damage after oxidative stress. *Experimental neurology* **1999,** *159* (1), 309-18. DOI: 10.1006/exnr.1999.7145.
58. Kelekar, A.; Thompson, C. B., Bcl-2-family proteins: the role of the BH3 domain in apoptosis. *Trends in Cell Biology* **1998,** *8* (8), 324-330. DOI: 10.1016/s0962-8924(98)01321-x.
59. Fleury, C.; Mignotte, B.; Vayssière, J.-L., Mitochondrial reactive oxygen species in cell death signaling. *Biochimie* **2002,** *84* (2-3), 131-141. DOI: 10.1016/s0300-9084(02)01369-x.
60. Hensley, K.; Robinson, K. A.; Gabbita, S. P.; Salsman, S.; Floyd, R. A., Reactive oxygen species, cell signaling, and cell injury. *Free Radical Biology and Medicine* **2000,** *28* (10), 1456-1462. DOI: 10.1016/s0891-5849(00)00252-5.
61. Halliwell, B., Biochemistry of oxidative stress. *Biochemical Society transactions* **2007,** *35* (Pt 5), 1147-50. DOI: 10.1042/BST0351147.
62. Halliwell, B.; Whiteman, M., Measuring reactive species and oxidative damage in vivo and in cell culture: how should you do it and what do the results mean? *British journal of pharmacology* **2004,** *142* (2), 231-55. DOI: 10.1038/sj.bjp.0705776.
63. Hong, V.; Steinmetz, N. F.; Manchester, M.; Finn, M. G., Labeling live cells by copper-catalyzed alkyne--azide click chemistry. *Bioconjugate chemistry* **2010,** *21* (10), 1912-6. DOI: 10.1021/bc100272z.
64. Dollwet, H. H. A.; Sorenson, J. R. J., HISTORIC USES OF COPPER-COMPOUNDS IN MEDICINE. *Trace Elements in Medicine* **1985,** *2* (2), 80-87.
65. Bienert, G. P.; Schjoerring, J. K.; Jahn, T. P., Membrane transport of hydrogen peroxide. *Bba-Biomembranes* **2006,** *1758* (8), 994-1003. DOI: DOI 10.1016/j.bbamem.2006.02.015.
66. Bernardin, A.; Cazet, A.; Guyon, L.; Delannoy, P.; Vinet, F.; Bonnaffe, D.; Texier, I., Copper-free click chemistry for highly luminescent quantum dot conjugates: application to in vivo metabolic imaging. *Bioconjugate chemistry* **2010,** *21* (4), 583-8. DOI: 10.1021/bc900564w.

67. Saxon, E., Cell Surface Engineering by a Modified Staudinger Reaction. *Science* **2000,** *287* (5460), 2007-2010. DOI: 10.1126/science.287.5460.2007.
68. Laughlin, S. T.; Agard, N. J.; Baskin, J. M.; Carrico, I. S.; Chang, P. V.; Ganguli, A. S.; Hangauer, M. J.; Lo, A.; Prescher, J. A.; Bertozzi, C. R., Metabolic labeling of glycans with azido sugars for visualization and glycoproteomics. *Methods Enzymol* **2006,** *415*, 230-50. DOI: 10.1016/S0076-6879(06)15015-6.
69. Laughlin, S. T.; Bertozzi, C. R., Metabolic labeling of glycans with azido sugars and subsequent glycan-profiling and visualization via Staudinger ligation. *Nat Protoc* **2007,** *2* (11), 2930-44. DOI: 10.1038/nprot.2007.422.
70. Ross, D. D.; Joneckis, C. C.; Ordonez, J. V.; Sisk, A. M.; Wu, R. K.; Hamburger, A. W. N. R. E.; Nora, R. E., Estimation of cell survival by flow cytometric quantification of fluorescein diacetate/propidium iodide viable cell number. *Cancer research* **1989,** *49* (14), 3776-82.
71. Jones, K. H.; Senft, J. A., An improved method to determine cell viability by simultaneous staining with fluorescein diacetate-propidium iodide. *Journal of Histochemistry & Cytochemistry* **1985,** *33* (1), 77-79. DOI: 10.1177/33.1.2578146.
72. Clarke, J. M.; Gillings, M. R.; Altavilla, N.; Beattie, A. J., Potential problems with fluorescein diacetate assays of cell viability when testing natural products for antimicrobial activity. *Journal of Microbiological Methods* **2001,** *46* (3), 261-267. DOI: 10.1016/s0167-7012(01)00285-8.
73. Jin, Q. H.; Zhao, B.; Zhang, X. J., Cytochrome c release and endoplasmic reticulum stress are involved in caspase-dependent apoptosis induced by G418. *Cellular and molecular life sciences : CMLS* **2004,** *61* (14), 1816-25. DOI: 10.1007/s00018-004-4143-7.
74. Schmittgen, T. D.; Livak, K. J., Analyzing real-time PCR data by the comparative CT method. *Nature Protocols* **2008,** *3* (6), 1101-1108. DOI: 10.1038/nprot.2008.73.

Chapter 4: Matrix Metalloproteinase Responsive Delivery of fibroblast growth factor 2

Marcus Gutmann[1], Valerie Spieler[1], Martina Raschig[1], Ulrike Potschka[2], Susanne Neidhold[2], Götz Münch[2], Lorenz Meinel[1] and Tessa Lühmann[1]*

[1]Institute of Pharmacy and Food Chemistry, University of Würzburg, DE-97074 Würzburg, Germany,
[2]AdvanceCOR GmbH, DE-82152 Martinsried, Germany

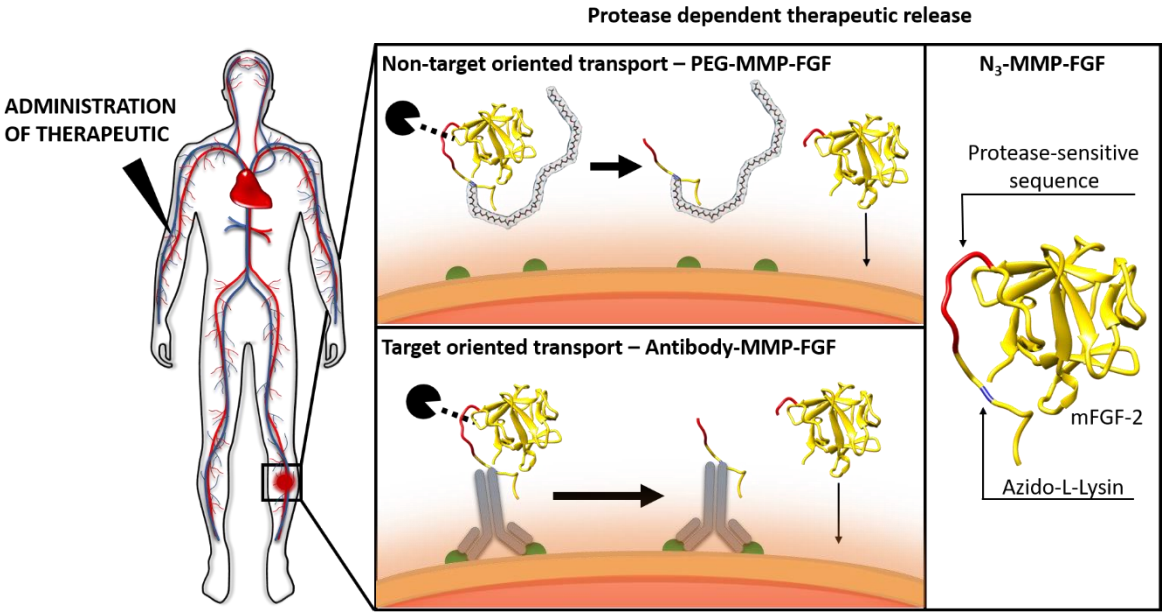

Unpublished manuscript

Introduction

Proteins and peptides offer great potential as therapeutic substances by providing superior drug properties such as customized structures to control their activity and interaction with specific targets, leading to less cross reactivity and a lower risk of possible side effects. However, their drawbacks are not negligible: Poor pharmacokinetic (PK) properties with short half-life due to rapid metabolism, fast degradation by endogenous proteases or rapid elimination by clearance through the kidneys. To overcome these limitations, appropriate high doses or frequent dosages are needed, causing problems like immune response through recognition/neutralization by antibodies or possible toxicity and aggregation through plasma level spikes.[1-3] The chemical modification of native proteins and peptides presents an appropriate tool to address these disadvantages. Here, depending on the modification, it has to be considered whether the focus should be set to a general improvement of protein/peptide properties – then synthetic and natural polymers can be chosen as modification – or to target a specific structure/substance – then a targeting-ligand is the adjustment of choice (vide infra) .[4-5]

Referring to the improvement of therapeutic properties, the attachment of polyethylene glycol (PEG) chains is a common, well studied and Food and Drug Administration approved method.[5-6] Through its flexibility, variability, hydrophobicity and low toxicity, the PEG structure provides (i) increased circulation half-life, mainly due to the increase in hydrodynamic size, (ii) reduced degradation and immunogenicity by masked surface epitopes and (iii) enhanced water solubility.[7-8] PEGylation may be obtained by different strategies and can easily alter the characteristics of the protein, affecting clinical effects due to reduced bioactivity through variation in quantity and position of attached PEG chains.[9-10] However, reduced bioactivity is compensated by improved PK profiles, which empowers the protein to be potent enough for clinical applications. Conventional conjugation strategies aiming at amines or thiols result into a mixture of products and batch-to-batch variation, thus compromising reproducible PK and Pharmacodynamic (PD) performances. At this point, new improved strategies come into play: by anchoring artificial functional groups into the protein sequence, bioorthogonal coupling of the modified protein to a carrier molecule is possible, leading to selective and site-specific conjugations.[11-13] Besides PEG, various other synthetic polymers like poly(N-vinylpyrrolidone), polyglycerol, polyoxazoline and natural polymers like polysaccharides, poly(amino acid)-based hybrids, polypeptides and lipids are available.[4-5] An advantage of those synthetic polymers is that molecular properties can be controlled more easily than those obtained from natural sources.

As far as targeting-ligands are concerned, antibody conjugates are the first choice of secure delivery systems. Antibody conjugates provide (i) increased circulation half-live through their molecular size

and salvage pathway capability of the Fc terminus, (ii) selective targeting of certain structures (e.g. healthy and diseased tissue), thereby avoiding nonspecific delivery of their payload, and (iii) minimal immunogenicity.[14-16] The payload plays a key role and must fulfill certain criteria to be suitable, including high level of potency and relative hydrophilicity. Other targeting-ligands under current clinical development range from small molecules and peptides to antibody fragments and protein scaffolds.[17]

Both strategies, target and non-target oriented, are challenged by the size difference between the protein cargo, typically small size in cases of growth factors and cytokines, and the chosen modification. Despite site-directed conjugation strategies, the bulkiness of the modification is able to cover essential parts of the therapeutic, thus shielding it effectively from its target site. To overcome these challenges, cleavable linkers between the modification and the cargo protein have to be implemented, to remove the modification at a clearly defined target site and thus revealing the full spectrum of the native protein.

The cleavable linker has to ensure, that the therapeutic remains attached to the modification during body circulation and is only released at the target site. Lysis of different cleavable linkers is based on chemical and biochemical properties and is performed through different processes (e.g. reduction, low pH, enzyme hydrolysis etc.) releasing an unmodified therapeutic and possible byproducts.[17-18] Reductively cleavable linkers are formed of disulfide bridges and are cleaved through reducing conditions. These linkers are more stable in bloodstream than in intracellular compartments and are predominantly lysed due to reduced glutathione concentration in the cellular cytoplasm. The disadvantages of this system are low half-time and possible byproducts depending on the chosen disulfide spacer. Sterically shielding of the disulfide bonds allows fine tuning of the half-time but delays or even prevents adequate release of the therapeutic.[19-24] Acid cleavable linkers are most commonly formed of hydrazones[19, 25], cis-aconityl[26], p-methoxybenzyl acetals[25] and trityl bonds[27] that ideally remain stable at the neutral pH of blood circulation and are cleaved through acidic conditions in the endosome. Disadvantages are derived from insufficient stability of the chemical linker with increased drug release during blood circulation. A great diversity of other acid cleavable linkers exists.[28] Enzymatic cleavable linkers, formed of small peptide sequences, enable the release of the attached therapeutic at a specific location via recognition by proteases. Such peptide linkers allow a “traceless release” of the therapeutic without byproducts by cleaving the linker peptides at the protease’s recognition site, thus leaving only two or three amino acid residues on the therapeutic which should be well tolerated.[29] Enzymatic cleavable linkers as an emerging technique overcome the pitfalls of reductively and acid cleavable linkers in terms of cytotoxicity of the chemical linker, byproducts and protein release during blood circulation as well as during shelf-storage. However,

precise investigation has to be conducted concerning the existence and the concentration of the selected protease at the targeted location to ensure proper release of the therapeutic payload.[30]

In the following chapter, we provide two delivery strategies – target and non-target oriented – for controlled release of basic fibroblast growth factor-2 (FGF-2) triggered by disease-associated matrix metalloproteinases (MMP).

Results

Preparation of fibroblast growth factor variants for bioorthogonal coupling

We developed two analogues of the FGF-2 to conjugate the therapeutic growth factor to targeting and non-targeting molecules to maintain its bioactivity and to improve the PK profile. The method took advantage of a genetic code expansion mechanisms found in archaebacteria, *Methanosarcina barkeri*, which enables the incorporation of an additional amino acid L-pyrrolysine (Pyl) - encoded by the amber codon UAG - into the protein biosynthesis. Two enzymes, the $tRNA^{Pyl}$, which recognizes the amber codon UAG during translation, and the Pyl-tRNA synthetase, which transfers Pyl to its specific tRNA ($tRNA^{Pyl}$), are essential for a correct incorporation of the unnatural amino acid (uAA).[13, 31] The pylRS/$tRNA^{Pyl}$ system was transferred to Escherichia coli (E. coli) and N_3-L-lysine (Alk) (Figure 1, S1), a Pyl derived analogue, was used as uAA for the incorporation.

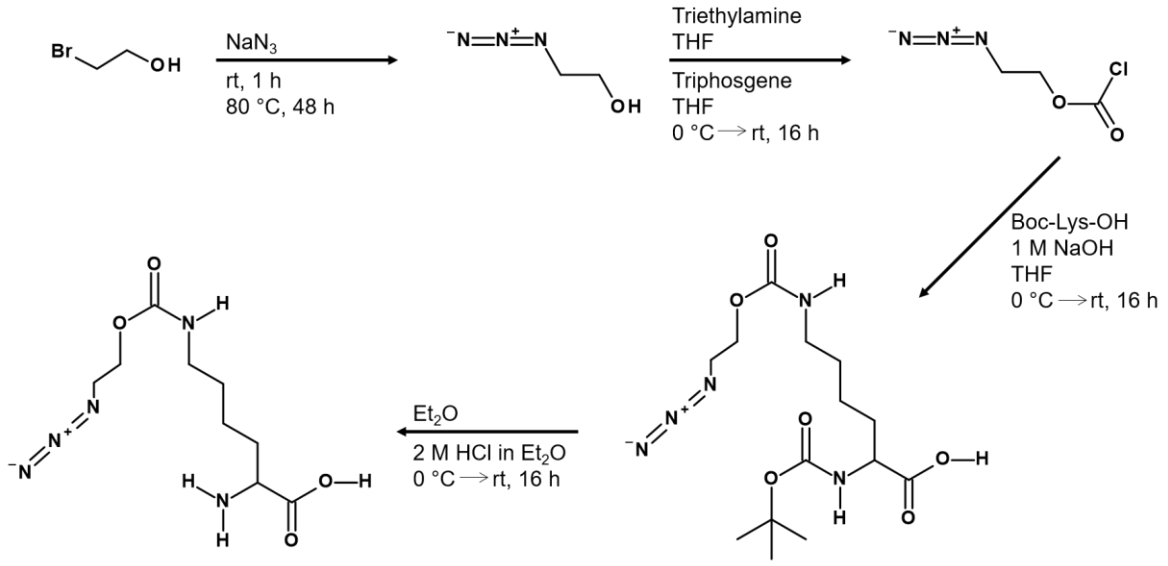

Figure 1: Synthesis of the unnatural amino acid N_3-L-lysine (Alk).

The first variant of FGF-2, the 8(TAG)-FGF-2, is derived from the murine fibroblast growth factor, where the 8th position of the 154 amino acid long FGF-2 sequence was changed from UCG, encoding for serine, to UAG, encoding for pyrrolysine (Figure 2) as described before[13]. The second variant of

FGF-2, the 8(TAG)-MMP-FGF-2, shows the same genetic modification as the 8(TAG)-FGF-2 but with additional changes in position #12 as well as #14-#19. The additional positions (#12, #14-#19) were changed to generate a protease sensitive region (-**GPQGIAGQ**-) within the N-terminal region of the FGF-2 (Figure 2). Both FGF-2 variants, with the incorporated N_3-L-lysine at position #8 allow the specific linkage of FGF-2 with a molecule bearing an alkyne-analogue via bioorthogonal click reaction (strain promoted azide-alkyne cycloaddition (SPAAC) and copper(I)-catalyzed azide-alkyne cycloaddition (CuAAC)).

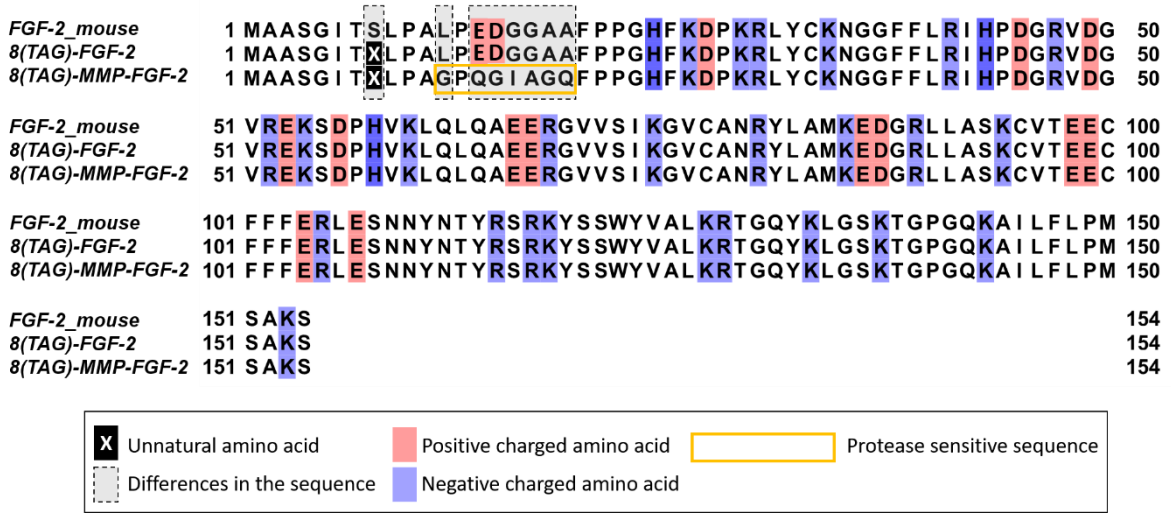

Figure 2: Amino acid sequence alignment of FGF-2_mouse, 8(TAG)-FGF-2 and 8(TAG)-MMP-FGF-2. Differences in the sequences are shown on grey framed background, position of the unnatural amino acid is marked by an X on black background and protease sensitive sequence is framed by an orange box. Charged residues are shown in blue (negative charged) and red (positive charged) colors.

After expression in *E. coli* and affinity chromatography for purification, purity of both FGF-2 variants was assessed by SDS-Page and/or by HPLC resulting in a single band after Coomassie staining at approximately 14 kDa on a 15% SDS-Page gel (Figure S2 A, S3 A) and a single signal in the HPLC chromatogram recorded at 214 nm (Figure S2 C). The correct incorporation of the uAA Alk at position 8 in the amino acid sequence of N_3-FGF-2 and N_3-MMP-FGF-2 was analyzed by MALDI-MS, resulting in an observed average mass of 17171.4122 Da (calc. average mass without methionine 17173.47 Da) for N_3-MMP-FGF-2 and an observed average mass of 17192.6834 Da (calc. average mass without methionine 17175.44 Da) for N_3-FGF-2. (Figure S2 B, S3 B), respectively.

To collaborate the MALDI-MS results as well as to confirm the correct formation of the protease sensitive sequence (GPQGIAGQ), N_3-MMP-FGF-2 was separated by SDS-Page chromatography, extracted and digested with elastase. The resulting peptides were analyzed by NanoLC MS/MS. Two most representative peptide sequences (AASGIT*Alk*LPA**GPQGIAG** and

AASGIT*Alk*LPA**GPQGIAGQ**FPPGHFKDPKRL) were found and masses of the fragments were calculated showing the correct incorporation of the Alk at position 8 by fragment b7 (Figure 3) with an observed mass of 742.38 Da (calc. mass 742.388 Da) as well as the correct formation of the protease sensitive sequence by fragment y23 with an observed mass of 2428.33 Da (calc. mass 2428.327 Da) (Figure 3 B).

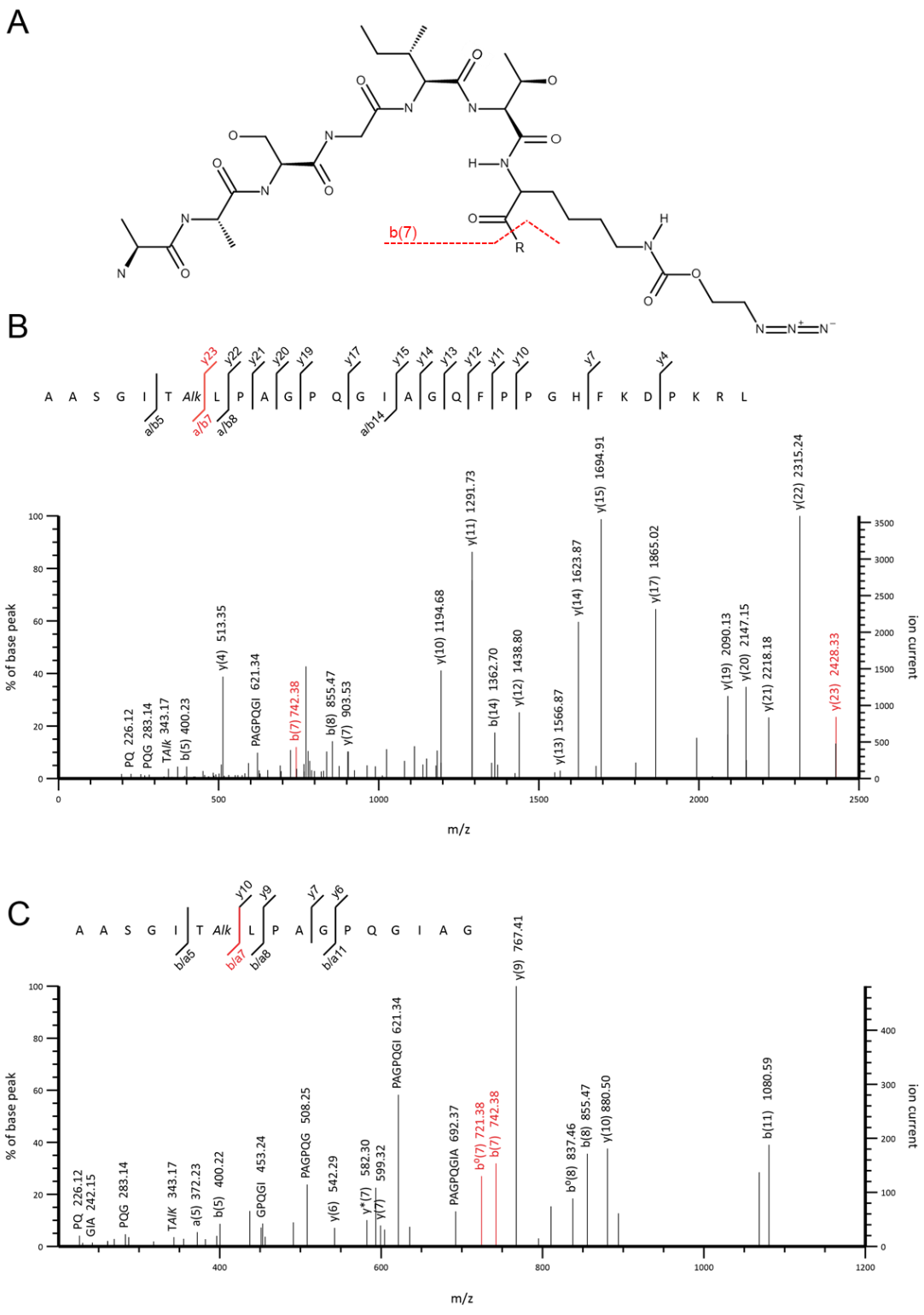

Figure 3: Elastase digestion of N_3-MMP-FGF-2 analyzed by LC MS/MS. (A) Structure of fragment b(7) displaying amino acid 2-8 of N_3-MMP-FGF-2, including N_3-L-lysine. Mass spectra of the N-terminal region displaying amino acid sequence 2-31 (B) and 2-18 (C) of all found peptides. Fragment b(7) shows the included Alk with the observed mass = 742.38 Da (calculated mass =742.388 Da) and fragment y(23) shows the protease sensitive sequence with the observed mass = 2428.33 Da (calculated mass = 2428.327 Da).

Preparation of PEGylated protease sensitive fibroblast growth factor 2

To prepare the PEGylated protease sensitive variant of FGF-2, N_3-MMP-FGF-2 was incubated with Dibenzocyclooctyne (DBCO)-mPEG 10 kDa for 48 h at 4 °C. After the SPAAC, the product (PEG-MMP-FGF-2) was purified from both educts (N_3-MMP-FGF-2 and DBCO-mPEG 10 kDa) by heparin-sepharose affinity chromatography (Figure 4 A). Both signals were analyzed by SDS-Page (Figure 4 B), resulting in PEG-MMP-FGF-2 for the first signal (Figure 4 A signal 1; 4 B lane 1) and N_3-MMP-FGF-2 for the second signal (Figure 4 A signal 2; 4 B lane 2). Purity of PEG-MMP-FGF-2 was assessed by SDS-Page and HPLC resulting in a single band after Coomassie staining at approximately 35 kDa on a 15% SDS-Page gel (Figure S4 A lane 3) and a single signal in the HPLC chromatogram (Figure S4 C) recorded at 214 nm. The correct formation of PEG-MMP-FGF-2 was analyzed by MALDI-MS, resulting in an observed average mass of 28293.139 Da. (Figure S4 B)

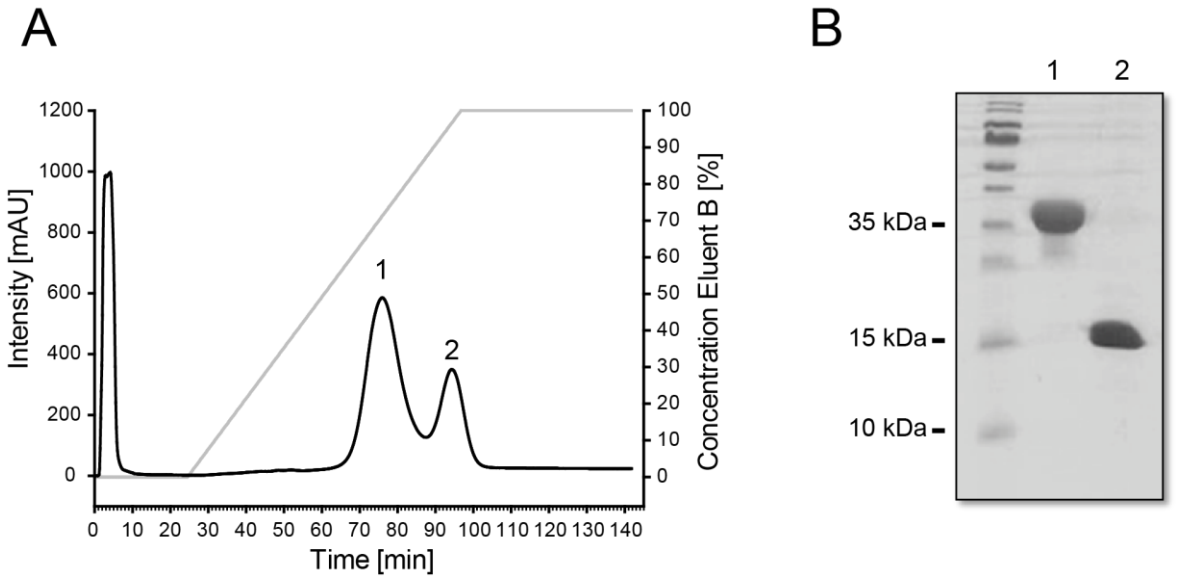

Figure 4: Heparin-sepharose purification of PEG-MMP-FGF-2 after SPAAC (N_3-MMP-FGF-2 + DBCO-PEG). (A) Elution profile of PEG-MMP-FGF-2 purified with heparin-sepharose affinity chromatography displaying PEG-MMP-FGF-2 (Signal 1) and N_3-MMP-FGF-2 (Signal 2). (B) SDS-PAGE after heparin-sepharose purification showing PEG-MMP-FGF-2 (Lane 1) and N_3-MMP-FGF-2 (Lane 2).

Biological activity of PEG-MMP-FGF-2 and N_3-MMP-FGF-2 was tested in cell-based assays employing NIH 3T3 mouse embryonic fibroblasts. Mouse FGF-2 as a natural stimulating agent was used in both assays as reference substance. The MAPK/Erk signaling cascade assay was used to study the downstream signaling effects of PEG-MMP-FGF-2 and N_3-MMP-FGF-2 on stimulated NIH 3T3 cells. ERK phosphorylation (an effector kinase of the MAPK/ERK pathway) was analyzed compared to total ERK expression by western blot (Figure 5 B). In contrast to not stimulated cells (Figure 5 B lane 1 and 5), both tested concentrations of N_3-MMP-FGF-2 (Figure 5 B; 10 ng/mL, lane 3; 100 ng/mL, lane 7), PEG-MMP-FGF-2 (Figure 5 B; 10 ng/mL, lane 4; 100 ng/mL, lane 8) and

mouse FGF-2 (Figure 5 B; 10 ng/mL, lane 2; 100 ng/mL, lane 6) induced strong ERK phosphorylation. WST-1 assay was used to study the proliferation of NIH 3T3 stimulated with PEG-MMP-FGF-2 and N_3-MMP-FGF-2. Different concentrations ranging from 0.125 ng/mL to 100 ng/mL of both variants were tested. The stable formazan salt WST-1 is cleaved by cellular mitochondria dehydrogenase to soluble formazan. An increase in the number of viable cells results in an increased formation of the formazan dye, which can be quantified by measuring the absorbance of the dye at 440 nm. The outcome shows that both PEG-MMP-FGF-2 and N_3-MMP-FGF-2 stimulated the growth of NIH 3T3 cells as potent as its natural stimulating agent, mouse FGF-2 (Figure 5 A).

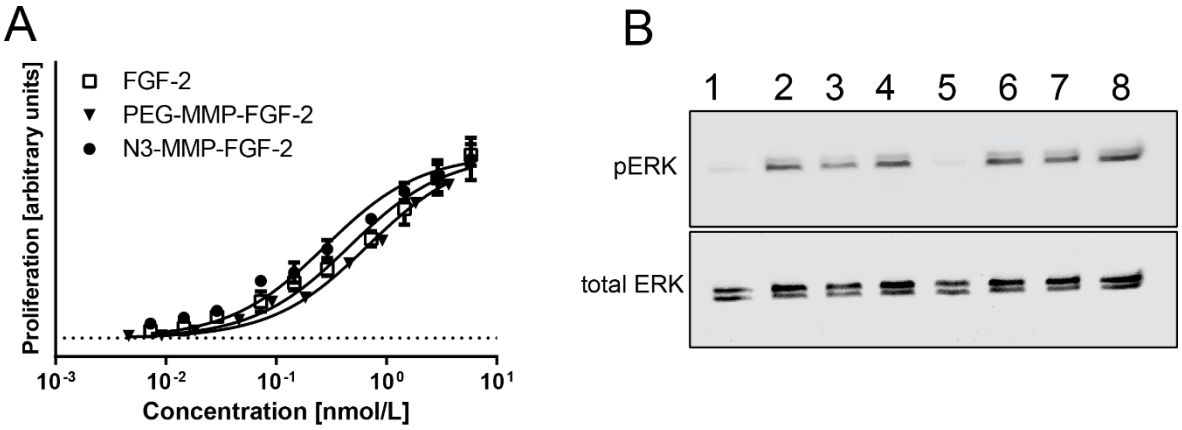

Figure 5: Bioactivity analysis of PEG-MMP-FGF-2 and N_3-MMP-FGF-2 compared to mouse FGF-2. (A) NIH 3T3 proliferation assay of PEG-MMP-FGF-2, N_3-MMP-FGF-2 and mouse FGF-2 as control (mean ± standard deviation, n=3). (B) ERK/ phosphorylated ERK assay of NIH 3T3 in 0.5% FCS containing growth medium (Lane 1 and 5) and after treatment with PEG-MMP-FGF-2 (10 ng/mL, lane 4 and 100 ng/mL, lane 8) N_3-MMP-FGF-2 (10 ng/mL, lane 3 and 100 ng/mL, lane 7), and mouse FGF-2 (10 ng/mL, lane 2; 100 ng/mL, lane 6) analyzed by Western blot.

The genetically inserted protease sensitive sequence features a MMP sensitive cleavable region, which was used to bioresponsively release the FGF-2 in inflammatory or MMPs enriched cellular environments. The appropriate functionality of this incorporated sequence was assessed by SDS-PAGE and HPLC after incubation with 16 nmol/L of MMP-2 and/or MMP-9, respectively. The SDS-PAGE chromatogram showed an almost complete removal of the FGF-2 from the covalently conjugated 10 kDa mPEG by changing from 35 kDa to 17 kDa after MMP digestion (Figure 6 A; MMP-2 lane 2; MMP-9 lane 3) compared to the non-MMP treated PEG-MMP-FGF-2 which remained unchanged (Figure 6 A lane 1). HPLC was performed to determine the cleavage rate of the incorporated protease sensitive site after MMP-9 digestion between 1 to 24 hours. The chromatogram shows two signals with increasing intensity over the time for the first signal and a decrease of the second signal (Figure 6 F, G, H). Non-treated PEG-MMP-FGF-2 shows no change during 24 h incubation (Figure 6 B, C, D, E). The third signal could not be found. To verify the identity of each

signal, PEG-MMP-FGF-2, N_3-MMP-FGF-2 as well as the cleavage product AASGIT*(10kDa mPEG)*LPAGPQG were used as control substances. The cleavage product AASGIT*(10kDa mPEG)*LPAGPQG was isolated after PEG-MMP-FGF-2 digestion using an excess of heparin-sepharose beads. The AASGIT*(10kDa mPEG)*LPAGPQG product remained in the supernatant, whereas the cleavage product containing the residuary FGF-2 stays on the heparin beads. The overlap of the controls with the digested PEG-MMP-FGF-2 revealed an overlap of the starting material PEG-MMP-FGF-2 and the cleavage product AASGIT*(10kDa mPEG)*LPAGPQG. (Figure S5)

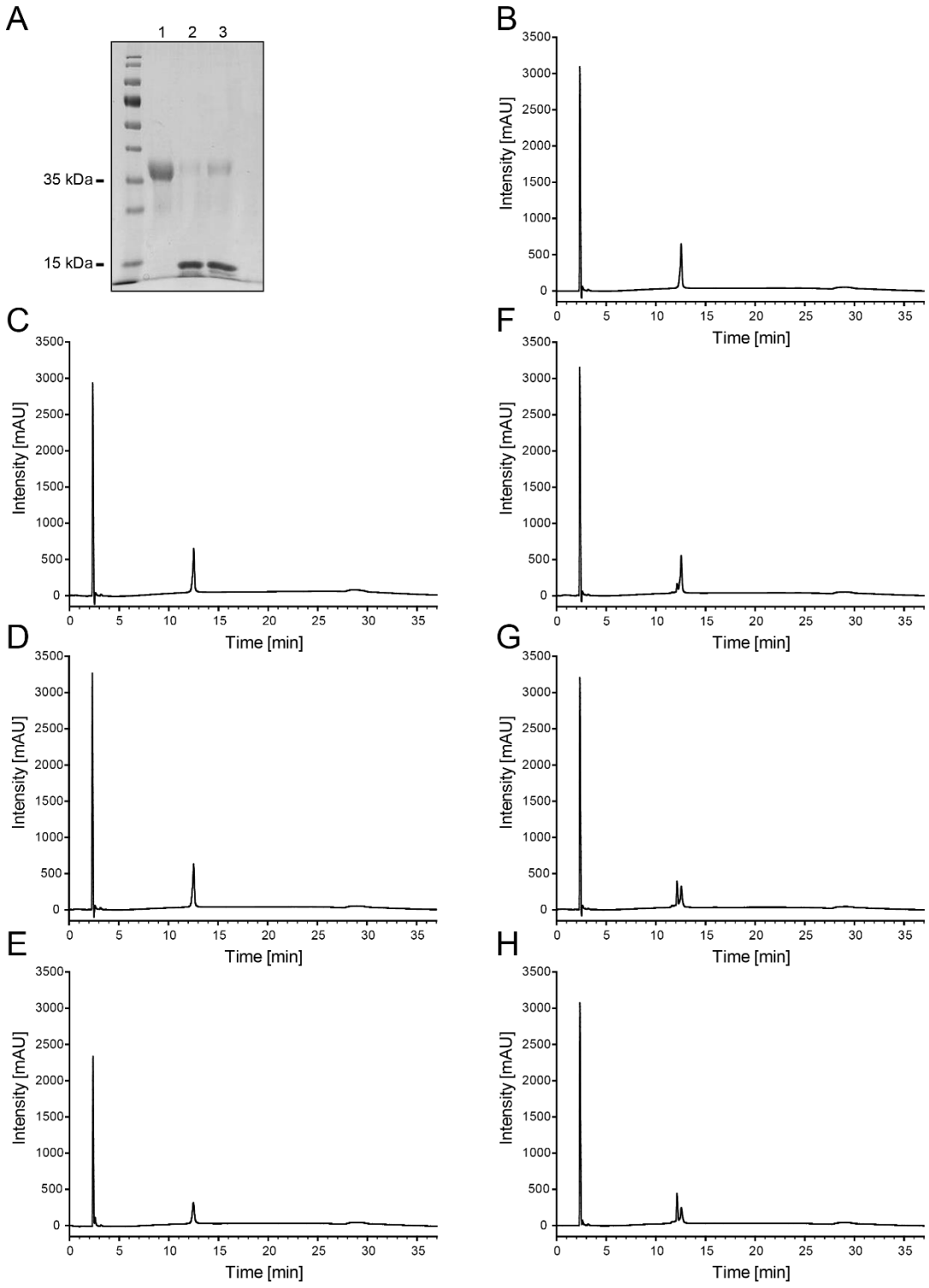

Figure 6: SDS-PAGE and HPLC analytics of the cleavage products after incubation of PEG-MMP-FGF-2 with MMP. (A) SDS-Page of PEG-MMP-FGF-2 cleavage after 24 hours with 16 nM MMP-2 (Lane 2) and MMP-9 (Lane 3) in comparison to untreated PEG-MMP-FGF-2 (Lane 1). HPLC analytics of PEG-MMP-FGF-2 after incubation with (F, G, H) and without (C, D, E) 16 nM of MMP-9 after 1 hour (F, C), 9 hours (G, D) and 24 hours (H, E) compared to untreated PEG-MMP-FGF-2 (B).

Preparation of Revacept coupled fibroblast growth factor variants

To prepare the Revacept fibroblast growth factor variants, DBCO moieties were integrated into the Revacept structure. At first, Revacept was reacted with NHS-DBCO and the amount of DBCO moieties were calculated by UV-VIS spectroscopy, resulting in two DBCO per Revacept. The SPAAC reactive Revacept-$(DBCO)_2$ was further incubated with N_3-FGF-2 and N_3-MMP-FGF-2, respectively. In a first step, remaining N_3-FGF-2 and N_3-MMP-FGF-2 were separated from Revacept-$(DBCO)_2$ and Revacept-FGF-2/Revacept-MMP-FGF-2 variants using size exclusion chromatography (SEC) (Figure 7 A signal 1). In a second step, the unreacted Revacept-$(DBCO)_2$ was separated from Revacept-MMP-FGF-2 and Revacept-FGF-2 variants (Figure 7 B signal 1) using heparin-sepharose affinity chromatography.

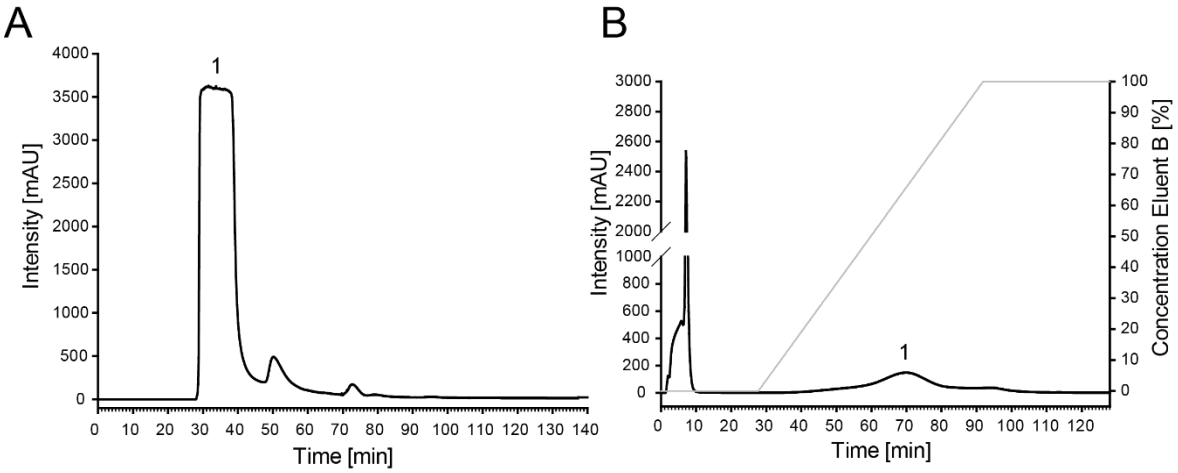

Figure 7: SEC and heparin-sepharose purification of Revacept-MMP-FGF-2 or Revacept-FGF-2 after SPAAC (N_3-MMP-FGF-2 + Revacept-DBCO). (A) Elution profile of Revacept-MMP-FGF-2 or Revacept-FGF-2 purified with SEC displaying Revacept-MMP-FGF-2 or Revacept-FGF-2 + Revacept-DBCO (Signal 1). (B) Elution profile of heparin-sepharose purification of Revacept-MMP-FGF-2 or Revacept-FGF-2 after SEC showing Revacept-MMP-FGF-2 or Revacept-FGF-2 (Signal 1).

The absence of unreacted FGF-2 variants as well as Revacept-$(DBCO)_2$ was assessed by SDS-PAGE. The 5 % SDS-PAGE shows a mass shift between Revacept-$(DBCO)_2$ (Figure 8 A lane 1,4) and Revacept-FGF-2 (Figure 8 A lane 2) as well as Revacept-MMP-FGF-2 (Figure 8 A lane 3). The 15 % SDS-PAGE shows no signal of remaining N_3-FGF-2/ N_3-MMP-FGF-2 at 17 kDa in the Revacept-MMP-FGF-2 (Figure 8 B lane 3) and Revacept-FGF-2 (Figure 8 B lane 4).

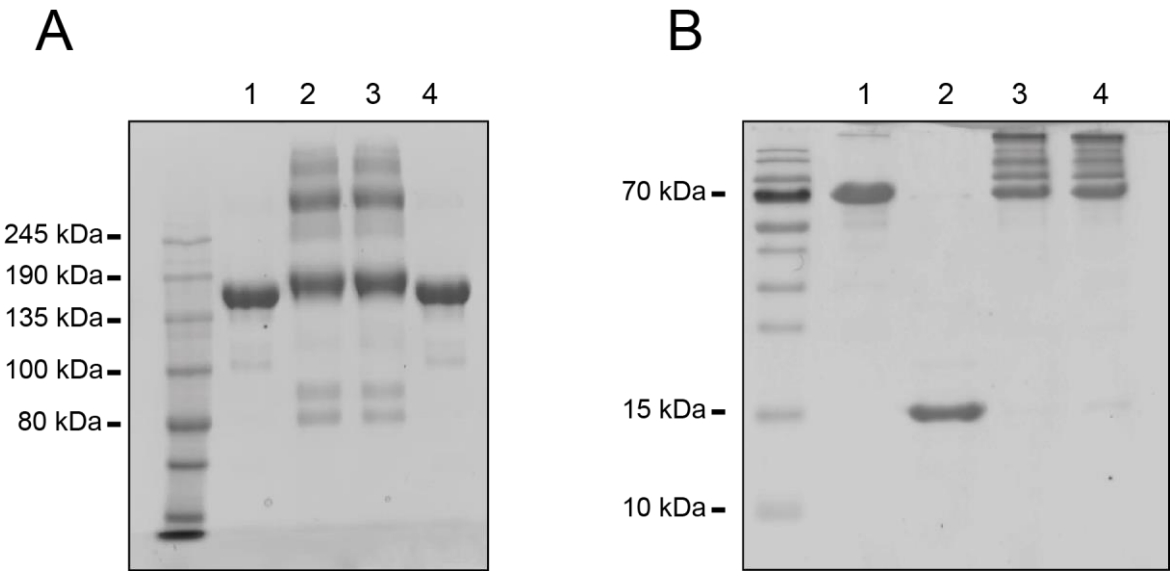

Figure 8: SDS-PAGE of Revacept-MMP-FGF-2 and Revacept-FGF-2 after SEC and heparin-sepharose purification. (A) 5% SDS-PAGE of purified Revacept-MMP-FGF-2 and Revacept-FGF-2 showing Revacept-DBCO (Lane 1,4), Revacept-FGF-2 (Lane 2) and Revacept-MMP-FGF-2 (Lane 3). (B) 15% SDS-PAGE of purified Revacept-MMP-FGF-2 and Revacept-FGF-2 showing Revacept-DBCO (Lane 1), N_3-MMP-FGF-2 (Lane2), Revacept-FGF-2 (Lane 3) and Revacept-MMP-FGF-2 (Lane 4).

Bioactivity of Revacept-MMP-FGF-2 and Revacept-FGF-2 was tested in a cell-based assay using NIH 3T3 mouse embryonic fibroblasts. Mouse FGF-2 as a natural stimulating agent was used as reference. A WST-1 proliferation assay was performed to study the effect of different Revacept-FGF-2 and Revacept-MMP-FGF-2 concentrations ranging from 0.125 ng/mL to 100 ng/m on NIH 3T3 cells. Revacept-FGF-2 and Revacept-MMP-FGF-2 show a left shift in the concentration/percentage response curve of NIH 3T3 cells compared to its natural stimulating agent (Figure 9 A). The specific binding of Revacept-MMP-FGF-2 and Revacept-FGF-2 to its natural ligand collagen was assessed compared to Revacept as reference substance using a collagen enzyme linked immunosorbent assay (ELISA). The results display equal binding specificity between the constructs and the control substance (Figure 9B).

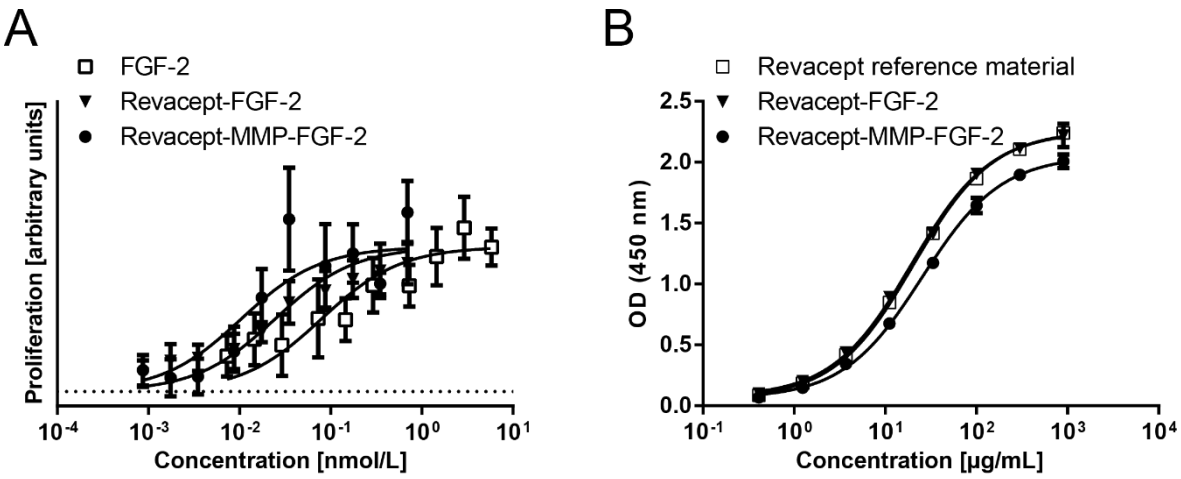

Figure 9: (A) Bioactivity analysis using NIH 3T3 proliferation assay of Revacept-MMP-FGF-2 and Revacept-FGF-2 compared to mouse FGF-2 as control (mean ± standard deviation, n=3). (B) Collagen ELISA of Revacept-MMP-FGF-2 and Revacept-FGF-2 compared to Revacept reference material as control (mean ± standard deviation, n=3).

Discussion

The therapeutic potential of FGF-2 is currently based on its important stimuli of angiogenesis[32-33], re-epithelization[34-35] and the potential to attenuate fibrotic effects[36] (scar deposition), driving more regenerative resolutions of wound healing (acute/chronic) in damaged tissue, ischemia and bacterial contamination.[37-38] Nevertheless, FGF-2 therapy suffers from substantial drawbacks like high diffusivity and short half-life, which is known to be less than one hour.[39-40] Aiming at a defined FGF-2 delivery to inflammatory or MMP enriched cellular environment and simultaneously increasing the half-life of the therapeutic, we developed two MMP-responsive FGF-2 drug delivery systems (DDS). Both DDS were designed to release their payload upon attendance of MMP to obtain increased and clinically relevant concentrations within the target structure. The protease sensitive cleavable linker -GPQGIAG- (MMP sequence) was selected to match the MMP profile in ischemia[41-42] as well as in wound healing of acute[43] and chronical wounds.[44] These states of injury show a predominately upregulation of MMP-2 and MMP-9 together with other MMPs. The sequence used in both approaches was chosen based on previous studies in the field of MMP derived drug delivery[30, 45-46] , showing excellent cleavage rates for MMP- 1, MMP-2, MMP-3, MMP-7, MMP-8, and MMP-9[45], respectively. By releasing the growth factor from the initial DDS due to MMP cleavage, the restored FGF-2 can not only activate cell surface receptors but can also be shuttled to the nucleus of the cell and thus activate nuclear targets.[47-48]

The first DDS (PEG-MMP-FGF-2) presents a classical and FDA approved approach[9] to increase the PK properties of therapeutic substances by coupling the therapeutic with a hydrophilic PEG polymer.[6] The 10 kDa mPEG was site-selectively conjugated under physiological conditions -

without altering protein function - to the N-terminal region, using SPAAC. The N-terminal region of the 154 aa long FGF-2 is highly flexible and the essential amino acids for fibroblast growth factor receptor (FGFR) binding are the hydrophobic aa Tyr-24, Tyr-103, Leu-140, Met-142 as well as the polar aa Arg-44 and Asn-101.[49] The N-terminal region consequently represents an attractive region for further modification (Figure 2). The introduction of N_3-L-lysine into 8(TAG)-FGF-2 and 8(TAG)-MMP-FGF-2 did not affect heparin binding in contrast to the PEG-MMP-FGF-2 which showed decreased affinity to heparin during purification (Figure 4 A signal 1), induced by 10 kDa PEG modification shielding parts of the protein. Both bioactivity tests, downstream signaling of FGF-2 through MAPK activation as well as stimulation of proliferation, were not impaired by the introduction of PEG and showed similar results to mouse FGF-2 and the unmodified N_3-MMP-FGF-2 (Figure 5). MMP-cleavage tests showed the good accessibility of the MMP-sequence in the protein with almost complete cleavage over 24 hours by the predominant MMPs, MMP-2 and MMP-9 (Figure 6).

The second DDS presents an antibody drug conjugate for specific targeting of injured and MMP enriched environmental. Here, Revacept, an antibody against human glycoprotein VI, that binds to exposed collagen I, III and VI after vascular lesions, was chosen as carrier for FGF-2. Revacept alone is used in clinical trials for patients suffering from stroke, transient ischemic attack or coronary heart disease. The antibody prevents upon binding to the exposed collagen the activation of thrombocytes along with the formation of blood clots without increasing bleeding time in patients. Initially, Revacept was modified with DBCO resulting in Revacept-$(DBCO)_2$, which offers an elegant way to couple the N_3-MMP-FGF-2 or N_3-FGF-2 to the antibody in a bioorthogonal manner using SPAAC. The resulting conjugates, the Revacept-MMP-FGF-2 and Revacept-FGF-2, could be purified from residual FGF-2 species (Figure 7, 8 B) and Revacept-DBCO (Figure 7, 8 A). Impurities after purification on the SDS-Page arose from oligomerization. Present studies with DBCO antibody conjugates reveal an increased tendency to oligomer formation based on the reactivity of the DBCO molecule.[50] Another issue concerns the thiol groups in both molecules, FGF-2 and Revacept, which contribute to the formation of aggregates. FGF-2 favors a reductive environment to stabilize its free thiol groups, whereas the Revacept needs a non-reductive environment to prevent the cleavage of dithiol bridges within the antibody. Both Revacept conjugates showed comparable results in binding to collagen and compared to unmodified Revacept, respectively (Figure 9 B). The bioactivity assay revealed improved effects in the concentration/percentage response curve of NIH 3T3 cells for both Revacept conjugates compared to mouse FGF-2, indicating that the Revacept prolongs the FGF-2 effect through interaction with formed ECM collagen or through protecting the FGF-2 form dissociating from the receptor (Figure 9 A).

Conclusion

By following bioinspired strategies, we developed two DDS, which differ in the nature of the carrier molecule to release the FGF-2 payload at the desired structure/environment. A 10 kDa mPEG was chosen as non-targeting carrier and Revacept, an antibody against human glycoprotein VI, was chosen as targeting carrier for FGF-2/MMP-FGF-2. The PEG conjugate showed similar bioactivity as observed for mouse FGF-2 and proper cleavage of the FGF-2 from the PEG by MMP-2 and MMP-9. Both Revacept conjugates maintained their collagen binding properties and showed improved bioactivity *in vitro* compared to the native mouse FGF-2. As a result, both the Revacept and the PEG represent a promising approach for establishing a regenerative therapeutic system for acute and chronical wounds and ischemic damaged tissues.

Nevertheless, this study presents only the preliminary work for both conjugates. Further and more precise characterization of the conjugates as well as additional analysis including serum stability, nuclear and cytosolic effects of the released growth factor and *in vivo* PK have to be conducted to draw a conclusion concerning the versatile applicability of these DDS in therapeutic fields.

Materials and Methods

Materials

Boc-protected L-lysine was from P3 BioSystems LLC (Shelbyville, KY, US). 2-Bromoethanol, triphosgene, sodiumazide, 1,4 dithiothreitol (DTT), Ioadacetamide (IAA), Dibenzocyclooctyne-N-hydroxysuccinimidyl ester (DBCO-NHS), carbenicillin, kanamycin, Isopropyl-β-D-thiogalactopyranosid (IPTG), penicillin-streptomycin and Dulbeco's Modified Eagle's Medium – high glucose were purchased from Sigma Aldrich (Schnelldorf, Germany). Restriction enzymes NdeI and BglII were from New England Biolabs (Ipswitch, USA). Fetal bovine serum (FCS/FBS) was from GIBCO life technologies (Carlsbad, CA). DBCO-mPEG, 10 kDa was purchased from Dundeecell Products (Dundee, Scotland, UK). PageRuler™ Prestained Protein Ladder (10 – 170 kDa), Coomassie Brilliant Blue G250, SuperSignal™ West Pico PLUS Chemiluminescent Substrate, Bradford Protein Assay Kit, Mammalian Cell Lysis Buffer, 1-Step™ Ultra TMB ELISA Substrate Solution were from Thermo Fischer Scientific (Dreieich, Germany). HiTrap Heparin HP, Superdex 75 10/30 and Superdex 75 16/60 were from GE Healthcare (Buckinghamshire, GB). P hospho-p44/42 MAPK (Erk1/2) (Thr202/Tyr204) Antibody #9101, p44/42 MAPK (Erk1/2) Antibody #9102 and Anti-rabbit IgG, HRP-linked Antibody #7074 were from Cell Signalling (Hitchin, UK). WST-1 was purchased from Roche (Basel, Switzerland). Vivaspin centrifugal concentrators were from Sartorius AG (Göttingen, Germany). 8(TAG)-MMP-FGF-2 sequence was from Eurofins genomics (Ebersberg, Germany). Zip Tip® C 18 resin was purchased from Merck Millipore (Billerica, USA).

BioTrace™ NT Nitrocellulose Transfer Membrane was purchased from Pall (Portsmouth, UK). Dialysis membrane tubing Spectra/Por® 6 - MWCO 10kDa, Spectrum was from Repligen (Ravensburg, Germany). Roti@-bock solution was from Carl Roth (Karlsruhe, Germany) All other chemicals used were at least pharmaceutical grade and were purchased from Sigma Aldrich (unless noted otherwise).

Methods

Synthesis of N_3-L-lysine ((S)-2-amino-6-((2-azidoethoxy)carbonylamino)hexanoic acid)

N_3-L-lysine was synthesized according to existing protocols provided by EMC Microcollections GmbH (Tübingen, Germany). N_3-L-lysine was prepared as HCl-salt. 25 g 2-Bromoethanol (1 eq., 200 mmol) was given in round bottom flask and 26 g sodiumazide (2 eq., 400 mmol) was slowly added. Ice cubes were added to form a suspension. The reaction was stirred for 1 hour at room temperature and subsequently heated to 80 °C for 48 hours under reflux cooling. The precipitate was centrifuged at 3000xg for 10 minutes at 4 °C and washed two times with Et_2O. The combined supernatants were dried over $MgSO_4$ and evaporated using a rotary evaporator. The remaining substance, 2-azidoethanol, was dissolved in CH_2Cl_2, dried overnight using a molecular sieve and solvent was evaporated until receiving a clear oil. 40 g triphosgene (0.9 eq., 135 mmol) was dissolved in THF using a round bottom flask with silicon sealing. The solution was cooled in an ice bath and a mixture of 13.1 g 2-azidoethanol (1 eq.,150 mmol) and 15.2 g triethylamine (150 mmol) dissolved in THF was added dropwise using a syringe pump, silicon tube and needle. The temperature of the mixture was slowly increased to room temperature and stirred overnight. The Precipitate was centrifuged at 3000xg for 10 minutes at 4 °C and washed two times with THF. The combined supernatants containing the azidoethylchloroformate were evaporated to a remaining volume of 30 mL. 40.6 g Boc-L-Lys-OH (1.1 eq., 165 mmol) were dissolved in 500 mL 1M NaOH and 100 mL THF. The solution was cooled in an ice bath and azidoethylchloroforamte was added dropwise under constant stirring. The temperature of the mixture was slowly increased to room temperature and stirred overnight. The solution was cooled in an ice bath and acidified with 6 M HCl under strong stirring until white clouding appears. 50 mL 1 M $KHSO_4$ was added and the mixture was extracted three times with EtOAc. The combined organic phases were washed twice with water, once with brine and dried over $MgSO_4$ prior to evaporation. The residual substance was dissolved in 50 mL Et_2O, cooled in an ice bath and 60 mL 2M HCL in Et2O was added dropwise under stirring. The temperature of the mixture was slowly increased to room temperature and stirred overnight. The precipitate was centrifuged at 3000xg for 10 minutes at 4 °C, washed twice with Et_2O and dried under

vacuum. The product was dissolved in water, 5 g charcoal was added, and the mixture was stirred for 3 hours at room temperature. The solution was filtered and lyophilized.

Expression and purification of N_3-FGF-2 and N_3-MMP-FGF-2

The gene encoding for full length 8(TAG)-MMP-FGF-2 in a pEX-A2 vector backbone was purchased from Eurofins Genomics. For the 8(TAG)-MMP-FGF-2, the initial DNA was amplified by PCR using a forward primer including a NdeI restriction site (5'-CCGCAAGCCATATGGCTGCCAGCG-3') and a reverse primer including a BglII restriction site (5'-GCAGGTAGATCTTTATCAGCTCTTAGCAGACATTGG-3'). After digestion with NdeI and BglII, the resulting 8(TAG)-MMP-FGF-2 was subcloned into the backbone of a pet11a construct, containing the gene for the pyrrolysine tRNA, the lipoprotein promotor lpp and the terminator RRN b/c. The pet11a vector, encoding the 8(TAG)-MMP-FGF-2 and pyrrolysine tRNA, was co-transformed with a pRSF-duet vector, encoding the pyrrolysine tRNA synthetase pylRS, via heat shock into the bacterial strain BL21 (DE3). Correct insert of the sequence was confirmed by sequencing. The sequence of 8(TAG)-MMP-FGF-2 on the pet11a vector is controlled by the lac-operon for selective regulation of the transcription using Isopropyl-β-D-thiogalactopyranoside (IPTG). Transformed cells were plated on a lysogeny broth agar plate containing carbenicillin (100 µg/mL) and kanamycin (40 µg/mL) and were incubated overnight at 37 °C. Expression was performed in terrific broth containing carbenicillin (100 µg/mL), kanamycin (40 µg/mL) and poly (propylene glycol) to reduce foam building. Cells were incubated at 37 °C and 1mM N_3-L-lysine was added at an OD_{600} of 0.3 and protein expression was induced with 3mM IPTG at an OD_{600} of 0.6. Cells were harvested after 6 hours and centrifuged at 4500xg for 20 minutes at 4 °C. The cell pellet was resuspended in lysis buffer (12 mM sodium phosphate, 300 mM NaCl, pH 7.4, substituted with 1 mM Phenylmethylsulfonyl fluoride (PMSF)) and ultrasonicated at 4 °C. The supernatant was centrifuged at 4500xg 30 minutes 4 °C, again at $1x10^5$x g 60 minutes 4 °C and filtered with a 0.22 µm syringe filter. The filtered supernatant containing N_3-MMP-FGF-2 was purified using heparin-sepharose high performance resin column (GE Healthcare, HiTrap Heparin HP affinity column) on an FPLC system (GE Healthcare, Äkta purifier) at 4 °C. N_3-MMP-FGF-2 was eluted with a linear gradient using buffer A (12 mM sodium phosphate, 300 mM NaCl, pH 7.4) and B (12 mM sodium phosphate, 1.5 M NaCl, pH 7.4). After purification, fractions containing N_3-MMP-FGF-2 were dialyzed against PBS containing 1 mM DTT at 4 °C and stored in PBS containing 3 mM DTT at -80 °C. Concentration was determined using Bradford assay or BCA assay following manufacturer instructions.

MALDI-MS

A solution of 20 µL (1 mg/ mL) of the sample protein was desalted using Zip Tip® C 18 resin (Merck Millipore, Billerica, USA) following manufacturer instructions. One µl of the desalted protein was emended in a matrix, consisting of 3,5-Dimethoxy-4-hydroxycinnamic acid in TA-solvent (30:70 [v/v] acetonitrile(ACN)/0.1 % trifluoroacetic acid (TFA) in water). Matrix assisted laser desorption ionization (MALDI) mass spectra were acquired in the linear positive mode with a 337 nm nitrogen laser using an Autoflex II LFR instrument (Bruker Daltonics Inc., Billerica, USA). Protein Standard I (Bruker Daltonics Inc., Billerica, USA) was used for calibration. Theoretical masses of proteins were calculated (https://web.expasy.org/peptide_mass/).

NanoLC MS/MS after elastase digestion

For in-gel digestion, 10 µg of the purified N_3-MMP-FGF-2 was mixed with 4x NuPAGE LDS sample buffer and Dithiothreitol (DTT)-solution (500 mM) was added to obtain a final concentration of 40 mM. The mixture was incubated for 10 minutes at 70 °C. After cooling, Iodoacetamide (IAA)-solution (500 mM) was added to obtain a final concentration of 80.5 mM. The mixture was kept in the dark for 20 minutes at room temperature and was loaded on a 15 % SDS-PAGE gel. After Coomassie staining, the bands were excised, destained with 30 % ACN, shrunk with 100 % ACN and dried in a Vacuum concentrator (Concentrator 5301, Eppendorf, Hamburg, Germany). The protein bands were digested with about 0.1 µg elastase per gel band. Elastase digest was performed overnight at 37 °C in 0.1 M NH_4HCO_3 (pH 8). Peptides were extracted from the gel slices with 5 % formic acid and analyzed using a NanoLC-MS/MS LTQ-Orbitrap Velos Pro (Thermo Scientific) equipped with an EASY-Spray Ion Source coupled to an EASY-nLC 1000 (Thermo Scientific) and the separation was performed on a trapping column (2 cm × 75 µm ID. PepMap C18 3 µm particles, 100 Å pore size) and EASY-Spray column (25 cm × 75 µm ID, PepMap C18 2 µm particles, 100 Å pore size) with a linear gradient from 3-30 % ACN with 0.1 % formic acid for 30 minutes.

Formation and purification of PEG-MMP-FGF-2

PEG-MMP-FGF-2 was generated using the SPAAC. N_3-MMP-FGF-2 in PBS with 3 mM DTT was incubated with a twofold molar excess of DBCO-mPEG 10 KDa for 48 h at 4 °C degree. The generated PEG-MMP-FGF-2 was subsequently separated from the unreacted N_3-MMP-FGF-2 by affinity chromatography using heparin-sepharose high performance resin column (GE Healthcare, HiTrap Heparin HP affinity column) on an FPLC system (GE Healthcare, Äkta purifier) at 4 °C (vide supra). The resulting peaks were dialyzed against PBS containing 1 mM DTT using a hydrophilic cellulose MWCO 10 kDa (Dialysis membrane tubing Spectra/Por® 6 - MWCO 10kDa, Spectrum) overnight at 4 °C. PEG-MMP-FGF-2 was identified by SDS-Page. Concentration was determined

using Bradford assay following manufacturer instructions and Protein was frozen at -80 °C in PBS containing 3 mM DTT.

Formation and purification of Revacept-MMP-FGF-2 and Revacept-FGF-2

Revacept was initially dialyzed against PBS using a hydrophilic cellulose MWCO 10 kDa (Dialysis membrane tubing Spectra/Por® 6 - MWCO 10kDa, Spectrum) overnight at 4 °C. An N-hydroxysuccinimide (NHS) reaction was performed to generate Revacept-DBCO. Revacept was incubated with a fivefold molar excess of NHS-DBCO, which was dissolved in PBS/DMF and reacted overnight at 4 °C. The resulting Revacept-DBCO was centrifuged at 3000xg for 20 minutes at 4 °C and the amount of DBCO per Revacept was determined following manufacturer instructions. N_3-MMP-FGF-2 was incubated with a 1.5 molar excess of Revacept-$(DBCO)_2$ overnight at 4 °C. The product was separated on a SEC column (Superdex 75 16/60 or Superdex 75 10/30, GE Healthcare) using FPLC system (GE Healthcare, Äkta purifier) at 4 °C. Revacept-MMP-FGF-2 and Revacept-$(DBCO)_2$ was eluted with an isocratic method using PBS. After SEC purification, the fractions containing Revacept-MMP-FGF-2 and Revacept-$(DBCO)_2$ were separated on an affinity chromatography column using heparin-sepharose high performance resin column and a FPLC system (GE Healthcare, Äkta purifier) at 4 °C. Revacept-MMP-FGF-2 was dialyzed against PBS using hydrophilic cellulose MWCO 10 kDa overnight at 4 °C. Concentration was determined using Bradford assay following manufacturer instructions and protein was frozen at -80 °C in PBS. Formation of Revacept-FGF-2 was conducted in the same way with identical steps.

SDS-Page

Recombinant proteins and proteins used in SPAAC were analyzed by standard tris-glycine SDS-polyacrylamide gel electrophoresis. Gels were stained with Coomassie brilliant blue (CBB) G-250 (80 mg/L CBB G-250, 3 mL/L HCl 37 %) and analyzed using a FluorChem FC2 imaging system (Protein Simple, Santa Clara, CA).

HPLC analysis

Protein purity was assessed on a HPLC system using a VWR Hitachi LaChromUltra HPLC system equipped with a diode array detector. 20 µg proteins sample was loaded on a Zorbax 300 SB-CN 4.6x150 mm 5-microns column, equilibrated with water containing 0.1 % TFA and ACN containing 0.1 % TFA (92:8). Proteins were eluted by a linear gradient 8 – 85 % for 29 minutes using ACN containing 0.1 % TFA and a flow rate of 1 mL/min. Column temperature was kept at 22 °C and absorbance was monitored at 214 nm as well as diode array from 200-400 nm, respectively.

Matrix metalloproteinase digestion

PEG-MMP-FGF-2 was dialyzed against MMP-Buffer (50 mM Tris, 150 mM NaCl, 1 µM $ZnCl_2$, 10 mM $CaCl_2$, pH 7.4) at 25 °C with slow agitation prior to the digestion using MMP-9 (16 nmol/L) and/or MMP-2 (16 nmol/L). For the experiments targeting the time-dependent cleavage, the samples were split, one half was incubated with one subtype of MMP and the other half with MMP buffer alone. For each time point, 20 µg of PEG-MMP-FGF-2 was used. The digestion was stopped by the addition of 50 mM EDTA and heating to 95 °C for 5 minutes. The solution was analyzed by SDS-PAGE standard protocol or analyzed by HPLC using a Zorbax 300 SB-CN 4.6x150 mm 5-microns column, equilibrated with water containing 0.1 % TFA and ACN containing 0.1 % TFA (92:8). Proteins were eluted by a linear gradient 8 – 85 % for 29 minutes using ACN containing 0.1 % TFA and a flow rate of 1 mL/min. Column temperature was kept at 22 °C and absorbance was monitored at 214 nm as well as diode array from 200-400 nm, respectively. The 24 hours time point was repeated as described before and the reaction was stopped with 50 mM EDTA. The solution was treated with an excess of heparin-sepharose beads and incubated for 4 hours on a roller mixer. The beads were centrifuged at $11x10^3$xg for 10 minutes and the supernatant was analyzed (vide supra) on a HPLC system.

Cell culture

NIH 3T3 fibroblast (CRL-1658; ATCC, Manassas, VA) were harvested from exponentially growing sub confluent monolayer. The cells were maintained in 75 cm² culture flasks in growth medium (DMEM high-glucose containing heat-inactivated FCS (10 %), penicillin G (100 U/mL) and streptomycin (100 µg/µL)) at 37 °C under 5 % CO_2.

WST-proliferation assay

Bioactivity of FGF-2 variants compared to mouse FGF-2 was conducted by formazan assay. NIH 3T3 fibroblasts were seeded in a 96-well plate ($33x10^3$ cells/mL, 125 µL per well) in growth medium overnight at 37 °C under 5 % CO_2. The medium was changed to assay medium (DMEM high-glucose containing heat-inactivated FCS (0.5 %), penicillin G (100 U/mL) and streptomycin (100 µg/µL)) and cells were grown for 24 hours. Dilution series of each protein from 0.25 ng/mL to 200 ng/mL were prepared in assay medium and added (1:1 [V/V]) to the cells. Cells were stimulated for 48 hours at 37 °C and 5% CO_2. After stimulation, 10 µL WST-1 reagent was added to each well and cells were incubated for at 37 °C according to manufacturer instructions. Every 30 minutes, cells were analyzed and the absorbance of the soluble formazan product at 450 nm as well as background noise at 630 nm was determined using a Spectramax 250 microplate reader (Molecular Devices, Sunnyvale). Relative proliferation with respect to mouse FGF-2 is expressed.

pERK/ERK activation assay

Extracellular signaling of FGF-2 variants in respect to mouse FGF-2 was conducted by pERK/ERK assay. NIH 3T3 fibroblasts were seeded in a 6-well plate ($37.5x10^3$ cells/mL, 2 mL per well) in growth medium overnight at 37 °C under 5 % CO_2. The medium was changed to assay medium (DMEM high-glucose containing heat-inactivated FCS (0.5 %), penicillin G (100 U/mL) and streptomycin (100 µg/µL)) and cells were grown for 24 hours. Cells were stimulated with 10 ng/mL and 100 ng/mL of each FGF-2 variant and incubated for 30 minutes at 37 °C. After stimulation, the cells were placed on ice, washed with ice cold PBS and proteins were extracted using mammalian extraction buffer (M-PER™ Mammalian Protein Extraction Reagent, Thermo Scientific). After extraction, proteins were immediately shock frozen using liquid nitrogen. The concentration of each condition was determined by Bradford assay following manufacturer instructions. 5 µg total protein of each condition was loaded on a 15 % SDS-Page gel and processed using standard SDS-PAGE and Western blotting procedures. Prior to phosphorylated MAPK/MAPK analysis, Ponceau red staining was performed. For detection of phosphorylated MAPK, a rabbit anti-phospho-p44/42 MAPK (Erk1/2) (Thr202/Tyr204) Antibody (1:1000) in Tris buffered saline (TBS), containing 0.1% (w/w) Tween-20 (TBST), was used overnight at 4 °C. After incubation with the first antibody, the blot was washed and incubated with an Anti-rabbit IgG, HRP-linked Antibody (1:2000 in TBST). Signals were detected using an enhanced chemiluminescence substrate and were subsequently monitored by a FluorChem FC 2 imaging system (Protein Simple, Santa Clara, USA). After detection of the phosphorylated MAPK, the blot was stripped with 2-Mercaptoethanol-Buffer (50 mM Tris-HCl, 2 % (w/w) SDS and 0.8 % 2-mercaptoethanol pH 6.8) for 45 minutes at 50 °C and was washed under rinsing water for 1 hour. For the detection of MAPK, a rabbit anti-p44/42 MAPK (Erk1/2) Antibody (1:1000 in TBST) and Anti-rabbit IgG (1:2000 in TBST), HRP-linked Antibody combination was used with identical steps.

Collagen Enzyme Linked Immunosorbent Assay (ELISA)

The specific binding of Revacept and Revacept-FGF-2 variants to its natural ligand collagen was assessed using a collagen ELISA. Bovine collagen type I (BD Bioscience, Heidelberg, Germany) was dissolved in coating buffer (1.59 g/L Na_2CO_3, 2.93 g/L $NaHCO_3$, pH 9.6) to a final concentration of 10 µg/mL. After each following step, the microtiter plate was thoroughly washed with 300 µL PBS containing 0.05 % Tween 20 for several times. Microtiter wells were coated with 100 µL collagen solution per well for 1 hour at room temperature under gently shaking. The coated wells were blocked 1 hour with 300 µL 1xRoti®-block solution. Revacept and Revacept-FGF-2 variants with concentration ranging from 0.041 – 900 µg/mL were added into the coated microtiter, plated and incubated for 1 hour at room temperature under gently shaking. 300µL of a horse radish

peroxidase (HRP)-coupled goat Antihuman IgG antibody (1:30000 in PBS) was added per well for 2 hours at room temperature. For detection, 100 µL 1-Step™ Ultra TMB ELISA Substrate Solution was added to each well and incubated for 30 minutes. The reaction was stopped by adding 100 µL 1 M sulfuric acid and the microtiter plate was measure at 450 nm with a microplate reader (Infinite® F200, Tecan, Meannedorf, Switzerland).

Supporting Information

Supporting Figures

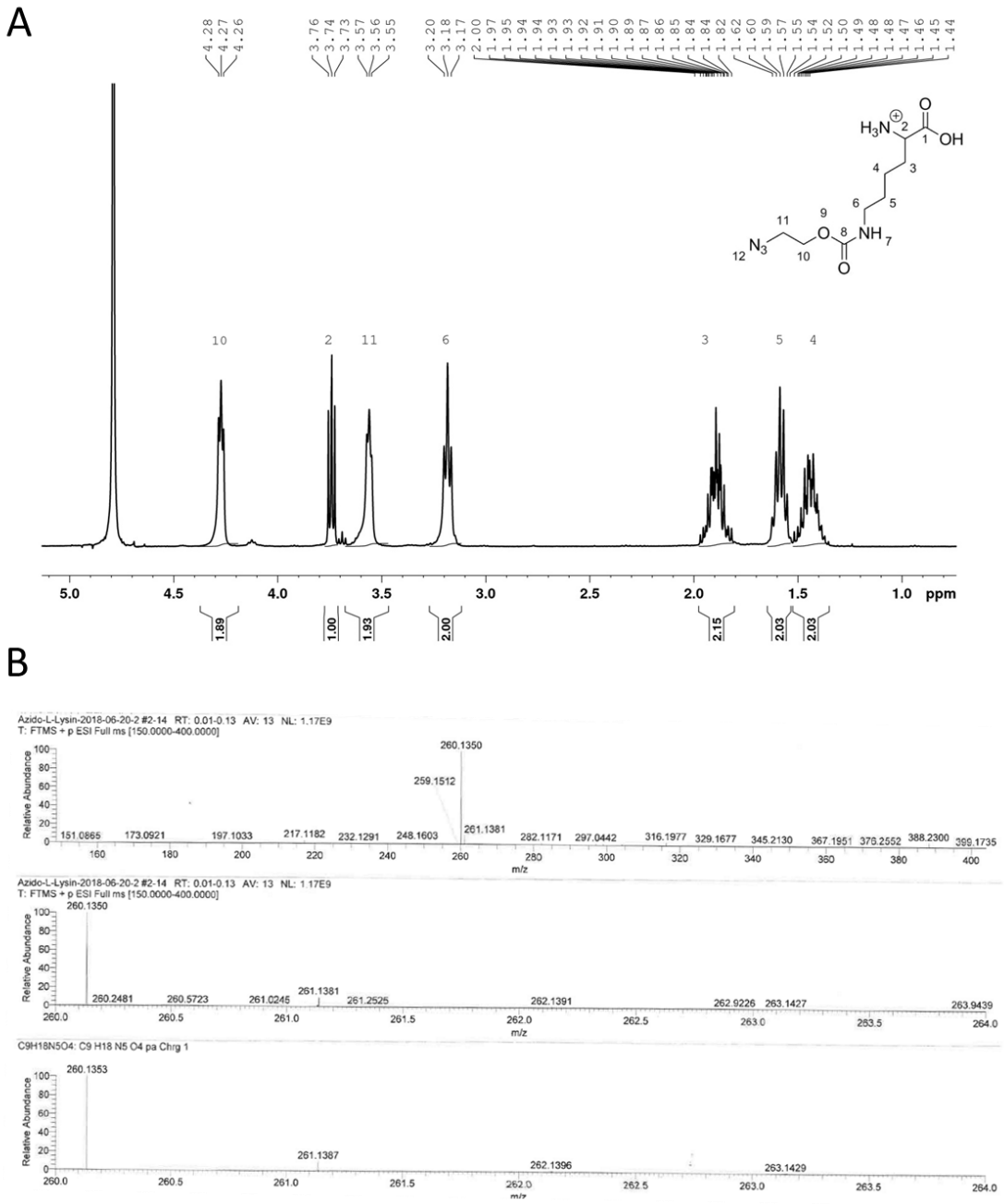

Figure S 1: (A) 1H-NMR spectra and (B) HRMS Esi-pos spectra of synthesized Alk to asses identification and purity. Observed average mass [M+] = 260.135 Da, calculated average mass [M+] = 260.128 Da.

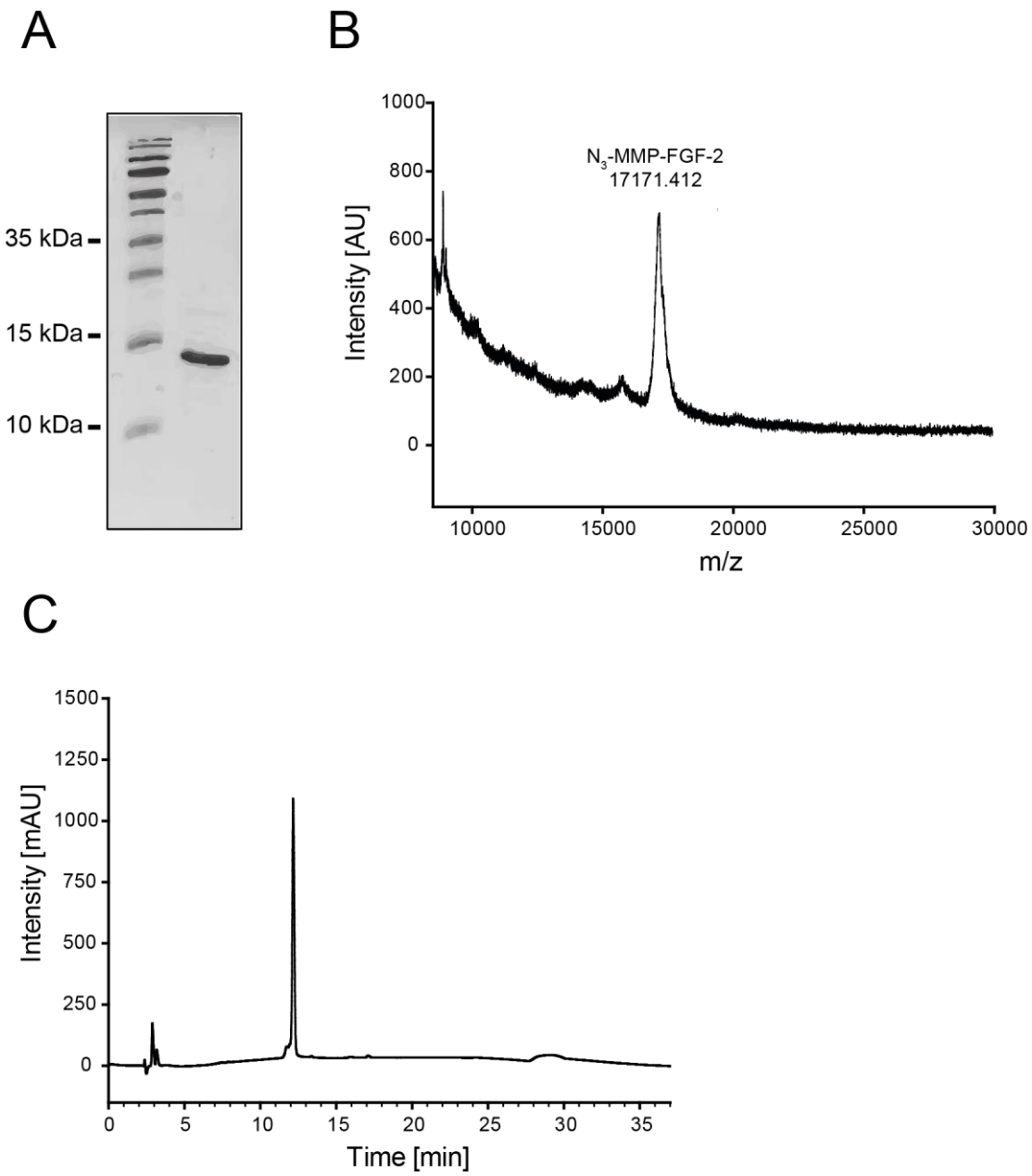

Figure S 2: Characterization of N_3-MMP-FGF-2. (A) SDS-PAGE of purified N_3-MMP-FGF-2. (B) MALDI-MS of N_3-MMP-FGF-2. Observed average mass = 17171.4122 Da; calculated average mass without methionine = 17173.47 Da. (C) RP-HPLC analysis of N_3-MMP-FGF-2.

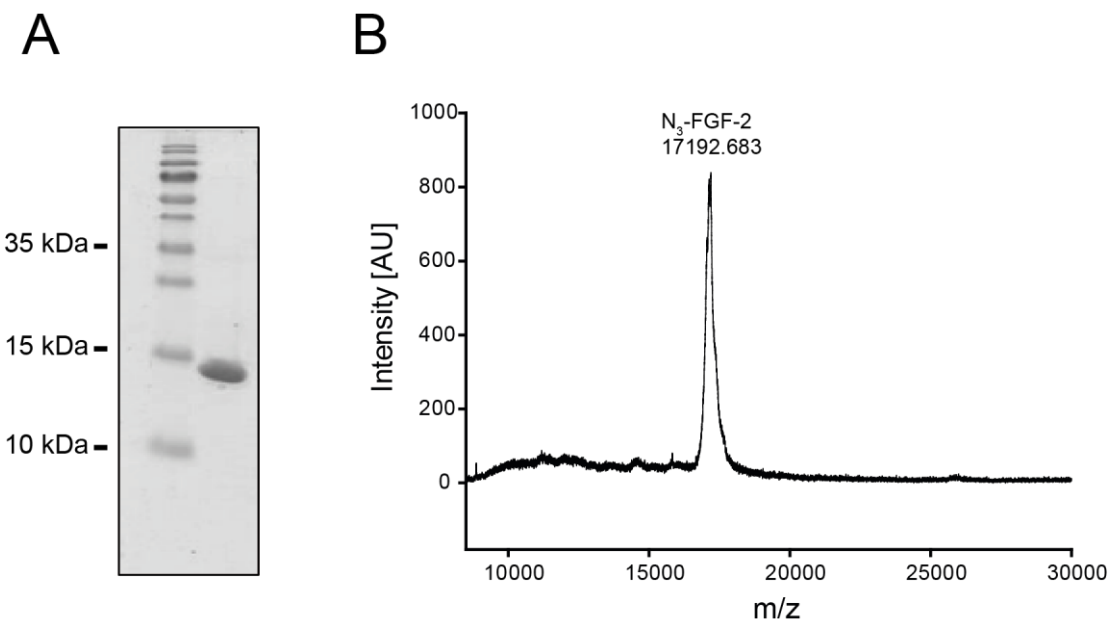

Figure S 3: Characterization of N_3-FGF-2. (A) SDS-PAGE of purified N_3-FGF-2. (B) MALDI-MS of N_3-FGF-2. Observed average mass = 17192.683 Da; calculated average mass without methionine = 17175.44 Da.

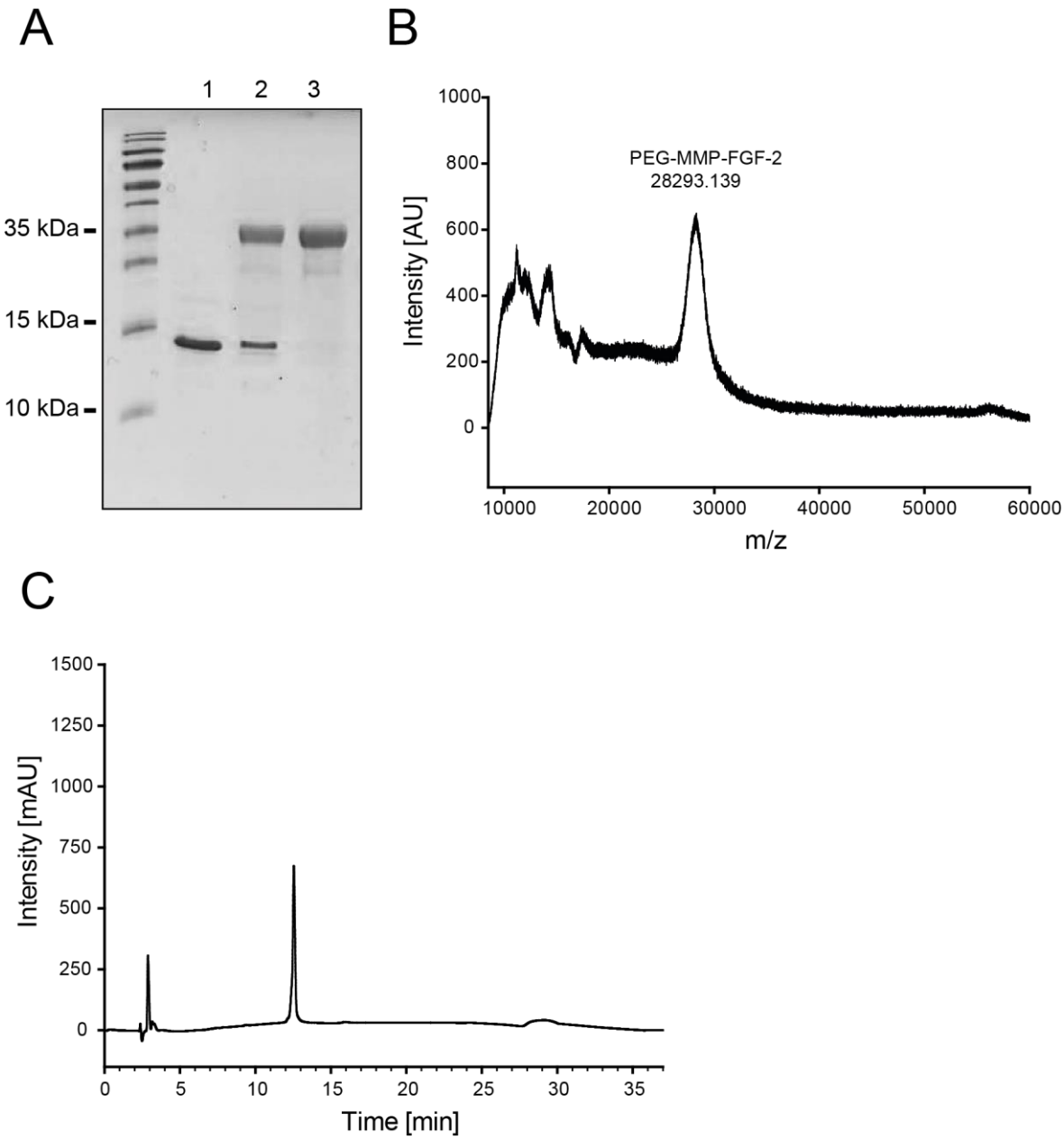

Figure S 4: Characterization of PEG-MMP-FGF-2. (A) SDS-PAGE of purified PEG-MMP-FGF-2 showing N_3-MMP-FGF-2 (Lane 1), N_3-MMP-FGF-2 together with PEG-MMP-FGF-2 prior to purification (Lane 2) and PEG-MMP-FGF-2 after purification (Lane 3). (B) MALDI-MS of PEG-MMP-FGF-2. Observed average mass = 28293.139 Da. (C) RP-HPLC analysis of PEG-MMP-FGF-2.

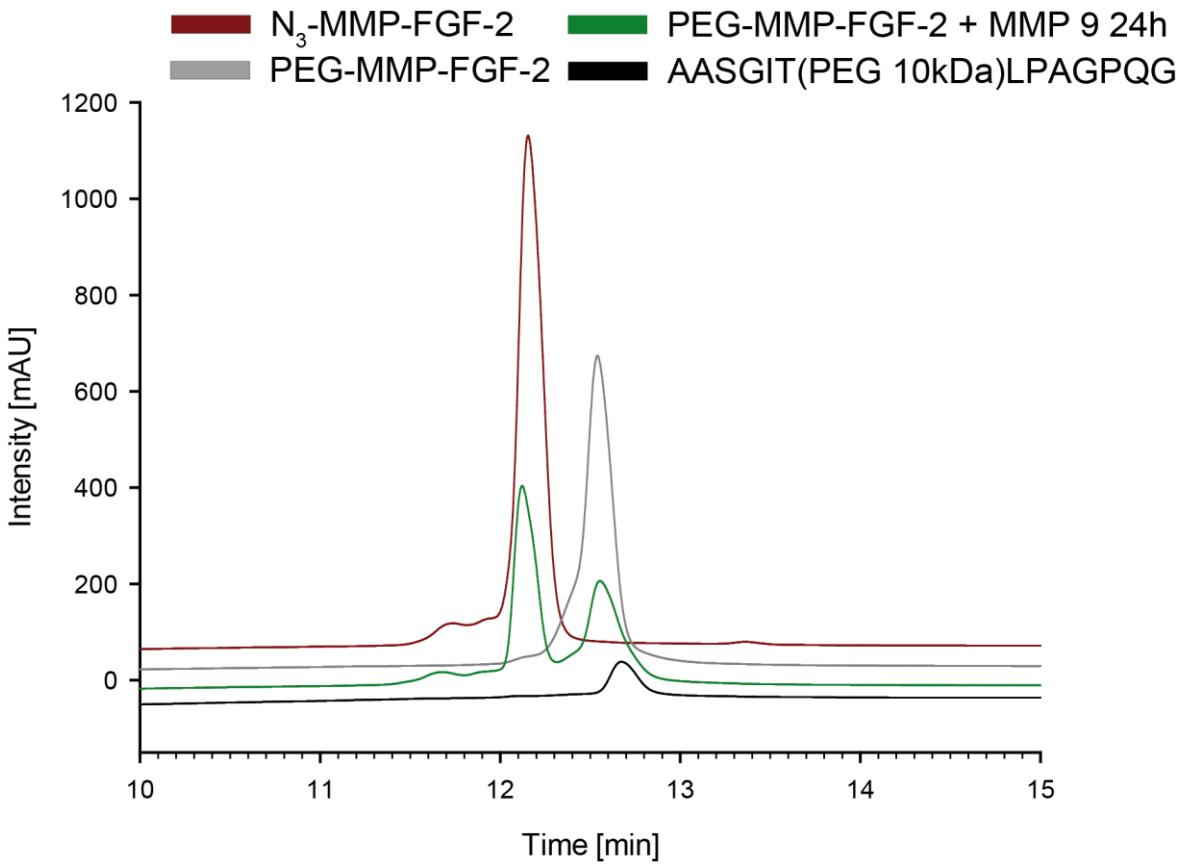

Figure S 5: HPLC analytics of the PEG-MMP-FGF-2 after cleavage with 16 nM MMP-9 for 24 hours (green). Signal of isolated cleavage product (black) compared to N_3-MMP-FGF-2 (red) and PEG-MMP-FGF-2 (grey).

References

1. De Groot, A. S.; Scott, D. W., Immunogenicity of protein therapeutics. *Trends Immunol* **2007,** *28* (11), 482-90. DOI: 10.1016/j.it.2007.07.011.
2. Krishna, M.; Nadler, S. G., Immunogenicity to Biotherapeutics - The Role of Anti-drug Immune Complexes. *Front Immunol* **2016,** *7*, 21. DOI: 10.3389/fimmu.2016.00021.
3. Salazar-Fontana, L. I.; Desai, D. D.; Khan, T. A.; Pillutla, R. C.; Prior, S.; Ramakrishnan, R.; Schneider, J.; Joseph, A., Approaches to Mitigate the Unwanted Immunogenicity of Therapeutic Proteins during Drug Development. *The AAPS Journal* **2017,** *19* (2), 377-385. DOI: 10.1208/s12248-016-0030-z.
4. van Witteloostuijn, S. B.; Pedersen, S. L.; Jensen, K. J., Half-Life Extension of Biopharmaceuticals using Chemical Methods: Alternatives to PEGylation. *ChemMedChem* **2016,** *11* (22), 2474-2495. DOI: 10.1002/cmdc.201600374.
5. Qi, Y.; Chilkoti, A., Protein-polymer conjugation-moving beyond PEGylation. *Curr Opin Chem Biol* **2015,** *28*, 181-93. DOI: 10.1016/j.cbpa.2015.08.009.
6. Dozier, J. K.; Distefano, M. D., Site-Specific PEGylation of Therapeutic Proteins. *Int J Mol Sci* **2015,** *16* (10), 25831-64. DOI: 10.3390/ijms161025831.
7. Lawrence, P. B.; Price, J. L., How PEGylation influences protein conformational stability. *Curr Opin Chem Biol* **2016,** *34*, 88-94. DOI: 10.1016/j.cbpa.2016.08.006.
8. Pasut, G.; Guiotto, A.; Veronese, F. M., Protein, peptide and non-peptide drug PEGylation for therapeutic application. *Expert Opinion on Therapeutic Patents* **2005,** *14* (6), 859-894. DOI: 10.1517/13543776.14.6.859.
9. Gaberc-Porekar, V.; Zore, I.; Podobnik, B.; Menart, V., Obstacles and pitfalls in the PEGylation of therapeutic proteins. *Curr Opin Drug Discov Devel* **2008,** *11* (2), 242-50.

10. Ginn, C.; Khalili, H.; Lever, R.; Brocchini, S., PEGylation and its impact on the design of new protein-based medicines. *Future Med Chem* **2014,** *6* (16), 1829-46. DOI: 10.4155/fmc.14.125.
11. Wu, F.; Braun, A.; Lühmann, T.; Meinel, L., Site-Specific Conjugated Insulin-like Growth Factor-I for Anabolic Therapy. *ACS Biomaterials Science & Engineering* **2018,** *4* (3), 819-825. DOI: 10.1021/acsbiomaterials.7b01016.
12. Luhmann, T.; Spieler, V.; Werner, V.; Ludwig, M. G.; Fiebig, J.; Mueller, T. D.; Meinel, L., Interleukin-4-Clicked Surfaces Drive M2 Macrophage Polarization. *Chembiochem* **2016,** *17* (22), 2123-2128. DOI: 10.1002/cbic.201600480.
13. Lühmann, T.; Jones, G.; Gutmann, M.; Rybak, J.-C.; Nickel, J.; Rubini, M.; Meinel, L., Bio-orthogonal Immobilization of Fibroblast Growth Factor 2 for Spatial Controlled Cell Proliferation. *ACS Biomaterials Science & Engineering* **2015,** *1* (9), 740-746. DOI: 10.1021/acsbiomaterials.5b00236.
14. Tsuchikama, K.; An, Z., Antibody-drug conjugates: recent advances in conjugation and linker chemistries. *Protein Cell* **2018,** *9* (1), 33-46. DOI: 10.1007/s13238-016-0323-0.
15. Beck, A.; Goetsch, L.; Dumontet, C.; Corvaia, N., Strategies and challenges for the next generation of antibody-drug conjugates. *Nat Rev Drug Discov* **2017,** *16* (5), 315-337. DOI: 10.1038/nrd.2016.268.
16. Chudasama, V.; Maruani, A.; Caddick, S., Recent advances in the construction of antibody-drug conjugates. *Nat Chem* **2016,** *8* (2), 114-9. DOI: 10.1038/nchem.2415.
17. Srinivasarao, M.; Low, P. S., Ligand-Targeted Drug Delivery. *Chem Rev* **2017,** *117* (19), 12133-12164. DOI: 10.1021/acs.chemrev.7b00013.
18. Rago, B.; Tumey, L. N.; Wei, C.; Barletta, F.; Clark, T.; Hansel, S.; Han, X., Quantitative Conjugated Payload Measurement Using Enzymatic Release of Antibody-Drug Conjugate with Cleavable Linker. *Bioconjug Chem* **2017,** *28* (2), 620-626. DOI: 10.1021/acs.bioconjchem.6b00695.
19. Lu, J.; Jiang, F.; Lu, A.; Zhang, G., Linkers Having a Crucial Role in Antibody-Drug Conjugates. *Int J Mol Sci* **2016,** *17* (4), 561. DOI: 10.3390/ijms17040561.
20. Wang, L.; Yuan, L.; Wang, H.; Liu, X.; Li, X.; Chen, H., New strategy for reversible modulation of protein activity through site-specific conjugation of small molecule and polymer. *Bioconjug Chem* **2014,** *25* (7), 1252-60. DOI: 10.1021/bc5000934.
21. Sun, T.; Morger, A.; Castagner, B.; Leroux, J. C., An oral redox-sensitive self-immolating prodrug strategy. *Chem Commun (Camb)* **2015,** *51* (26), 5721-4. DOI: 10.1039/c5cc00405e.
22. Staegemann, M. H.; Grafe, S.; Haag, R.; Wiehe, A., A toolset of functionalized porphyrins with different linker strategies for application in bioconjugation. *Org Biomol Chem* **2016,** *14* (38), 9114-9132. DOI: 10.1039/c6ob01551d.
23. Riber, C. F.; Smith, A. A.; Zelikin, A. N., Self-Immolative Linkers Literally Bridge Disulfide Chemistry and the Realm of Thiol-Free Drugs. *Adv Healthc Mater* **2015,** *4* (12), 1887-90. DOI: 10.1002/adhm.201500344.
24. Liang, Y.; Li, S.; Wang, X.; Zhang, Y.; Sun, Y.; Wang, Y.; Wang, X.; He, B.; Dai, W.; Zhang, H.; Wang, X.; Zhang, Q., A comparative study of the antitumor efficacy of peptide-doxorubicin conjugates with different linkers. *J Control Release* **2018,** *275*, 129-141. DOI: 10.1016/j.jconrel.2018.01.033.
25. Vlahov, I. R.; Leamon, C. P., Engineering folate-drug conjugates to target cancer: from chemistry to clinic. *Bioconjug Chem* **2012,** *23* (7), 1357-69. DOI: 10.1021/bc2005522.
26. Maier, K.; Wagner, E., Acid-labile traceless click linker for protein transduction. *J Am Chem Soc* **2012,** *134* (24), 10169-73. DOI: 10.1021/ja302705v.
27. Patel, V. F.; Hardin, J. N.; Mastro, J. M.; Law, K. L.; Zimmermann, J. L.; Ehlhardt, W. J.; Woodland, J. M.; Starling, J. J., Novel acid labile COL1 trityl-linked difluoronucleoside immunoconjugates: synthesis, characterization, and biological activity. *Bioconjug Chem* **1996,** *7* (4), 497-510. DOI: 10.1021/bc960038u.
28. Jacques, S. A.; Leriche, G.; Mosser, M.; Nothisen, M.; Muller, C. D.; Remy, J. S.; Wagner, A., From solution to in-cell study of the chemical reactivity of acid sensitive functional groups: a rational approach towards improved cleavable linkers for biospecific endosomal release. *Org Biomol Chem* **2016,** *14* (21), 4794-803. DOI: 10.1039/c6ob00846a.

29. Bottger, R.; Knappe, D.; Hoffmann, R., Readily adaptable release kinetics of prodrugs using protease-dependent reversible PEGylation. *J Control Release* **2016,** *230*, 88-94. DOI: 10.1016/j.jconrel.2016.04.010.
30. Braun, A. C.; Gutmann, M.; Mueller, T. D.; Luhmann, T.; Meinel, L., Bioresponsive release of insulin-like growth factor-I from its PEGylated conjugate. *J Control Release* **2018,** *279*, 17-28. DOI: 10.1016/j.jconrel.2018.04.009.
31. James, C. M.; Ferguson, T. K.; Leykam, J. F.; Krzycki, J. A., The amber codon in the gene encoding the monomethylamine methyltransferase isolated from Methanosarcina barkeri is translated as a sense codon. *J Biol Chem* **2001,** *276* (36), 34252-8. DOI: 10.1074/jbc.M102929200.
32. Yun, Y. R.; Won, J. E.; Jeon, E.; Lee, S.; Kang, W.; Jo, H.; Jang, J. H.; Shin, U. S.; Kim, H. W., Fibroblast growth factors: biology, function, and application for tissue regeneration. *J Tissue Eng* **2010,** *2010*, 218142. DOI: 10.4061/2010/218142.
33. Werner, S., A novel enhancer of the wound healing process: the fibroblast growth factor-binding protein. *Am J Pathol* **2011,** *179* (5), 2144-7. DOI: 10.1016/j.ajpath.2011.09.001.
34. Pastar, I.; Stojadinovic, O.; Yin, N. C.; Ramirez, H.; Nusbaum, A. G.; Sawaya, A.; Patel, S. B.; Khalid, L.; Isseroff, R. R.; Tomic-Canic, M., Epithelialization in Wound Healing: A Comprehensive Review. *Adv Wound Care (New Rochelle)* **2014,** *3* (7), 445-464. DOI: 10.1089/wound.2013.0473.
35. Yang, H. S.; Shin, J.; Bhang, S. H.; Shin, J. Y.; Park, J.; Im, G. I.; Kim, C. S.; Kim, B. S., Enhanced skin wound healing by a sustained release of growth factors contained in platelet-rich plasma. *Exp Mol Med* **2011,** *43* (11), 622-9. DOI: 10.3858/emm.2011.43.11.070.
36. Dolivo, D. M.; Larson, S. A.; Dominko, T., Fibroblast Growth Factor 2 as an Antifibrotic: Antagonism of Myofibroblast Differentiation and Suppression of Pro-Fibrotic Gene Expression. *Cytokine Growth Factor Rev* **2017,** *38*, 49-58. DOI: 10.1016/j.cytogfr.2017.09.003.
37. Meier, K.; Nanney, L. B., Emerging new drugs for wound repair. *Expert Opin Emerg Drugs* **2006,** *11* (1), 23-37. DOI: 10.1517/14728214.11.1.23.
38. Beenken, A.; Mohammadi, M., The FGF family: biology, pathophysiology and therapy. *Nat Rev Drug Discov* **2009,** *8* (3), 235-53. DOI: 10.1038/nrd2792.
39. Edelman, E. R.; Nugent, M. A.; Karnovsky, M. J., Perivascular and intravenous administration of basic fibroblast growth factor: vascular and solid organ deposition. *Proc Natl Acad Sci U S A* **1993,** *90* (4), 1513-7.
40. Shamloo, A.; Sarmadi, M.; Aghababaie, Z.; Vossoughi, M., Accelerated full-thickness wound healing via sustained bFGF delivery based on a PVA/chitosan/gelatin hydrogel incorporating PCL microspheres. *Int J Pharm* **2018,** *537* (1-2), 278-289. DOI: 10.1016/j.ijpharm.2017.12.045.
41. Cheung, P. Y.; Sawicki, G.; Wozniak, M.; Wang, W.; Radomski, M. W.; Schulz, R., Matrix metalloproteinase-2 contributes to ischemia-reperfusion injury in the heart. *Circulation* **2000,** *101* (15), 1833-9.
42. Phatharajaree, W.; Phrommintikul, A.; Chattipakorn, N., Matrix metalloproteinases and myocardial infarction. *Can J Cardiol* **2007,** *23* (9), 727-33.
43. Caley, M. P.; Martins, V. L.; O'Toole, E. A., Metalloproteinases and Wound Healing. *Adv Wound Care (New Rochelle)* **2015,** *4* (4), 225-234. DOI: 10.1089/wound.2014.0581.
44. McCarty, S. M.; Percival, S. L., Proteases and Delayed Wound Healing. *Adv Wound Care (New Rochelle)* **2013,** *2* (8), 438-447. DOI: 10.1089/wound.2012.0370.
45. Nagase, H.; Fields, G. B., Human matrix metalloproteinase specificity studies using collagen sequence-based synthetic peptides. *Biopolymers* **1996,** *40* (4), 399-416. DOI: 10.1002/(sici)1097-0282(1996)40:4<399::aid-bip5>3.0.co;2-r.
46. Braun, A. C.; Gutmann, M.; Ebert, R.; Jakob, F.; Gieseler, H.; Luhmann, T.; Meinel, L., Matrix Metalloproteinase Responsive Delivery of Myostatin Inhibitors. *Pharm Res* **2017,** *34* (1), 58-72. DOI: 10.1007/s11095-016-2038-6.
47. Bailly, K.; Soulet, F.; Leroy, D.; Amalric, F.; Bouche, G., Uncoupling of cell proliferation and differentiation activities of basic fibroblast growth factor. *FASEB J* **2000,** *14* (2), 333-44.

48. Sheng, Z.; Lewis, J. A.; Chirico, W. J., Nuclear and nucleolar localization of 18-kDa fibroblast growth factor-2 is controlled by C-terminal signals. *J Biol Chem* **2004,** *279* (38), 40153-60. DOI: 10.1074/jbc.M400123200.
49. Springer, B. A.; Pantoliano, M. W.; Barbera, F. A.; Gunyuzlu, P. L.; Thompson, L. D.; Herblin, W. F.; Rosenfeld, S. A.; Book, G. W., Identification and concerted function of two receptor binding surfaces on basic fibroblast growth factor required for mitogenesis. *J Biol Chem* **1994,** *269* (43), 26879-84.
50. van Geel, R.; Wijdeven, M. A.; Heesbeen, R.; Verkade, J. M.; Wasiel, A. A.; van Berkel, S. S.; van Delft, F. L., Chemoenzymatic Conjugation of Toxic Payloads to the Globally Conserved N-Glycan of Native mAbs Provides Homogeneous and Highly Efficacious Antibody-Drug Conjugates. *Bioconjug Chem* **2015,** *26* (11), 2233-42. DOI: 10.1021/acs.bioconjchem.5b00224.

Conclusion and outlook

Despite tremendous progress in drug development leading to a multitude of new therapeutics like peptides, proteins, RNAs, DNAs and highly potent small molecules, physiological characteristics (anatomic and physiologic barriers) drastically restrict an adequate drug deposition at the site of action[1-5]. Innovative solutions that go beyond the scope of conventional dosage forms have to be found to overcome off target effects resulting in reduced effectiveness and toxicity of the therapeutic agent.[3, 5-7] Smart drug delivery systems (DDS), that are precisely tailored to pre-existing conditions, can be a promising keystone for future medical treatment of difficult accessible and complex diseases.[1, 8-9] They can be roughly broken down in the category of passive and active targeting systems. Passive target delivery systems, generally composed of an active pharmaceutical ingredient together with a cleavable linker and a carrier substance, circulate through the vascular system and are distributed by their physicochemical properties of the carrier and/or therapeutic agent.[10-12] In contrast, active target delivery systems are comprised of a targeting structure, which preferentially aims for the desired destination.[11-12] A profound knowledge of the target structure's conditions e.g. existence of specific proteases, presence of certain cell types, physiological barriers and vascularization, that affect the fate of the therapeutic agents, is necessary for adapting the DDS.

This thesis establishes the scientific basis of three different drug delivery platforms – **cells, matrices** and **protein conjugates** – based on (i) glycoengineered cell surfaces, (ii) glycoengineered cell derived matrices and (iii) improved classical protein conjugate systems for targeting acute and chronical wounds.

Present therapeutic options for the treatment of acute and chronical wounds including various numbers of wound dressings, skin substitutes, hyperbaric oxygen, negative pressure wound therapy and biopharmaceutical formulations often result in unsatisfying clinical solutions and may lead to the formation of scar tissue or persisting impaired healing.[13-15] Growth factors, among them fibroblast growth factor-2 (FGF-2), platelet-derived growth factor (PDGF) and vascular endothelial growth factor (VEGF), are key signaling molecules regulating cell migration, survival, adhesion, proliferation, growth and differentiation.[6, 16-18] However, their efficient deployment in clinical application is restricted due to poor stability, short half-life, safety, cost effectiveness and lack of appropriate delivery methods.[6, 19-20]

To overcome this, the decoration of biodegradable matrices with therapeutic agents has recently become more and more into focus in fields of tissue engineering applications and regenerative medicine, including cell and cancer drug delivery.[17, 21-23] These 3D scaffolds can be based on synthetic materials[24-26], providing excellent mechanical support and stability, or formed by natural

materials[27-30], providing biological cues to cells and surrounding tissues.[21] The novel extracellular matrix (ECM) based scaffold, detailed in the first two chapters of this work, belongs to the category of natural biodegradable materials and provides enhanced control of the attachment sites for therapeutic agents by the incorporation of a unique reactive moiety into the glycan structure via metabolic glycoengineering.[31] The ECM is a non-cellular, highly organized 3D microenvironment, assembled by secreted macromolecules from various resident cells, composed of a core structure and a gel like intermediate space. The core structure, a complex interlocking mesh formed by fibrous proteins, provides tensile strength of tissue, whereas the gel like intermediate space is formed by glycoproteins and proteoglycans and provides buffering and hydration properties.[23, 32-33] ECM by nature provides exceptional characteristics by anchoring cells and growth factors as well as improving the stability of embedded molecules and enabling their spatiotemporal release, thus acting as a key element concerning the regulation of cellular function, development and homeostasis.[31, 34-35] In contrast to other scaffold materials, ECMs display a versatile and adaptable material by selecting the type of cells to generate the ECM and by reason of their exceptional characteristics.[23] Commercially available ECM scaffold materials have been already used in clinical trials.[36-37] However, the potential of currently clinically used natural ECM scaffold materials is not exhausted, yet, offering the possibility to expand.

An improvement of the applicability of ECMs is realized by metabolic glycoengineering. The strategy of metabolic glycoengineering takes the advantage of the natural cell machinery by introducing a metabolic engineered monosaccharide into the glycan structure of de novo synthesized and assembled glycoconjugates.[38-39] Chemically tunable monosaccharides – in this work a tetra acetylated azide bearing monosaccharide ($Ac_4GlcNAz$) – enter the cytosol by passive diffusion or active transport.[40-42] Inside the cytosol, they are recognized as natural substrates for enzymatic co-translational and post-translational modification processes and are thus inserted via the glycosylation machinery through endoplasmic reticulum and/or Golgi apparatus into glycoproteins and glycolipids. These tailored glycoconjugates in turn are shuttled through the cell membrane by secretory pathways and become part of the extracellular surface (glycocalyx) and of the interstitial space.[43] Through the incorporation of tailored monosaccharides, new coupling strategies come into play which pave the way for covalent immobilization of active compounds onto ECM derived materials with maximal control over attachment sites at the active compound.[39, 44-49] Using the presented approach, the glycoengineered ECM is featured for bioorthogonal conjugation reactions, particularly the copper(I)-catalyzed azide-alkyne cycloaddition (CuAAC) or strain-promoted alkyne-azide cycloaddition (SPAAC).[31]

The advantages of both reactions are (i) the toleration of wide ranges of pH (4-12) and temperature (0-100 °C), (ii) a covalent and stable reaction product and (iii) the usage of very unique reaction

groups (azides, alkynes and strain promoted alkynes).[50-53] Using these unique reaction groups, both click reactions strongly vary from the common used N-hydroxysuccinimide (NHS) or maleimide reaction, that are based on ubiquitous amine or thiol groups, thus leading to unspecific coupling.[54] Despite the advantages of a simpler technical applicability of the alkyne group, excellent water solubility of the educts and faster reaction kinetics, the CuAAC comes at a price[55-56]: Quite apart from the problems of capturing free copper ions by macromolecules and the formation of aggregates by compromising free thiol groups, the generation of reactive oxygen species (ROS) has a profound cytotoxic effect.[43, 57-59] The formation of ROS, induced by the dynamic interaction between the copper species ($Cu^{o/+/++}$), is associated with DNA strand breaks, oxidative processes as well as the cleavage and cross-linking of amino acids and proteins.[57-58, 60-61] To overcome these limitations, a precisely defined window for the CuAAC reaction conditions was determined by detail in chapter III, providing biological compatible concentrations and reaction times.[43]

With the strategy of metabolic glycoengineering, many perspectives in the field of medicine are possible: Glycoengineered ECM scaffolds offer (i) the decoration of multiple therapeutic substances by different enzymatic and bioorthogonal immobilization strategies, (ii) the ability to sequester growth factors with natural occurring binding sites within the matrix and (iii) the induction of synergistic effects (matricrin effects[62]), resulting in an increased and prolonged growth factor signaling due to the recruitment of integrin receptors on the cell surface and growth factor bound to ECM-molecules.[17, 31] According to this, glycoengineered ECM scaffolds represent a delivery platform and provide superior functionality and flexibility by tailoring the system for specific needs e.g. by loading antibiotics together with growth factors in wound healing.[63] In fact, many more perspectives are possible like covering synthetic materials with glycoengineered ECM making them accessible biomedical applications or allowing exciting studies of the degradation profile or development of different cell derived matrices.[21] Glycoengineered ECM can easily be expanded with protease cleavable linkers (vide infra) giving access to more precise tunable release determined by the activity and upregulation of enzymes, pH etc.[54, 64-65]

Another delivery platform detailed in chapter I and III of this work addresses the modification of living organisms via metabolic glycoengineering and bioorthogonal coupling without jeopardizing cellular homeostasis. Using the strategy of metabolic glycoengineering, a chemical tunable monosaccharide is incorporated into the cell surface (vide supra), thus open up new opportunities for elegant chemical decoration strategies of the glycocalyx.[43] Chapter I outlines the method for metabolic glycoengineered cells, whereas Chapter III primarily focusses on providing a design space for the effective and rapid decoration of healthy glycoengineered cells using CuAAC and SPAAC. By scrutinizing cell metabolism, membrane integrity and apoptotic gene response, an optimized CuAAC and SPAAC protocol for efficient and rapid decoration of the glycocalyx is established, thus

pioneering this strategy to be applicable to biological mechanism studies, diagnostic cell imaging, development of new biomaterials and drug delivery.

Metabolic glycoengineering has effectively been used in tumor cell diagnostic and therapy, but the heterogeneity of tumor tissue still remains a challenge in effective targeting for diagnostic and therapy. Traditionally, the targeting of tumor cells draws on proteins, peptides and other small molecules that specifically bind to the target tissue. However, limitations like low amount of target receptor or unknown target receptor on the tumor surface bring us to the limit of feasible techniques.[66-67] The introduction of precursor azide-bearing monosaccharides into the tumor tissue enables the exogenously generated azide group to be used as target molecule for a Dibenzocyclooctyne (DBCO)-bearing diagnostic or therapeutic, thus making it possible to address tumors with unknown location and hallmarks.[5] Another approach for effective tumor therapy addresses the metabolic glycoengineering of T cells. Small molecules were immobilized on the surface to design tumor-specific cytotoxic T cells for targeted therapy.[68]

A further field of application concerning metabolic glycoengineering uses the incorporation and conjugation of the engineered monosaccharide for *in vivo* tracking. Cells are decorated *in vitro*, prior to transplantation, and for *in vivo* monitoring to understand biological processes like survival, fate, location, distribution and migration. Along with cell tracking, metabolic glycoengineering is used for the spatiotemporal imaging of tissue development and change by alteration of monosaccharide administration together with the diagnostic substance.[69-71]

Both highlighted delivery platforms, glycoengineered cells surfaces and glycoengineered ECM present exceptional characteristics but yet are still in their initial stages. In addition to these systems, traditional carrier – spacer – payload systems can be developed into advanced DDS by exchanging the conventional spacer molecules with a cleavable linker. Degradation of cleavable linkers is performed by different physicochemical and biochemical processes (reduction, low pH, enzyme hydrolysis, etc.). It has to be ensured that (i) the therapeutic remains attached to the modification during circulation and shelf-storage (ii) the payload bound to the linker is not impaired during cleavage and (iii) no unsafe degradation products are generated and released after cleavage. Enzymatic cleavable linkers overcome the reductive and acid cleavable linkers by meeting all conditions and allowing a traceless release without byproducts, leaving only two or three amino acid residues on the payload. The residual amino acids should in principal be well tolerated, but possible effects like immunogenic behavior or lowered bioactivity of the therapeutic has to be evaluated. By tailoring these enzymatic cleavable linkers to specific requirements, the release profiles of the therapeutic can be adapted to address specific target structures or to respond to different states within the desired structure.[10, 54, 64-65, 72-74] Following bioinspired strategies, Chapter IV of this thesis outlines

two versatile delivery systems – target and non-target oriented – based on an enzymatic cleavable linker and triggered by disease-associated proteases. The protease sensitive cleavable linker, an eight amino acid long peptide sequence (-GPQGIAGQ-)[72-73, 75], was genetically inserted into the N-terminal protein sequence of FGF-2, a highly flexible region without essential amino acids for receptor binding and consequently, representing an attractive region for modification without jeopardizing protein activity.[76] Matrix metalloproteinase (MMP), a protease, which shows elevated profiles in tissue repair of acute and chronical wounds as well as in ischemia, was chosen as enzymatic trigger for the linker sequence.[77-80] In addition to the possibility of genetically insertion of the cleavable sequence, a bifunctional peptide including the eight amino acid long sequence can be used. However, two different and selective conjugation techniques have to be chosen to avoid additional purification efforts and to ensure the selective connection of one tail of the peptide to the carrier system and the other tail of the peptide to the payload.

As non-targeting carrier system, PEG, a well-studied, Food and Drug Administration approved substance and very common tool to increase the pharmacokinetic (PK) properties of therapeutic agents, was chosen.[81-82] Through its optimal properties (flexibility, viability, hydrophobicity and low cytotoxicity), PEG provides increased circulation half-life, reduced degradation and immunogenicity as well as enhanced water solubility of the attached payload.[83-84] Through the combined strategy of a PEG carrier and a cleavable linker, FGF-2 shifts from a common growth factor to an advanced DDS with MMP-triggered release of FGF-2.

In addition to PEG, Revacept, a human glycoprotein VI antibody, was chosen as targeting carrier system. Revacept (provided by AdvanceCor GmbH, München, Germany) specifically binds to exposed collagen I, III and VI after vascular lesions, inhibiting the activation of thrombocytes along with the formation of blood clots without impairing hemostasis. Recently, Revacept alone is used in clinical trials for patients suffering from stroke, transient ischemic attack and coronary heart disease. By covalently coupling MMP sensitive FGF-2 to this antibody, a combined system is created, interlocking in the treatment of tissue defects by providing antithrombotic properties through Revacept and regenerative properties through the released growth factor.[6, 16-18] In fact, unreleased FGF-2, bound to one of the carrier systems, exhibits cell stimulating characteristics by interacting with its specific cell surface receptor. Free FGF-2, in contrast, is shuttled into the nucleus via nuclear localization signals, activating nuclear targets to stimulate RNA expression and to unfold its full mitogenic effect.[85-86]

In conclusion, cancer treatment and wound healing is a global medical concern, which still remains an extremely important challenge. With the increasing incidence of obesity, diabetes, cardiovascular disorders, autoimmune diseases and the fact, that our society is constantly aging, issues involved in

healing and regeneration can be affected, which may favor cancerous diseases and non-healing wounds.[18, 87-90] However, tumor growth as well as surgical and traumatic wounds, where the patient immunogenicity is reduced and the risk of bacterial infection and complication is elevated, reveal to be a steadily growing global burden with significant discomfort and distress for the patient while exhausting the medical system through tremendous consumption of finances and human resources.[15, 91-93]

The inevitable pathogenesis ties our hands concerning meticulous treatment and results in the urgent needs for new treatment options. By focusing on various delivery platforms, this thesis establishes an essential cornerstone for promising strategies in the development of disease treatment. The outlined delivery systems ensure high flexibility due to exchanging single or multiple elements of the system, individually tailoring them to the respective disease or target site. In short: the here presented delivery platforms evince an enormous potential in wound and cancer treatment of the future.

References

1. Sun, W.; Hu, Q.; Ji, W.; Wright, G.; Gu, Z., Leveraging Physiology for Precision Drug Delivery. *Physiological Reviews* **2017,** *97* (1), 189-225. DOI: 10.1152/physrev.00015.2016.
2. Alsaggar, M.; Liu, D., Organ-based drug delivery. *J Drug Target* **2018,** *26* (5-6), 385-397. DOI: 10.1080/1061186X.2018.1437919.
3. Tibbitt, M. W.; Dahlman, J. E.; Langer, R., Emerging Frontiers in Drug Delivery. *J Am Chem Soc* **2016,** *138* (3), 704-17. DOI: 10.1021/jacs.5b09974.
4. Mitragotri, S.; Burke, P. A.; Langer, R., Overcoming the challenges in administering biopharmaceuticals: formulation and delivery strategies. *Nat Rev Drug Discov* **2014,** *13* (9), 655-72. DOI: 10.1038/nrd4363.
5. Yoo, J. W.; Irvine, D. J.; Discher, D. E.; Mitragotri, S., Bio-inspired, bioengineered and biomimetic drug delivery carriers. *Nat Rev Drug Discov* **2011,** *10* (7), 521-35. DOI: 10.1038/nrd3499.
6. Wang, Z.; Wang, Z.; Lu, W. W.; Zhen, W.; Yang, D.; Peng, S., Novel biomaterial strategies for controlled growth factor delivery for biomedical applications. *NPG Asia Materials* **2017,** *9* (10). DOI: 10.1038/am.2017.171.
7. Kwon, I. K.; Lee, S. C.; Han, B.; Park, K., Analysis on the current status of targeted drug delivery to tumors. *J Control Release* **2012,** *164* (2), 108-14. DOI: 10.1016/j.jconrel.2012.07.010.
8. Lu, Y.; Aimetti, A. A.; Langer, R.; Gu, Z., Bioresponsive materials. *Nature Reviews Materials* **2016,** *2* (1). DOI: 10.1038/natrevmats.2016.75.
9. Cobo, I.; Li, M.; Sumerlin, B. S.; Perrier, S., Smart hybrid materials by conjugation of responsive polymers to biomacromolecules. *Nat Mater* **2015,** *14* (2), 143-59. DOI: 10.1038/nmat4106.
10. Mura, S.; Nicolas, J.; Couvreur, P., Stimuli-responsive nanocarriers for drug delivery. *Nat Mater* **2013,** *12* (11), 991-1003. DOI: 10.1038/nmat3776.
11. Rosenblum, D.; Joshi, N.; Tao, W.; Karp, J. M.; Peer, D., Progress and challenges towards targeted delivery of cancer therapeutics. *Nat Commun* **2018,** *9* (1), 1410. DOI: 10.1038/s41467-018-03705-y.
12. Kobsa, S.; Saltzman, W. M., Bioengineering approaches to controlled protein delivery. *Pediatr Res* **2008,** *63* (5), 513-9. DOI: 10.1203/PDR.0b013e318165f14d.

13. Moura, L. I.; Dias, A. M.; Carvalho, E.; de Sousa, H. C., Recent advances on the development of wound dressings for diabetic foot ulcer treatment--a review. *Acta Biomater* **2013,** *9* (7), 7093-114. DOI: 10.1016/j.actbio.2013.03.033.
14. Powers, J. G.; Morton, L. M.; Phillips, T. J., Dressings for chronic wounds. *Dermatol Ther* **2013,** *26* (3), 197-206. DOI: 10.1111/dth.12055.
15. Han, G.; Ceilley, R., Chronic Wound Healing: A Review of Current Management and Treatments. *Adv Ther* **2017,** *34* (3), 599-610. DOI: 10.1007/s12325-017-0478-y.
16. Martino, M. M.; Briquez, P. S.; Maruyama, K.; Hubbell, J. A., Extracellular matrix-inspired growth factor delivery systems for bone regeneration. *Advanced drug delivery reviews* **2015,** *94*, 41-52. DOI: 10.1016/j.addr.2015.04.007.
17. Briquez, P. S.; Hubbell, J. A.; Martino, M. M., Extracellular Matrix-Inspired Growth Factor Delivery Systems for Skin Wound Healing. *Adv Wound Care (New Rochelle)* **2015,** *4* (8), 479-489. DOI: 10.1089/wound.2014.0603.
18. Eming, S. A.; Martin, P.; Tomic-Canic, M., Wound repair and regeneration: mechanisms, signaling, and translation. *Sci Transl Med* **2014,** *6* (265), 265sr6. DOI: 10.1126/scitranslmed.3009337.
19. Mitchell, A. C.; Briquez, P. S.; Hubbell, J. A.; Cochran, J. R., Engineering growth factors for regenerative medicine applications. *Acta biomaterialia* **2016,** *30*, 1-12. DOI: 10.1016/j.actbio.2015.11.007.
20. Shamloo, A.; Sarmadi, M.; Aghababaie, Z.; Vossoughi, M., Accelerated full-thickness wound healing via sustained bFGF delivery based on a PVA/chitosan/gelatin hydrogel incorporating PCL microspheres. *Int J Pharm* **2018,** *537* (1-2), 278-289. DOI: 10.1016/j.ijpharm.2017.12.045.
21. Hinderer, S.; Layland, S. L.; Schenke-Layland, K., ECM and ECM-like materials - Biomaterials for applications in regenerative medicine and cancer therapy. *Adv Drug Deliv Rev* **2016,** *97*, 260-9. DOI: 10.1016/j.addr.2015.11.019.
22. Hussey, G. S.; Dziki, J. L.; Badylak, S. F., Extracellular matrix-based materials for regenerative medicine. *Nature Reviews Materials* **2018**. DOI: 10.1038/s41578-018-0023-x.
23. Fitzpatrick, L. E.; McDevitt, T. C., Cell-derived matrices for tissue engineering and regenerative medicine applications. *Biomater Sci* **2015,** *3* (1), 12-24. DOI: 10.1039/C4BM00246F.
24. Jiang, B.; Akar, B.; Waller, T. M.; Larson, J. C.; Appel, A. A.; Brey, E. M., Design of a composite biomaterial system for tissue engineering applications. *Acta Biomater* **2014,** *10* (3), 1177-86. DOI: 10.1016/j.actbio.2013.11.029.
25. Chiono, V.; Mozetic, P.; Boffito, M.; Sartori, S.; Gioffredi, E.; Silvestri, A.; Rainer, A.; Giannitelli, S. M.; Trombetta, M.; Nurzynska, D.; Di Meglio, F.; Castaldo, C.; Miraglia, R.; Montagnani, S.; Ciardelli, G., Polyurethane-based scaffolds for myocardial tissue engineering. *Interface Focus* **2014,** *4* (1), 20130045. DOI: 10.1098/rsfs.2013.0045.
26. Dash, T. K.; Konkimalla, V. B., Poly-small je, Ukrainian-caprolactone based formulations for drug delivery and tissue engineering: A review. *J Control Release* **2012,** *158* (1), 15-33. DOI: 10.1016/j.jconrel.2011.09.064.
27. Williams, P. A.; Campbell, K. T.; Gharaviram, H.; Madrigal, J. L.; Silva, E. A., Alginate-Chitosan Hydrogels Provide a Sustained Gradient of Sphingosine-1-Phosphate for Therapeutic Angiogenesis. *Ann Biomed Eng* **2017,** *45* (4), 1003-1014. DOI: 10.1007/s10439-016-1768-2.
28. Mejia Oneto, J. M.; Gupta, M.; Leach, J. K.; Lee, M.; Sutcliffe, J. L., Implantable biomaterial based on click chemistry for targeting small molecules. *Acta Biomater* **2014,** *10* (12), 5099-105. DOI: 10.1016/j.actbio.2014.08.019.
29. Uebersax, L.; Mattotti, M.; Papaloizos, M.; Merkle, H. P.; Gander, B.; Meinel, L., Silk fibroin matrices for the controlled release of nerve growth factor (NGF). *Biomaterials* **2007,** *28* (30), 4449-60. DOI: 10.1016/j.biomaterials.2007.06.034.
30. Germershaus, O.; Lühmann, T.; Rybak, J. C.; Ritzer, J.; Meinel, L., Application of natural and semi-synthetic polymers for the delivery of sensitive drugs. *International Materials Reviews* **2014,** *60* (2), 101-131. DOI: 10.1179/1743280414y.0000000045.

31. Gutmann, M.; Braun, A.; Seibel, J.; Lühmann, T., Bioorthogonal Modification of Cell Derived Matrices by Metabolic Glycoengineering. *ACS Biomaterials Science & Engineering* **2018,** *4* (4), 1300-1306. DOI: 10.1021/acsbiomaterials.8b00264.
32. Frantz, C.; Stewart, K. M.; Weaver, V. M., The extracellular matrix at a glance. *J Cell Sci* **2010,** *123* (Pt 24), 4195-200. DOI: 10.1242/jcs.023820.
33. Mecham, R. P., Overview of extracellular matrix. *Curr Protoc Cell Biol* **2001,** *Chapter 10*, Unit 10 1. DOI: 10.1002/0471143030.cb1001s00.
34. Mouw, J. K.; Ou, G.; Weaver, V. M., Extracellular matrix assembly: a multiscale deconstruction. *Nat Rev Mol Cell Biol* **2014,** *15* (12), 771-85. DOI: 10.1038/nrm3902.
35. Theocharis, A. D.; Skandalis, S. S.; Gialeli, C.; Karamanos, N. K., Extracellular matrix structure. *Adv Drug Deliv Rev* **2016,** *97*, 4-27. DOI: 10.1016/j.addr.2015.11.001.
36. Badylak, S. F.; Freytes, D. O.; Gilbert, T. W., Extracellular matrix as a biological scaffold material: Structure and function. *Acta Biomater* **2009,** *5* (1), 1-13. DOI: 10.1016/j.actbio.2008.09.013.
37. Parmaksiz, M.; Dogan, A.; Odabas, S.; Elcin, A. E.; Elcin, Y. M., Clinical applications of decellularized extracellular matrices for tissue engineering and regenerative medicine. *Biomed Mater* **2016,** *11* (2), 022003. DOI: 10.1088/1748-6041/11/2/022003.
38. Du, J.; Meledeo, M. A.; Wang, Z.; Khanna, H. S.; Paruchuri, V. D.; Yarema, K. J., Metabolic glycoengineering: sialic acid and beyond. *Glycobiology* **2009,** *19* (12), 1382-401. DOI: 10.1093/glycob/cwp115.
39. Saxon, E., Cell Surface Engineering by a Modified Staudinger Reaction. *Science* **2000,** *287* (5460), 2007-2010. DOI: 10.1126/science.287.5460.2007.
40. Sarkar, A. K.; Fritz, T. A.; Taylor, W. H.; Esko, J. D., Disaccharide uptake and priming in animal cells: inhibition of sialyl Lewis X by acetylated Gal beta 1-->4GlcNAc beta-O-naphthalenemethanol. *Proceedings of the National Academy of Sciences* **1995,** *92* (8), 3323-3327. DOI: 10.1073/pnas.92.8.3323.
41. Laughlin, S. T.; Bertozzi, C. R., Metabolic labeling of glycans with azido sugars and subsequent glycan-profiling and visualization via Staudinger ligation. *Nat Protoc* **2007,** *2* (11), 2930-44. DOI: 10.1038/nprot.2007.422.
42. Homann, A.; Qamar, R. U.; Serim, S.; Dersch, P.; Seibel, J., Bioorthogonal metabolic glycoengineering of human larynx carcinoma (HEp-2) cells targeting sialic acid. *Beilstein journal of organic chemistry* **2010,** *6*, 24. DOI: 10.3762/bjoc.6.24.
43. Gutmann, M.; Memmel, E.; Braun, A. C.; Seibel, J.; Meinel, L.; Luhmann, T., Biocompatible Azide-Alkyne "Click" Reactions for Surface Decoration of Glyco-Engineered Cells. *Chembiochem : a European journal of chemical biology* **2016,** *17* (9), 866-75. DOI: 10.1002/cbic.201500582.
44. Collins, B. E.; Fralich, T. J.; Itonori, S.; Ichikawa, Y.; Schnaar, R. L., Conversion of cellular sialic acid expression from N-acetyl- to N-glycolylneuraminic acid using a synthetic precursor, N-glycolylmannosamine pentaacetate: inhibition of myelin-associated glycoprotein binding to neural cells. *Glycobiology* **2000,** *10* (1), 11-20. DOI: 10.1093/glycob/10.1.11.
45. Mahal, L. K., Engineering Chemical Reactivity on Cell Surfaces Through Oligosaccharide Biosynthesis. *Science* **1997,** *276* (5315), 1125-1128. DOI: 10.1126/science.276.5315.1125.
46. Sampathkumar, S. G.; Li, A. V.; Jones, M. B.; Sun, Z.; Yarema, K. J., Metabolic installation of thiols into sialic acid modulates adhesion and stem cell biology. *Nat Chem Biol* **2006,** *2* (3), 149-52. DOI: 10.1038/nchembio770.
47. Niederwieser, A.; Spate, A. K.; Nguyen, L. D.; Jungst, C.; Reutter, W.; Wittmann, V., Two-color glycan labeling of live cells by a combination of Diels-Alder and click chemistry. *Angew Chem Int Ed Engl* **2013,** *52* (15), 4265-8. DOI: 10.1002/anie.201208991.
48. Patterson, D. M.; Nazarova, L. A.; Xie, B.; Kamber, D. N.; Prescher, J. A., Functionalized cyclopropenes as bioorthogonal chemical reporters. *J Am Chem Soc* **2012,** *134* (45), 18638-43. DOI: 10.1021/ja3060436.
49. Agarwal, P.; Beahm, B. J.; Shieh, P.; Bertozzi, C. R., Systemic Fluorescence Imaging of Zebrafish Glycans with Bioorthogonal Chemistry. *Angew Chem Int Ed Engl* **2015,** *54* (39), 11504-10. DOI: 10.1002/anie.201504249.

50. Hein, C. D.; Liu, X. M.; Wang, D., Click chemistry, a powerful tool for pharmaceutical sciences. *Pharm Res* **2008,** *25* (10), 2216-30. DOI: 10.1007/s11095-008-9616-1.
51. Hein, J. E.; Fokin, V. V., Copper-catalyzed azide-alkyne cycloaddition (CuAAC) and beyond: new reactivity of copper(I) acetylides. *Chem Soc Rev* **2010,** *39* (4), 1302-15. DOI: 10.1039/b904091a.
52. Kislukhin, A. A.; Hong, V. P.; Breitenkamp, K. E.; Finn, M. G., Relative performance of alkynes in copper-catalyzed azide-alkyne cycloaddition. *Bioconjug Chem* **2013,** *24* (4), 684-9. DOI: 10.1021/bc300672b.
53. McKay, C. S.; Finn, M. G., Click chemistry in complex mixtures: bioorthogonal bioconjugation. *Chem Biol* **2014,** *21* (9), 1075-101. DOI: 10.1016/j.chembiol.2014.09.002.
54. Braun, A. C.; Gutmann, M.; Luhmann, T.; Meinel, L., Bioorthogonal strategies for site-directed decoration of biomaterials with therapeutic proteins. *J Control Release* **2018,** *273*, 68-85. DOI: 10.1016/j.jconrel.2018.01.018.
55. Elchinger, P.-H.; Faugeras, P.-A.; Boëns, B.; Brouillette, F.; Montplaisir, D.; Zerrouki, R.; Lucas, R., Polysaccharides: The "Click" Chemistry Impact. *Polymers* **2011,** *3* (4), 1607-1651. DOI: 10.3390/polym3041607.
56. Lang, K.; Chin, J. W., Bioorthogonal reactions for labeling proteins. *ACS chemical biology* **2014,** *9* (1), 16-20. DOI: 10.1021/cb4009292.
57. Hong, V.; Presolski, S. I.; Ma, C.; Finn, M. G., Analysis and optimization of copper-catalyzed azide-alkyne cycloaddition for bioconjugation. *Angewandte Chemie* **2009,** *48* (52), 9879-83. DOI: 10.1002/anie.200905087.
58. Brewer, G. J., Risks of copper and iron toxicity during aging in humans. *Chemical research in toxicology* **2010,** *23* (2), 319-26. DOI: 10.1021/tx900338d.
59. Kay, P.; Wagner, J. R.; Gagnon, H.; Day, R.; Klarskov, K., Modification of peptide and protein cysteine thiol groups by conjugation with a degradation product of ascorbate. *Chem Res Toxicol* **2013,** *26* (9), 1333-9. DOI: 10.1021/tx400061e.
60. Gaetke, L., Copper toxicity, oxidative stress, and antioxidant nutrients. *Toxicology* **2003,** *189* (1-2), 147-163. DOI: 10.1016/s0300-483x(03)00159-8.
61. Stadtman, E. R.; Oliver, C. N., Metal-catalyzed oxidation of proteins. Physiological consequences. *The Journal of biological chemistry* **1991,** *266* (4), 2005-8.
62. Tada, S.; Kitajima, T.; Ito, Y., Design and synthesis of binding growth factors. *Int J Mol Sci* **2012,** *13* (5), 6053-72. DOI: 10.3390/ijms13056053.
63. Park, S. N.; Kim, J. K.; Suh, H., Evaluation of antibiotic-loaded collagen-hyaluronic acid matrix as a skin substitute. *Biomaterials* **2004,** *25* (17), 3689-98. DOI: 10.1016/j.biomaterials.2003.10.072.
64. Srinivasarao, M.; Low, P. S., Ligand-Targeted Drug Delivery. *Chem Rev* **2017,** *117* (19), 12133-12164. DOI: 10.1021/acs.chemrev.7b00013.
65. Beck, A.; Goetsch, L.; Dumontet, C.; Corvaia, N., Strategies and challenges for the next generation of antibody-drug conjugates. *Nat Rev Drug Discov* **2017,** *16* (5), 315-337. DOI: 10.1038/nrd.2016.268.
66. Denison, T. A.; Bae, Y. H., Tumor heterogeneity and its implication for drug delivery. *J Control Release* **2012,** *164* (2), 187-91. DOI: 10.1016/j.jconrel.2012.04.014.
67. Dagogo-Jack, I.; Shaw, A. T., Tumour heterogeneity and resistance to cancer therapies. *Nature Reviews Clinical Oncology* **2017,** *15*, 81. DOI: 10.1038/nrclinonc.2017.166.
68. Wang, W.; Zhao, Z.; Zhang, Z.; Zhang, C.; Xiao, S.; Ye, X.; Zhang, L.; Xia, Q.; Zhou, D., Redirecting Killer T Cells through Incorporation of Azido Sugars for Tethering Ligands. *Chembiochem* **2017,** *18* (21), 2082-2086. DOI: 10.1002/cbic.201700340.
69. Gu, E.; Chen, W. Y.; Gu, J.; Burridge, P.; Wu, J. C., Molecular imaging of stem cells: tracking survival, biodistribution, tumorigenicity, and immunogenicity. *Theranostics* **2012,** *2* (4), 335-45. DOI: 10.7150/thno.3666.
70. Kang, S. W.; Lee, S.; Na, J. H.; Yoon, H. I.; Lee, D. E.; Koo, H.; Cho, Y. W.; Kim, S. H.; Jeong, S. Y.; Kwon, I. C.; Choi, K.; Kim, K., Cell labeling and tracking method without distorted signals by phagocytosis of macrophages. *Theranostics* **2014,** *4* (4), 420-31. DOI: 10.7150/thno.7265.

71. Laughlin, S. T.; Baskin, J. M.; Amacher, S. L.; Bertozzi, C. R., In vivo imaging of membrane-associated glycans in developing zebrafish. *Science* **2008,** *320* (5876), 664-7. DOI: 10.1126/science.1155106.
72. Braun, A. C.; Gutmann, M.; Ebert, R.; Jakob, F.; Gieseler, H.; Luhmann, T.; Meinel, L., Matrix Metalloproteinase Responsive Delivery of Myostatin Inhibitors. *Pharm Res* **2017,** *34* (1), 58-72. DOI: 10.1007/s11095-016-2038-6.
73. Braun, A. C.; Gutmann, M.; Mueller, T. D.; Luhmann, T.; Meinel, L., Bioresponsive release of insulin-like growth factor-I from its PEGylated conjugate. *J Control Release* **2018,** *279*, 17-28. DOI: 10.1016/j.jconrel.2018.04.009.
74. Ritzer, J.; Luhmann, T.; Rode, C.; Pein-Hackelbusch, M.; Immohr, I.; Schedler, U.; Thiele, T.; Stubinger, S.; Rechenberg, B. V.; Waser-Althaus, J.; Schlottig, F.; Merli, M.; Dawe, H.; Karpisek, M.; Wyrwa, R.; Schnabelrauch, M.; Meinel, L., Diagnosing peri-implant disease using the tongue as a 24/7 detector. *Nat Commun* **2017,** *8* (1), 264. DOI: 10.1038/s41467-017-00340-x.
75. Nagase, H.; Fields, G. B., Human matrix metalloproteinase specificity studies using collagen sequence-based synthetic peptides. *Biopolymers* **1996,** *40* (4), 399-416. DOI: 10.1002/(sici)1097-0282(1996)40:4<399::aid-bip5>3.0.co;2-r.
76. Springer, B. A.; Pantoliano, M. W.; Barbera, F. A.; Gunyuzlu, P. L.; Thompson, L. D.; Herblin, W. F.; Rosenfeld, S. A.; Book, G. W., Identification and concerted function of two receptor binding surfaces on basic fibroblast growth factor required for mitogenesis. *J Biol Chem* **1994,** *269* (43), 26879-84.
77. Caley, M. P.; Martins, V. L.; O'Toole, E. A., Metalloproteinases and Wound Healing. *Adv Wound Care (New Rochelle)* **2015,** *4* (4), 225-234. DOI: 10.1089/wound.2014.0581.
78. McCarty, S. M.; Percival, S. L., Proteases and Delayed Wound Healing. *Adv Wound Care (New Rochelle)* **2013,** *2* (8), 438-447. DOI: 10.1089/wound.2012.0370.
79. Cheung, P. Y.; Sawicki, G.; Wozniak, M.; Wang, W.; Radomski, M. W.; Schulz, R., Matrix metalloproteinase-2 contributes to ischemia-reperfusion injury in the heart. *Circulation* **2000,** *101* (15), 1833-9.
80. Phatharajaree, W.; Phrommintikul, A.; Chattipakorn, N., Matrix metalloproteinases and myocardial infarction. *Can J Cardiol* **2007,** *23* (9), 727-33.
81. Dozier, J. K.; Distefano, M. D., Site-Specific PEGylation of Therapeutic Proteins. *Int J Mol Sci* **2015,** *16* (10), 25831-64. DOI: 10.3390/ijms161025831.
82. Qi, Y.; Chilkoti, A., Protein-polymer conjugation-moving beyond PEGylation. *Curr Opin Chem Biol* **2015,** *28*, 181-93. DOI: 10.1016/j.cbpa.2015.08.009.
83. Lawrence, P. B.; Price, J. L., How PEGylation influences protein conformational stability. *Curr Opin Chem Biol* **2016,** *34*, 88-94. DOI: 10.1016/j.cbpa.2016.08.006.
84. Pasut, G.; Guiotto, A.; Veronese, F. M., Protein, peptide and non-peptide drug PEGylation for therapeutic application. *Expert Opinion on Therapeutic Patents* **2005,** *14* (6), 859-894. DOI: 10.1517/13543776.14.6.859.
85. Sheng, Z.; Lewis, J. A.; Chirico, W. J., Nuclear and nucleolar localization of 18-kDa fibroblast growth factor-2 is controlled by C-terminal signals. *J Biol Chem* **2004,** *279* (38), 40153-60. DOI: 10.1074/jbc.M400123200.
86. Bailly, K.; Soulet, F.; Leroy, D.; Amalric, F.; Bouche, G., Uncoupling of cell proliferation and differentiation activities of basic fibroblast growth factor. *FASEB J* **2000,** *14* (2), 333-44.
87. Gould, L.; Abadir, P.; Brem, H.; Carter, M.; Conner-Kerr, T.; Davidson, J.; DiPietro, L.; Falanga, V.; Fife, C.; Gardner, S.; Grice, E.; Harmon, J.; Hazzard, W. R.; High, K. P.; Houghton, P.; Jacobson, N.; Kirsner, R. S.; Kovacs, E. J.; Margolis, D.; McFarland Horne, F.; Reed, M. J.; Sullivan, D. H.; Thom, S.; Tomic-Canic, M.; Walston, J.; Whitney, J. A.; Williams, J.; Zieman, S.; Schmader, K., Chronic wound repair and healing in older adults: current status and future research. *J Am Geriatr Soc* **2015,** *63* (3), 427-38. DOI: 10.1111/jgs.13332.
88. Park, Y.; Colditz, G. A., Diabetes and adiposity: a heavy load for cancer. *The Lancet Diabetes & Endocrinology* **2018,** *6* (2), 82-83. DOI: 10.1016/s2213-8587(17)30396-0.
89. Global Burden of Disease Cancer, C.; Fitzmaurice, C.; Dicker, D.; Pain, A.; Hamavid, H.; Moradi-Lakeh, M.; MacIntyre, M. F.; Allen, C.; Hansen, G.; Woodbrook, R.; Wolfe, C.; Hamadeh, R. R.; Moore, A.; Werdecker, A.; Gessner, B. D.; Te Ao, B.; McMahon, B.; Karimkhani, C.; Yu,

C.; Cooke, G. S.; Schwebel, D. C.; Carpenter, D. O.; Pereira, D. M.; Nash, D.; Kazi, D. S.; De Leo, D.; Plass, D.; Ukwaja, K. N.; Thurston, G. D.; Yun Jin, K.; Simard, E. P.; Mills, E.; Park, E. K.; Catala-Lopez, F.; deVeber, G.; Gotay, C.; Khan, G.; Hosgood, H. D., 3rd; Santos, I. S.; Leasher, J. L.; Singh, J.; Leigh, J.; Jonas, J. B.; Sanabria, J.; Beardsley, J.; Jacobsen, K. H.; Takahashi, K.; Franklin, R. C.; Ronfani, L.; Montico, M.; Naldi, L.; Tonelli, M.; Geleijnse, J.; Petzold, M.; Shrime, M. G.; Younis, M.; Yonemoto, N.; Breitborde, N.; Yip, P.; Pourmalek, F.; Lotufo, P. A.; Esteghamati, A.; Hankey, G. J.; Ali, R.; Lunevicius, R.; Malekzadeh, R.; Dellavalle, R.; Weintraub, R.; Lucas, R.; Hay, R.; Rojas-Rueda, D.; Westerman, R.; Sepanlou, S. G.; Nolte, S.; Patten, S.; Weichenthal, S.; Abera, S. F.; Fereshtehnejad, S. M.; Shiue, I.; Driscoll, T.; Vasankari, T.; Alsharif, U.; Rahimi-Movaghar, V.; Vlassov, V. V.; Marcenes, W. S.; Mekonnen, W.; Melaku, Y. A.; Yano, Y.; Artaman, A.; Campos, I.; MacLachlan, J.; Mueller, U.; Kim, D.; Trillini, M.; Eshrati, B.; Williams, H. C.; Shibuya, K.; Dandona, R.; Murthy, K.; Cowie, B.; Amare, A. T.; Antonio, C. A.; Castaneda-Orjuela, C.; van Gool, C. H.; Violante, F.; Oh, I. H.; Deribe, K.; Soreide, K.; Knibbs, L.; Kereselidze, M.; Green, M.; Cardenas, R.; Roy, N.; Tillmann, T.; Li, Y.; Krueger, H.; Monasta, L.; Dey, S.; Sheikhbahaei, S.; Hafezi-Nejad, N.; Kumar, G. A.; Sreeramareddy, C. T.; Dandona, L.; Wang, H.; Vollset, S. E.; Mokdad, A.; Salomon, J. A.; Lozano, R.; Vos, T.; Forouzanfar, M.; Lopez, A.; Murray, C.; Naghavi, M., The Global Burden of Cancer 2013. *JAMA Oncol* **2015,** *1* (4), 505-27. DOI: 10.1001/jamaoncol.2015.0735.

90. Pearson-Stuttard, J.; Zhou, B.; Kontis, V.; Bentham, J.; Gunter, M. J.; Ezzati, M., Worldwide burden of cancer attributable to diabetes and high body-mass index: a comparative risk assessment. *The Lancet Diabetes & Endocrinology* **2018,** *6* (6), e6-e15. DOI: 10.1016/s2213-8587(18)30150-5.

91. Boateng, J.; Catanzano, O., Advanced Therapeutic Dressings for Effective Wound Healing--A Review. *J Pharm Sci* **2015,** *104* (11), 3653-80. DOI: 10.1002/jps.24610.

92. Frykberg, R. G.; Banks, J., Challenges in the Treatment of Chronic Wounds. *Adv Wound Care (New Rochelle)* **2015,** *4* (9), 560-582. DOI: 10.1089/wound.2015.0635.

93. Kang, R.; Goodney, P. P.; Wong, S. L., Importance of cost-effectiveness and value in cancer care and healthcare policy. *J Surg Oncol* **2016,** *114* (3), 275-80. DOI: 10.1002/jso.24331.

Abbreviations

A	Absorbance
AA	Amino acids
ACN	Acetonitrile
APTES	(3-Aminopropyl)triethoxysilane
ActRIIB	Activin receptors IIB
Ac_4GlcNAz	N-azidoacetylglucosamine-tetraacylated
Alg	Glycosyltransferase
Alk	(S)-2-amino-6-((2-azidoethoxy)carbonylamino)hexanoic acid
ALK4/5	Activin receptor-like kinase receptor
au	Arbitrary units
BCA	Bicinchoninic acid
BCS	Bovine calf serum
BSA	Bovine serum albumin
CDM	Cell derived matrix
cDNA	Complementary deoxyribonucleic acid
CF	5(6)-Carboxyfluorescein
CMP	Cytidine monophosphate
CuAAC	Copper (I)-catalyzed azide-alkyne cycloaddition
DBCO	Dibenzocyclooctyne
DDS	Drug delivery system
DMEM	Dulbecco’s Modified Eagle Medium
DMSO	Dimethyl sulfoxide
DNA	Deoxyribonucleic acid
DTT	Dithiothreitol
ECM	Extracellular matrix
E. coli	Escherichia coli
EDTA	Ethylenediaminetetraacetate
ELISA	Enzyme linked immunosorbent assay
ER	Endoplasmic reticulum
ERK	Extracellular-signal Regulated Kinases
FACS	Fluorescent activated cell sorting
FCS	Fetal calf serum
FDA	Fluoresceindiacetate
FGF-2	Fibroblast growth factor

FPLC	Fast protein liquid chromatography
Fuc	Fucose
Gal	Galactose
GalNAc	*N*-acetylgalactosamine
GalNAz	*N*-azidoacetylgalactosamine
Glc	Glucose
GlcA	Glucuronic acid
GlcNAc	*N*-acetylglucosamine
GlcNAz	*N*-azidoacetylglucosamine
GPI	glycosylphosphatidylinositol
HPLC	High-performance liquid chromatography
HRP	Horseradish peroxidase
IdoA	Iduronic acid
IgG	Immunoglobulin G
IPTG	Isopropyl ß-D-1-thiogalactopyranosid
LAF	Laminar Air Flow
LB	Lysogeny broth
MALDI-MS	Matrix-assisted laser desorption ionization mass spectrometry
Man	Mannose
ManNAc	*N*-acetylmannosamine
ManNAz	*N*-azidoacetylmannosamine
MMP	Matrix metalloproteinase
MI	Myostatin inhibitor
mRNA	Messenger ribonucleic acid
MS	Mass spectrometry
MWCO	Molecular weight cut-off
m/z	mass to charge ratio
NHS	*N*-hydroxysuccinimide
OD	Optical density
PBS	Phosphate buffered saline
PCR	Polymerase chain reaction
PD	Pharmacodynamic
PEG	Polyethylene glycol
Pen/Strep	Penicillin and streptomycin
pERK	Phosphorylated Extracellular-signal Regulated Kinases
PI	Propidium Iodide

PK	Pharmacokinetic
PMSF	Phenylmethylsulfonyl fluoride
PTFE	Polytetrafluoroethylene
Pyl	L-pyrrolysine
PylRS	Pyrrolysyl-tRNA synthetase
RNA	Ribonucleic acid
RT	Room temperature
RT-PCR	Quantitative real time polymerase chain reaction
RPM	Rounds per minute
SA	Sialic acid
SDS	Sodium dodecylsulfate
SDS-PAGE	Sodium dodecylsulfate polyacrylamide gel electrophoresis
SEC	Size exclusion chromatography
SEM	Scanning electron microscopy
SPAAC	Strain-promoted alkyne-azide cycloadditions
TB	Terrific broth
TFA	Trifluoracetic acid
THPTA	Tris(3-hydroxypropyltriazolylmethyl) amine
TMB	Tetramethylbenzidine
uAA	Unnatural amino acids
UV	Ultraviolet
UDP	Uridine diphosphate
VIS	Visible
WST-1	Water soluble tetrazolium salt
Xyl	Xylose

Curriculum vitae

Publications

Reggane, M., J. Wiest, et al., (2018). "Bioinspired co-crystals of Imatinib providing enhanced kinetic solubility." Eur J Pharm Biopharm.

Braun, A. C., M. Gutmann, et al., (2018). "Bioresponsive release of insulin-like growth factor-I from its PEGylated conjugate." J Control Release 279: 17-28.

Gutmann, M., A. Braun, et al., (2018). "Bioorthogonal Modification of Cell Derived Matrices by Metabolic Glycoengineering." ACS Biomaterials Science & Engineering 4(4): 1300-1306.

Braun, A. C., M. Gutmann, et al., (2018). "Bioorthogonal strategies for site-directed decoration of biomaterials with therapeutic proteins." J Control Release 273: 68-85.

Griesbeck, S., Z. Zhang, et al.,(2016). "Water-Soluble Triarylborane Chromophores for One- and Two-Photon Excited Fluorescence Imaging of Mitochondria in Cells." Chemistry 22(41): 14701-14706.

Braun, A. C., M. Gutmann, et al., (2017). "Matrix Metalloproteinase Responsive Delivery of Myostatin Inhibitors." Pharm Res 34(1): 58-72.

Steiger, C., K. Uchiyama, et al., (2016). "Prevention of colitis by controlled oral drug delivery of carbon monoxide." J Control Release 239: 128-136.

Dechnik, J., F. Mühlbach, et al., (2016). "Luminescent Metal-Organic Framework Mixed-Matrix Membranes from Lanthanide Metal-Organic Frameworks in Polysulfone and Matrimid." European Journal of Inorganic Chemistry 2016(27): 4408-4415.

Gutmann, M., E. Memmel, et al., (2016). "Biocompatible Azide-Alkyne "Click" Reactions for Surface Decoration of Glyco-Engineered Cells." Chembiochem 17(9): 866-875.

Lühmann, T., G. Jones, et al., (2015). "Bio-orthogonal Immobilization of Fibroblast Growth Factor 2 for Spatial Controlled Cell Proliferation." ACS Biomaterials Science & Engineering 1(9): 740-746.

Steiger, C., J. Wollborn, et al., (2015). "Controlled therapeutic gas delivery systems for quality-improved transplants." Eur J Pharm Biopharm 97(Pt A): 96-106.

Posters

Gutmann, M., Braun, A., et al., (2016) “Site-directed functionalization of cell derived matrices by metabolic glycoengineering and click chemistry” ChemSyStM, Würzburg

Gutmann, M., Memmel, E., et al., (2015) “Modification of glycoengineered living cells by copper-free (SPAAC) and copper catalyzed azide alkyne cycloaddition (CuAAC)” DPhG annual meeting, Düsseldorf

Gutmann, M., Wurzel, J., et al., (2014) “Decoration of living cell surfaces by copper catalyzed azide-alkyne cycloaddition” DPhG annual meeting, Frankfurt

Gutmann, M., Memmel, E., et al., (2013) “Decoration of living cell surfaces by site-directed covalent coupling” CRS Germany Local Chapter Meeting, Kiel

Acknowledgments

First of all, I would like to sincerely thank Prof. Dr. Dr. Lorenz Meinel for giving me the opportunity to join his research group and to perform my PhD thesis in this fascinating field of research. During these eventful years, I have gratefully appreciated his guidance through permanent support, helpful advice, his wide scientific skills as well as providing excellent equipment conditions.

Furthermore, I would like to express my sincere gratitude to my supervisor PD Dr. Tessa Lühmann for her expert guidance, her constant support, her encouragement and honest scientific advice during my PhD.

I am very grateful to Prof. Dr. Jürgen Seibel and Dr. Elisabeth Memmel, of the Institute of Organic Chemistry in Würzburg for the supply of the engineered monosaccharides, their contributions to the manuscripts and productive discussions. This thank is also extended to Prof. Dr. Andreas Schlosser and Stephanie Lamer of the Rudolf Virchow Centrum as well as Dr. Werner Schmitz of the Chair of Biochemistry and Molecular Biology for the knowledge and support in mass spectrometry analysis. In addition, I would like to thank Prof. Dr. Götz Münch, Dr. Susanne Neidhold and Ms. Ulrike Potschka from AdvanceCor GmbH in Munich for the expertise and great collaboration in the Revacept project.

I also would like to thank my PhD colleagues and other members of the team as well as my colleagues from the group of Prof. Dr. Petra Högger and Prof. Dr. Ulrike Holzgrabe for the enjoyable time in Wuerzburg. Special thanks go to Alexandra Braun for the intensive collaboration, Valerie Spieler for the fruitful discussions and extracurricular projects as well as Cecilia Amstalden and Cornelius Hermann for their true friendship. Apart from this I would like to thank Dr. Vera Werner for her constant advice and her deep friendship. Many thanks also to the family Kuhn for the warm welcome and the pleasant hours.

Finally, I would like to thank my family, my girlfriend and her family – I am eternally grateful for their constant and unlimited advice and support.

Documentation of authorship

This section contains a list of the individual contribution for each author to the publications reprinted in this thesis. Unpublished manuscripts are handled, accordingly.

P1	**Gutmann M, Bechold J, Seibel J, Meinel L, Lühmann T** (2018). Metabolic glycoengineering of cell derived matrices and cell surfaces - a detailed guidance [Submitted]				
Author	**1**	**2**	**3**	**4**	**5**
Procedure – Synthesis	x	x			
Procedure – Cell derived matrices	x				
Procedure – Cells	x				
Manuscript planning	x			x	x
Manuscript writing	x			x	x
Design of the graphics	x				
Correction of manuscript	x	x	x	x	x
Supervision of Marcus Gutmann					x

P2	**Gutmann M, Braun A C, Seibel J, Lühmann T** (2018) Bioorthogonal Modification of Cell Derived Matrices by Metabolic Glycoengineering. ACS Biomater. Sci. Eng.2018, 4, 1300−1306			
Author	**1**	**2**	**3**	**4**
Synthesis, chemical modification, and molecular weight of the myostatin inhibitors	x	x		
Glass surface modification	x			
Generation and extraction of cellular derived matrices (CDMs)	x			
SDS-PAGE and Western Blot of different Sera	x			
Immobilization of fluorescent dyes on CDMs	x			
Cell viability during matrix deposition	x			
Characterization of resident cells from unextracted CDMs	x			
Characterization of re-seeded fibroblasts on CDMs	x			
SDS-PAGE and Western Blot of modified fibronectin	x			
Immobilization of myostatin inhibitor on CDMs	x	x		
Scanning electron microscopy	x			
Fluorescence microscopy	x			
Confocal laser scanning microscopy	x			
Flow cytometry	x			
Statistics analysis	x			
Study design/concept development	x		x	x
Data analysis and interpretation	x	x		x
Manuscript planning	x		x	x
Manuscript writing	x			x
Correction of manuscript	x	x	x	x
Supervision of Marcus Gutmann				x

P3	**Gutmann M, Memmel E, Braun A C, Seibel J, Meinel L, Lühmann T** (2016) Biocompatible Azide Alkyne"Click" Reactions for Surface Decoration of Glyco-Engineered Cells Chembiochem. 17(9), pp. 866-75

Author	**1**	**2**	**3**	**4**	**5**	**6**
Synthesis and purification of 2-azidoacetylamino-2-deoxy-(1,3,4,6)-tetra-O-acetyl-d-glucopyranoside		x				
Glycoengineering of HEK 293 Freestyle and NIH3T3	x					
Cell viability of CuAAC	x		x			
Cell recovery after CuAAC	x					
RT-PCR (Quantitative real-time PCR of apoptotic markers)	x					
Quantification of reactive oxygen species	x		x			
Quantification of cell-surface labeling after CuAAC and SPAAC	x					
Kinetic of cell-surface labeling after CuAAC and SPAAC	x					
Flow cytometry (FACSCalibur and FACS Aria III)	x					
Confocal laser scanning microscopy	x					
Statistical analysis	x					
Study design/concept development	x			x	x	x
Data analysis and interpretation	x		x		x	x
Manuscript planning	x					x
Manuscript writing	x					x
Correction of manuscript	x	x	x	x	x	x
Supervision of Marcus Gutmann						x

P4	**Gutmann M, Spieler V, Raschig M, Potschka U, Neidhold S, Münch G, Meinel L, Lühmann T** (2018) Matrix Metalloproteinase Responsive Delivery of fibroblast growth factor 2 [unpublished]

Author	**1**	**2**	**3**	**4**	**5**	**6**	**7**	**8**
Synthesis and purification of ((S)-2-amino-6-((2-azidoethoxy)carbonylamino)hexanoic acid)	x		x					
Sub cloning of 8(TAG)-MMP-FGF-2	x	x						
Expression and purification of N3-FGF-2 and N3-MMP-FGF-2	x							
Elastase digestion and mass spectrometric characterization	x							
Formation and purification of PEG-MMP-FGF-2	x							
Formation and purification of Revacept-MMP-FGF-2 and Revacept-FGF-2	x							
High performance liquid chromatography	x							
Cell proliferation assay (WST-1)	x							
Cell signaling and Western immunoblotting	x							
Collagen Enzyme Linked Immunosorbent Assay (ELISA)				x				
Statistical analysis	x							
Study design/concept development	x				x	x	x	x
Data analysis and interpretation	x							x
Manuscript planning	x				x	x	x	x
Manuscript writing	x							x
Correction of manuscript	x	x	x				x	x
Supervision of Marcus Gutmann								x

Erklärung zu den Eigenanteilen des Doktoranden sowie der weiteren Doktoranden als Koautoren an Publikationen und Zweitpublikationsrechten bei einer kumulativen Dissertation.

Für alle in dieser kumulativen Dissertation verwendeten Manuskripte liegen die notwendigen Genehmigungen der Verlage (‚reprint permission') für die Zweitpublikation vor, außer das betreffende Kapitel ist noch gar nicht publiziert. Dieser Umstand wird einerseits durch die genaue Angabe der Literaturstelle der Erstpublikation auf der ersten Seite des betreffenden Kapitels deutlich gemacht oder die bisherige Nichtveröffentlichung durch den Vermerk „unpublished" oder „nicht veröffentlicht" gekennzeichnet.

Die Mitautoren der in dieser kumulativen Dissertation verwendeten Manuskripte sind sowohl über die Nutzung als auch über die oben angegebenen Eigenanteile informiert.

Die Beiträge der Mitautoren an den Publikationen sind in den vorausgehenden Tabellen aufgeführt.

PD Dr. Tessa Lühmann	25. Oktober 2018	Unterschrift
Marcus Gutmann	25. Oktober 2018	Unterschrift